

G3798

**PHOTOACOUSTIC EFFECT : SOME APPLICATIONS IN  
LASER TECHNOLOGY**

**M. K. SATHEESHKUMAR**

THESIS SUBMITTED  
IN PARTIAL FULFILMENT OF THE REQUIREMENTS  
FOR THE DEGREE OF  
**DOCTOR OF PHILOSOPHY**

DEPARTMENT OF PHYSICS  
COCHIN UNIVERSITY OF SCIENCE AND TECHNOLOGY


**1987**

*To*  
**MY PARENTS**

## CERTIFICATE

*Certified that the work presented in this thesis entitled **Photoacoustic effect: Some applications in laser technology** is based on the original work done by **Mr. M. K. Satheeshkumar**, under my guidance in the Department of Physics, Cochin University of Science and Technology, and has not been included in any other thesis submitted previously for the award of any degree.*

Cochin-682 022  
27 - 08 - 1987

  
**Dr. C. P. Girijavallabhan**  
Supervising Teacher

## DECLARATION

*Certified that the work presented in this thesis entitled **Photoacoustic effect: Some applications in laser technology** is based on the original work done by me under the guidance of **Dr. C. P. Girijavallabhan**, Professor, Department of Physics, Cochin University of Science and Technology, and has not been included in any other thesis submitted previously for the award of any degree.*

Cochin-682 022  
27 - 08 - 1987

  
**M. K. Satheeshkumar**

## ACKNOWLEDGEMENTS

*The investigations presented in this thesis have been carried out under the guidance and supervision of Dr. C. P. Girijavallabhan, Professor, Department of Physics, Cochin University of Science and Technology. I express my sincere gratitude for his able guidance and competent advice given to me throughout the period of this work.*

*I am extremely thankful to Prof. M. G. Krishna Pillai, Prof. & Head of the Dept. of Physics, for providing all the necessary facilities to carry out this work.*

*I am highly indebted to Prof. K. Sathianandan, former Prof. & Head of this department for encouraging me with necessary guidance to take up research work in laser physics.*

*I would like to thank Dr. C. K. N. Patel, Director, Physics Division, AT&T Bell Labs., U.S.A., for the timely help given to me during the early stages of this work. Thanks are also due to Dr. A. C. Tam, IBM Labs., San Jose, California and Dr. P. Poulet, Institute de Physique Biologique, France, for the help and advice. I extend my thanks to Dr. U. Syamaprasad, Scientist, Regional Research Lab., Bhubaneswar, for providing silicon samples.*

*Mr. C. Raghavan, Technical Assistant, Dept. of Physics, helped me a great deal in the design and fabrication of electronic circuits used in this work. I extend my sincere thanks*

to him for his kind co-operation and help. Thanks are also due to Dr. K. Mohanachandran and Dr. N. Subhash for their timely help and advice.

A special note of gratitude goes to Prof. R. Pratap, visiting professor, Dr. V.P.N. Nampoori, Dr. Jacob Philip and Dr. K.P. Vijayakumar, faculty members of this department for their help and advice.

I express my sincere thanks to all my colleagues especially those in Laser Division and Thin Film Division for their kind co-operation and immense help given to me throughout the entire programme.

Thanks are also due to the technical, administrative and library staff of this department and staff of the University Science Instrumentation Centre for their help and co-operation.

I take this opportunity to thank Indian Space Research Organisation, Bangalore; Dept. of Atomic Energy, Bombay, and Council of Scientific and Industrial Research, New Delhi, for the award of research fellowships.

It would be impossible to name every one to whom I would like to convey my thanks for making my stay in the Cochin University Campus pleasant and memorable.

Finally I extend my thanks to Mr. John Palathingal for typing this manuscript neatly.

**M. K. Satheeshkumar**

## PREFACE

The discovery of the Photoacoustic (PA) effect was a remarkable achievement and was relegated to the scientific footnotes of the nineteenth century. However, after the advent of lasers and sophisticated electronics this effect was rediscovered and it has established itself as an important research and analytical tool in numerous areas, including physics, chemistry, biology and medicine. Quite recently, this phenomenon has made its impact in the field of laser technology for applications such as the developments of highly efficient active media for lasers, high quality optics and sensitive laser power monitoring devices. This thesis presents the work carried out by the author in this field during the past few years at the Department of Physics in Cochin University of Science and Technology.

The studies discussed here are mostly based on the development of a sensitive PA laser power meter and its various applications using different laser systems available in the laboratory. This includes the development of a current regulated CW  $\text{CO}_2$  laser and its application in material processing. The major achievements outlined in the present thesis are the following :

1. Development of a PA set up and the studies related to the different aspects of the system.
2. Use of the PA set up as a sensitive laser power meter and its application to laser beam attenuation studies in atmosphere.
3. The studies related to the influence of backing materials in PA effect for the identification of multi-layered thin film structures and experimental evaluation of the thermal diffusivities of bulk copper samples and  $\text{CeO}_2$  thin films.
4. Design and fabrication of a 30 W current stabilised CW  $\text{CO}_2$  laser.

5. Detailed studies of operating characteristics of such a laser made for the first time with the help of a PA laser power meter.
6. The absolute measurement of absorption coefficient at  $10.6 \mu\text{m}$  region in an undoped silicon wafer using the PA laser power meter.

The thesis contains seven chapters which by and large are self contained with separate abstracts and references. The first chapter which is divided into two parts presents an introduction to the PA effect and its present status. Part A reviews the basic theory of laser and gives a summary of various lasers and their applications. Part B presents a brief description of PA effect and its suitability as a spectroscopic tool followed by its applications to various branches of science and technology.

Chapter II presents a comprehensive overview of Rosencwaig-Gersho [RG] theory which is considered to be the basic theory for PA effect. A detailed account of the thermal diffusion equation and its solutions at gas-sample-backing interface are presented. The thermal piston model is briefly outlined and the results for special cases such as optically opaque, optically transparent, thermally thick and thermally thin samples are given. The applications of this theory under different conditions of the experimental set up are briefly discussed.

In chapter III the details of the fabrication of a PA cell and the experimental set up for the measurement of PA effect using a laser, mechanical chopper and a lock-in amplifier are described. It also describes how the basic PA cell can be converted to measure the power of the incident laser beam. Elaborate measurements using different types of lasers like He-Ne, Ar ion and Dye laser demonstrate the flat wavelength response, large dynamic range and excellent linearity of

the PA laser power meter. It also describes the utility of this laser power meter in the total atmospheric attenuation of laser beams when it propagates through a long distance in the atmosphere.

Chapter IV presents the experimental observation of the effect of backing materials on the amplitude and phase of the PA signal. With a thin film backing material sudden changes in both amplitudes and phase are found to occur as the thermal diffusion length exceeds the sample thickness. The phase and amplitude of PA signal are measured as a function of chopping frequency for copper sample of different thicknesses using three different backing materials. (water, isopropyl alcohol and castor oil). Analysis of the result shows agreement with R-G theory and from the observed characteristic frequencies which correspond to different thicknesses of copper samples, thermal diffusivity is precisely calculated. Similarly using rear surface illumination method, the thermal diffusivity of  $\text{CeO}_2$  thin films of thicknesses 1000 Å and 2000 Å are accurately determined using PA technique.

Chapter V is divided into two parts in which Part A gives a concise review of the various stages in the development of  $\text{CO}_2$  lasers along with a detailed description of theoretical backgrounds. It also provides an account of design and fabrication of a current regulated CW  $\text{CO}_2$  laser system. This laser contains two water cooled plasma tubes of length 75 cms each which are optically in series but electrically in parallel. A brief description of the design and fabrication of its anodes, cathodes, and gas filling system is presented. Part B describes the complete details of the high voltage power supply which ensures simultaneous excitation of both plasma tubes of the laser system. It also incorporates a solid state net work to regulate the plasma tube current with high stability, precision and protection circuits to safeguard the laser system from over voltages and over currents.



In chapter VI extensive parameter studies of the current stabilised CO<sub>2</sub> laser using the PA laser power meter are described. Study of variation of output power with current levels at a fixed gas mixture ratio gives the parameters for optimising the operating conditions. A peak with large negative slope is found to occur for a definite plasma tube current for a particular gas mixture ratio and this suggests the possibility of efficient intensity modulation of laser beam by modulating the plasma tube current within this operating region. Addition of water vapour at 0.3 torr improves the power level beyond 30 W. Spectral response at different current values for a fixed gas pressure reveals that intensity peaks for laser emission occurs at 9.6  $\mu\text{m}$  and 10.6  $\mu\text{m}$ . With the increase of pressure, the number of lasing lines reduces and P(20) line become more dominant. The divergence of the CO<sub>2</sub> laser beam is found to be extremely small due to fairly long laser cavity.

Chapter VII deals with the application of the CO<sub>2</sub> laser for material processing. It briefly describes the necessary theory and a concise review of the laser material processing. The optical transmission through a commercial grade silicon wafer is measured as a function of time using PA laser power meter. It is observed that the transmission coefficient decreases with time and in 15-20 seconds it reaches a steady value which is about 20% of its original magnitude. The unchanged reflection coefficient in air and in vacuum reveals the absence of oxide layer formation on the surface of silicon. Absolute value of the absorption coefficient under steady state condition helps to determine the free carrier concentration at 1100 K.

Part of the investigations presented in this thesis has been published/accepted for publication in the form of the following papers/reports :

1. A photoacoustic set up for atmospheric attenuation studies using a He-Ne laser beam.  
M. K. Satheeshkumar and C.P.G. Vallabhan,  
Proceedings of National Conference on Instrumentation (CSIO),  
India, p.332 (1983).
2. A simple and inexpensive optical chopper with in-built reference signal shaped for maximum phase accuracy.  
M.K. Satheeshkumar, C. Raghavan and C.P.G. Vallabhan,  
Proceedings of National Conference on Instrumentation (CSIO),  
India, p.324 (1983).
3. A sensitive photoacoustic laser power meter.  
M.K. Satheeshkumar and C.P.G. Vallabhan,  
Lasers and Applications, Ed. Bist and Goela (Tata McGraw Hill, New Delhi), p. 83 (1983).
4. Use of a photoacoustic cell as a sensitive laser power meter.  
M.K. Satheeshkumar and C.P.G. Vallabhan,  
J. Phys. E. (Scientific Instruments), 18, 434 (1985).
5. Effect of thin film backing material on the photoacoustic signal.  
M.K. Satheeshkumar, K.P. Vijayakumar and C.P.G. Vallabhan,  
Proceedings of Quantum Electronics Symposium, DAE, (BARC, Bombay), p. 164 (1985).
6. Thermal diffusivity of  $CeO_2$  thin film using photoacoustic effect.  
M.K. Satheeshkumar and C.P.G. Vallabhan,  
Proceedings of Solid State Physics Symposium, DAE, (Nagpur) 28c, p. 328 (1985).

7. Laser monitoring of atmospheric pollution.  
M.K. Satheeshkumar and C.P.G. Vallabhan,  
Technical Report, ISRO Sponsored Space Technology and  
Space Application Projects (RESPOND), TR-54-86, p. 82 (1986).
8. Design and fabrication of a current stabilised power supply  
system for CW CO<sub>2</sub> laser.  
V.P.N. Namboori, C. Raghavan, M.K. Satheeshkumar and  
C.P.G. Vallabhan,  
Proceedings of Quantum Electronics Symposium, DAE, (Cochin  
University of Science & Technology), p. 1 (1986).
9. CO<sub>2</sub> laser beam transmission through silicon wafers : Obser-  
vation of time dependent effects.  
M.K. Satheeshkumar, C.P.G. Vallabhan and K. Mohanachandran,  
Proceedings of International Conference on Laser Application  
in Spectroscopy and Optics, COSTED (IIT, Madras), paper 12,  
(1987).
10. High voltage solid state power supply for a CW CO<sub>2</sub> laser  
with current stabilisation.  
M.K. Satheeshkumar, C. Raghavan and C.P.G. Vallabhan,  
International Journal of Electronics (in press).

## CONTENTS

	Acknowledgements	i
	Preface	iii
<b>Chapter I</b>	<b>General Introduction</b>	
1.1	Introduction to lasers	2
1.2	Interaction of radiation with matter	3
1.3	Laser resonator	8
1.4	Properties of laser beam	15
1.5	Various types of lasers and its applications	17
1.6	Conclusion	27
1.7	Photoacoustic effect and its spectroscopic applications	29
1.8	PAS of solids	34
1.9	Weak absorptions in gases	35
1.10	Thin films	36
1.11	Photoacoustic microscopy	37
1.12	PAS in biology and medicine	40
1.13	Conclusion	43
<b>Chapter II</b>	<b>General theory of photoacoustic effect in solids and its applications</b>	
2.1	Introduction	51
2.2	Early history	52
2.3	Rosencwaig-Gersho theory	54
2.4	Special cases	67
2.5	Applications	76
<b>Chapter III</b>	<b>Experimental set up for a photoacoustic measurement system and some of its applications</b>	
3.1	Introduction	84
3.2	Details of the PA experimental set up	85
3.3	Conversion of the PA cell into a laser power meter	104

<b>Chapter IV</b>	<b>Determination of thermal diffusivity of metallic and dielectric samples from photoacoustic measurements</b>	
4.1	Introduction	124
4.2	Historical background	125
4.3	Front surface illumination of the sample:theory	127
4.4	Experimental set up	130
4.5	Results and discussion	134
4.6	Thermal diffusivity of CeO <sub>2</sub> thin film using rare surface illumination method	141
4.7	Depth profiling studies using PA technique	148
<b>Chapter V</b>	<b>Design and fabrication of a current stabilised CW CO<sub>2</sub> laser</b>	
5.1	Introduction	161
5.2	Theoretical considerations for laser action	163
5.3	Design and fabrication of a CW CO <sub>2</sub> laser	184
5.4	High voltage power supply	192
5.5	Operation of the laser	201
<b>Chapter VI</b>	<b>Parametric studies of a current stabilised CW CO<sub>2</sub> laser</b>	
6.1	Introduction	206
6.2	Earlier work	207
6.3	Variation of CO <sub>2</sub> laser power with plasma tube current	210
6.4	Variation of output power with total pressure at fixed plasma tube current levels	220
6.5	Effect of the addition of water vapour on the laser beam intensity	223
6.6	Effect of plasma tube current on the spectral distribution in CO <sub>2</sub> laser emission	226
6.7	Measurement of divergence of the laser beam	229

Chapter VII	CO <sub>2</sub> laser beam transmission through silicon wafer	
7.1	Introduction	240
7.2	Earlier work on infrared transmission through semiconductors	240
7.3	Theory	242
7.4	Changes in optical properties due to high intensity laser beams	245
7.5	Experimental set up for the measurement of CO <sub>2</sub> laser beam through silicon wafer	254
7.6	Results and discussion	257
7.7	Conclusion	260

## CHAPTER I

### GENERAL INTRODUCTION

#### ***Abstract***

*This chapter is divided into two parts. Part A gives a brief account of laser theory, different laser systems and their applications related to science and technology. Part B presents a concise review of the various applications of photoacoustic spectroscopy.*

## PART A

### 1.1 Introduction to lasers :

The 20th century is earmarked by the two remarkable revolutions in optics, viz., the discovery of quantum nature of light and the invention of laser. The concept of energy quanta introduced by Max Planck at the turn of this century has deeply influenced the fundamental understandings of light and matter. Then the laser made it possible to generate light with entirely new properties. This in turn led to the discovery of completely new types of optical processes such as harmonic frequency generation in matter, up and down conversion at optical frequencies, coherent scattering and several other non-linear phenomena. Consequently many new branches in physics, viz., quantum optics, laser physics and non-linear optics were developed rapidly. These breathtaking advances have made it abundantly clear that there is hardly any other field in physics in which a profound understanding of the fundamental processes is so intimately interwoven with various applications of great practical importance in the field of science and technology.

**LASER** which is an acronym for Light Amplification by Stimulated Emission of Radiation is in fact an unique source of radiation in the wide wavelength range between x-rays and microwaves in the electromagnetic spectrum. This intense beam of optical radiation possesses many desirable properties like monochromaticity, coherence and directionality which make it a potential light source with immense possibilities for application in many branches of science, medicine and engineering. Pulsed as well as Continuous Wave (CW) output is obtained



from different lasers, with a pulse duration as short as femtosecond while some CW lasers can provide an output power of several kilowatts. Recently laser was successfully employed to reveal the identity of single atoms and molecules. Similarly high resolution spectroscopic studies using lasers could bring out the complete dynamics of the chemical reactions and this has opened up a new era in photochemistry [1]. The use of laser as a tool for bloodless surgery is indicative of the potential application of this light source in the field of medicine. Material processing studies using high power lasers have provided promising results in the field of engineering sciences.

Thus there can be no doubt that laser represents one of the most remarkable scientific and technical milestones of the present century. The laser revolution has brought out a rebirth of science and technology of optics and has led to the development of whole new industries.

In the first part of this chapter a brief account of the laser emission process and its characteristic features are presented. A comprehensive review of the development of various laser systems and their applications are discussed in the sub sections followed by the theoretical description.

## **1.2 Interaction of radiation with matter :**

In order to visualise laser action a thorough understanding of the quantum mechanical description of interaction of electromagnetic radiation with matter is essential. A laser exploits three fundamental phenomena which occur when an electromagnetic wave interacts with

matter, viz., the processes absorption, spontaneous emission and stimulated emission. If the frequency of the wave corresponds to the energy difference between two energy levels in the medium, then the system absorbs energy from the wave and gets excited to the upper energy level. This process is often termed as absorption and the condition for the same can be expressed as

$$h\nu = E_2 - E_1 \quad (1.01)$$

where  $E_1$  and  $E_2$  are energy levels in the medium,  $h$  is the Planck's constant and  $\nu$  is the frequency of the interacting wave. After a photon is absorbed by an atom or molecule in the medium an excited atomic or molecular species is produced. The rate of absorption depends on the intensity of radiation and hence it can be expressed as

$$\frac{dN_1}{dt} = -B_{12} U(\omega) N_1 \quad (1.02)$$

where  $N_1$  is the total number of atoms or molecules in the energy level  $E_1$  and  $B_{12}$  is the probability of absorption at an energy density  $U(\omega)$ , is known as Einstein's B coefficient. Subsequently, the excited atom may relax to the lower energy level in the absence of any external agency and this radiative relaxation process is termed as spontaneous emission. The rate of spontaneous emission can be expressed as

$$\frac{dN_2}{dt} = -AN_2 \quad (1.03)$$

where  $N_2$  is the population density in the excited state, and  $A$  is the spontaneous emission probability which is Einstein's A coefficient [2].

Instead of leaving the excited atom to decay by virtue of its finite life time, if it is irradiated with another photon which has the same energy as one emitted spontaneously, then the irradiation may trigger the release of a photon from the medium which in effect amplifies the input radiation. This process in which the emission of radiation with the aid of an external stimulation is known as stimulated emission. Since this process is closely connected with the characteristics of the incident electromagnetic wave, there exists a definite phase relationship between the emitted photon and the interacting photon. The rate of stimulated emission process is expressed as

$$\frac{dN_2}{dt} = - B_{21} U(\omega) N_2 \quad (1.04)$$

where  $N_2$  is the population density of the upper energy level,  $U(\omega)$  is the energy density of the interacting electromagnetic wave and  $B_{21}$  is the probability of stimulated emission which is also known as Einstein's B coefficient. Therefore the stimulated emission process is apparently a complementary process of absorption. The ratio of Einstein's A and B coefficients essentially determines the probability of spontaneous emission over stimulated emission process in the medium which in turn determines the efficiency of laser action in the medium. The ratio of A and B coefficient is

$$\frac{A}{B} = \frac{\hbar \omega^3}{\pi^2 c^3} \quad (1.05)$$

where  $C$  is the velocity of light and  $\hbar = h/2\pi$ ,  $h$  being the Planck's constant. From this relation it is evident that the spontaneous emission

probability is higher in the short range wavelengths. These three processes namely absorption, spontaneous emission and stimulated emission are schematically illustrated in fig. 1.1.

The stimulated emission process governs the laser emission from a medium. In order to obtain the stimulated emission from an active medium a condition known as 'population inversion' is highly essential. Consider a case in which two arbitrary energy levels 1 and 2 of a given medium and let  $N_1$  and  $N_2$  be their respective population densities. If a plane electromagnetic wave with an intensity corresponding to a photon flux  $F$  is travelling along the  $Z$  direction of the medium, then the elemental change of this photon flux due to both stimulated emission and absorption process is given by

$$dF = F (N_2 - N_1) dz \quad (1.06)$$

Therefore the material behaves as an amplifier if  $N_2 > N_1$ , and it acts as an absorber if  $N_2 < N_1$ . In the case of thermal equilibrium, the energy level populations are described by Maxwell-Boltzmann statistics as

$$\frac{N_2^e}{N_1^e} = \exp \left[ - (E_2 - E_1) / kT \right] \quad (1.07)$$

where  $N_1^e$  and  $N_2^e$  are the population densities at the thermal equilibrium,  $k$  is the Boltzmann constant and  $T$  is the absolute temperature of the medium. At thermal equilibrium ( $N_2 < N_1$ ), the medium acts as an absorber at frequency  $\nu = (E_2 - E_1)/h$ . But if a non-equilibrium

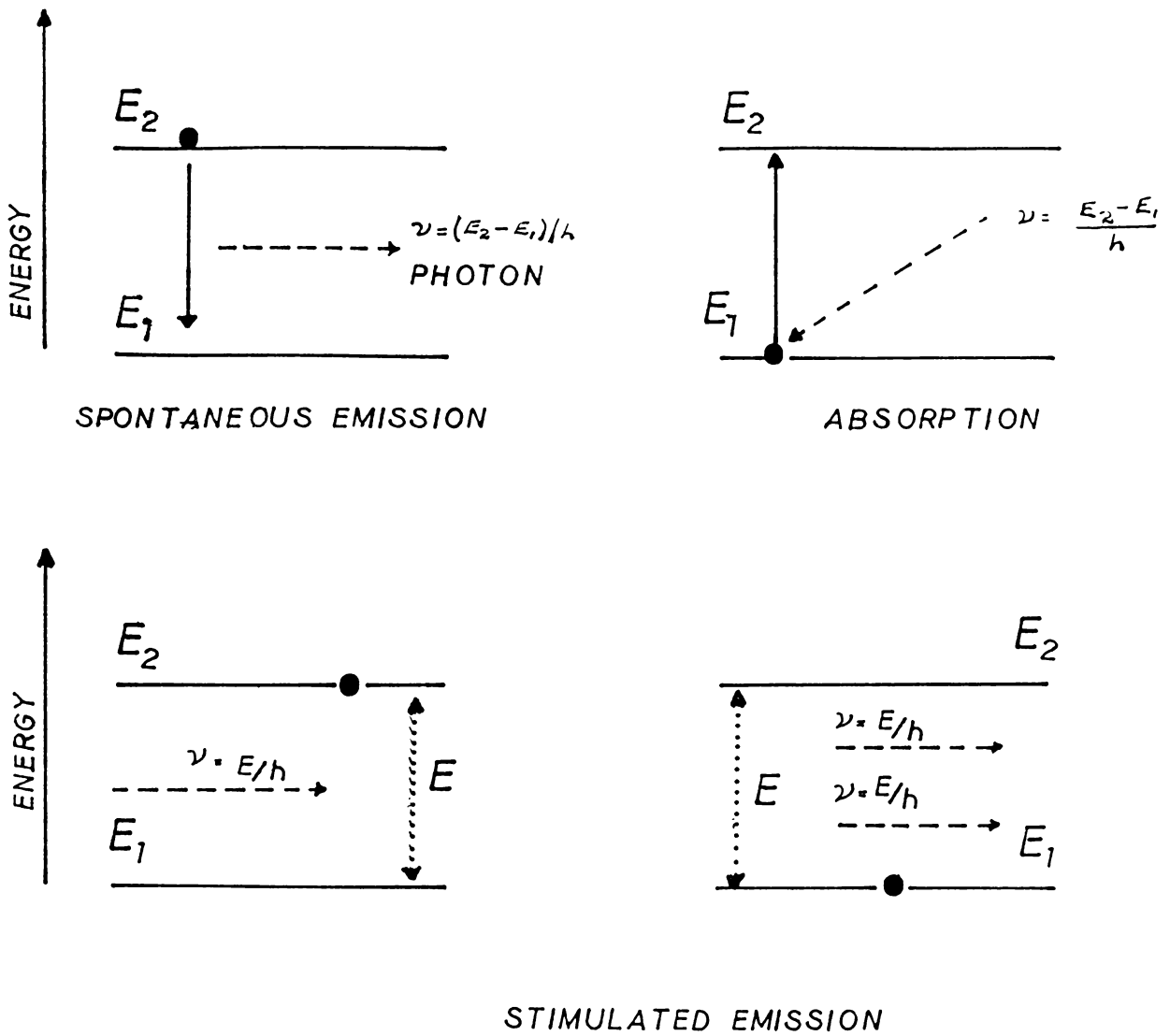


Fig. 1.1 Schematic representation of absorption, spontaneous emission and stimulated emission.

condition is reached for which  $N_2 > N_1$ , then the medium behaves as an amplifier. Therefore this condition in which  $N_2 > N_1$  is termed as population inversion and it is one of the necessary conditions for establishing laser action in the medium. To create a population inversion, the active medium of the laser is energised by means of electrical discharge, optical excitation with lamps or with other laser systems, collisional processes with excited molecules, exothermic chemical reactions and electron beam excitation. Once the deexcitation from the upper level begins, further radiative deexcitation can be stimulated by creating the proper feedback conditions. This is achieved by enclosing the active medium inside an optical resonator cavity. The details of an optical resonator cavity is briefly described in the following section.

### **1.3 Laser resonator :**

Once a laser medium is excited such that the population inversion condition is achieved, some kind of optical feedback is often necessary to establish a continuous stimulated emission [3]. This optical feedback is provided by placing the active medium between two highly reflecting mirrors. In this case a plane electromagnetic wave travelling in a direction orthogonal to the mirrors will bounce back and forth between the mirrors which in turn provides sufficient amplification of the wave on each passage through the medium. Therefore the oscillator cavity which forms an integral part of the laser system characterises the

laser beam. A schematic representation of a laser resonator cavity is shown in fig. 1.2. Here one of the mirrors is partially transmitting so as to couple the energy out of the resonator. Positive feedback, of course, does not occur until a threshold is reached, that is, until the optical gain exceeds the losses within the cavity. This is primarily because the oscillations in the cavity may be damped out due to the loss of energy and consequently, the energy of the wave does not reach at the threshold point. The basic loss mechanism in the resonator cavity are absorption and scattering processes by the components which form the resonator cavity and transmission losses through the output coupling mirror. The oscillations will be sustained when the gain for the beam compensates the losses in the cavity of the laser. The gain per pass in the active material is given by the exponential relation

$$\exp [\sigma (N_2 - N_1) l] \quad (1.08)$$

where  $\sigma$  is the absorption coefficient and  $l$  is the cavity length. If the only losses present in the cavity are those due to transmission, the condition for the threshold will be

$$R_1 R_2 \exp [2\sigma (N_2 - N_1) l] = 1 \quad (1.09)$$

where  $R_1$  and  $R_2$  are the reflectivities of the end mirrors of the cavity. From the above relation it is evident that the threshold is reached when the population difference  $(N_2 - N_1)$  reaches a critical value known as critical inversion. Once the critical inversion is reached, oscillations will build up in the cavity initiated by a spontaneously emitted photon.

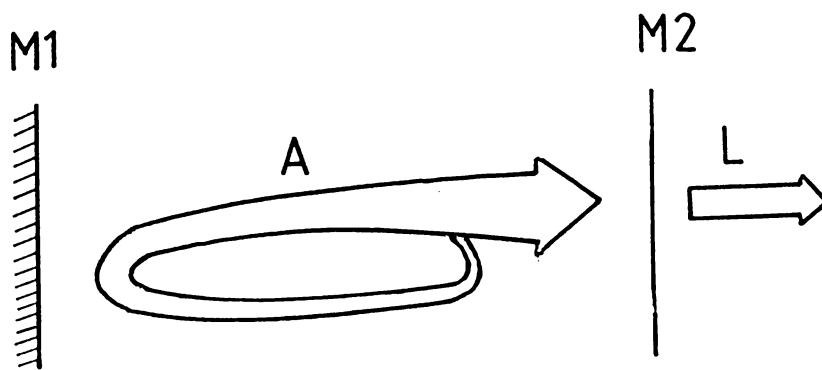


**Fig. 1.2** Schematic representation of oscillations in a laser resonator. (M1 - 100% reflecting mirror; M2 - output coupling mirror, A - Active medium and L - laser beam).



This photon is subsequently amplified when it traverses back and forth between the mirrors and part of the energy of the oscillation is emitted from the output mirror. Consequently, the laser resonator plays an important role on the total efficiency of the laser system.

Since the active medium is always confined in a cavity consisting of two mirrors, the medium experiences gain over only a small spectral range, usually determined by the width of the absorption line. Within this spectral range there may be several narrower laser oscillations. These oscillations have high gain since they undergo constructive interference within the laser cavity. They satisfy the relationship

$$l = \frac{1}{2} m \lambda \quad (1.10)$$

where  $l$  is the cavity length,  $\lambda$  is the laser wavelength and  $m$  is an integer. The corresponding resonant frequencies are given by

$$\nu = \frac{m c}{2 l} \quad (1.11)$$

where  $c$  is the velocity of light. Depending on various  $m$  values different frequencies tend to oscillate within the gain profile of the medium. These discrete frequencies designed by different  $m$  values are known as modes of oscillations. In low pressure gases and vapours which have narrow natural absorption line widths, only few cavity mode exists with sufficient gain to reach the threshold condition. Other materials such as dyes and solids can support a large number of cavity modes because of their relatively broad natural line width. The gain of

a particular mode often depends on the quality factor of the cavity which is defined as

$$Q = \frac{\omega_0 \times \text{energy stored in the mode}}{\text{energy dissipated per second from the mode}} \quad (1.12)$$

where  $\omega_0 = 2\pi\nu_0$ ,  $\nu_0$  being the central frequency of the gain profile.

Quality factor of the cavity can be theoretically expressed as

$$Q = \omega_0 t_c \quad (1.13)$$

where  $t_c$  is the cavity decay time.

The most widely used laser resonators have either plane or spherical mirrors separated by the total cavity length  $l$ . There are various cavity configurations which determine the oscillation strength and stability of different modes oscillating in the cavity. The following are the stable configuration wherein the beam is usually trapped inside and losses are only due to diffraction.

1. Large radii mirror configuration
2. Confocal configuration
3. Plane parallel (Fabry-Parot) configuration.
4. Concentric mirror configuration
5. Hemispherical configuration.

The above mentioned configurations are schematically shown in the fig. 1.3.

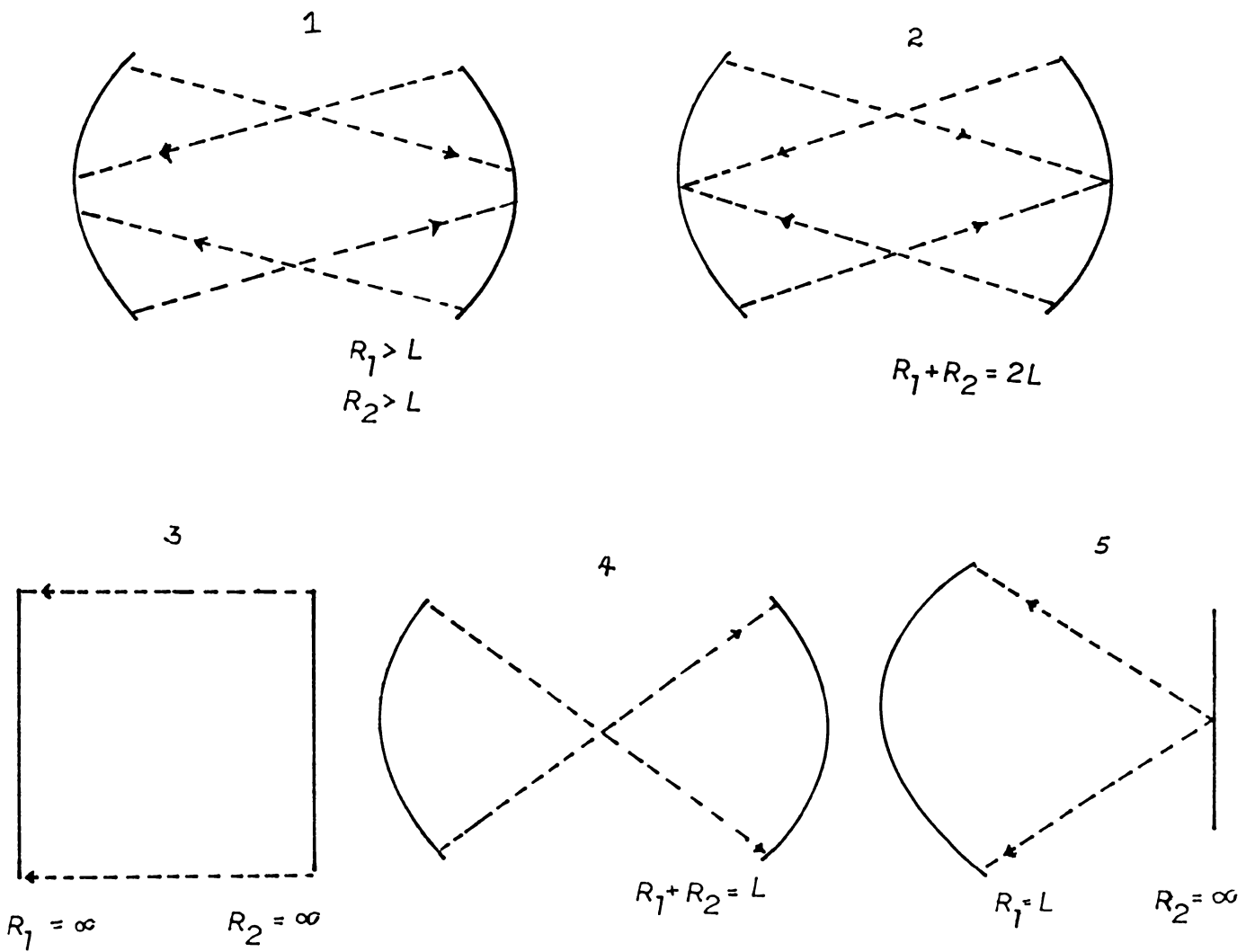


**Fig. 1.3** Various optical resonator configurations (1. Large radii mirror configuration; 2. Confocal configuration; 3. Plane parallel (Fabry-Perot) configuration; 4. Concentric mirror configuration; 5. Hemispherical configuration).

In a similar manner transverse modes are also existing in the laser cavity because of the various distributions of the electromagnetic field associated with the photons in the cavity. These field distribution determine the intensity profile of the beam which oscillates in the laser cavity. The different modes are designated by the notiations  $TEM_{mnq}$  where TEM denotes Transverse Electromagnetic owing to the transverse electromagnetic field distribution associated with the photons oscillating in the cavity.  $m$  and  $n$  are the transverse indices and  $q$  is the longitudinal index of the mode. A mode has a characteristic spatial structure of the electromagnetic field, that is, a certain distribution of the field amplitude and phase. In the plane perpendicular to the resonator axis, specifically on the mirror surface, this distribution is described by transverse indices  $m$  and  $n$ . To each combination of  $m$  and  $n$  there correspond a number of modes having various  $q$  values. But in the case of transverse modes only  $m$  and  $n$  in the indices are considered to get the field distribution. Since transverse indices  $m$  and  $n$  specify the electromagnetic field variation in the transverse direction, each type of mode has a characteristic light pattern observed on the resonator mirror. It is seen that the lower the values of the transverse indices, the denser the light field of the mode concentrates at the mirror's centre. The transverse mode  $TEM_{00}$  is the lowest order symmetric mode, termed as the fundamental mode and it presents the simplest structure of the light spot. Light spots observed in actual conditions often result from the superposition of

a few transverse modes which evidently shows that the laser normally contains a few closely spaced spectral lines.

#### 1.4 Properties of laser beam :

The outstanding properties of a laser beam are its high degree of monochromaticity, coherence, directionality and brightness. Laser beam possesses both temporal and spatial coherence. Temporal coherence can be thought of as the correlation between the values of the radiation field at the same point in space at two different times and spatial coherence is measured by the correlation between the values of radiation field at two different points in space at the same time interval. The directionality of the laser beam is due to its high degree of spatial coherence so that the laser beam propagates in the form of an almost plane wave whose divergence does not exceed greatly the minimum divergence due to the diffraction of light wave represented by,

$$\theta_{diff} \approx \frac{\lambda}{a} \quad (1.14)$$

where  $a$  is the laser beam diameter and  $\lambda$  is the wavelength. Such spatially coherent wave can be focussed by an optical system of lenses or mirrors of an area of size approximately equal to one wavelength and this makes the laser a very precise light source. Similarly monochromaticity of laser beam results from the high degree of temporal coherence of the beam.

Brightness of a given source of electromagnetic radiation is defined as the power emitted per unit area per unit solid angle and since the laser power density is enormously large, it possesses a very large value of brightness.

It is well known that the quality factor of the resonant cavity  $Q$  shows the capacity to store the energy in the cavity [4]. A high  $Q$  factor implies that the cavity will rapidly dissipate its energy. In most of the applications the temporal behaviour of laser power is of greater importance than its frequency characteristics. Therefore in order to obtain high powered laser pulses a technique is often adopted and this is known as Q-switching by which power stored in the cavity is suddenly released in the form of a giant pulse. Various techniques have been developed for a Q-switching of lasers. One method consists in a mechanical rotation of one of the laser mirrors about an axis normal to the resonator axis. In this case when the mirrors are not parallel the losses in the resonator are large and thus the pump increases the inversion beyond the threshold corresponding to the case when the mirrors are parallel. If the timing of the pump pulse is such that it reaches a maximum as the two mirrors are getting parallel a giant pulse would appear at the output. Similarly electro-optical shutters which employ Kerr and Pockels effects are widely being used for Q-switching. Saturable dye absorbers when placed in the optical cavity provide an efficient way of Q-switching. These methods make it possible the generation of peak laser powers of several gigawatts.

Q-switching in fact provides high peak power from the laser from the laser system while the technique termed as mode locking results the generation of ultra short pulses of time duration  $\approx 10^{-15}$  sec. As already mentioned that laser radiation contains various longitudinal

It is well known that the quality factor of the resonant cavity  $Q$  shows the capacity to store the energy in the cavity [4]. A high  $Q$  factor implies that the cavity will rapidly dissipate its energy. In most of the applications the temporal behaviour of laser power is of greater importance than its frequency characteristics. Therefore in order to obtain high powered laser pulses a technique is often adopted and this is known as  $Q$ -switching by which power stored in the cavity is suddenly released in the form of a giant pulse. Various techniques have been developed for a  $Q$ -switching of lasers. One method consists in a mechanical rotation of one of the laser mirrors about an axis normal to the resonator axis. In this case when the mirrors are not parallel the losses in the resonator are large and thus the pump increases the inversion beyond the threshold corresponding to the case when the mirrors are parallel. If the timing of the pump pulse is such that it reaches a maximum as the two mirrors are getting parallel a giant pulse would appear at the output. Similarly electro-optical shutters which employ Kerr and Pockels effects are widely being used for  $Q$ -switching. Saturable dye absorbers when placed in the optical cavity provide an efficient way of  $Q$ -switching. These methods make it possible the generation of peak laser powers of several gigawatts.

$Q$ -switching in fact provides high peak power from the laser from the laser system while the technique termed as mode locking results the generation of ultra short pulses of time duration  $\approx 10^{-15}$  sec. As already mentioned that laser radiation contains various longitudinal

modes whose frequencies are equidistant and separated by a frequency interval of  $\frac{2\pi}{c}$ . If the phase difference between any two adjacent modes has a definite fixed value, there exists a mutual interference of longitudinal modes giving rise to a train of ultra short light pulses. Therefore longitudinal mode locking provides a train of ultra short laser pulses. In order to obtain such pulses two conditions are to be satisfied. First, a laser must generate a fairly large number of longitudinal modes. Secondly, these modes must be equidistant in frequency and synchronised in phase. These ultra short pulses can generate high peak powers of the order of  $10^{12}$ W.

Thus in general laser offers a unique and intense source of radiation which finds its application in various branches of science and technology. Based on different active media, variety of lasers with different wavelength have been developed so far. They are solid state lasers, atomic and ion lasers, gas lasers, chemical lasers and semiconductor lasers. A brief account of various laser systems and their important applications are presented in the following sections.

### **1.5 Various types of lasers and its applications :**

Since the first demonstration of laser action in Ruby by Maiman in 1960 [5] the world has witnessed a phenomenal growth of activity in laser area both in its fundamental and applied aspects. Another area showing a similar growth in this category has been semiconductor technology, culminating in the development of microprocessors and fast computers. The impressive progress in both these areas has, in fact,



been possible due to the timely availability of appropriate scientific technique together with right technological processes. With the advent of lasers new areas of research have emerged both in fundamental and applied sciences. High resolution spectroscopy, non-linear spectroscopy, time and frequency domain spectroscopy of atoms and molecules material processing, light wave communication in space, under water and through optical fibres, holography, information processing and optical computing, chemical kinetics, isotope separation, micro and macro surgery and laser fusion are a few prominent applications so far conceived, planned and achieved. It is neither possible nor within the scope of the present thesis to describe all the lasers and its applications in detail. However, a brief of the prominent laser systems and their applications is presented in this section.

#### 1.5.1 Gas lasers :

One of the most important lasers in this category is the Helium-Neon laser. It was discovered by Ali Javan in 1961 [6]. Since it is comparatively cheap, compact and reliable, this laser finds its application in almost every branch of physics. It lases on the transitions of neutral Ne atom and He assists in pumping the upper state of Ne by collisionally transferring of its excited metastable state (3s) energy. CW power in excess of 100 mW has been obtained from this laser. It operates in the wavelength 632.8 nm, 1.15  $\mu\text{m}$  and 3.39  $\mu\text{m}$ . Recently green wavelength ( $\lambda = 543.5$  nm) emission from this laser has been reported [7]. This laser is often being used in optical aligning

processes, absorption studies of methane gas at  $3.39 \mu\text{m}$ , short distance communication, optical radar, etc. Today He-Ne lasers with life-times in the range of 20,000 hours are commercially available.

#### 1.5.2 Noble gas ion lasers :

Laser based on noble gas discharges and involving levels of ions like  $\text{Ar}^+$ ,  $\text{Kr}^+$ ,  $\text{Xe}^+$ , etc, have been successfully developed since 1974. Both CW and pulsed laser operations have been achieved on a number of visible and ultraviolet lines. Lasers with both RF and De-excitation are available with life time of a few thousand hours.  $\text{Ar}^+$  and  $\text{Kr}^+$  lasers are commercially available with multiline power levels ranging from 5 mW to 20 Watts, distributed over a few discrete lines. The prominent transitions are 351 nm, 488 nm and 514.5 nm in  $\text{Ar}^+$  and 530.9 nm and 647.1 nm in  $\text{Kr}^+$ .  $\text{Xe}^+$  lasers are not yet popularised due to inherent technological problems in the development. A major application of these lasers is in CW dye laser pumping for producing a continuously tunable output. The other applications in medicine include photocoagulation in ophthalmology to destroy cataractous layers on the eyelens. These lasers are widely being used as the light source for carrying out Raman Spectroscopy, non-linear spectroscopy, phase conjugation and optical bistability.

#### 1.5.3 Metal ion vapour lasers :

Copper vapour laser is found to be one of the most prominent laser in this category because it operates in the 510.6 nm and 578.2 nm

with maximum power. Presently, this laser is operated at a very high repetition rate upto 50 KHz., delivering an average power output of about 100 Watts. With furnace heating of copper changed to heating by excess discharge energy, efficiencies upto 1% have been achieved. Therefore its higher efficiency provides its application in isotope separation by selective excitation process. With similar technology, gold vapour lasers are developed, which emit at 628 nm a key wavelength for photoradiation therapy of tumours, cancerous tissues, etc. Another type is the He-Cd laser which produces a CW output distributed primarily at 327.5 nm and 441.6 nm. This is considered as an ideal tool in blood analyses, electronic printers, etc. Since 441.6 nm emission suffers less attenuation when it traverses through water medium, this wavelength is widely being used as a source in under water communication.

#### 1.5.4 Molecular lasers :

C. K. N. Patel in 1964 [8] reported the discovery of laser action in a molecular system, viz.,  $\text{CO}_2$ . At present, all  $\text{CO}_2$  lasers use a mixture of  $\text{CO}_2$ ,  $\text{N}_2$  and He in the appropriate proportion which varies with the geometry of the laser system. In this laser,  $\text{N}_2$  helps in the inversion mechanism through vibrational energy transfer and He de-populates the lower level of  $\text{CO}_2$  molecule.  $\text{CO}_2$  lasers operate both CW and pulsed, span the low to very large power range, and operate at several rotational lines centered around 9.6  $\mu\text{m}$  and 10.6  $\mu\text{m}$ . Therefore appropriate tuning of  $\text{CO}_2$  provides about 100 rotational lines over 8-11  $\mu\text{m}$  range. This makes them an important tool in spectroscopic applications in high resolution spectroscopy and as high power pump

sources in Spin Flip Raman Laser (SFRL) which provides the emission in far infrared region (9 - 14  $\mu\text{m}$ ). Since this laser is highly efficient among all varieties of lasers, because of the rotational-vibrational transitions, high powers of the order of tens of kilowatts has been achieved. Therefore this laser is widely being used in industrial applications, laser fusion, laser surgery, material processing in semiconductor technology, etc [9]. The details of the design and fabrication of a CW  $\text{CO}_2$  laser and its application in material processing are described in chapter V and VII respectively. Various geometries have been adopted to increase the efficiency of this laser. Some of them are Transverse Electric Atmospheric (TEA) laser in which the electric field for exciting the molecules is applied perpendicular to the gas flow which is usually at atmospheric pressure, and the gas dynamic laser in which the proper mixture of  $\text{CO}_2$ ,  $\text{N}_2$  and He gases at higher pressure is allowed to flow through a region where low pressure and large volume are maintained. Thus the abrupt expansion provides cooling of the mixture which produces population inversion by quenching process. Consequently this system produces a high peak power of 20 KW and ensures a better efficiency. Similarly  $\text{CO}_2$  wave guide lasers have received considerable attention in recent years. In these lasers the optical beam is constrained in a small ceramic capillary of 1-2 mm diameter, which results in increased cooling by the walls of the discharge tube. This, can make high pressure operation of such lasers feasible.

A related type of molecular laser is the CO laser, which operates on 5  $\mu\text{m}$  band. The cooling requirements for this laser are far more stringent than those of  $\text{CO}_2$  laser and the CO gas handling problems have adversely affected its developments and applications [10].

Nitrogen laser is the another one which utilises the electronic transitions in  $N_2$  molecules [11]. It operates in the ultraviolet region in a single line of 331.7 nm. In these electronic transitions the lower laser level possesses large lifetime, thereby making them self terminating. In view of this, only very high speed electronic discharges can pump these lasers for creating inversion. Due to low cost and reliability,  $N_2$  lasers have become very prominent pump lasers for the tunable pulsed dye lasers.

#### 1.5.5 Chemical lasers :

In chemical lasers, often the active medium is formed by a chemical reaction from its constituents, initiated by an electric discharge. Lasers with HF and DF as the active medium have been developed which emits output at 2.6  $\mu\text{m}$  and 4.0  $\mu\text{m}$  bands. CW output power in the range of a few watts are obtained from these lasers and they are widely being used in defence applications.

#### 1.5.6 Excimer lasers :

Excimer laser works on the principle that for some pairs of the atoms the ground states are usually repulsive, but a combination of a ground state and an excited state often forms chemical binding resulting in a molecule usually referred as excimer (excited dimer). This excimer relaxes radiatively to the repulsive (dissociative) ground state and subsequently emit UV radiation around 193 nm for ArF. Because of the short life-time, these lasers have a self scavenging feature, which is highly essential for high efficiency laser. Since the upper level has a short lifetime, excimer lasers cannot be operated in CW

fashion. Application of these lasers are mainly in scientific research like photochemistry and in electronic industry, particularly in photolithography in making ICs, etc., and in weapon development [12]. However, only a very small part of their promising features have been tapped so far and many more will be appreciated as the technology advances.

#### 1.5.7 Solid state lasers :

Most of the solid state lasers involve a host material, incorporating the active atoms at very low concentrations and the host material is usually in the crystalline form. Typical examples of active and host materials are chromium in sapphire lattice (Ruby), neodymium in yttrium-aluminium garnet (YAG) and neodymium in silicate, phosphate glasses. In all cases the purity of the host material and the quality of the grown crystals are highly demanding for an efficient performance of the laser. All solid state lasers show the following common features:

1. They are optically pumped, the only exceptions being the semiconductor lasers.
2. During the excitation process, quite a lot of energy is absorbed by the host, which goes as lattice heat. Therefore the resulting change in temperature and refractive index of the crystal is to be taken into account in the laser design.
3. All solid state lasers deliver higher power density relative to their size and in majority of the cases they exhibit multiple pulsing known as spiking.

- Both CW and pulsed operations are possible with these lasers. The pulsed operation includes Q-switching, mode-locking and cavity damping. Consequently intense and very high peak power outputs can be generated.

The Ruby laser, the first laser invented, emits at 694.3 nm. It can generate approximately 200 J of output in the long-pulsed mode (300 - 3000  $\mu$ sec) and 15 J in the short-pulsed (15-20 nsec) in the Q-switched mode. Applications of this laser include holography, non-destructive material testing, atmospheric sciences, plasma diagnostics, ophthalmic surgery, etc.

Nd:YAG and Nd:Glass lasers operate at 1.06  $\mu$ m band and are 4 level lasers with inherently operating thresholds. These lasers differ in the host material and in the case of Nd:Glass lasers the host material is amorphous and the relevant transitions are broadened by two orders of magnitudes, thereby increasing the pumping threshold. The optical pump bands of these lasers are in the red region and therefore, krypton-arc lamps are mostly used for pumping. The 2nd, 3rd and 4th harmonics at 532 nm, 355 nm and 268 nm are also generated from this laser using appropriate non-linear medium for harmonic generation. Q-switching provides high energy output and subsequently these lasers are often used as a source in material processing, plasma studies and damage studies [13].

#### 1.5.8 Semiconductor lasers :

The most promising new development in coherent infrared sources is the advent of semiconductor lasers [14, 15]. These lasers operate

by the stimulated emission occurring across the gap between the conduction and valence bands of a semiconductor. Population inversion is achieved by electron injection across the band gap either by use of an electrical current or by optical pumping or electron beam excitation. Infrared semiconductor laser materials in the 1-30  $\mu\text{m}$  range include such binary compounds as InAs, InSb, GaSb, PbSe, PbS and PbTe and such pseudobinary alloys as  $\text{Pb}_{1-x}\text{Sn}_x\text{Te}$ ,  $\text{PbS}_{1-x}\text{Se}_x$ ,  $\text{Hg}_{1-x}\text{Cd}_x\text{Te}$ ,  $\text{InGa}_{1-x}\text{As}_x$  and  $\text{GaAs}_x\text{Sb}_{1-x}$ . The coarse tuning of the infrared wavelength emitted by the lead salt diode lasers can be achieved by adjusting the chemical composition which essentially determines the band gap energy in a semiconductor. At present these semiconductor lasers can be continuously tuned over only  $0.1 - 1 \text{ cm}^{-1}$  by varying the operating temperature or drive current [16] or alternately by varying an externally applied magnetic field. With the broadband wavelength coverage available using hydrostatic pressure tuning, only the binary semiconductor compounds and one or two alloy semiconductor is necessary to cover the entire wavelength range from 2-35  $\mu\text{m}$ . Semiconductor laser has relatively low output power, providing only 1-20 mW CW power in single mode operation. Very often semiconductor lasers operate at low temperature because at relatively higher temperatures a fairly large threshold current is necessary to sustain lasing action. Recently laser diodes operating at room temperature are available commercially at a reasonable cost. Diode lasers are used in air pollution measurements, optical communication, information processing and video-audio discs. At present active research is being carried out to develop efficient diode lasers for optical communication.,



### 1.5.9 Dye lasers :

Dye lasers occupy a very prominent position in the family of lasers as such, and also in their applications. This is because they are the ideal tunable laser available in the range of wavelengths from near IR to near UV. With the use of selective dyes, this laser can be continuously tuned with a spectral width of less than 1 nm. Dyes are often used in the liquid form by dissolving them in suitable solvents and they are optically pumped by using discrete line lasers which coincide with the absorption band of the dye. Subsequent luminescent emission from the dye is effectively amplified in a cavity and selectively tuned using dispersion elements like gratings, prisms and etalons. In CW dye laser, the dye is often made to flow at a reasonably high speed and further to improve the optical quality of laser, open dye jets at Brewster angle are employed for pumping by using high power lasers. While in pulsed dye laser the dye is always kept in a cuvette on which the pump beam is irradiated [17]. Usually the pump lasers used are  $N_2$  laser,  $Ar^+$  laser,  $Kr^+$  laser and excimer laser which have their wavelength near the UV region. CW dye lasers are mode locked and cavity dumped to obtain picosecond and femtosecond pulses by pumping them synchronously with a mode-locked ion laser. Applications of these tunable lasers are numerous in spectroscopy, non-linear optics, photochemistry, colour illumination and in optical displays [18].

### 1.5.10 Free electron lasers :

All charged particles emit electromagnetic radiation when accelerated or decelerated. However, by mounting undulators (devices which

spatially modulate the magnetic field periodically along the length) on a linear accelerator can produce much brighter spontaneous visible to x-ray radiations. These undulators can also be used to produce coherent and tunable radiation over a large spectral range and it has resulted the development of free electron laser in 1976 [19]. Therefore by incorporating tuning elements in the laser cavity, highly precise tuning could be achieved. Recently, this technique has been extended into the visible region with an optical klystron consisting of two undulators separated by a dispersive element. Free electron laser phenomenon has real potentialities as a wide range tunable source from IR to x-rays. However, the requirements of high currents of relativistic monoenergetic electrons are formidable and such laser sources may, costwise, compare with nuclear accelerators.

### 1.6 Conclusion :

Thus the area to which lasers make a significant contribution are growing in parallel with the progress in the domain of laser technology. In some fields lasers already have established a high standing, in other areas only first application have appeared, while in still other ones the possibility of their applications are only at the infant stage. Consequently, serious attempts are in progress to develop lasers having higher power and ultrashort pulse width which can be utilised to initiate various techniques to explore the frontier areas in science and technology. With the rapid growth in lasers, the traditional electronics is now re-

placed by **optoelectronics** in which the combination of electronic and optical methods are used for data processing in high speed computers. Hence the use of lasers can create several more miracles in the field of science and technology in the days to come.

## PART B

### Photoacoustic effect and its spectroscopic applications :

#### 1.7 Introduction :

Spectroscopy has been a scientific tool for well over a century, and it has proven to be a remarkable method to analyse the physical properties of solids, liquids and gaseous phases of matter. It in fact, is the science devoted to the study of the interaction of radiation with matter. As such, it is a science encompassing many techniques and practiced by a large number of scientists of various disciplines. Because of its versatility, range and non-destructive nature, optical spectroscopy remains a widely used and most important tool for investigating and characterising the properties of matter. There are, however, several instances where conventional optical spectroscopic methods are quite inadequate for the complete analysis of the interaction of optical radiation with matter. These include the situations like the study of weak absorption which involves the measurement of very small change in the intensity of the transmitted beam through the material and of weak intensity which arises due to the reflection and scattering from the opaque surfaces. Consequently, several techniques have been developed to permit optical investigations of highly light scattering and opaque materials. The most common among them are diffuse reflectance spectroscopy [20], attenuated total reflection method [21], internal reflection method [22] and Raman scattering [23]. All these techniques

have proven to be very useful, yet each suffers from serious limitations. In particular, each method is found to utilise only for a relatively small wavelength range and very often the data obtained are difficult to interpret. Thus, a method which yields sufficient information regarding the interacting photons rather than non-interacting photons has successfully been developed in recent times based on photoacoustic (PA) effect. This technique thus provides enormous potential to study those materials that are unsuitable for the conventional transmission or reflection methodologies [24] and is termed as Photoacoustic Spectroscopy (PAS).

PAS is a method recently being used as a potential tool which finds its application in almost all disciplines in science. It is based on the photoacoustic effect discovered in the last century. PA effect is essentially the generation of acoustic waves or other thermoelastic effects by any type of modulated electromagnetic radiation ranging from radio frequency to x-rays. Thus, when a sample is irradiated by a modulated electromagnetic wave, absorption of photons causes an excited internal energy levels in the sample. Upon subsequent de-excitation of these energy levels, all or part of the absorbed photon energy is then transformed into heat energy through non-radiative relaxation process in the sample. In a gas this heat energy appears as kinetic energy of the gas molecules, while in a solid or liquid, it appears as vibrational energy of ions or atoms. Since the incident radiation onto the sample is intensity modulated, the internal heating of the sample is also modulated at the same frequency. The sample to be

studied is often enclosed in a PA cell. For the case of gases and liquids the sample generally fills the entire chamber whereas in the case of solids, the sample fills only a portion of the chamber, and the rest of the chamber is filled with a non-absorbing gas such as air. In addition, the cell also contains a sensitive microphone which acts as a transducer. Thus the periodic heating of the sample due to the absorption of modulated electromagnetic radiation results in a periodic heat flow from the sample to the gas, which itself does not absorb the radiation. This periodic heat flow in turn produces pressure variation in the gas medium at the same frequency at which the incident beam is modulated. These pressure variations are directly monitored by a sensitive microphone placed in the PA cell and converted into electrical signal. In the case of samples in the form of thin films, bulk solid samples and liquids, it is possible to measure heat production through subsequent pressure or stress variation in the sample itself by means of a piezoelectric transducer which is in intimate contact with the sample. Thus the output signal amplitude directly gives the absorption of incident beam of radiation. This output is often processed by a phase sensitive detection system.

Since PA technique measures the internal heating of the sample, it clearly is a form of calorimetry, as well as a form of optical spectroscopy. This technique therefore offers the detection of pressure variation corresponding to  $10^{-6}$ °C rise of temperature at the sample - gas interface. There are several advantages to PA effect as a form of spectro-

scopy, that is, when it is used to perform PA spectroscopy. Since absorption of electromagnetic radiation is required before a PA signal can be generated, light that is transmitted or elastically scattered by the sample is not detected and hence does not interfere with the inherently absorptive PA measurements. This is of crucial importance when one is working with essentially transparent media, such as pollutant-containing gases, which have few absorbing centres. This insensitivity to scattered radiation also permits one to obtain optical absorption data on highly light scattering materials, such as powders, gels, amorphous solids and colloids. Another advantage is the capability of obtaining optical absorption spectra on materials that are completely opaque to transmitted light since this technique does not depend on the detection of photons. Coupled with this unique capability, non-destructive depth profiling studies in opaque materials can be performed with extreme sensitivity. This study, in fact, reveals the absorption property of the material at each layer below the sample surface. Furthermore, since the sample itself constitutes the electromagnetic radiation detector no photoelectric or photoconductive device is necessary, and thus studies over a wide range of optical and electromagnetic wavelengths are possible without the need to change the detector system. This provides the experimental procedure becomes<sup>4</sup> more simple and straightforward. The limitations in this regard are that the source be sufficiently energetic and that whatever windows are used in the system be reasonably transparent to the radiation. These limitations can however be eliminated by using laser as the optical radiation source and the absorption can be

minimised by using dielectric coated windows to provide maximum transmission at the wavelength of interest. Finally, PA effect results from a radiationless energy conversion process and is therefore complementary to radiative and photochemical processes. Thus PAS itself may be used as a sensitive, though indirect, method for studying the phenomena of fluorescence and photosensitivity in materials using PA effect.

Since the PA technique involves the processes as optical absorption, non-radiative relaxation and thermal diffusion in a material, this method can be effectively used to study the optical absorption coefficient, quantum yield, lifetime and thermal diffusivity of the material with high precision [25]. Thus it reveals the enormous capability of this method to analyse the various physical properties of the sample simultaneously. Furthermore, the study of optical absorption and the thermal diffusion at various layers of the sample has opened up a new branch of science namely **Photoacoustic Microscopy (PAM)**. This new and promising technique provides the identification of flaws and defects in a material from the detailed analysis of heat flow through the material [26]. In particular, PAM appears to hold considerable promise both as a general analytical tool and as a dedicated process-control instrument for the semiconductor industry [27]. PA microscopes can be employed in semiconductor fabrication line to monitor the presence of electrical shorts or leaks in integrated circuits at a very early stage of the device fabrication. They are often used on-line to visualise and inspect patterns



and structures that are below the surface and to perform localised thin film thickness measurements [28]. With these various capabilities, PA microscopes may well be able to effect a considerable cost savings in the manufacture of large scale integrated circuits and other electronic devices.

With its various spectroscopic and non-spectroscopic attributes, PA techniques have already found many important applications in the research and characterisation of materials.

A brief summary of the applications of PAS which are directly related to the technological importance are presented in the following section.

### **1.8 PAS of solids :**

In recent years substantial progress has been made in the fabrication of low loss optical materials for use in the visible and infrared spectral regions. This work has made necessary developments of new techniques for measuring bulk and surface absorption at low levels. The absorption studies carried out in the infrared transmitting materials like ZnSe and uncoated Sapphire could reveal the absorption coefficients at  $10.6 \mu\text{m}$  and the influence of thicknesses  $\text{ThF}_4$  layer which acts as an anti-reflection coating on the surface of these materials at this wavelength region [29]. This in turn brings out the development of precision optics which can improve the  $\text{CO}_2$  laser efficiency. Similarly, the methods

for the accurate determination of photoluminescence quantum efficiencies and relaxation processes are of considerable importance. Such photophysical parameters have proved difficult to measure accurately using conventional photometric methods and calorimetric techniques. The quantum efficiency measurement of <sup>Al</sup> ruby crystal shows its utility as a material for laser active medium [30]. The visible region PA spectra of silicon samples under open circuit and loaded conditions provide the detailed information regarding the wavelength dependence of solar cell performance [31]. Recently PAS method has been effectively utilised to measure optical absorption of  $10^{-6} \text{ cm}^{-1}$  with a cell volume of  $3 \text{ cm}^3$  and with a pulsed laser of 1 mJ energy and 1  $\mu\text{sec}$  duration for excitation [32].

### 1.9 Weak absorption in gases :

One of the most significant applications of PA effect is the sensitive detection of pollutant gas species present in the atmosphere. These studies could attain a sensitivity limit of few parts per billion which is considered to be a remarkable achievement of the PA spectroscopic technology [32]. Another important aspect of this technology is the in-situ measurement of absorption in optical fibres [33] which is highly useful for the development of low loss optical fibres needed for optical communications. Similarly absorption in transparent solids [34] and liquids [35] provide the development of various optics to be used in laser technology. The overtone absorption measurements [36] provide the basic understandings of the molecular structures and its photokinetics. Further-

more, this novel technique might allow the study of the details of absorption spectra of rare earth oxides such as holmium, erbium, neodymium, samarium, dysprosium, gadolinium and terbium. From these measurements it is found that the non-fluorescent levels of the rapidly ionised rare earth atoms are easily detected by this novel technique. [37].

#### 1.10 Thin films :

The use of PA technique for measuring absorption due to thin films, monolayers or even submonolayers have been reported recently [38]. For thin films of powders or liquids the pulsed PA technique provides measurement of an absorption coefficient as low as  $10^{-3} \text{ cm}^{-1}$  for a thickness of  $10^{-8} \text{ cm}$  [31]. Recently PA method has been successfully employed to measure the enthalpy of absorbed materials like pyridine on evaporated polycrystalline nickel films [39] and this provides the absolute rate of deposition of a single monolayer of surface adsorbate very precisely. Therefore this technique, is a non-destructive method for analysing the properties of thin films such as its optical absorption coefficient at various monolayers and the rate of deposition of layers on the substrate [40]. Consequently, this technique finds its application in the field of semiconductor industry in which the detailed analysis of the changes in physical properties at each monolayer is often necessary to develop highly efficient semiconductor devices.

Since the PA signal is a function of the thermal propagation within the sample, it is possible to determine the thermal properties like thermal diffusivity and thermal conductivity with great accuracy [41, 42]. There-

fore the study of thermal wave propagation through the various layers of the sample provides the thermal properties of the sample in a non-destructive fashion. Using PA technique, thermal diffusivities of glass, copper [43] and various polymer samples [44] have been determined precisely and these measurements provide the study of absolute value of thermal diffusivity of samples with temperature. Since the thermal parameters of a material generally vary when the material undergo a phase transition, monitoring the PA signal as a function of temperature should provide information on the occurrence of phase transitions. Thus first order phase transition measurements have been carried out in materials like  $K_2SnCl_6$  [45],  $NaNO_2$  [46], Indium and Gallium [47] and these studies reveal that the application of PA effect to phase transition studies should constitute a useful complementary technique to the conventional calorimetric methodology. Similarly, the depth profiling studies in solids can be effectively utilised to obtain the physical properties at various layers in the sample by controlling the thermal wave propagation through the layers with great precision [48]. These data often provide the information regarding the heat flow through various layers or even monolayers and any discontinuity in the thermal wave propagation can be easily monitored from the PA signal amplitude and phase. Thus, these investigations in the microscopical level could open up a new field termed as **Photoacoustic Microscopy (PAM)** and a brief discussion of the same is given in the following section.

### **1.11 Photoacoustic microscopy (PAM) :**

The generation and propagation of acoustic waves in a sample depend critically on the thermoeleastic and physical properties of the sample.

By monitoring the PA signal amplitude and phase, it is possible to probe or measure such properties, as acoustic velocities, elasticity, density, thickness, specific heat, material discontinuities, crystallinity, phase transition, etc. Therefore, this technique can provide information on the thickness of a surface layer, depth of a sublayer, thermal diffusivity of a coating material, thermal barriers, or other irregularities below the surface and depth dependent optical absorption features [49].

The basic principle involved in PAM is the thermal wave analysis at each layer of the sample using PA technique. If any irregularity or flaw is present in any of the layers of the sample, the thermal diffusion process through these layers may vary depending on the nature of the defect at the sample. Therefore by controlling the thermal diffusion through the sample very precisely, the nature and location of the defect can be easily identified using this method. Subsequently, the PA signal amplitude and phase will vary rapidly due to the discontinuity in the heat flow through the layer of the sample. Thus the PA signal amplitude and phase directly reveal the detailed information regarding the defect present in the material. In order to obtain the exact location of the irregularity, the laser beam is scanned across the sample surface and the variations in PA signal are recorded simultaneously. From the change in amplitude and phase, the location and its size can be precisely determined. This method, therefore, is a non-destructive tool for studying the defects or irregularities in a sample at the microscopic level.

Thus, PAM is an exciting field that is very quickly expanding and being actively investigated by many research groups because of its potential

applications in thin film technology, chemical engineering, biology, medical diagnostics, etc. It provides a unique method for obtaining subsurface imaging of irregularities, flaws, doping concentrations, etc, that cannot be obtained by other non-destructive methods. The first remarkable attempt made in this direction is the pulsed PA imaging to obtain the subsurface holes in an aluminium cylinder using a piezoelectric transducer [50]. The variations in PA signal could detect subsurface inhomogeneities not visible with an optical microscope [51]. Furthermore, the PA imaging studies in multilayer films on germanium substrate revealed the irregularities with a fairly high resolution and the samples with inhomogeneities located by PAM will usually be damaged by sufficiently intense radiation at the positions where it is located. Therefore, this method may actually be useful to predict the tendency towards the laser induced damages [52]. Similarly, PA imaging of compositional variation in  $\text{Hg}_{1-x}\text{Cd}_x\text{Te}$  semiconductors, which are useful for mid-ir-radiation detection [53]. This experiment shows the suitability of PAM for use in industrial quality control; the  $\text{Hg}_{1-x}\text{Cd}_x\text{Te}$  can be photoacoustically scanned for homogeneity before fabrication into infrared detector arrays, which require compositional uniformity to ensure uniform spectral response across the arrays. One of the most remarkable achievements in PAM technique is the demonstration of PA mapping of damages due to ion implantation and subsequent recrystallisation due to annealing in Si or GaAs using a CW Nd:YAG laser operating at  $1.06 \mu\text{m}$  for excitation [54]. The spurious PA signals from the substrate could be eliminated by suitable phase adjustments of the lock-in amplifier. This result shows that laser annealing can change the sample to single crystal structure or to a polycrystalline

structure. Recently, this method has been successfully used to detect the subsurface features of integrated circuits and this provided information on absolute spatial distribution of dopant concentration [55].

To summarise, PAM techniques have been used for non-destructive imaging of various subsurface features : holes in metals, flaws in ceramics, absorption sites in laser windows, water content in porous materials, inhomogenities in layered materials, foreign material inclusion in biological samples [56], defects in ICs and in substrates [57], compositional variations in alloys, ion implantation damage in semiconductors [58] etc. Excitation can be made by modulated CW lasers, pulsed lasers or other energetic beams, and detection is possible by sensitive microphone or piezoelectric transducers. PAM is considered as a promising non-destructive technique which has direct applications in the field of semiconductor industry which essentially controls the entire growth of technology.

#### **1.12 PAS in biology and medicine :**

PA methods of determining the absorption property of a material is widely being used in biological samples as well as in medicine. Many of the above mentioned samples occur naturally in insoluble states, many others are membrane bound or are part of bone or tissue structure. These materials are found to function biologically within a more or less solid matrix. PAS through its capability of providing optical data on intact biological matter, even with material which is optically opaque, holds great promise as both a research and diagnostic tool in biology and medicine.

This novel technique has been effectively utilised to study the optical absorption spectrum of the oxidised and reduced form of cytochrome C in various aqueous solutions and the detailed analysis shows its variation of its concentration during cellular respiration [59]. This microanalysis ensures a basic understanding of the fundamental process in the case of living organisms. The studies on an intact green leaf clearly shows the absorption characteristics of the chlorophyll tissues in leaves and its changes during photosynthesis [60]. In addition, the depth profiling studies in a biological specimen gives the different layers associated with the material and this provides a clear layout of chemical combinations in tissue structures [61]. Recently, PAS has been employed to study the photo-damage caused to thiamine derivatives and the analysis clearly shows the suitability of this method to monitor the time dependent behaviour of light absorption in some biological samples and packed formulation of pharmaceuticals [62].

Similarly one of the most exciting areas in PA studies lies in the field of medicine. Because PAS provides optical data on medical specimens that are not amenable to conventional methods since conventional spectroscopic techniques often suffer excessive light scattering from these types of samples. An example of the use of PAS in medical studies is the identification of bacterial states [63]. The absorption spectrum shows a strong band at 410 nm when the bacteria is in its spore state and it is absent when it is in the vegetative state. Therefore, these measurements can identify the living states of a biologically active material.



PA spectroscopic measurement on human eye lens reveals the formation of tryptophan and tyrosine residues which essentially causes cataract [64]. This method has the added advantage that the laser irradiation onto the eye lens destroys the cataractous layer by photocoagulation and the deformation of this layer is sensitively monitored by real time analysis. Similarly, PA studies in blood provide the absorption spectrum from which the concentration of haemoglobin, which is the basic constituent of the blood, could be precisely determined [65]. The investigations carried out in this direction make it possible to monitor the spectral properties of abnormal or cancerous tissues and their molecular structure which helps the early detection of such growths in the human body [66]. These results in turn reveal the utility of this method in the field of medicine which is a direct application of PA effect in the day to day life.

While extensive applications of PA generation and detection has been developed as described earlier, there are two other related effects that are less well known. The first is the effect of sonoluminescence [67] which is the reverse PA effect, viz., the generation of optical radiation by acoustic waves. One mechanism for sonoluminescence is acoustic cavitations followed by bubble collapse, which drives the interior gases to high temperature, resulting in production of free radicals and subsequent radiative recombinations. The second effect is the inverse PA effect [68, 69], which is reported very recently and the details of which are yet to be classified.

### 1.13 Conclusion :

In conclusion, PA technique is a valuable tool, particularly, for the probing of physical properties of matter and it is being utilised in every branch of science and technology. Though the PA effect was originally discovered in 1880, it has been effectively utilised since 1973 after the advent of tunable lasers, sensitive microphones and sophisticated signal processing techniques. During the past 14 years it showed a rapid growth in all respects. The literature survey shows that a great deal of work has been carried out and this has resulted in the publication of a large number of research papers and several review articles [31, 49, 60, 70-81] within this short period. Moreover, four International Conferences were held in the field of Photoacoustics, Thermal and Related Sciences which substantiate the importance of this technique and an international journal namely *Journal of Photoacoustics* has been published since 1982. All these essentially show the immense growth of activities in this field. The next few years promise an exciting period of growth for the rediscovered sciences of photoacoustics and photoacoustic spectroscopy.

## References :

1. V.S. Letokhov, Phys. Today, **30**, 23 (1977).
2. A.Einstein, Physikalische Zeitschrift., **18**, 121 (1917).
3. H. Kogelnik and T. Li, Proc. IEEE, **54**, 1312 (1966).
4. G.D. Boyd and J.P. Gordon, Bell Syst. Tech. J., **40**, 489 (1961).
5. T.H. Maiman, R.H. Hoskins, I.J. D'Haenes, C.K. Asawa and V. Evtuhov, Phys. Rev., **123**, 1145 (1961).
6. A. Javan, W.R. Bennell and D.R. Herriott, Phys. Rev. Lett., **6**, 106 (1971).
7. D.L. Perry, IEEE J. Quantum Electron., **QE-7**, 107 (1971).
8. C.K.N. Patel, Phys. Rev. Lett., **12**, 588 (1964a).
9. M.F. Kimmitt, Proc. of the Second International Conference on lasers in Manufacturing, Birmingham, U.K. (1985).
10. L. Tarasov, 'Laser Physics and Applications' (Mir Publishers : USSR) (1986).
11. C.K.N. Patel in 'Lasers' (Ed: A.K. Levine, Marcel Decker : New York) p.1 (1968).
12. C.K. Rhodes, 'Excimer Lasers' (Springer-Verlag : Berlin) p. 165 (1979)
13. D. Finaly and D.W. Goodwin in 'Advances in Quantum Electronics', (Ed. D.W. Goodwin, Academic Press : New York), p. 78 (1970).
14. M.I. Nathan, Proc. IEEE, **54**, 1276 (1966).
15. I. Melngailis and A. Mooradian in 'Laser Applications of Optics and Spectroscopy' (Ed. S.F. Jacob, Addison-Wesley : New York) (1976).
16. E.D. Hinkley, T.C. Hartman and C. Fread, Appl. Phys. Lett., **13**, 49 (1968).

17. Donald C. O'shea, W. Russel Callen and William T. Rhodes, 'Introduction to Lasers and Their Applications', (Addison-Wesley, USA) (1978).
18. F.P. Schafer 'Dye Lasers' (Springer-Verlag : Berlin) (1977).
19. L.R. Elias, W.M. Fairbank, J.M.J. Madey, H.A. Schwettman and T.I. Smith, Phys. Rev. Lett., **36**, 717 (1976).
20. W.W. Wendlandt and H.G. Hect, 'Reflectance Spectroscopy' (Wiley & Sons : New York) (1966).
21. P.A. Wills and T.Hirschfeld, Appl. Spectroscopic Rev. **1**, 99 (1968).
22. W.D. Ashby, 'Developments in Applied Spectroscopy' (Plenum : New York) (1962).
23. G.B. Wright, 'Light Scattering of Solids', (Springer-Verlag : Berlin) (1969).
24. A. Rosencwaig, Opt. Commun., **7**, 305 (1973).
25. A. Rosencwaig, 'Photoacoustics and Photoacoustic Spectroscopy' (Wiley & Sons : New York) (1980).
26. S.K. Wickramasinghe, R.C. Bray, V. Jipson, C.F. Quate and H.R. Salcedo, Appl. Phys. Lett., **33**, 923, (1978).
27. A. Rosencwaig and G. Busse, Appl. Phys. Lett., **36**, 725 (1980).
28. P. Poulet, Ph.D. Thesis, L'universit e Louis Paster de strasbourg, France (1985).
29. J. Fernandez, J. Etxebarria, J. Zubillaga and M.J. Tello, Digest of the 4th Topical Meeting on Photoacoustics, Thermal and Related Sciences, Villed Esteral (Qubec), Canada, paper ThB4 (1985).

30. J.P. Roger, D. Fournier, A.C. Boccara, R. Noufi and D. Cahen, Digest of the 4th Topical Meeting of Photoacoustics, Thermal and Related Sciences, Villed Esteral (Qubec), Canada, paper MD.6 (1985).
31. C.K.N. Patel and A.C. Tam, Rev. Mod. Phys., **53**, 517 (1981).
32. L.B. Kreuzer, N.D. Kenyon and C.K.N. Patel, Science, **177**, 347 (1972).
33. S.J. Huard and D. Chardon, Opt. Commun., **39**, 59 (1981).
34. T. Sawada and S. Oda, Anal. Chem., **53**, 471 (1981).
35. C.K.N. Patel and A.C. Tam, Appl. Phys. Lett., **36**, 7 (1980).
36. H.L. Fang and R.L. Swafford, Appl. Opt., **21**, 55 (1982).
37. V.N. Rai, L.B. Tiwari, S.N. Thakur and D.K. Rai, Pramana, **19**,, 579 (1982).
38. A.C. Tam and C.K.N. Patel, Appl. Phys. Lett., **35**, 243 (1979c)
39. H.F. Chen, M.R. Wixom and A.H. Francis, Digest of the 4th Topical Meeting on Photoacoustics, Thermal and Related Sciences, Ville'd Esteral (Qubec), Canada, paper, MD.7 (1985).
40. A. Rosencwaig, Am. Lab., **11**, 39 (1979).
41. K.O. Park, S.I. Yun and C.S. Sol, New Physics (Korean Physical Society) **3**, 183 (1981).
42. Andre' Lacharine and Patric Poulet, Appl. Phys. Lett., **45**, 953 (1984).
43. M.J. Adams and G.F. Kirkbright, Analyst, **102**, 81 (1977a).
44. P. Hefferie and H. Coufal, Digest of the 4th International Topical Meeting on Photoacoustics, Thermal and Related Sciences, Ville'd Esteral (Quebec), Canada, paper WA2 (1985).

45. R. Florian, J. Pelzel, M. Rosenberg, H. Vargas and R. Wernhardt, *Phys. Status Solidi*, A48, K 35 (1978).
46. T. Somasundaram, P. Ganguly and C.N.R. Rao, *J. Phys. C.*, 19, 2137 (1986).
47. P. Korpium, A Faber and J. Weiser, *Digest of the 4th International Topical Meeting on Photoacoustics, Thermal and Related Sciences, Ville'd Esteral (Quebec), Canada, paper WA 10* (1985).
48. C.E. Yeak, R.L. Melcher and H.E. Klauses, *Appl. Phys. Lett.*, 41, 1043 (1982).
49. A.C. Tam, *Rev. Mod. Phys.*, 58, 2, 381 (1986).
50. A.C. Tam and H. Coufal, *Appl. Phys. Lett.*, 42, 33 (1983a).
51. E. Brandis and A. Rosencwaig, *Appl. Phys. Lett.*, 37, 98 (1980).
52. G. Busse, *Appl. Opt.*, 21, 107 (1982).
53. J.F. McClelland and R.N. Kinsely, *Appl. Phys. Lett.*, 35, 585 (1979).
54. R.A. Macfarlane and L.D. Hess, *Appl. Phys. Lett.*, 36, 137 (1981).
55. Shu-yi Zang and Lichen, *Digest of the 4th International Topical Meeting on Photoacoustics, Thermal and Related Sciences, Ville'd Esteral (Quebec), Canada, paper WD.12* (1985).
56. O. Pessoa, C.L. Cesar, C.A.S. Lima, H. Vargas and L.C.M. Miranda *Digest of the 4th International Topical Meeting on Photoacoustics, Thermal and Related Sciences, Ville'd Esteral (Quebec) Canada, paper Th.A 5* (1985).
57. E.A. Ash, E.Dieulesaint and H. Rakouth, *Electron. Lett.*, 16, 470 (1980).
58. A. Rosencwaig, *J. Photoacoustics*, 1, 371 (1982).

59. A. Rosencwaig, *Science*, **181**, 657 (1973).
60. A. Rosencwaig in 'Advances in Electronics and Electron Physics' (Ed. L. Martin, Academic Press : New York), Vol. 46 (1978).
61. D. Balasubramanian and Ch. Mohan Rao, Digest of the 4th International Topical Meeting on Photoacoustics, Thermal and Related Sciences, Ville'd Esteral (Quebec), Canada, paper Th.A 1 (1985).
62. G.J. Diebold and J.S. Hayden, Digest of the 4th International Topical Meeting on Photoacoustics, Thermal and Related Sciences, Ville'd Esteral (Quebec) Canada, paper Th. A 2 (1985).
63. R.B. Somoano, *Angew. Chem. Int.*, **17**, 234 (1978).
64. A. Rosencwaig and E. Pines, *J. Invest. Dermatol.*, **69**, 296 (1977a).
65. F.W. Karasek, *J. Research and Development (USA)*, **9**, 38 (1977).
66. E.J. Stadler, P. Bithe, M. Frank and C. Rensch, Technical Digest of the 2nd International Topical Meeting on Photoacoustic Spectroscopy (Berkeley, USA), paper Tu.B. 21 (1981).
67. L.A. Crum and G.T. Reynolds, *J. Acoust. Soc. Am.*, **78**, 137 (1985).
68. S. Didascalou, R. Stewart and G. Diebold, Digest of the 4th International Topical Meeting on Photoacoustics, Thermal and Related Sciences, Ville'd Esteral (Quebec), Canada, paper MA.7 (1985).
69. B.S.H. Royce and J.B. Benziger, (Private Communication).
70. W.R. Harshbarger and M.B. Robin, *Acc. Chem. Res.*, **6**, 329 (1973).
71. A. Hordvick, *Appl. Opt.*, **16**, 2827 (1977).
72. M.B. Robin, *J. Lumin*, **13**, 131 (1976).
73. M.J. Golles, N.R. Geddes and E. Mehdizadeh, *Contemp. Phys.*, **20**, 11 (1979).

74. G.F. Kirkbright and S.L. Castelden, Chem. Br., 16, 661 (1980).
75. L.M. Lyamshev and L.N. Sedov, Akust., Zh. 27, 5 [Sov. Phys. Acoustics] 27, 4 (1981).
76. P. Ganguly and C.N.R. Rao, Proc. Indian Acad. Sci. (Chem. Sci.) 3, 153 (1981).
77. M.J. Adams, Prog. analyt. atom. spectrosc., 5, 153 (1982).
78. J.B. Kinney and R.H. Staley, Annual Rev. Mater. Sci., 12, 295 (1982).
79. A.C. Tam in 'Ultrasensitive Laser Spectroscopy', (Ed. Klinger, Academic Press : New York) (1983).
80. G. A. West, J.J. Basrett, D.R. Siebert and K.V. Reddy, Rev. Sci. Instrum., 54, 797 (1983).
81. Markus W. Sigrist, J. Appl.Phys., 60(7), R 83 (1986).



## CHAPTER II

### GENERAL THEORY OF PHOTOACOUSTIC EFFECT IN SOLIDS AND ITS APPLICATIONS

#### ***Abstract***

*The first section of this chapter gives a historical survey of the various theories developed in the case of PA spectroscopy of solids. A detailed account of the Rosencwaig-Gersho theory is presented and its experimental verification is briefly discussed. A summary of the instrumentation aspect of PA spectroscopy and some of its applications are presented.*

## 2.1 Introduction :

The term photoacoustic (PA) effect usually refers to the generation of acoustic waves by a sample by the interaction with a modulated electromagnetic radiation. In its broader sense, PA effect may mean the production of acoustic waves or other thermoelastic effects by any type of energy sources, including electromagnetic radiation ranging from radio frequency to X-ray, electrons, protons, ions and other particles. Despite the fact that PA phenomenon is a very weak effect discovered nearly a century ago, there has been a great resurgence of interest in this subject during the past few years. This is mainly due to the development of highly intense sources like lasers, extremely sensitive transducers and highly sophisticated signal processing techniques. Recently, the PA effect is being successfully employed in various branches of physics, chemistry, biology, engineering and medicine as an ultra sensitive detection and diagnostic tool. This has caused the emergence of a new area of technology which has enormous potential for measurement of the various physical properties of materials.

A brief account of the development of the theories of PA effect and a detailed version of Rosencwaig-Gersho theory and its suitability to interpret the experimental observations are given in the subsequent sections.

## 2.2 Early History :

The PA effect was discovered by Alexander Graham Bell [1] in 1880 who observed that sound is produced when chopped sunlight is incident on optically absorbing materials. He suggested that this effect was due to a cyclic expulsion and reabsorption of air contained within the sample when it is heated with an intermittent light source. About the same period Rayleigh [2] explained that this signal was derived primarily from a thermally induced mechanical vibration of the solid. Mercadier [3] investigated solid and liquid samples, gases and vapours. Finally he was convinced that the effect is caused by the absorption of light in the gas or vapour but not by a solid or liquid sample. A lot of experimental evidences led Tyndall [4] to a similar conclusion. Preece [5] recognised that the gas plays an important part in the generation of sound. From his experimental observations he made a conclusion that the thermal strain developed in the sample due to the temperature gradient can in turn contribute to acoustic signal. At about the same time Rontgen [6] reported that acoustical effects as a result of pressure variations are due to the absorption of light in various gases.

In the following years no appreciable interest was shown in PA effect. Moreover, none of the explanations suggested in the eighties of the last century could give a satisfactory quantitative description. Later Veingerov [7] conducted a series of experiments to analyse the gas

mixtures using this technique. In this regard, Luft [8] could make an exciting achievement to monitor the abundance of trace gases by using an infrared source. Thus gas analysis became the most widespread and important applications of the photoacoustic effect [9,10]. Later in 1971 Kreuzer and Patel [11] developed a PA spectrometer which could detect very low concentrations of contaminants in a gas by tuning an infrared laser to the vibrational frequency of the contaminants and recording the microphone signal resulting from the absorption. This experiment infact made a landmark in PA spectroscopy since a laser could be most effectively used as a light source in this experiment.

The first theoretical analysis of PA effect was reported by Kaiser [12] on the basis of a two-state gas model. But a remarkable attempt at a modern, quantitative theory was made in 1973 by Parker [13]. While conducting experiments with gases he noticed a weak signal apparently emanating from the cell windows. This led Parker to derive the theoretical expression for PA signal by which many of the salient features of the more general theories could be established.

Subsequently in 1975 Rosencwaig and Gersho [14,15] formulated a more general theory of PA effect in condensed media. This theory now commonly referred to as RG theory, reveals that in a gas-microphone set up for measurement of PA signal, the signal apparently

depends both on the generation of acoustic pressure disturbance at the sample-gas interface and on the transport of this disturbances through the gas to the microphone. The generation of the surface pressure disturbance in turn depends on the periodic temperature fluctuation at the sample-gas interface. Therefore RG theory could exactly predict the temperature variation in the gas medium which directly depends on the absorption of light by the sample. This theory could thus trigger a world-wide rebirth of interest in PA methods and since then, there has been a real boom in the growth of this field. The details of RG theory are described in the next section.

In the following years, Bennett and Forman [16] and Aamdot et al [17] refined RG theory by treating the transport of the acoustic disturbances in gases more exactly, with Navier-Stokes equations. Later in 1978 McDonald and Wetsel [18] modified the thermal piston model suggested in RG theory by incorporating the mechanical vibrations of the sample at low frequencies. This in fact led Quimby [19] to make appropriate changes in the RG theory by making use of the three dimensional heat flow at relatively low chopping frequencies. Recently in 1982 Guli [20] formulated a theory based on thermoelastic considerations in the sample which is in agreement with RG theory. However, these refinements did not change the basic results of the RG theory in most of the experimental conditions.

### 2.3 Rosencwaig-Gersho theory :

Rosencwaig-Gersho [RG] theory is considered to be the most

successful theory developed so far, and it is found to be effective in the commonly encountered experimental conditions. The prominent feature of this theory is its simplicity and straightforwardness in its approach to provide a basic understanding of the various physical process in the generation of PA signal. This treatment is essentially based on the thermal diffusion through the sample which in turn produces the acoustic signal. Most of the experimental observations on PA studies can be interpreted on the basis of this theory.

RG theory starts with a one dimensional analysis of the generation of PA signal in a simple cylindrical cell as shown in fig. 2.1. The sample is considered to be in the form of a disc having a diameter equal to the cell diameter and thickness  $l_s$ . This sample is mounted in such a way that its rear surface is in perfect contact with a poor thermal conductor of thickness  $l_b$ . The gas column which serves as the coupling medium between the sample and microphone, has a length  $l_g$ . Optical absorption in the gas medium and at the backing material are considered to be negligible compared to the sample material.

The intensity of a monochromatic light beam modulated at a frequency  $\omega$  allowed to be incident on the sample is given by,

$$\hat{I} = \frac{1}{2} I_0 (1 + e^{i\omega t}) \quad (2.01)$$

where  $I_0$  is the incident intensity of the light flux. If the absorption coefficient of the sample is  $\beta$ , then the absorbed intensity in the

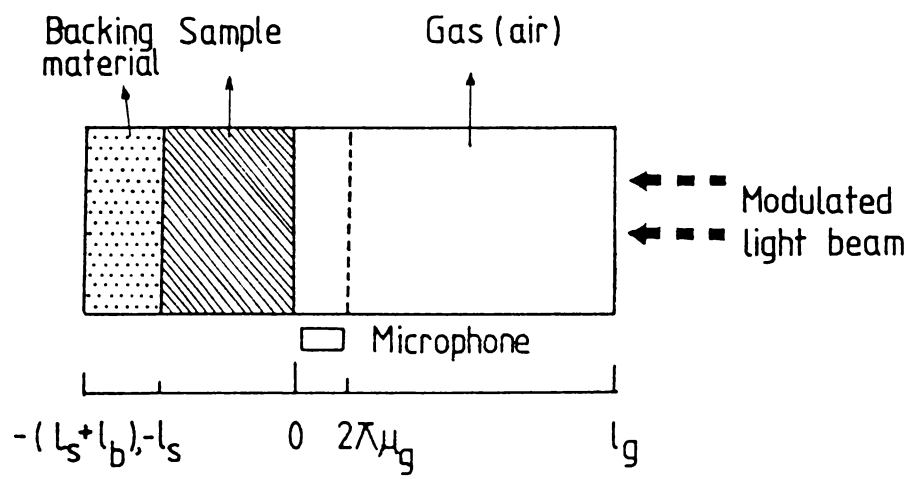


Fig. 2.1 Schematic diagram of a cylindrical PA cell

sample along the distance  $x$  can be determined from Lambert-Beer law as,

$$\bar{I}_{abs} = \frac{1}{2} \bar{I}_0 (1 + e^{i\omega t}) (1 - e^{\beta x}) \quad (2.02)$$

where  $\beta x$  is positive because  $x$  is taken as negative. Similarly the intensity absorbed by a layer of thickness  $dx$  in the sample is given by

$$\bar{I}_{abs} = \frac{1}{2} \bar{I}_0 (1 + e^{i\omega t}) \left[ (1 - e^{\beta x}) - (1 - e^{\beta(x+dx)}) \right] \quad (2.03)$$

which is approximated as

$$\bar{I}_{abs} \simeq \frac{1}{2} \beta \bar{I}_0 e^{\beta x} (1 + e^{i\omega t}) dx \quad (2.04)$$

assuming that  $\beta dx$  is small. The above expression represents the heat energy generated per unit volume at the layer of thickness  $dx$  provided that the non-radiative transition probability is assumed to be unity. Here  $x$  takes on negative values since the solid extends from  $x = 0$  to  $x = l_s$  with the light incident at  $x = 0$ .

### 2.3.1 Temperature Distribution :

The heat generated in the sample represented by eq. (2.04) warms up the sample, gas and backing by an amount  $\theta(x, t)$  above the ambient temperature  $T_0$ . Therefore, the rise in temperature can be expressed as

$$\theta(x, t) = T(x, t) - T_0 \quad (2.05)$$



As soon as the heat is generated in the sample due to the absorption of light, it starts conducting to the gas and backing and the amount of heat transfer depends on the thermal conductivity of these media. Therefore, in order to analyse the temperature distribution at the sample, air and backing, the thermal diffusion equations at these regions have to be considered and these provide a basic idea of heat transfer process. Consequently the solutions of these thermal diffusion equations give the temperature at the respective regions. Thus taking into account of the distributed heat source due to the absorption of modulated light beam, the thermal diffusion equation in the sample can be expressed as

$$\frac{\partial^2 \theta_s}{\partial x^2} - \frac{1}{\alpha_s} \frac{\partial \theta_s}{\partial t} + \frac{1}{2} \frac{\beta I_0}{k_s} e^{\beta x} (1 + e^{i\omega t}) = 0 \quad (2.06)$$

$$\text{for } -l_s \leq x \leq 0$$

where  $k_s$  is the thermal conductivity of the sample,  $\alpha_s$  the thermal diffusivity of the sample which is

$$\alpha_s = \frac{k_s}{\rho_s C_{p_s}} \quad (2.07)$$

$C_{p_s}$  the specific heat capacity of the sample at constant pressure and  $\rho_s$  the density of the sample. The last term in the equation (2.06) represents the heat generated in the sample. Since the heat generated in the sample is transferred to the air and backing material, the temperature rise in these media will be entirely due to the heat transfer from the sample. Therefore, in the case of air and backing

material there is no localised heat centres and the respective thermal diffusion equations in these regions are,

$$\frac{\partial^2 \theta_g}{\partial x^2} - \frac{1}{\alpha_g} \frac{\partial \theta_g}{\partial t} = 0 \quad (2.08)$$

where  $0 \leq x \leq l_g$

$$\frac{\partial^2 \theta_b}{\partial x^2} - \frac{1}{\alpha_b} \frac{\partial \theta_b}{\partial t} = 0 \quad (2.09)$$

where  $-(l_s + l_b) \leq x \leq -l_s$

The solutions of these equations which are of physical interest, representing the temperature in the sample, gas and backing relative to ambient temperature, as a function of position and time, are given by the real part of the complex valued solution of equations (2.06), (2.08), (2.09) respectively.

The general solution for  $\theta_s(x, t)$  in the sample neglecting transients can be written as

$$\theta_s(x, t) = b_1 + b_2 + b_3 e^{\beta x} + \left[ u e^{\sigma_s x} + v e^{-\sigma_s x} - F e^{\beta x} \right] e^{i\omega t} \quad (2.10)$$

where  $-l_s \leq x \leq 0$

similarly in the gas medium the temperature is

$$\theta_g(x, t) = \left(1 - \frac{x}{l_g}\right) F + \theta_0 e^{-\sigma_g x + i\omega t} \quad (2.11)$$

where  $0 \leq x \leq l_g$

the temperature at the backing material is

$$\theta_b(x,t) = \frac{1}{l_b} (x + l_s + l_b) W_0 + W e^{\sigma_b(x + l_s) + i\omega t} \quad (2.12)$$

where  $-(l_s + l_b) \leq x \leq -l_s$

Here  $W, U, V, E$  and  $\theta_0$  are complex valued constants,  $b_1, b_2, b_3$ ,  $W_0$  and  $F$  are real. The parameter which plays an important role on the thermal diffusion process is  $\sigma$  which is given by

$$\sigma = (1+i) a \quad (2.13)$$

where  $a$  is the thermal diffusion coefficient represented by  $a = \sqrt{\frac{\omega}{2\alpha}}$

$\theta_0$  and  $W$  represent the complex amplitudes of the periodic temperature at the sample-gas boundary ( $x=0$ ) and the sample-backing boundary ( $x=l_s$ ) respectively. The quantities  $W_0$  and  $F$  represent the steady component of the temperature relative to the ambient temperature at the front and rear surfaces of the sample respectively. The term with amplitude  $U$  represents a temperature wave propagating to the left and  $V$  represents a temperature wave propagating in the opposite direction in the sample. These waves will be effectively attenuated when it starts propagating through the gas medium. The distance upto which these waves can propagate through the gas medium without any appreciable change in its amplitude is approximately one wavelength of this wave which is represented by

$$\lambda_g = 2\pi \mu_g \quad (2.14)$$

where  $\mu_g$  is the thermal diffusion length in the gas.

In order to solve the thermal diffusion equations, it is necessary to apply proper boundary conditions. Here the boundary conditions for the temperature and heat flux at the sample surfaces are given by

$$\theta_g(0, t) = \theta_s(0, t) \quad (2.15)$$

$$\theta_b(-l_s, t) = \theta_s(-l_s, t) \quad (2.16)$$

Similarly

$$k_g \frac{\partial \theta_g(0, t)}{\partial x} = k_s \frac{\partial \theta_s(0, t)}{\partial x} \quad (2.17)$$

$$k_b \frac{\partial \theta_b(0, t)}{\partial x} = k_s \frac{\partial \theta_s(-l_s, t)}{\partial x} \quad (2.18)$$

Using the above conditions in the eqn.(2.10)(2.11) and(2.12)the constants can be determined as

$$b_3 = -\bar{I}_0 / 2\beta k_s \quad (2.19)$$

$$E = \beta \bar{I}_0 / 2k_s (\beta^2 - \sigma_s^2) \quad (2.20)$$

$$F_0 = b_1 + b_3 \quad (2.21)$$

$$W_0 = b_1 - b_2 l_s + b_3 e^{-\beta l_s} \quad (2.22)$$

$$-\frac{k_g}{l_g} F_0 = k_s b_2 + \beta k_s b_3 \quad (2.23)$$

$$\frac{k_b}{l_b} W_0 = k_s b_2 + \beta k_s b_3 e^{-\beta l_s} \quad (2.24)$$

$$\theta_0 = U + V - E \quad (2.25)$$

$$W = e^{-\sigma_s l_s} U + e^{\sigma_s l_s} V - e^{-\beta l_s} E \quad (2.26)$$

$$-k_g \sigma_g \theta_0 = k_s \sigma_s U - k_s \sigma_s V - k_s \beta E \quad (2.27)$$

$$k_b \sigma_b W = k_s \sigma_s e^{-\sigma_s l_s} U - k_s \sigma_s e^{\sigma_s l_s} V - k_s \beta e^{-\beta l_s} E \quad (2.28)$$

These solutions are essential for evaluating the temperature distribution in the cell in terms of optical, thermal and geometric parameters of the system. Therefore, the temperature at the sample gas interface (at  $x=0$ ) is given by

$$\theta_0 = \frac{\beta I_0}{2k_s(\beta^2 - \sigma_s^2)} \left[ \frac{(h-1)(b+1)e^{\sigma_s l_s} - (h+1)(b-1)e^{-\sigma_s l_s} + 2(b-h)e^{-\beta l_s}}{(g+1)(b+1)e^{\sigma_s l_s} - (g-1)(b-1)e^{-\sigma_s l_s}} \right] \quad (2.29)$$

$$b = \frac{k_b a_b}{k_s a_s} \quad (2.30)$$

$$g = \frac{k_g a_g}{k_s a_s} \quad (2.31)$$

$$h = (1-i)\beta / 2a_s \quad (2.32)$$

$$\sigma_s = (1+i)a_s \quad (2.33)$$

From these relations it is evident that  $a_s$ ,  $a_g$  and  $a_b$  play an important role on the heat transfer process in the sample, gas and backing material respectively. The thermal diffusion coefficient  $a = \frac{\mu}{\mu} = \left( \frac{\pi f P c_p}{k} \right)^{1/2}$  where  $\mu$  is the thermal diffusion length,  $f$  represents the modulation frequency,  $P$  denotes the density,  $c_p$  is the specific heat and  $k$  is the thermal conductivity. Therefore the thermal diffusion length in

a medium is inversely proportional to the square root of the modulation frequency which means that at higher chopping frequencies, the amount of heat transferred from the inner layer of the sample to the gas medium is much less. This causes a decrease in PA signal at higher chopping frequencies.

### 2.3.2 Production of Acoustic Signal :

The acoustic signal originates as a result of the periodic heat flow from the sample to the surrounding gas medium. This periodic heat diffusion process produces a temperature fluctuations of the same frequency in the gas which is given by the sinusoidal (a.c.) component of the solution of eqn.(2.11)

$$\theta_{ac}(x,t) = \theta_0 e^{-\sigma_g x + i\omega t} \quad (2.34)$$

This expression represents the temperature distribution in the gas medium. The term  $e^{-\sigma_g x}$  denotes the damping of temperature wave when it propagates through gas medium. Therefore the time dependent component of the temperature in the gas attenuates rapidly with increasing distance from the sample surface. Since the thermal diffusion coefficient  $a_g$  represents the wave number of the temperature diffusion wave, the corresponding wavelength in the gas medium is  $\lambda_g = \frac{2\pi}{a_g} = 2\pi\mu_g$ . Consequently at a distance of  $2\pi\mu_g$  which corresponds to one wavelength of acoustic wave in the gas medium, (where  $\mu_g$  is the thermal diffusion

length in the gas), the periodic temperature variation in the gas is assumed to be fully damped out.

Thus the spatially averaged temperature of the gas within this boundary layer as a function of time can be determined by

$$\bar{\theta}(t) = \frac{1}{2\pi\mu_g} \int_0^{2\pi\mu_g} \theta_{ac}(x,t) dx \quad (2.35)$$

$$\bar{\theta}(t) = \frac{1}{2\pi\mu_g} \int_0^{2\pi\mu_g} \theta_0 e^{-\sigma_g x + i\omega t} dx \quad (2.36)$$

$$\bar{\theta}(t) = \frac{1}{\sqrt{2}\pi} \theta_0 e^{i(\omega t - \pi/4)} \quad (2.37)$$

Using the relations  $\sigma_g = (1+i) \sqrt{\mu_g}$  and  $(1+i) = \sqrt{2} e^{i\pi/4}$  and the approximation made was  $e^{-2\pi} \ll 1$ .

Due to the periodic heating of the gas-sample interface a thin layer of gas which is close to the sample surface may expand and contract periodically and this can be considered as an acoustic piston acting on the rest of the gas column. This in fact produces an acoustic signal which travels through the entire gas column. The displacement of this gas piston is solely due to the periodic heating at the surface of the sample. This can be determined using the ideal gas law.

$$\delta x(t) = 2\pi\mu_g \frac{\bar{\theta}(t)}{T_0} \quad (2.38)$$

Substituting the values from eqn.(2.36) for  $\bar{\theta}(t)$

$$\delta x(t) = \frac{\theta_0 \mu_g}{\sqrt{2} T_0} e^{i(\omega t - \pi/4)} \quad (2.39)$$

Where  $T_0$  is the temperature at the sample surface. This displacement of the acoustic piston therefore makes an adiabatic change in the gas pressure. Thus the corresponding acoustic pressure in the cell due to the displacement of this gas piston is derived from the adiabatic gas law

$$PV^\gamma = \text{Constant} \quad (2.40)$$

where  $P$  is the gas pressure,  $V$  volume of the gas in the cell and  $\gamma$  the ratio of specific heats. From the above relation the variation in pressure

$$\delta P(t) = \frac{\gamma P_0}{V_0} \delta V = \frac{\gamma P_0}{l_g} \delta x(t) \quad (2.41)$$

Where  $P_0$  and  $V_0$  are the ambient pressure and volume respectively. Therefore substituting values for  $\delta x(t)$  from eqn.(2.38).

$$\delta P(t) = \frac{\gamma P_0 \theta_0}{\sqrt{2} l_g a_g T_0} e^{i(\omega t - \pi/4)} \quad (2.42)$$

where

$$\frac{\gamma P_0 \theta_0}{\sqrt{2} l_g a_g T_0} = Q \quad (2.43)$$

$Q$  specifies the complex envelope of the sinusoidal pressure variation in the gas medium which is detected by microphone placed in the cavity.

Therefore combining eqns. (2.28) and (2.42),  $Q$  becomes

$$Q = \frac{\beta T_0 \gamma P_0}{2\sqrt{2} T_0 k_s l_g a_g (\beta^2 - \sigma_s^2)} \left[ \frac{(\kappa-1)(b+d)e^{\sigma_s l_s} - (\kappa+1)(b-d)e^{-\sigma_s l_s} + 2(b-\kappa)e^{-\beta l_s}}{(g+1)(b+1)e^{\sigma_s l_s} - (g-1)(b-1)e^{-\sigma_s l_s}} \right] \quad (2.44)$$

$$\sigma_s = (1+i)/\mu_s \quad (2.45)$$



This expression represents the amplitude and phase of the acoustic waves generated in the cell by PA effect. This expression provides an explicit formula for the pressure variation within the photoacoustic chamber, but it is somewhat difficult to interpret the results due to its complexity. However, a physical insight may be gained by examining special cases where the expression for  $Q$  becomes relatively simple. To illustrate the use of the equation, Rosencwaig and Gersho considered its application to a variety of special cases. For these examples the optical absorption length is defined by  $l_{\beta} = 1/\beta$  where  $\beta$  is the optical absorption coefficient of the sample. The special cases of the eqn. (2.41) essentially deal with the relative magnitude of  $l_{\beta}$  with respect to the sample thickness  $l_s$  and the variation of thermal diffusion length of the sample  $\mu_s$  with respect to the sample thickness  $l_s$ . Based on these conditions sample can be classified into mainly two groups. They are optically transparent samples in which the optical absorption length exceeds the sample thickness i.e., ( $l_{\beta} > l_s$ ) and optically opaque samples in which the optical absorption length must be smaller than the sample thickness ( $l_{\beta} < l_s$ ). Now considering the thermal property of the samples, it can be again divided into two categories. They are thermally thin samples in which the thermal diffusion length exceeds the sample thickness  $\mu_s > l_s$  and thermally thick samples in which thermal diffusion length is smaller than the sample thickness  $\mu_s < l_s$ .

Where  $T_0$  is the temperature at the sample surface. This displacement of the acoustic piston therefore makes an adiabatic change in the gas pressure. Thus the corresponding acoustic pressure in the cell due to the displacement of this gas piston is derived from the adiabatic gas law

$$PV^\gamma = \text{Constant} \quad (2.40)$$

where  $P$  is the gas pressure,  $V$  volume of the gas in the cell and  $\gamma$  the ratio of specific heats. From the above relation the variation in pressure

$$\delta P(t) = \frac{\gamma P_0}{V_0} \delta V = \frac{\gamma P_0}{l_g} \delta x(t) \quad (2.41)$$

Where  $P_0$  and  $V_0$  are the ambient pressure and volume respectively. Therefore substituting values for  $\delta x(t)$  from eqn.(2.38).

$$\delta P(t) = \frac{\gamma P_0 \theta_0}{\sqrt{2} l_g a_g T_0} e^{i(\omega t - \pi/4)} \quad (2.42)$$

where

$$\frac{\gamma P_0 \theta_0}{\sqrt{2} l_g a_g T_0} = Q \quad (2.43)$$

$Q$  specifies the complex envelope of the sinusoidal pressure variation in the gas medium which is detected by microphone placed in the cavity.

Therefore combining eqns. (2.28) and (2.42),  $Q$  becomes

$$Q = \frac{\beta I_0 \gamma P_0}{2\sqrt{2} T_0 k_s l_g a_g (\beta^2 - \sigma_s^2)} \left[ \frac{(\lambda - 1)(b + 1)e^{\sigma_s l_s} - (\lambda + 1)(b - 1)e^{-\sigma_s l_s} + 2(b - \lambda)e^{-\beta l_s}}{(g + 1)(b + 1)e^{\sigma_s l_s} - (g - 1)(b - 1)e^{-\sigma_s l_s}} \right] \quad (2.44)$$

$$\sigma_s = (1 + i) / \mu_s \quad (2.45)$$

This expression represents the amplitude and phase of the acoustic waves generated in the cell by PA effect. This expression provides an explicit formula for the pressure variation within the photoacoustic chamber, but it is somewhat difficult to interpret the results due to its complexity. However, a physical insight may be gained by examining special cases where the expression for  $Q$  becomes relatively simple. To illustrate the use of the equation, Rosencwaig and Gersho considered its application to a variety of special cases. For these examples the optical absorption length is defined by  $l_{\beta} = 1/\beta$  where  $\beta$  is the optical absorption coefficient of the sample. The special cases of the eqn. (2.41) essentially deal with the relative magnitude of  $l_{\beta}$  with respect to the sample thickness  $l_s$  and the variation of thermal diffusion length of the sample  $\mu_s$  with respect to the sample thickness  $l_s$ . Based on these conditions sample can be classified into mainly two groups. They are optically transparent samples in which the optical absorption length exceeds the sample thickness i.e., ( $l_{\beta} > l_s$ ) and optically opaque samples in which the optical absorption length must be smaller than the sample thickness ( $l_{\beta} < l_s$ ). Now considering the thermal property of the samples, it can be again divided into two categories. They are thermally thin samples in which the thermal diffusion length exceeds the sample thickness  $\mu_s > l_s$  and thermally thick samples in which thermal diffusion length is smaller than the sample thickness  $\mu_s < l_s$ .

Therefore, by choosing these special conditions a clear physical insight into the PA process can be easily obtained. These conditions and their significances are discussed in the following section.

## 2.4. Special Cases :

### 2.4.1 Optically Transparent Solids ( $l_\beta > l_s$ ):

In the case of these samples light is absorbed throughout the length of the sample and part of the light is transmitted through the sample. Here also three special cases are to be considered depending on the thermal diffusion length and length of the solid sample and they are given below :

a) Thermally thin solids.

In this case,  $\mu_s \gg l_s$  and  $\mu_s \gg l_\beta$  so that  $e^{-\beta l_s} \approx (1 - \beta l_s)$ ;  $e^{\pm \alpha_s l_s} \approx 1$ ,  $|\alpha l_s| \gg 1$  in eqn.(2.41). Therefore  $Q$  can be expressed as

$$Q = \frac{Y}{2 a_g a_b k_b} (\beta - 2 a_s b - i \beta) \approx \frac{(1-i) \beta l_s}{2 a_g} \left( \frac{\mu_b}{k_b} \right) \quad (2.46)$$

where

$$Y = \frac{\gamma P_0 I_0}{2 \sqrt{2} T_0 l_g} \quad (2.47)$$

From the above expression it is evident that the acoustic signal is thus proportional to  $\beta l_s$  and since  $\frac{\mu_b}{a_g}$  is proportional to  $\bar{\omega}^{-1}$  the acoustic signal has an  $\bar{\omega}^{-1}$  dependence. For this case where  $\mu_s \gg l_s$ , the thermal properties of the backing material play an important role on the PA signal. This is due to the fact that the heat generated along

the path of the light beam will be transferred to the backing material since the thermal diffusion length of the sample is large compared to its thickness.

b) Thermally thin solids.

Here the conditions  $\mu_s > l_s$  and  $\mu_s < l_\beta$  consequently  $e^{-\beta l_s} \approx (1 - \beta l_s)$ ,  $e^{\pm \sigma_s l_s} \approx (1 \pm \sigma_s l_s)$  and  $|R| < 1$  in eqn. (2.41).

Therefore the final expression will be

$$Q = \frac{\beta l_s \gamma}{4k_s a_g a_s^3 b} \left[ (\beta^2 + 2a_s^2) + i(\beta^2 - 2a_s^2) \right] \quad (2.48)$$

$$Q \approx \frac{(1-i)\beta l_s}{2a_g} \left( \frac{\mu_b}{k_b} \right) \gamma \quad (2.49)$$

The acoustic signal is again proportional to  $\beta l_s$  which varies as  $\omega^{-1}$  and also depends on the thermal properties of the backing material.

c) Thermally thick solids.

In this case  $\mu_s < l_s$  and  $\mu_s \ll l_\beta$ . Therefore  $e^{-\beta l_s} \approx (1 - \beta l_s)$ ,  $e^{-\sigma_s l_s} \approx 0$  and  $|R| \ll 1$ . The acoustic signal then becomes

$$Q \approx -\frac{i\beta\mu_s}{2a_g} \left( \frac{\mu_s}{k_s} \right) \gamma \quad (2.50)$$

Here also the signal is proportional to  $\beta\mu_s$  rather than  $\beta l_s$ . This means that the light absorbed within the first thermal diffusion length contri-

tribution to the signal, in spite of the fact that light is being absorbed throughout the length  $l_s$  of the solid. Also, since  $\mu_s < l_s$ , the thermal properties of the backing material do not have any influence on the signal and it mainly depends on the thermal properties of the sample itself. Since the equation contains  $\mu_s^2 \mu_g$ , the frequency dependence  $Q$  varies as  $\omega^{-3/2}$ .

These above mentioned cases which are applicable for an optically transparent sample demonstrate a unique capability of PA technique which enables one to obtain a depth profile of the optical absorption within a sample. Consequently such depth profile analysis becomes practicable and thus opens up exciting possibilities for studying layered and amorphous materials in determining overlay and thin film patterns.

#### 2.4.2 Optically Opaque Solids. ( $l_\beta \ll l_s$ )

In these cases, most of the light is absorbed within a distance which is small compared to the sample thickness, and consequently no light is transmitted. Here also depending on the sample geometry and thermal diffusion length there exist three special cases. They are described below.

##### a. Thermally thin solids.

In this case obviously  $\mu_s \gg l_s$  and  $\mu_s \gg l_\beta$  as seen in the previous case. Therefore  $e^{-\beta l_s} \approx 0$ ;  $e^{\pm \sigma_s l_s} \approx 1$  and  $|k| \gg 1$

The final expression becomes

$$Q \approx \frac{(1-i)}{2a_g} \left( \frac{\mu_b}{k_b} \right) \gamma \quad (2.51)$$

In this case, there exists PA opaqueness as well as optical opaqueness in the sense that the acoustic signal is independent of  $\beta$ . This would be the case for a very black absorber such as carbon black. Since the sample possesses large absorption coefficient the acoustic signal is quite strong. The signal depends on the thermal properties of the backing material because the heat generated in the sample can be transferred to the backing material owing to its large thermal diffusion length. Here also the signal varies as

b. Thermally thick solids

Here  $\mu_s < l_s$  and  $\mu_s > l_p$ ; which corresponds to  $e^{-\beta l_s} \approx 0$ ,  $e^{-\sigma_s l_s} \approx 0$  and  $|r| > 1$ . Therefore the expression becomes

$$Q \approx \frac{1}{2a_g a_s k_s \beta} (\beta - 2a_s - i\beta) \gamma \quad (2.52)$$

$$Q \approx \frac{(1-i)}{2a_g} \left( \frac{\mu_s}{k_s} \right) \gamma \quad (2.53)$$

Here since the thermal diffusion length is confined into the sample thickness, in the above expression thermal parameters of the backing are replaced by the solid. Also acoustic signal is independent of  $\omega$  and varies with  $\omega^{-1}$ .

c. Thermally thick solids

Here the condition is  $\mu_b \ll l_s$  and  $\mu_s < l_p$ . Consequently  $e^{-\beta l_s} \approx 0$ ,  $e^{-\sigma_s l_s} \approx 0$  and  $|r| < 1$ . Therefore by incorporating these simplifications, the final expression becomes

$$Q \approx \frac{-i\beta}{4a_g a_s^3 k_s} (2a_s - \beta + i\beta) \gamma \quad (2.54)$$

$$Q \simeq \frac{-i\beta\mu_s}{2\alpha g} \left(\frac{\mu_s}{k_s}\right) \gamma \quad (2.55)$$

This case is found to be the most important one in the class of optically opaque solids. Optically opaque samples satisfy the condition  $\beta l_s \gg 1$ . However, as  $\beta\mu_s < 1$  or  $\mu_s < l_\beta$ , this solid is no longer photoacoustically opaque, since only the light absorbed within the first thermal diffusion length,  $\mu_s$  contributes to the acoustic signal. Therefore, even though the solid is optically opaque, the PA signal is proportional to — Also the signal depends on the thermal parameters of the sample and varies as  $\omega^{-3/2}$ .

The complete illustration of these special cases has been schematically represented in fig. 2.2. Also the frequency dependence and phase of PA signal of these various cases are listed in Table 2.1.

one of the most obvious predictions of RG theory is the PA signal is always linearly proportional to the power of the incident radiation and this dependence holds good for any sample or cell geometry. In the case of an optically opaque sample, when the thermal diffusion length  $\mu_s$  is greater than the optical absorption length  $l_\beta$  the PA signal is independent of optical absorption coefficient  $\beta$  of the sample. Therefore in this case the PA signal is directly proportional to the incident intensity  $\hat{I}_0$ . Therefore, it is evident that the PA spectrum of an opaque sample is simply the power spectrum of the light source [21].



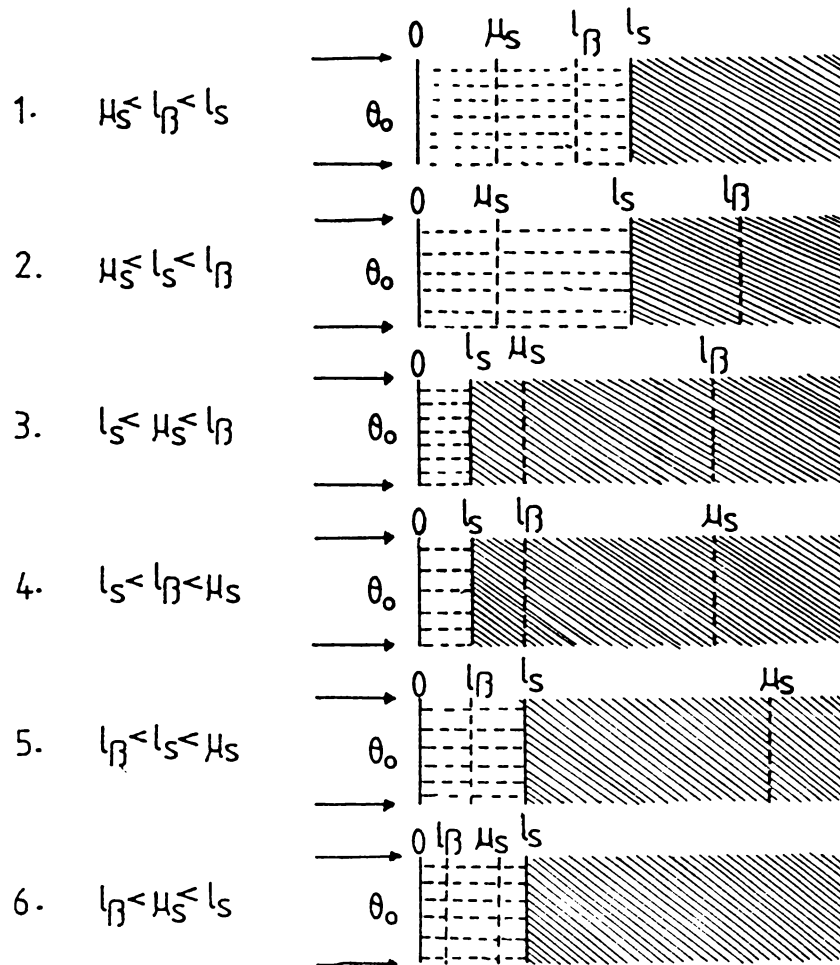


Fig. 2.2 Various cases of 'thermal piston' in PA generation, depending on the relative magnitude of the sample, thermal diffusion length  $\mu_s$ , sample optical absorption length  $l_\beta$  and sample thickness  $l_s$ .  $\theta_0$  is the amplitude of the temperature oscillation at the sample surface in contact with the coupling gas. The dotted area indicates the sample in contact with the backing material (shaded region). When  $\mu_s$  or  $l_\beta$  is larger than  $l_s$ , the location of  $\mu_s$  or  $l_\beta$  is indicated assuming that the backing has the same thermal diffusivity and optical absorption coefficient as the sample.

Table 2.1 Various cases of PA signal observed for a sample of thickness  $l_s$  mounted on a semi-infinite substrate

condition	case	approx. expression for PA signal	Phase
1 $\mu_s > l_\beta > l_s$	Thermally thin optically transparent	$(1-i)\beta l_s \left(\frac{\mu_b}{k_b}\right) \gamma$	$-45^\circ$
2 $l_\beta > \mu_s > l_s$	Optically transparent thermally thin	$(1-i)\beta l_s \left(\frac{\mu_b}{k_b}\right) \gamma$	$-45^\circ$
3 $l_\beta > l_s > \mu_s$	Optically transparent thermally thick	$-i\beta \mu_s \left(\frac{\mu_s}{k_s}\right) \gamma$	$-90^\circ$
4 $\mu_s > l_s > l_\beta$	Thermally thin optically opaque	$(1-i)\left(\frac{\mu_b}{k_b}\right) \gamma$	$-45^\circ$
5 $l_s > \mu_s > l_\beta$	Thermally thick optically opaque	$(1-i)\left(\frac{\mu_s}{k_s}\right) \gamma$	$-45^\circ$
6 $l_s > l_\beta > \mu_s$	Thermally thick optically opaque	$-i\beta \mu_s \left(\frac{\mu_s}{k_s}\right) \gamma$	$-90^\circ$

Another important aspect of RG theory is it provides the absolute value of the optical absorption coefficient by measuring the dependence of PA signal on modulation frequency. McDonald and Wetsel [22] confirmed this fact by measuring the absolute optical absorption coefficient of phenol red sodium salt in distilled water. RG theory also predicts that for an opaque material ( $l_p < l_s$ ), the PA signal varies as  $\omega^{-1}$  when  $\mu_s > l_p$ , and  $\omega^{-3/2}$  when  $\mu_s < l_p$ . This was proved by Rosencwaig [23] using a 0.1 cm thick GaP disc.

The PA effect thus provides a method for the study of optical absorption process in the sample by an indirect way. The corresponding temperature rise is due to the relaxation and thermal diffusion process taking place in the sample. This can in turn be detected by sensing the accompanying pressure fluctuations produced in the gas column in contact with the sample surface, using a microphone and its output can be processed electronically to get the PA signal amplitude as well as the phase.

Therefore in order to carry out the measurement in PA spectroscopy, the basic requirements are :

- a) Light Source
- b) Modulator
- c) PA cell
- d) Transducer
- e) Signal processing unit

Intense light sources are often required in PA experiments because the acoustic detectors like microphones and piezoelectric receivers impose fundamental detector noise limitations. The most popular incoherent source in PA spectroscopy is the high pressure Xenon lamp which provides a continuous spectrum from 230 to 2000 nm. Therefore by using a source monochromator along with the lamp-different wavelengths can be appropriately selected. But this system possesses relatively low efficiency since the output from monochromator is always of low intensity.

Tunable lasers have now replaced the lamp/monochromator system since they possess higher spectral brightness, monochromaticity and coherence. A variety of lasers which find their use as light sources in PA spectroscopy are available. They include gas lasers, metal vapour lasers, solid state lasers and semiconductor lasers. But the higher cost and relatively shorter life of the laser systems impose some limitations in their use in most applications in PA spectroscopy.

Intensity modulation of the light source is a necessary requirement for the production of the PA signal as it is the periodic heating and cooling of the samples, following absorption, which induces the measurable acoustic signal. The most common method of modulation is the mechanical chopper and the details of which are described in chapter III. For high frequency modulation, electro-optic modulator as well as acousto-optic modulators are used. Very often pulsed lasers are used as the light source in PA spectroscopy. PA cell is considered as the heart of the

experimental set up in PA spectroscopy. Since the geometry of the PA cell has a significant role on the sensitivity of the experiment, a careful design ensures one to obtain better signal to noise ratio. Various types of cell designs have been adopted and the details of some of these are described in chapter III. Usually there are three types of PA cells which are widely being employed in PA experiments. They are longitudinal/radial resonant cells, non resonant cells and Helmholtz resonant cells, Of which non resonant cells are commonly employed in most experimental arrangements. Commercial microphone is the most sensitive transducer widely being used in PA studies of gases and solids because its response in sensing acoustic signals in a gas medium is extremely high. Electret microphones provide higher sensitivity and compactness which make it suitable for PA spectroscopy. Recently piezoelectric transducers like PZT, PVDF and ZnO have been used as the transducers in the study of liquids [24].

## 2.5 Applications :

The PA effect provides a means of monitoring the absorption of radiation by a sample in which the sample itself forms an integral component of the detector assembly. The PA signal is a function of two fundamental processes, the absorption of electromagnetic radiation and the thermal propagation within the sample. Therefore, based on the above facts the PA experiments can be classified mainly into two categories.

The first category mainly deals with the spectroscopic applications using PA effect. This provides an efficient method for studying the absorption spectra of different samples such as solids, liquids and gases. Extensive work has been carried out in pollution monitoring using PA effect. The sensitivity of PA detection in gases has advanced to an absorption measurement capability of  $10^{-10} \text{ cm}^{-1}$  with a cell length of 10 cm [25].

Similarly, the minimum absorption detectability in a liquid has been shown to be  $10^{-6} \text{ cm}^{-1}$  with a PA cell length of 1 cm using a pulsed laser of 1 mJ energy and 1- $\mu\text{sec}$  pulse duration for the excitation [26]. Therefore PA technique is considered to be an efficient tool to carry out high resolution spectroscopy [27]. Consequently, Photoacoustic Antistokes Raman Spectroscopy (PARS) has been developed in the field of non-linear spectroscopy which is considered to be an ideal method for studying the non-linear susceptibilities of a Raman active medium [28]. The use of PA technique for measuring absorption due to thin films, monolayers or even sub monlayers has been recently reported [29]. Therefore by incorporating this technique, PA detection sensibility of  $10^{-3} \text{ cm}^{-1}$  of a monolayer of  $\text{NH}_3$  on silver is achieved [30]. Another important application is the study of quantum efficiency of  $\text{Nd}^{3+}$  ions in an ED-2 glass matrix [31] and this turns out to be a prominent method for the appropriate choice of Nd: glass rods, which helps to increase the Nd: Glass laser efficiency. Further more it was shown that the

band gap of an indirect band gap semiconductor could be determined with high accuracy [32] with PA technique. Thus in general, PA measurements are applicable to samples like powders, aerosols, gels and flames, since non radiative thermal relaxation occur generally during ion attachment, diffusion, recombination and quenching and these phenomena may impose serious limitations on the other detection schemes involving ionisation or luminescence.

The technique of PA spectroscopy has been increasingly used to study biological molecules, organelles, cells and tissues in the last few years. Subsequently, photo damage caused to thiamine derivatives has been evaluated by using this novel technique [33] and it has been found that this method can be used to monitor the time dependent degradation probability of samples and packaged formulation of pharmaceuticals. Further more, PA technique can be effectively utilised to study the transmission characterisation of human eye lenses which resulted the early detection of cataractous layer formation on the eye lens [34].

Since the generation and propagation of thermal waves in a sample depend critically on the thermo-elastic and other physical properties, a detailed analysis of the amplitude and phase of the PA signal provide the determination of properties like thermal diffusivity, specific heat, thermal conductivity and phase transition of the sample. This ensures the possibility to carry out non destructive testing of samples which possess defects.

PA technique offers a congenial method for determining the thermal diffusivity of samples. The variation of phase with the modulation frequency provides a thorough understanding of the thermal diffusion process which in turn measures the thermal diffusivity. Extensive amount of work has been carried out to determine the thermal parameters of solids [35]. Adams could determine the thermal diffusivity of copper and glass accurately by using PA effect [36]. Recently thermal parameters of polymer samples have been reported by Poulet et al in 1985 [37]. The details of the set up and experimentation are described in chapter IV.

Another important non-spectroscopic application is phase transition measurement using PA effect. Essentially amplitude and phase angle of the thermal wave depend on the thermal conductivity and specific heat or latent heat which determine refraction, reflection and damping of temperature waves. Because of a temperature gradient exists in the sample, different parts of the sample, are involved in the phase transition process at different temperatures. Thus a variation in PA signal amplitude or phase can monitor the phase transition because the temperature distribution changes rapidly at the temperature of phase transition. The most significant achievement in this regard was the observation of phase transitions in  $TaH_{0.5}$ ,  $NbH_{0.8}$  [38] and in  $NaNO_2$  crystals [39].

Another important application of PA effect is the development of Photoacoustic Microscopy [40] which is capable of detecting flaws and defects in solids. This infact is widely being employed in semiconductor industry to carry out the quality control measurements [34].



**References:**

1. A. G. Bell., *Am.J.Sci.*, **20**, 305 (1880)
2. Rayleigh (Lord)., *Nature*, **23**, 274 (1881)
3. M. E. Mercadier, *Phil. Mag.*, **11**, 78 (1881).
4. J. Tyndal, *Proc. Roy. Soc.*, **31**, 307 (1881).
5. W. H. Preece, *Proc. Roy. Soc.*, **31**, 506 (1881)
6. W. C. Roentgen, *Ann. Phys. U. Chem.*, **3,12**, 155 (1881).
7. M. L. Veingerov, *Dokl. Acad. Nauk., USSR*, **19**, 687 (1938)
8. K. F. Luff., *Z. Techn. Phys.*, **24**, 97 (1943)
9. S. M. Luchin., *Dokl. Acad. Nauk., USSR*, **49**, 418 (1945)
10. W. G. Fastie, and A. U. Pfund., *J. Opt. Soc. America*, **37**, 762 (1947).
11. L. B. Kreuzer and C. K. N. Patel, *Science*, **173**, 45 (1971)
12. R. Kaiser, *Cau. J. Phys.*, **37**, 1499 (1959).
13. J. G. Parker., *Appl. Opt.*, **12**, 2974 (1973)
14. A. Rosencwaig and A. Gersho., *Science*, **190**, 556 (1975)
15. A. Rosencwaig and A. Gersho. *J. Appl. Phys.*, **47**, 64 (1976).
16. H. S. Bennett and R. A. Forman, *Appl. Opt.*, **15**, 2405 (1976).
17. L. C. Aamodt, J. C. Murphy and J. G. Parker, *J. Appl. Phys.* **48**, 927 (1972).
18. G. C. Wetzel and F. A. McDonald., *Appl. Phys. Lett.*, **30**, 252 (1977).
19. R. S. Quimby and W. M. Yen, *Appl. Phys. Lett.*, **95**, 43 (1979).
20. Guli, *Appl. Opt.*, **5**, 955 (1982).
21. A. Rosencwaig, *Rev. Sci. Instrum.*, **48**, 1133 (1977).

22. F. A. McDonald and G. C. Wetsel, *Bull. Am. Phys. Soc.*, **22**, 295 (1977).
23. A. Rosencwaig, In 'Advances in Electronics and Electron Physics', Vol. 46, (L. Marton Ed.), New York, Academic Press (1978).
24. A. C. Tam. In 'Ultrasensitive Spectroscopic Techniques', Ed., D. Kliger (New York: Academic Press) (1982).
25. C. K. N. Patel and R. J. Kerl, *Appl. Phys. Lett.*, **30**, 578 (1977).
26. A. C. Tam and C. K. N. Patel, *Appl. Opt.*, **18**, **19**, 3348 (1979).
27. A. C. Tam., *Rev. Mod. Phys.*, **58**, **2**, 381 (1986).
28. G. A. West, J. J. Barrett, D. R. Siebert and K. V. Reddy, *Rev. Sci. Instrum.*, **54**, 797 (1983).
29. C. K. N. Patel and A. C. Tam., *Appl. Phys. Letts*, **36**, 7 (1980).
30. H. Coufal, F. Trager, T. J. Chuang and A. C. Tam., *Surf. Sci.*, **145**, L504, (1984).
31. R. S. Quimby and W. M. Yen., *J. Appl. Phys.*, **51**, **3**, 1780 (1980).
32. A. Rosencwaig., *Annal. Chem.*, **47**, 592A (1975).
33. D. Balasubramnian and Ch. Mohan Rao, Digest of the 4th International Topical Meeting on Photoacoustic, Thermal and Related Sciences, Ville D'estereel (Qubec), Canada, 1985, paper Th. 1.1
34. R. Rosencwaig, 'Photoacoustic and Photoacoustic spectroscopy' (New York: Wiley and Sons) (1980).
35. M. J. Adams, *Prog. analyst. atom. Spectrosc.*, **5**, 153 (1982).
36. M. J. Adams, A. A. King and G. F. Krikbright., *Analyst*, **101**, 73 (1976).

37. Patrick Poulet, Ph.D. Thesis, L' Universite Louis Pastere de Strasbourg, France (1985).
38. P. Korpium, J. Appl. Phys., 51 12, 6115 (1980).
39. T. Somasundaram, P. Ganguly and C. N. R. Rao, J. Phys. C., 19, 2137 (1986).
40. A. Rosencwaig, J. Photoacoustics., 1, 1, 75 (1982).

## CHAPTER III

### EXPERIMENTAL SET UP FOR A PHOTOACOUSTIC MEASUREMENT SYSTEM AND SOME OF ITS APPLICATIONS

#### ***Abstract***

*This chapter deals with some specific aspects of PA instrumentation. It essentially describes the fabrication of a light chopper and a PA cell developed for the present experimentation. The complete details regarding the use of PA set up as a sensitive laser power meter are presented. The utility of this power meter in the atmospheric visibility measurements is illustrated.*

### 3.1 Introduction :

The PA effect provides an efficient method by which the absorption process in a sample is measured indirectly by monitoring the change in pressure in the PA cell. This phenomenon is not wavelength limited and PA measurements have been recorded in the ultraviolet, visible, infrared and microwave region of the spectrum [1]. Therefore this technique can be effectively utilised as a prominent and sensitive tool for measuring the absorption process in a material with utmost efficiency [2,3]. Since a PA experimental set up consists of various subsystems like intensity modulated light source, PA cell and electronics for signal processing, the overall sensitivity of the experimental set up depends entirely on these subsystems. Consequently a careful design of these elements ensures a better accuracy and sensitivity for PA measurements.

In the early stages of the developments of PA effect various types of PA spectrometers were used [4] and the sensitivity was relatively low. But after the advent of lasers and sophisticated signal processing techniques the efficiency of these spectrometers were found to be large enough to detect even very weak absorption process in the sample [5]. Recently commercial PA spectrometers are available which provides extremely high sensitivity [6].

In this chapter a detailed account of the instrumentation needed for PA set up is given. It mainly describes the fabrication details and performance of an optical chopper used for intensity modulation and a non-resonant PA cell. The use of this PA cell as a sensitive laser power meter is described here in detail and the application of this power meter in the atmospheric visibility measurements using a He-Ne laser is given.

### 3.2 Details of the PA experimental set up :

A typical PA experimental arrangement will require the subsystem as shown in fig. 3.1. The important components needed are :

1. Light source
2. a means of modulating the intensity of the light source [e.g. by pulsing of laser sources or by using a mechanical chopper]
3. PA cell incorporating a sensitive microphone.
4. the electronics used for data acquisition and processing.

The details of these items are given below :

#### 3.2.1 Light sources :

Two general classes of light sources are commonly being used in PA studies. The first type includes arc lamps, filament lamps and glow bars, while the second type includes the lasers. The details of the various light sources are already described in chapter II. In the present experimentation lasers have been used as light sources. Discrete wavelengths from He-Ne laser (Jodon, USA) and argon ion laser (Spectra

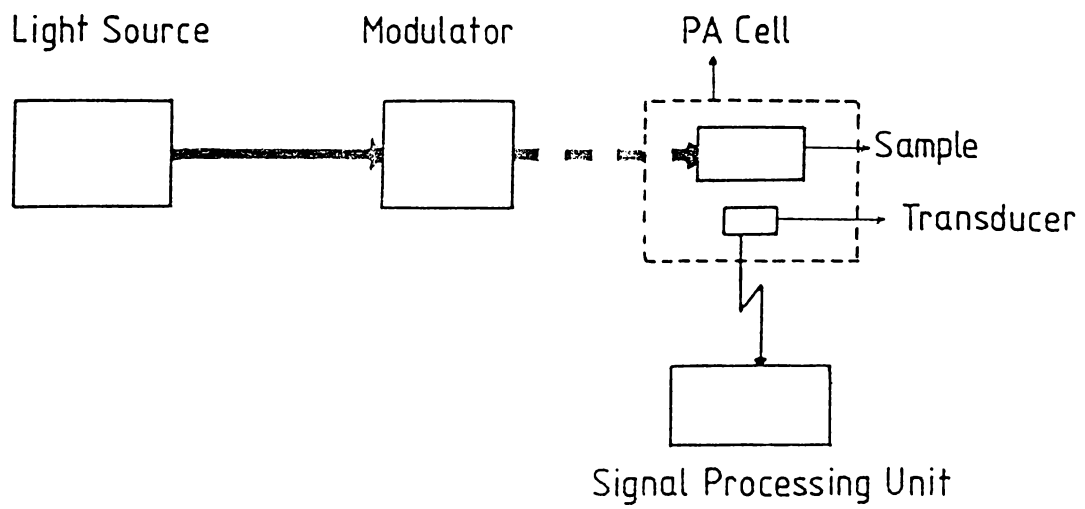


*Fig. 3.1 A schematic representation of the PA experimental set up*

Physics, USA) have been employed to study the performance of the PA set up developed in the laboratory. Similarly, a tunable ring dye laser (Spectra Physics, USA) has been used to study the wavelength response of the PA cell.

### 3.2.2 Modulation :

Modulation of the light source is a necessary requirement for the production of the PA signal as this generates the periodic heating and cooling of the samples which in turn produces the PA signal. The most common method adopted for modulation is the use of a simple rotating sector driven by a motor. Very often these mechanical choppers are designed to be used along with a lock-in amplifier for the purpose of synchronous detection. On many occasions the trigger pulse to drive the reference channel of the lock-in amplifier is derived from the chopped beam itself by using a beam splitter and photodiode arrangements.

But the use of such a beam splitter may cause additional attenuation of the beam which can affect the total sensitivity of the system. Commercially available light choppers with built-in reference voltage facility often have only a fixed output. Voltage waveshape and the phase accuracy may be lost, when such measurements have to be made as in the case of PA experiments [7]. Therefore a mechanical chopper is fabricated which provides an adjustable reference voltage having the required output waveshape designed to give maximum phase accuracy when used with a lock-in amplifier [8].



The details of the design of the chopper are shown schematically in fig. 3.2. The symmetrical sector type chopper wheel is made out of black perspex sheet of thickness 2 mm. The diameter of the wheel is 11 cms. and it has a hole at the centre enabling this to be fixed on to the shaft of a small DC motor. This wheel is mounted vertically and it is driven directly by a 6V DC motor working on a stabilised power supply shown in fig. 3.3. Here the 230V AC supply is rectified using two diodes (ISMI) and smoothened by using a combination of 1000  $\mu\text{F}$  and 0.1  $\mu\text{F}$  capacitors. A zener diode of 6.2V is connected to provide a constant voltage and SL 100 transistor connected in series with the zener diode regulates the output voltage in the circuit. This is further filtered by using a 10  $\mu\text{F}$  capacitor and is fed to the DC motor.

This stabilised power supply thus ensures a constant speed of revolution for the motor which provides better stability for the chopper.

Since a reference signal with sufficient amplitude is often necessary to drive a lock-in amplifier, provisions are made for obtaining such a reference output from the chopper unit itself. This is achieved by using a lamp and a photodiode arrangement provided with stabilised DC power supply. The bias voltage required for photodiode is derived from the same power supply. The photodiode is connected to the base of the transistor so that it amplifies the current variation in the base due to the action of the photodiode. As the light beam from the lamp falls on the photodiode it induces an increase in the reverse current flow in the photodiode which in turn provides sufficient base current

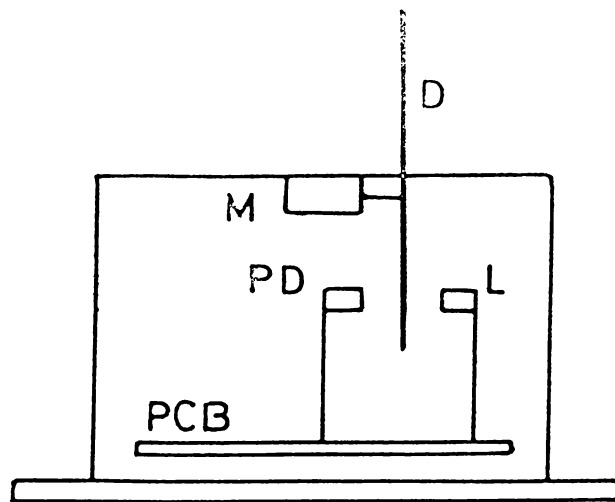
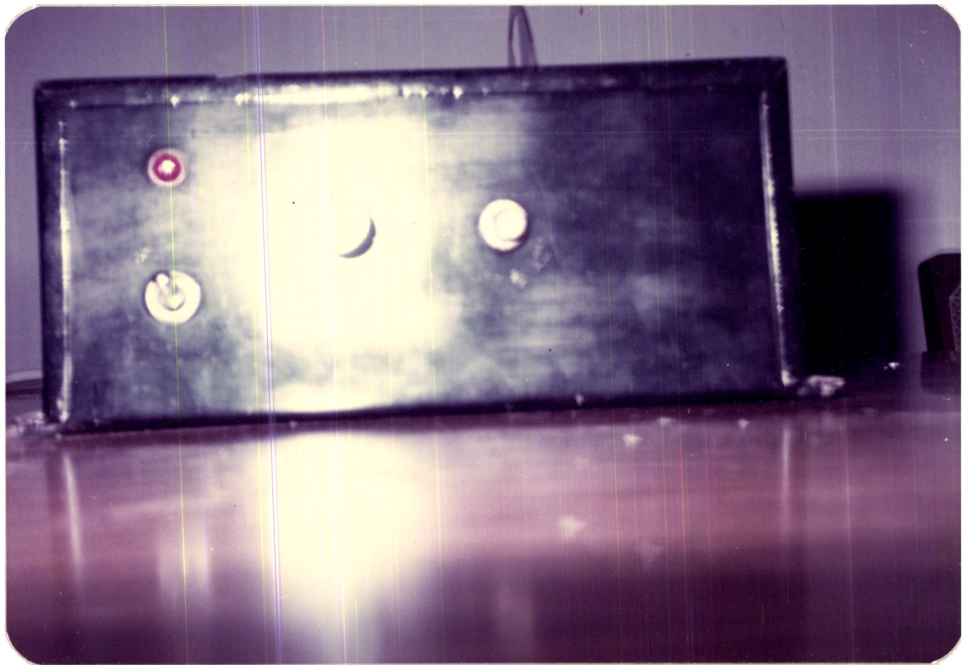


**Fig. 3.2** Schematic representation of the optical chopper.

*D - Acrylic disc, M - Motor, PD - Photodiode,  
L - Lamp, PCB - Printed Circuit Board*





*Photograph of the mechanical chopper*

to the transistor to drive it into conducting stage. Thus the amplified signal derived from the photodiode after further wave shaping provides the reference voltage output. A silicon signal diode connected on the output side clips the original symmetric wave form below  $-0.6\text{V}$  whereas the positive level is limited at  $10.9\text{V}$  by the zener diode. This arrangement gives the appropriate relative magnitude for positive and negative voltage swings. For example, at a reference voltage of  $1\text{V}$  peak to peak, the positive part is  $900\text{ mV}$  while the negative part is  $100\text{mV}$  as shown in fig. 3.4. Such a wave form is often recommended for maximum phase accuracy in commercial lock-in amplifier [9]. Reference level can be adjusted by the potentiometer ( $22\text{K}\Omega$ ) connected across the output of the system.

The entire power supply system and motor is enclosed in a black-end aluminium box measuring  $20 \times 10 \times 13\text{ cm}^3$ . The upper portion of the chopper wheel, which projects outside the rectangular aluminium box through a slot made on the top of it, chops the light beam as the wheel rotates at a fixed speed. At the same time the lower portion of the wheel which is well inside the enclosure chops the light beam falling on the photodiode from the lamp kept inside the box. Thus the light beam from the internal light source is periodically interrupted from falling on the photodiode in synchronism with the chopping action of the external light beam.

Since the motor rotates at a fixed speed, different blades are used to get various frequencies. These discrete frequencies possible

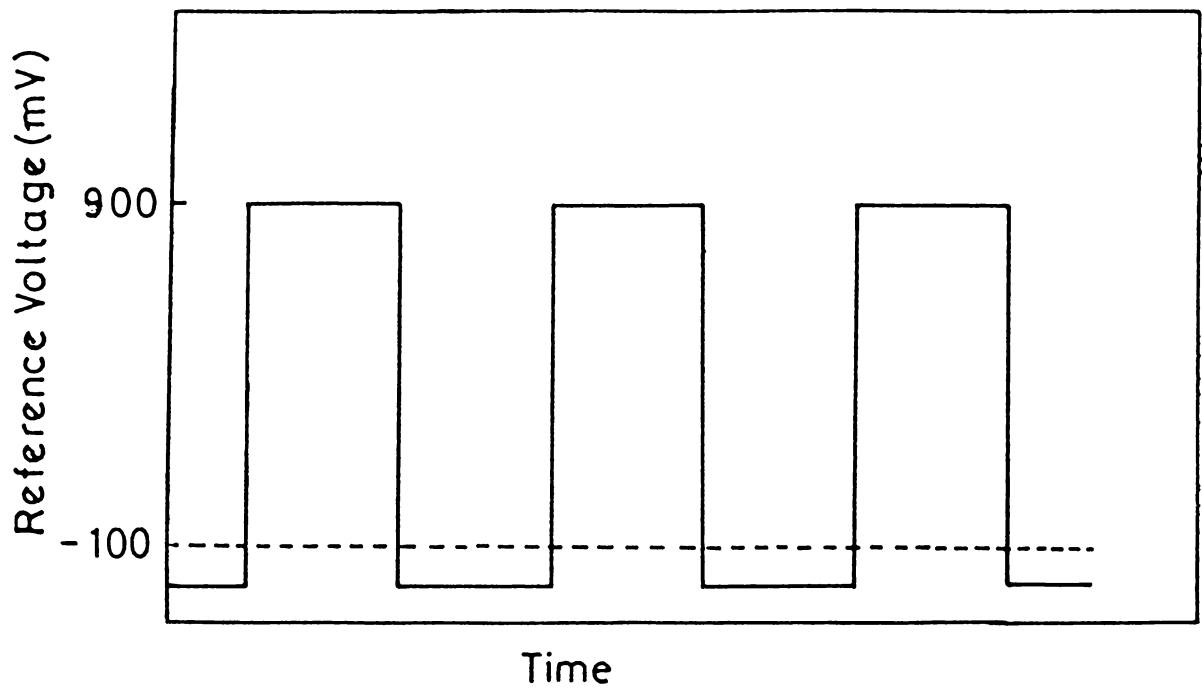


*Fig. 3.4 Reference output voltage from the chopper*

with different chopper wheels are 74, 146, 220 and 441 Hz as measured with a frequency counter. The blades are in the form of sectors of the circles enclosed between two radii with an angle equal to  $90^\circ$  for the two blade system and  $15^\circ$  for 12 blade system. Acoustic isolation has been achieved with proper rubber mountings at the base of the system. An indicator lamp, variable output control and a BNC connector are fixed on a side panel of the enclosure. This chopper is found to give very good long term stability and it shows a variation of only 0.1Hz per hour.

### 3.2.3 PA cell :

The PA cell can be considered as the heart of the PA spectrometers and the literature contains many references to cell designs both for general use and more limited, special applications [10]. The ultimate aim in cell design is to maximise the signal to noise ratio. Therefore in order to achieve maximum sensitivity, there are certain criteria [11] which govern the design of the PA cell are,

- a) The acoustic isolation of the cell from external vibrations. To achieve this one should as far as possible use chopping frequencies different from those present in the acoustic and vibrational spectrum of the environment. In addition to this, the walls of the PA cell should be fairly thick so that it prevents any acoustic disturbances from interfering with the signal.

External acoustic isolation like vibration free tables also can be used for this purpose.

- b) To minimise any PA signal that may arise from the interaction of the light beam with the walls and windows of the PA cell, the windows must be selected such that they are as much optically transparent as possible for the wavelength region of interest. Also the body of the PA cell should be made out of polished aluminium or stainless steel. Although the aluminium or stainless steel walls absorb some of the incident and scattered light, the resultant PA signal will be quite weak, as long as the thermal mass of these walls is large. A large thermal mass results in a very small temperature rise at the surface and it thus reduces the magnitude of the background signal. In addition to this the cell should be designed in such a way that the scattered light must be a minimum inside the cell.
- c) The PA signal generated in the cell should be as high as possible to detect it with a sensitive microphone placed in the PA cell. The amplitude of the PA signal varies in an inverse manner with the cell volume and therefore it is necessary to keep the cell volume as small as possible to achieve an appreciable signal to noise ratio. The dimensions of the cell, however should not allow the acoustic signal produced from the sample surface to suffer appreciable dissipation at the cell window or cell walls. The distance between the sample surface and the cell window



should always be greater than the thermal diffusion length in the gas medium adjacent to the sample. Therefore an optimum gas column length  $l_g$  should be provided for a maximum PA signal amplitude, and the PA signal decreases for both larger and smaller  $l_g$ . Experimentally the optimum value for  $l_g$  is found to be [12].

$$l_g = 1.8\mu g \quad (3.01)$$

where  $g$  is the thermal diffusion length in the gas. From this it is obvious that the PA signal amplitude is directly related to the thermal diffusion length in the gas which in turn depends on the physical properties of the gas medium. Thus a careful selection of the gas medium can somehow enhance the signal to noise ratio. Recent investigations reveal that helium gas improves the sensitivity of the PA cell by a factor of 3.2 compared with that for  $N_2$  gas at the same chopping frequency [12]. This is because helium gas possesses large thermal conductivity which enhances the thermal diffusion process through the gas medium.

Considering the operation of the PA cells, it can be broadly classified into two groups. They are resonant and non resonant PA cells. Resonant cells which utilises the longitudinal or radial resonances occur in the cylindrical cavity of the PA cell when the PA signal frequency becomes equal to the inherent frequency of the PA cell. Therefore

when these two frequencies are exactly same, maximum acoustic energy transfer occurs in the PA cell which essentially increases the PA signal amplitude. These types of PA cells are often used with a single modulation frequency which is the same as the resonant frequency so as to increase the signal to noise ratio.

Since the PA cell is a simple cylinder of radius  $a$  and a length  $l$  the continuity equation for the pressure variation in the cell can be expressed in spherical polar coordinates as

$$\frac{1}{r} \frac{\partial}{\partial r} \left( r \frac{\partial p}{\partial r} \right) + \frac{1}{r^2} \frac{\partial^2 p}{\partial \theta^2} + \frac{\partial^2 p}{\partial z^2} + k^2 p = 0 \quad (3.02)$$

where  $p$  represents the pressure variation in the cell. The solution of the above equation can be written as [13].

$$p = \frac{\cos}{\sin} (m\phi) \left[ A J_m(k_r r) + B N_m(k_r r) \right] \left[ C \sin(k_z z) + D \cos(k_z z) \right] \quad (3.03)$$

where  $J_m$  and  $N_m$  are Bessel functions of the first and second kind respectively. For a cylinder  $B = 0$  since  $N_m(0) = \infty$ . To satisfy the boundary conditions, the gradient of  $p$  normal to the cell wall must be zero. Thus,

$$\left[ \frac{\partial p}{\partial r} \right]_{r=a} = 0 \quad (3.04)$$

and

$$\left[ \frac{\partial p}{\partial z} \right]_{z=0} = 0 \quad (3.05)$$

This then sets  $C = 0$  in eqn. (3.03). Therefore,

$$k_z = \left[ \frac{\pi}{l} \right] n_z \quad (3.06)$$

where  $n_z = 0, 1, 2, 3, \dots$

$$K_r = \frac{\pi \alpha_{mn}}{a} \quad (3.07)$$

where  $\alpha_{mn}$  is the  $n$ th root of the equation involving  $m$ th order Bessel function. Thus

$$p = \frac{\cos(m\phi)}{\sin(m\phi)} [A J_m(k_\lambda r)] [D \cos k_z z] \quad (3.08)$$

substituting this value in eqn. (3.02) and expressing  $K = \omega/c_0$ , the resonant frequency of the PA cell is

$$\omega = c_0 [k_z^2 + k_\lambda^2]^{1/2} \quad (3.09)$$

where  $c_0$  is the velocity of sound. This expression represents the frequency at which resonance occurs in the PA cell with a cylindrical cavity. Therefore in order to fabricate a resonant PA cell the dimensions must be appropriately selected to achieve cell resonances governed by the above relation.

Another class of PA cell is the Helmholtz resonator [14]. It essentially contains three volumes, the sample chamber, the microphone housing chamber and an interconnecting channel between these two chambers. The gas column to the interconnecting channel can be considered to form a plunger as it moves from one chamber to the other chamber during the PA signal generation. Therefore the gas column essentially experiences a restoring force proportional to its displacement along the channel. Consequently the resulting pressure oscillation in

the microphone chamber is equivalent to that of a damped harmonic oscillator. Hence the signal enhancement occurs when the signal modulation frequency becomes equal to the resonant frequency of the cell  $F$  given by :

$$F = \frac{C}{2\sqrt{\pi}} R \left[ \frac{V_1 + V_2}{V_1 V_2 (L + 1.7R)} \right] \quad (3.10)$$

where  $C$  is the velocity of sound in the gas medium,  $R$  is the radius of the interconnecting channel,  $V_1$  is the volume of the sample chamber,  $V_2$  the volume of the microphone chamber and  $L$  is the length of the connecting channel [15]. The details of construction of such a cell are described in the literature [16].

However, for the present experimental set up a non-resonant PA cell has been designed and fabricated and it is shown in fig. 3.5. A commercially available electret microphone (Model 1753, Knowles, USA) is used as the pressure transducer kept within the PA cell. This microphone has a flat frequency response upto 3 KHz and sensitivity is 6 mV/Pa. Its dimensions are small enough to accommodate the same in a miniature PA cell. The PA cell is machined from a cylindrical block of aluminium which satisfies the criteria described in section 3.2.3. The body of the cell has 5 cms diameter having a length 5 cms. The cavity is made by drilling an axial bore of diameter 1 cm. The entrance and exit windows are held tightly in position by means of two annular aluminium discs (5 cms in diameter) with the help of o-rings and screws. This arrangement provides vacuum sealing of the cell and therefore considerable amount of external noise reduction can be achieved.

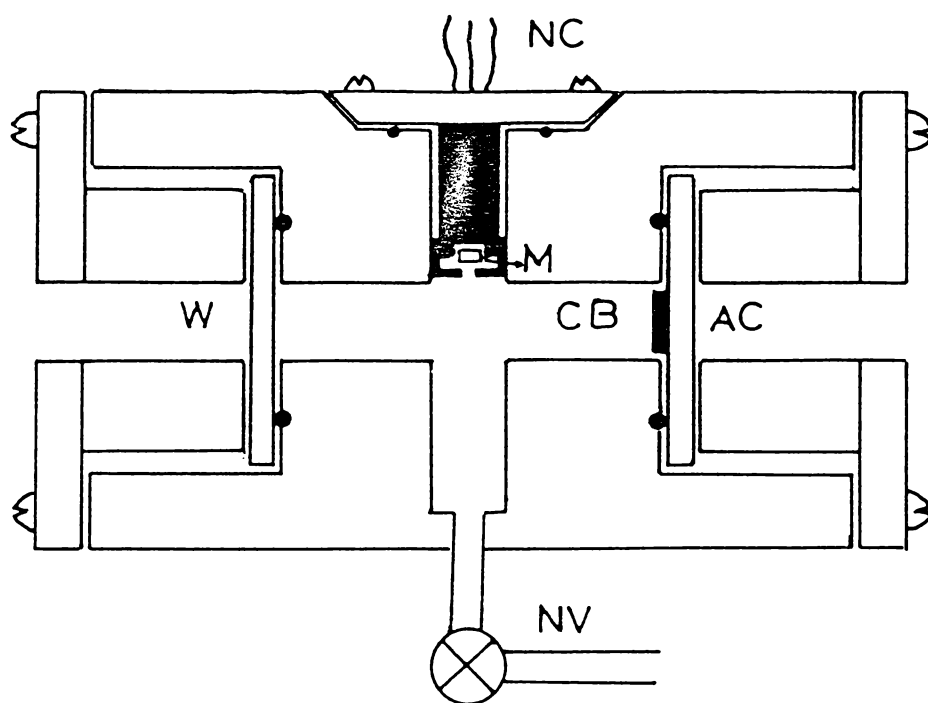


*Fig. 3.5 Schematic diagram of the PA cell.*

*M - Microphone, NC - Nylon cap, W - CaF<sub>2</sub> window,  
CB - Carbon black, AC - Acrylic disc, NV - Needle valve.*

The entrance window is placed at a couple of thermal diffusion length (which corresponds to the lowest modulation frequency possible) in air away from the microphone, whereas the exit window at which the sample is attached is kept close to the microphone. The volume of the PA cell constructed is approximately  $4 \text{ cm}^3$  which is found to give an appreciable PA signal amplitude [17]. The resonance occurs at 1.62 KHz which is always well beyond the operating range of the PA cell. However, this cell can be effectively employed to get the PA spectrum in the case of weakly absorbing species at the resonant frequency of the PA cell. This cell has the added advantage that it can be used to carry out experiments with solid and also with gas phase samples. By using the needle valve attached in the PA cell, different gases can be fed into it and the absorption of these gases can be studied in detail. Similarly an adapter is provided near the exit window which can be inserted into the cavity to mount the solid sample rigidly.

Electrical leads are taken out through a nylon housing provided for the encapsulation of the microphone as shown in fig. 3.5. This nylon housing is tightly fixed to the PA cell using O-rings and screws and this in fact provides an efficient sealing for the microphone. Nylon housing is used to prevent any short circuiting between microphone leads which can damage the electret microphone. BNC connectors are provided for the leads to connect the output to the signal processing unit. A polished circular calcium fluoride disc of diameter 20 mm is used as the entrance window since this material provides low absorption in the uv, visible and mid infrared region. This PA cell shows extreme

sensitivity and the design is such that the PA signal is almost free from the effect of external acoustic noises. This design therefore improves the signal to noise ratio.

### 3.2.4 Signal Processing :

The most common electronic system employed for extracting and amplifying the PA signal is the lock-in amplifier with phase sensitive detection. The phase sensitive detector can be simply represented by a two position switch which alternately gates the signal or inverted signal into a low pass filter. When the signal and the suitable reference input have the same frequency and are in phase, the output of the lock-in amplifier shows the time average amplitude of the signal. A phase difference between the signal and the reference affects the output of the lock-in amplifier. Generally the signal voltage be represented as

$$e_s = E_s \cos(\omega t + \phi) \quad (3.11)$$

where  $e_s$  the amplitude of the signal,  $\omega$  the frequency of modulation and  $\phi(t)$  is the phase angle. The corresponding reference signal derived from the chopper be

$$e_r = E_r \cos \omega t \quad (3.12)$$

The output of the multiplier is given by the product of the above terms. Therefore the output voltage can be represented as

$$V_{out} = e_s e_r = E_s E_r \cos(\omega t + \phi) \cos \omega t \quad (3.13)$$

which can be written as

$$V_{\text{out}} = 1/2 E_s E_r [\text{Cos}(2\omega t + \phi) + \text{Cos}\phi] \quad (3.14)$$

The first term is an AC signal occurring at twice the frequency of modulation and the second term is a DC term. A low pass filter is used to remove the AC signal and the remaining term is

$$V_{\text{out}} = 1/2 E_s E_r \text{Cos}\phi \quad (3.15)$$

which represents the output of the lock-in amplifier. From this it is evident that the output of the lock-in amplifier is a DC voltage which is proportional to the signal amplitude and magnitude of the phase angle. Many technical details regarding phase sensitive detection system is described in the literature [18]. From the above expression a phase shift of  $\pi/2$  degrees reduces the output to zero, while a phase shift  $\pi$  results the original amplitude but reverse polarity. To monitor the phase shift between the reference signal and the PA signal an external phase adjustment is provided at the reference channel of the lock-in amplifier. Therefore in order to measure the phase shift, the potentiometer provided for creating additional phase shift is adjusted to get a maximum signal in the lock-in amplifier. Thus the reading of the calibrated potentiometer directly gives the phase angle between the reference signal and PA signal. The lock-in amplifier also provides filtering out of voltage fluctuations at a frequencies other than the



reference frequency. Thus the device is fully capable of rejecting noise and it therefore serves as a filter and line rectifier. Consequently lock-in amplifier itself provides an efficient way of signal processing which substantially improves the signal to noise ratio.

In the present experimentation, a commercially available lock-in amplifier (Model 5101, EG&G, Princeton Applied Research Corp.) is used. This system provides a signal detection level from  $0.05 \mu\text{V}$  to 250 mV with adjustable steps in between this range. Phase difference between the signal and reference can be directly recorded from the lock-in amplifier. The noise level in the signal can be further limited by selecting appropriate time constants. The signal level can be directly read off from the meter provided at the front panel of the lock-in amplifier or recorded on a chart recorder.

### 3.3 Conversion of the PA cell into a laser power meter :

This PA set up described in proceeding sections could be effectively converted into a sensitive laser power meter [19]. There are standard commercial optical detectors which works on the basis of thermoelectric effect, photovoltaic effect [20] and proton drag phenomenon [21]. The most sensitive device in this category is the Golay cell [20] which has a noise equivalent power of  $10^{-10}$  watts  $\text{Hz}^{-1/2}$ , but it is less sensitive in the higher ranges of modulation frequencies of the incident intensity. Further its response is limited to low intensity levels. The laser power meter developed in the present investigation possesses

a fairly large dynamic range, a flat wavelength response and it works satisfactorily over a wide range of modulation frequencies. Moreover it is possible to calibrate this device accurately on the basis of Rosencwaig-Gersho theory. This theoretical support ensures its effectiveness as a device for absolute measurement of laser beam intensities.

In the laser power meter described here, the PA signal amplitude is proportional to the intensity of the laser beam falling on the PA cell at a constant modulation frequency. Since carbon black is employed as the sample material in the PA cell it comes under the category of optically opaque and thermally thin samples described in chapter II. Here carbon black acts as a true light trap from X-rays to the far infrared region ( $25 \mu\text{m}$ ) [22] which ensures the generation of the PA signal for incident radiation covering a wide range of frequencies. Since the signal amplitude mainly depends on the optical absorption coefficient  $\beta$  of the sample, the choice of carbon black can yield a greater amount of PA signal in proportion to the intensity of the incident radiation [19]. Rosencwaig in the 1973 [23] formulated a relationship for this case which is as follows.

The acoustic signal obtained from the PA cell is proportional to a term of the form,

$$I(\omega) \kappa(\omega) P_{\alpha}(\omega) f_{\delta}(\omega) f_{\gamma}(\omega) \quad (3.16)$$

where  $I(\omega)$  is the intensity of the illuminating source,  $\kappa\omega$  is the energy of the incident photons,  $P_{\alpha}(\omega)$  is the probability of the incident photons

being absorbed,  $f_g(\omega)$  is the fraction of the absorbed light energy that is converted into photons or heat energy by non radiative process.  $f_r(\omega)$  is the fraction of the phonon energy that is, in turn, imparted to the gas medium in the form of acoustic energy. Therefore from this relation the PA signal in the case of carbon black is strongly dependent on the incident light beam intensity. Based on this theory Rosencwaig could record the complete emission spectrum of the Xe lamp.

Later in 1975 [24] Rosencwaig and Gersho developed a detailed theory by accounting the thermal diffusion process which is already described in chapter II. According to RG theory in an optically opaque and thermally thin sample like a thin layer of carbon black, the PA signal entirely depends on the incident intensity. This is because carbon black possesses a large optical absorption coefficient and hence it generates a greater amplitude of PA signal depending on the intensity falling on sample. Since the sample is thermally thin, the heat diffusion process in the sample is quite rapid so that the thermal waves thus produced due to PA effect suffers minimum attenuation when it reaches to the microphone. The PA signal amplitude in the case of an optically opaque and thermally thin sample is

$$Q \approx \frac{(1-i) \gamma P_0 I_0}{4\sqrt{2} a_g T_0 l_g} \left( \frac{\mu_b}{k_b} \right) \quad (3.17)$$

where  $a_g$  is the thermal diffusion coefficient in the gas,  $\mu_b$  the thermal diffusion length in the backing material,  $k_b$  is the thermal conductivity of the backing material,  $\gamma$  the ratio of specific heat of air which serves

as the gas medium in the PA cell,  $P_0$  is the ambient pressure,  $T_0$  the ambient temperature of the PA cell,  $l_g$  the air column length and  $I_0$  is the incident modulated intensity of the laser. This expression shows that the PA signal amplitude is independent of  $l_g$  and is proportional to the incident intensity.

Since the equation( 3.17) is a complex one, taking the modulus of  $Q$  and the intensity of the laser beam

$$I_0 = \frac{4 T_0 a_g l_g k_b}{\gamma P_0 \mu_b} |Q| \quad (3.18)$$

where  $|Q|$  is the magnitude of change in pressure in the PA cell which can be directly measured from the microphone output. Thus the laser power levels can be theoretically calculated using the above relation which ensures the calibration of the device with extreme accuracy

Based on the above principle, a nonresonant PA cell described in the previous section which employs a commercially available sensitive (6 mV/Pa) miniature microphone (Knowles BT 1753) is effectively converted into a laser power meter. The windows used in the PA cell are a plane glass disc of 90.2% transmittance at normal incidence.  $\text{CaF}_2$  windows also can be used if desired. Air at atmospheric pressure is chosen to be the gas medium in the PA cell. Laser radiation from a CW argon ion laser (Spectra Physics Model 171-17) is chopped at a fixed frequency and allowed to fall on the carbon black sample as shown in fig. 3.6. The PA cell output is processed by the lock-in amplifier. From the

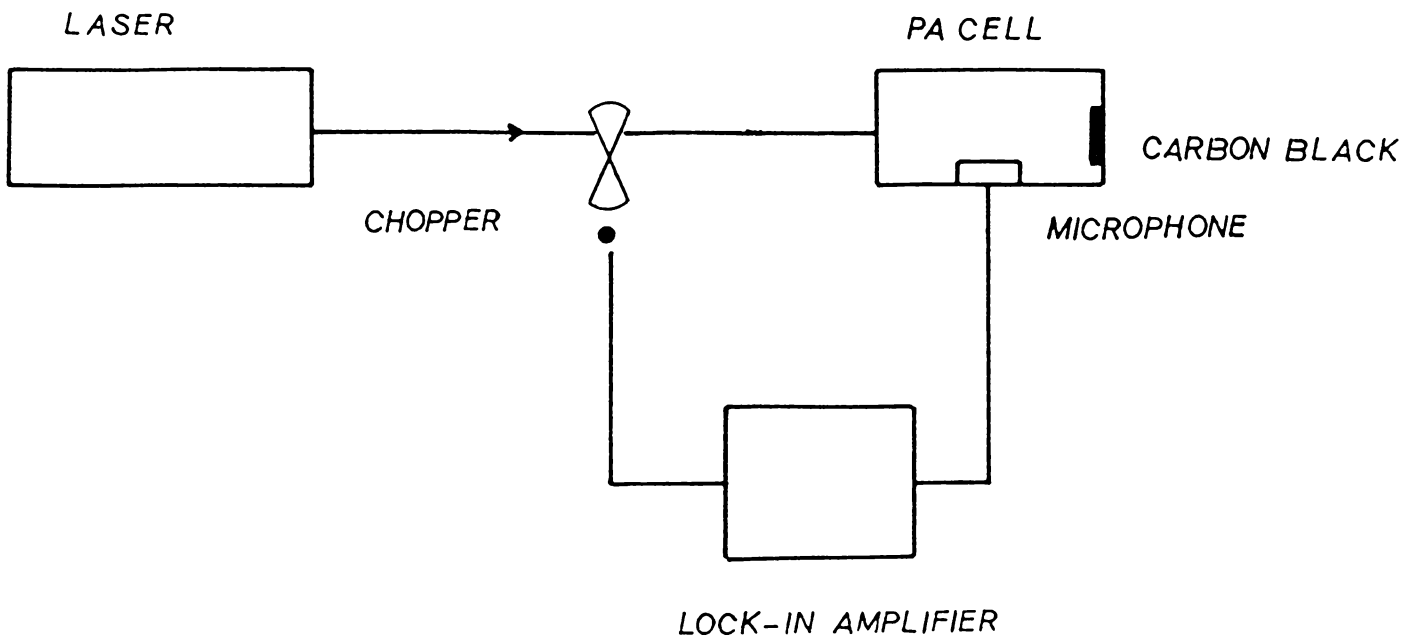


*Fig. 3.6 Experimental set-up for the use of a PA cell as a laser power meter*

measured amplitudes of the PA signal the laser power levels have been theoretically calculated using the above relation. The numerical values of the above constants are taken from the literature and these are summarised in Table 3.1 [25]. The power levels have been theoretically calculated using the above relation and compared with those measured with a standard laser power meter [Scientech Model : 38 - 0101], for three different chopping frequencies. Thus the percentage of deviations from the power meter readings for different calculated laser power levels using the above relation have been recorded and is shown in fig. 3.7. The PA signal amplitudes for various values of incident laser power levels at 514.5 nm are shown in fig. 3.8 for a chopping frequency of 500 Hz. This infact reveals the linear response of the PA signal output with the incident beam intensity as as described by the eqn. (3.18) and consequently this behaviour is very useful for calibration of the device when it is used as a laser power meter. From fig. 3.7 it is evident that the theoretically calculated laser power levels at 78Hz and 300Hz show only a small deviation from the standard laser power meter reading, while at 18Hz it shows a higher deviation. This is because at lower chopping frequencies the thermal diffusion length in the gas is relatively large so that the thermal waves can interact with the walls of the cell which results in additional heat loss. Therefore at relatively low chopping frequencies the heat flow along three mutually perpendicular axes must be considered rather than in a single direction as described in RG theory. This phenomenon in which the heat flow

Table 3.1 Approximate value for various materials of the thermal conductivity, density, specific heat and thermal diffusivity.

<i>Material</i>	$K$ <i>Cal. Sec.<sup>-1</sup> . cm<sup>-1</sup> deg<sup>-1</sup></i>	$\rho$ <i>gm. cm<sup>-3</sup></i>	$C$ <i>cal. gm<sup>-1</sup> . deg<sup>-1</sup></i>	$\alpha = k/\rho c$ <i>cm<sup>2</sup> . sec<sup>-1</sup></i>
<i>Air</i>	$5.7 \times 10^{-5}$	$1.29 \times 10^{-3}$	0.24	0.18
<i>Carbon</i>	$7 \times 10^{-5}$	$5.7 \times 10^{-2}$	0.16	$7.6 \times 10^{-3}$
<i>Glass</i>	$2.5 \times 10^{-3}$	2.5	0.12	$8.3 \times 10^{-3}$

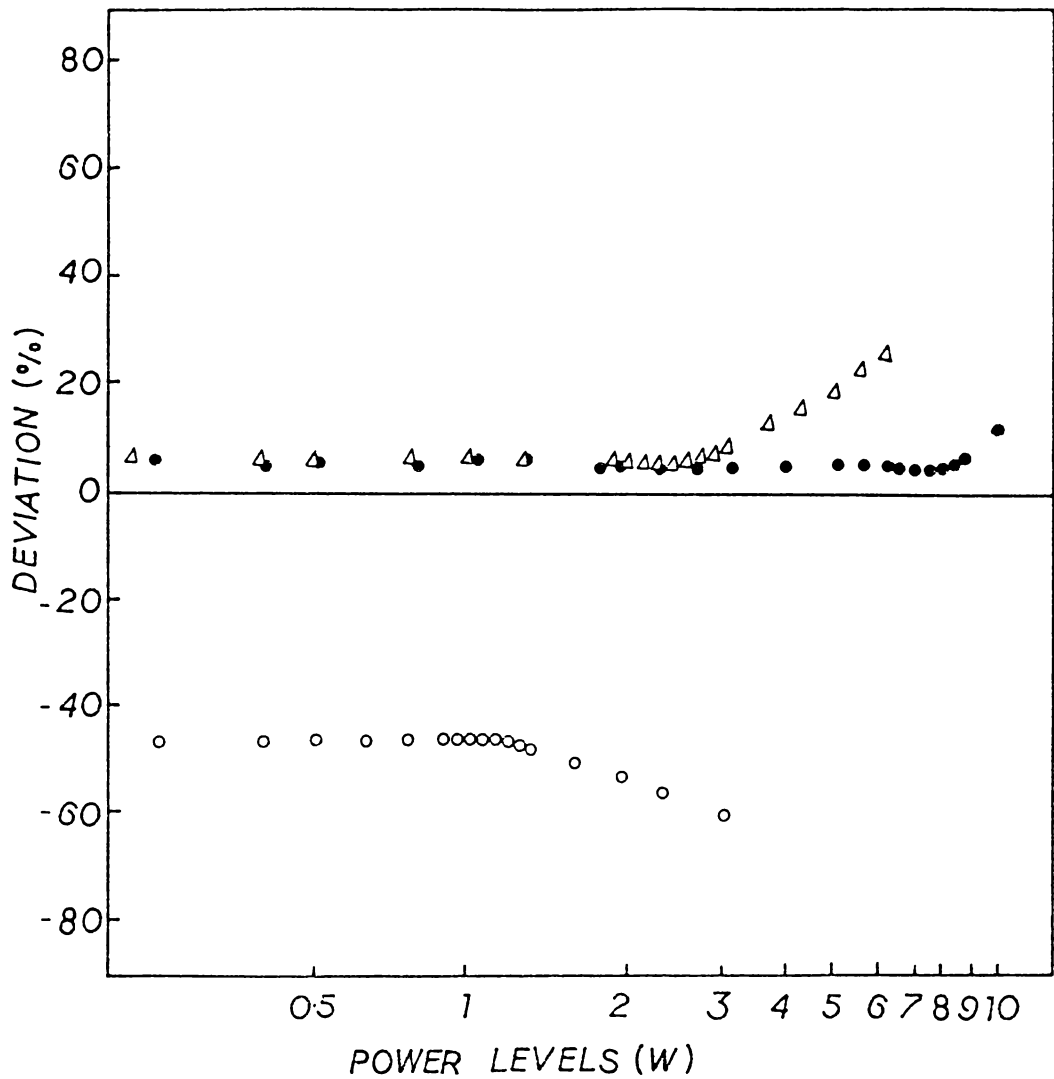


Fig. 3.7 Graph showing percentage of deviation for different power levels at three different chopping frequencies : 0 - 18 Hz;  $\Delta$  - 78 Hz and  $\bullet$  - 300 Hz. (Percentage of deviation is taken as (calculated power standard power meter reading  $\times$  100/standard power meter reading)



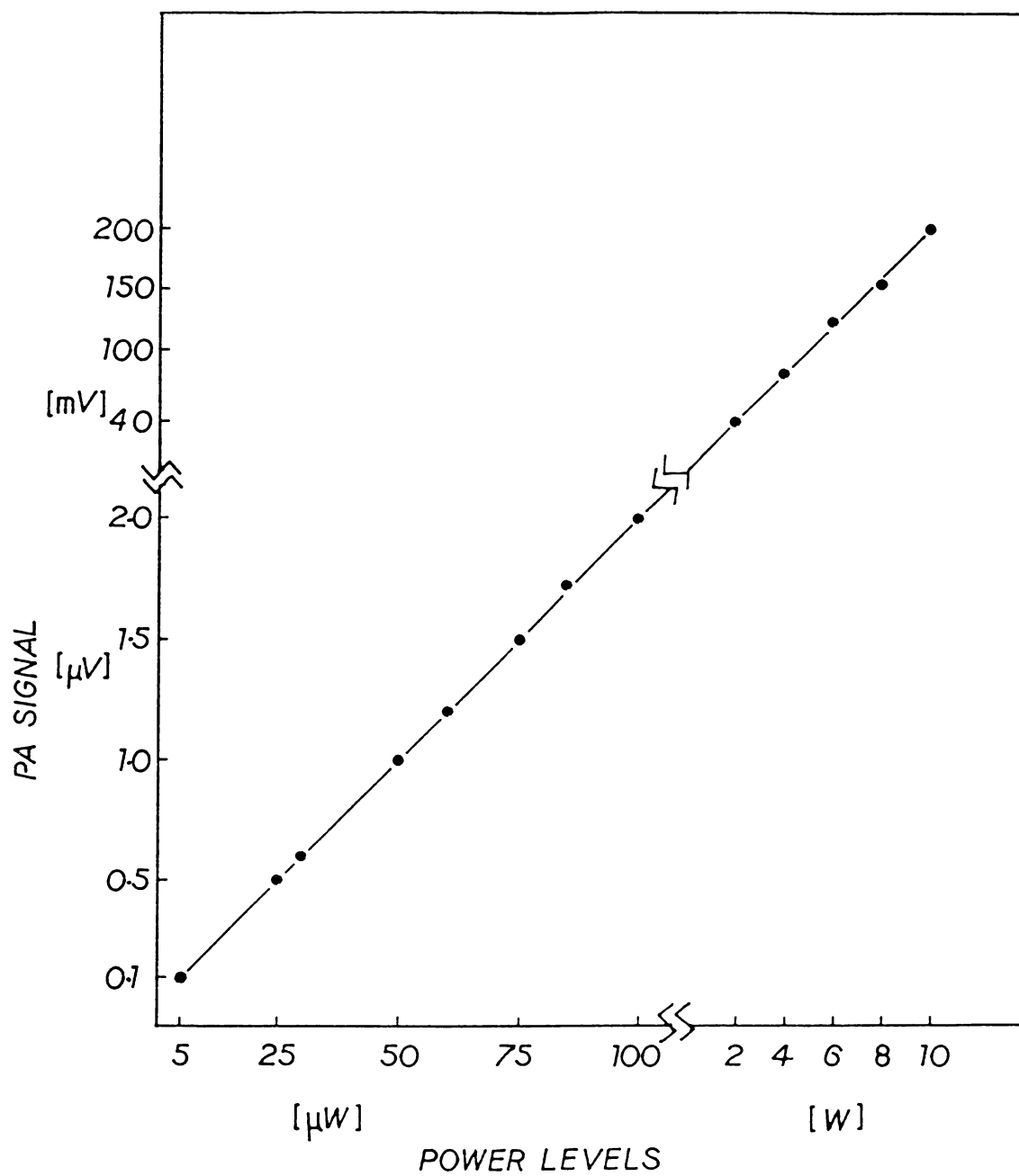
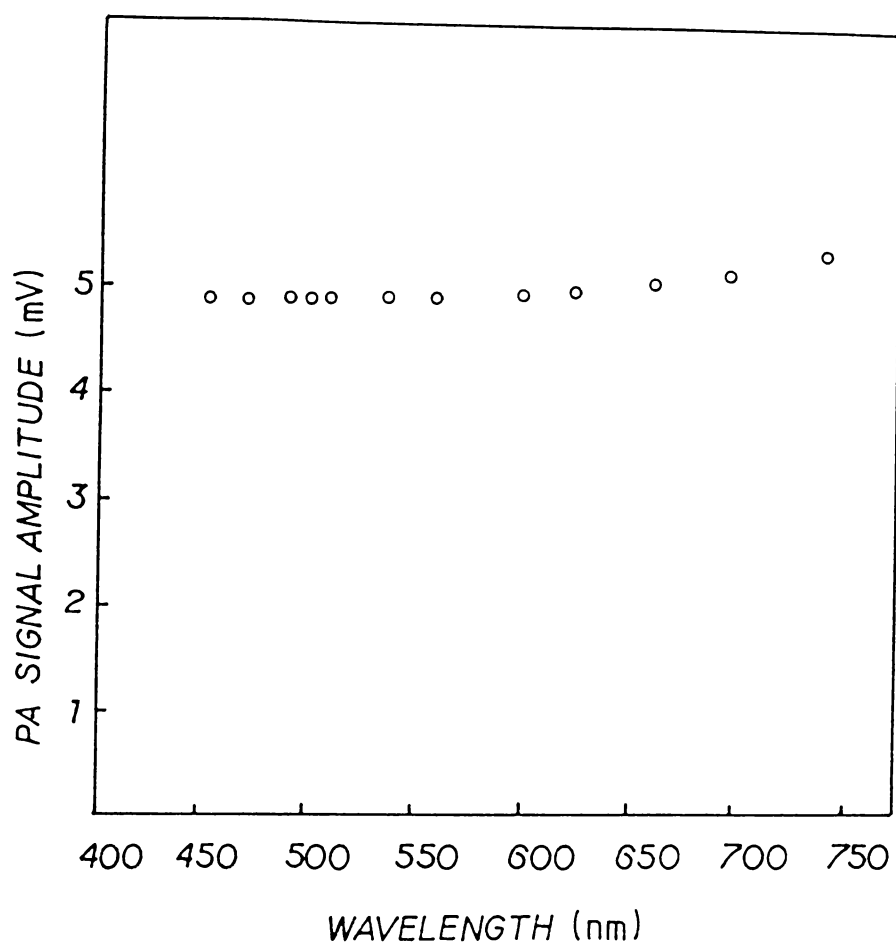


Fig. 3.8 Graph showing the linear behaviour of PA signal at different incident laser power levels obtained using a CW argon ion laser of wavelength  $\lambda = 514.5 \text{ nm}$

along the three dimension in the PA cell at low chopping frequencies is termed as three dimensional heat flow problem which was treated in detail in the context of PA effect by Quimby in 1979 [26]. Thus one may conclude that three dimensional heat flow at 18 Hz causes a reduction in PA signal amplitude which creates a large percentage of deviation as shown in fig. 3.7. As the chopping frequency increases, heat flow will become confined in one direction as described in RG theory because the thermal diffusion length will then be further reduced at the higher chopping frequencies. Moreover as the microphone response is found to be virtually identical at 18 Hz and 78 Hz, the 3 dimensional heat flow can be the main reason for the larger percentage of deviation observed at 18 Hz. In carbon black, since the heat generated within the thermal diffusion length is fully transferred to the air medium surrounding the sample, the PA signal increases with the intensity at lower power levels. But at higher laser power levels, though the incident intensity is high, the optical absorption length  $1/\beta$  is less than thermal diffusion length in the carbon black when the chopping frequencies are fairly low. Consequently the PA signal variation is no longer linear with respect to the laser power variation at higher power levels for a fixed modulation frequency. This may cause a saturation of the PA signal output at higher power levels resulting in a larger deviation in this region as can be seen from fig. 3.7. However an increase in the chopping frequency can shift the saturation regime as can be seen from the plot for 300 Hz. But the thermal diffusion length and hence the PA signal amplitude are inversely proportional to the chopping

and hence an increased chopping rate gives a smaller signal to noise ratio. Thus a frequency range between 30 Hz and 500 Hz is found to be satisfactory for most practical purposes. Since carbon black is employed as the sample material in the PA cell the response of the cell remains the same over a wide range of wavelengths. This is experimentally verified by using laser beams at discrete wavelengths derived from different laser sources (Spectra Physics Argon ion laser, Model : 171-17, Ring dye laser, Model 380 A). In this case a fixed laser power level of 250 mW is allowed to be incident on the carbon black and the corresponding PA signal is recorded. This is repeated for different wavelengths and a graph is plotted between wavelengths and corresponding PA signal is shown in fig. 3.9. From this it is evident that the PA laser power meter works satisfactorily over a wide range of wavelength. However, there is a slightly enhanced response in the 750 nm region and this presumably, is due to the inherent direct heating of the gas medium due to absorption at this wavelength. This effect can be minimised by filling PA cell with an inert gas like helium which in turn can enhance the PA signal due to its large thermal conductivity. A proper choice of the window material is needed for the measurement of intensities in the ultra violet and infrared region.

The maximum power level which the PA cell measures in this experiment is 10 W with a chopping frequency of 500 Hz. However, a similar device is effectively utilised in measuring a CW CO<sub>2</sub> laser operating at 30 W power level at 10.6 $\mu$ m region and a detailed account of



*Fig. 3.9* Variation of PA signal with wavelength for an input laser power of 250 mW at a chopping frequency 500 Hz.

the same is presented in chapter VI. Therefore higher intensities can be directly measured by using such devices with appropriate chopping frequencies. This evidently is one of the outstanding advantages of this system over other detectors which generally saturates at higher intensity levels. Also an absolute determination of the power levels using RG theory is possible in this case. This power meter is thus found to be useful to measure an intensity level as small as  $5 \mu W$  on the lower intensity side and several tens of watts on the higher intensity side. This lower detectable limit provides a noise equivalent power of about  $5 \times 10^{-6} \text{WHz}^{-1/2}$  and which gives a signal to noise ratio of  $10^3 \text{Hz}^{-1/2}$  at 5mW laser power with a chopping frequency of 500 Hz. Therefore considering its dynamic range, sensitivity and wavelength response, it shows excellent improvement over similar devices which use a gaseous absorbing medium described in the literature [27].

The PA laser power meter described in the previous section is efficiently employed as a detection system for atmospheric attenuation studies using a He-Ne laser [17]. Very often detectors like photodiodes and photomultiplier tubes are used in these experiments to determine the variation of the intensity of the laser beam after it is allowed to propagate through a certain region of the atmosphere. If the variation of the laser beam is small enough to develop any appreciable change in the output voltage due to saturation effects then these detectors are not very much useful to carry out atmospheric attenuation measurements. Therefore a detector with large dynamic range must be employed

in these experiments. The PA laser power meter described above could be effectively used to monitor the atmospheric visibility. The experimental set up used to measure the laser beam attenuation in the atmosphere is shown in fig. 3.10. The beam from a 5 mW He-Ne laser (Jodon, USA ) is chopped by means of an optical chopper at 440 HZ described in the previous section. A plane mirror kept at 30 meters from the laser returns the beam to the PA cell kept adjacent to the light source. The signal from the PA cell is given to a pre-amplifier with adjustable gain. The output from the pre-amplifier is fed to a lock-in amplifier (Model 5101, EG & G PARC) along with the reference voltage derived from the chopper. The lock-in amplifier output is given to a chart recorder for continuous monitoring. The original intensity of the laser beam is monitored by a laser power meter which receives a part of the beam before chopping (instead of a laser power meter, a photodiode also may be used).

Fig. 3.11 gives a typical variation of relative attenuation of laser beam over a 24 hour period in Cochin University campus (in the month of February). From this it is clear that the attenuation of laser beam is maximum at 2 a.m. in the night. Evidently this is due to the formation of fog present in the atmosphere. The gases like  $\text{NH}_3$ ,  $\text{SO}_2$  etc., released from the nearby industries also contribute to the reduction in the intensity at this hour of the day. This value of attenuation will include scattering as well as absorption losses of the laser beam.

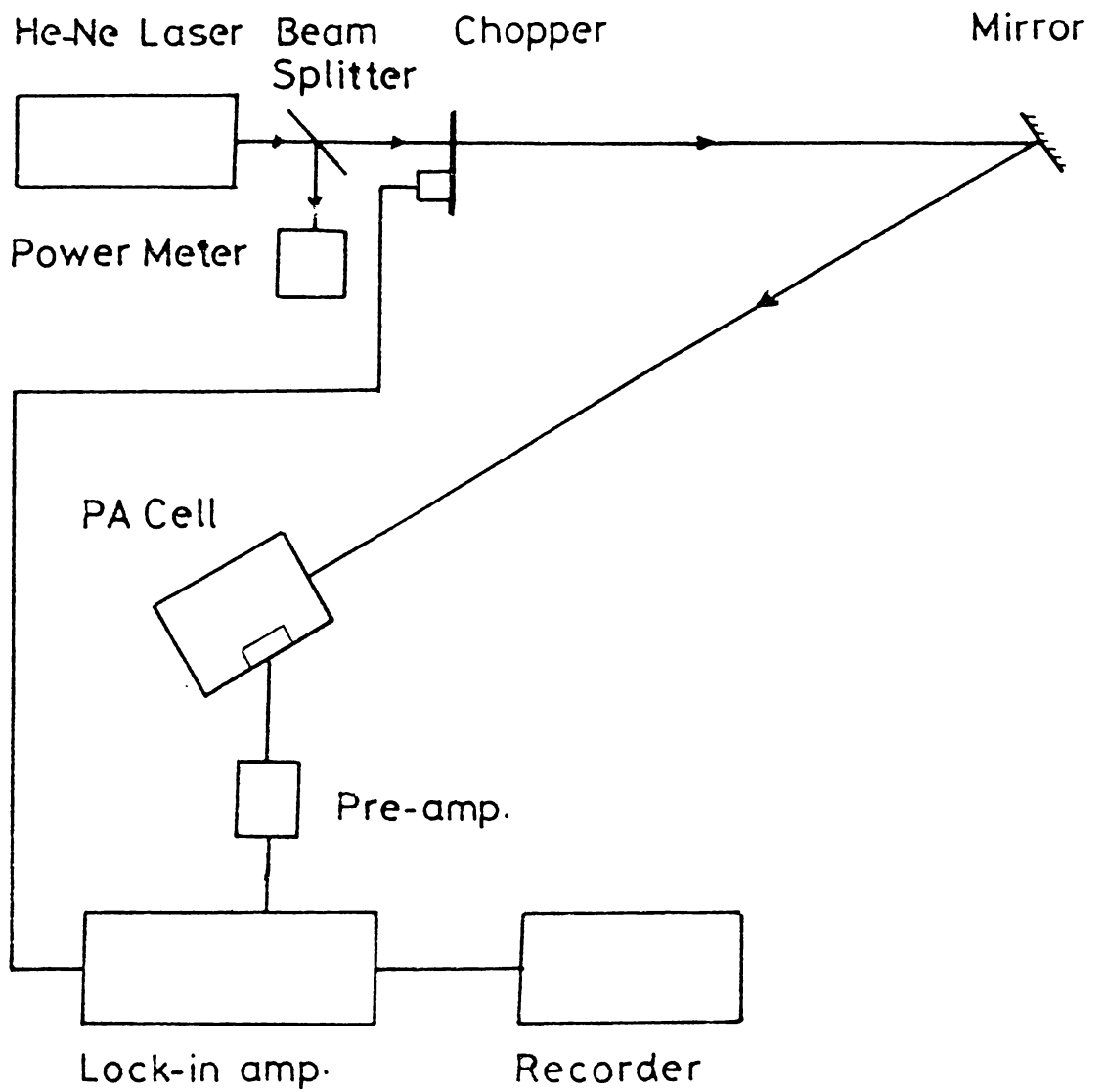


**Fig. 3.10** *Experimental set-up for the measurement of laser beam attenuation in the atmosphere.*

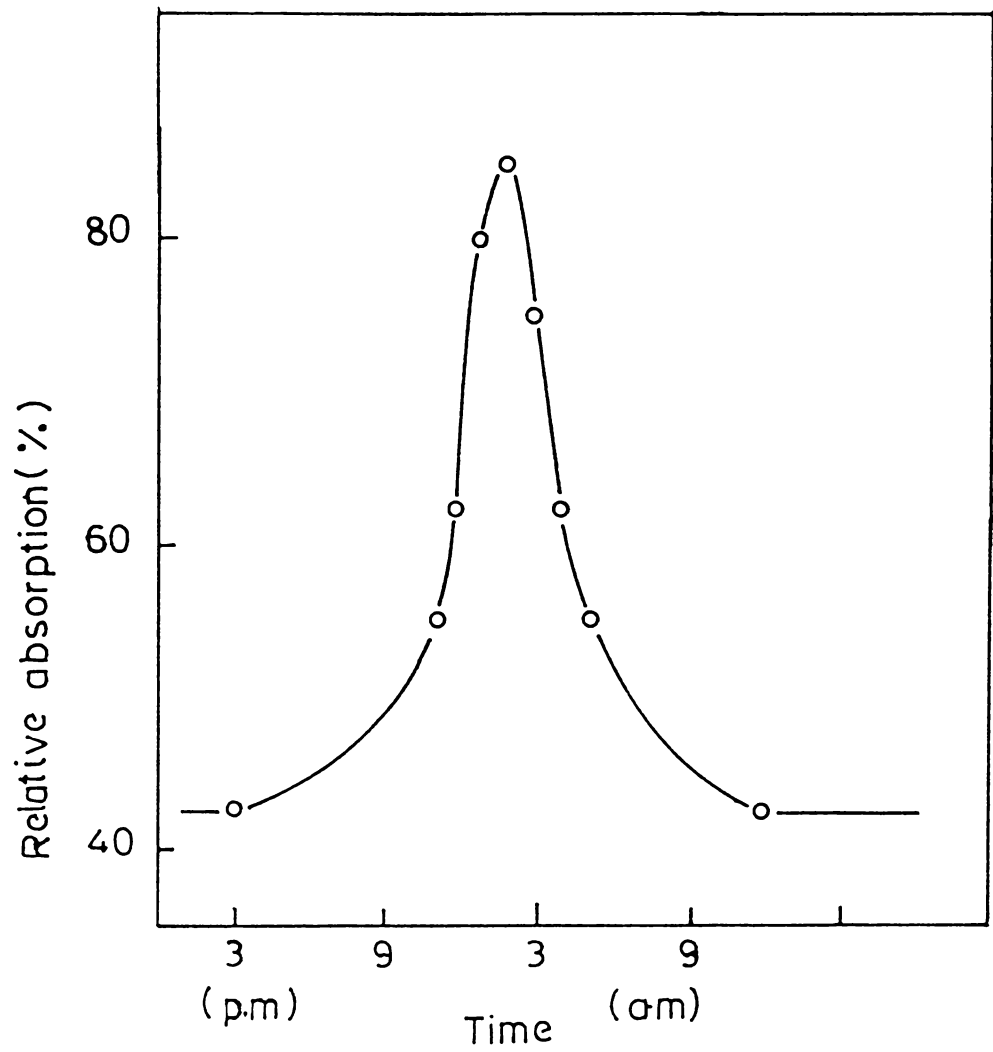


*Fig. 3.11 Typical variation of relative atmospheric absorption for 632.8 nm laser beam over a 24 hour period in February in Cochin area using 60 m path length*



The method described here is very convenient one for the measurement of total atmospheric attenuation suffered by a laser beam as it is made to propagate through selected regions of the atmosphere. The above method is also well suited for the quantitative measurement of visibility of atmosphere in large open areas like air ports, highways, etc.

**References :**

1. A. Rosencwaig, 'Photoacoustic and Photoacoustic Spectroscopy (Wiley and Sons: New York) (1980)
2. A. C. Tam, Rev. Mod. Phys. 58, 2, 381 (1986)
3. P. Ganguly and C. N. R. Rao, Proc. Indian Acad. Sci. (Chem. Sci.), 90, 3, 153 (1981).
4. J. G. Parker, Appl. Opt., 12, 2974 (1973).
5. A. C. Tam, 'Ultrasensitive Spectroscopic Techniques' (Ed. D. Kliger, Academic Press : New York) (1982).
6. F. W. Karasek, Research and Development (USA), 28, 9, 38 (1977).
7. Technical Report on Lock-in Amplifier, EG&G, PARC.
8. Instruction Manual of EG&G 5101 Model Lock-in Amplifier.
9. M. K. Satheeshkumar, C. Raghavan and C. P. G. Vallabhan, Proceedings of National Conference on Instrumentation, (CS10), India, p. 332 (1983).
10. Y. H. Pao, 'Optoacoustic Spectroscopy and Detection, (Academic Press : New York) (1977).
11. M. J. Adams, Prog. analyst. atom. Spectrosc., 5, 153 (1982).
12. A. C. Tam and Y. H. Wong, Appl. Phys. Lett., 36, 471 (1980)
13. P. M. Morse, 'Vibration and Sound,' (McGraw Hill: New York), 1948.
14. N. C. Fernelius, Appl. Opt. 18, 1785 (1979).
15. R. S. Quimby, P. M. Selzer and W. M. Yen, Appl. Opt., 16, 2630, (1977).

16. D. Cahen, E. I. Lerner, and A. Auerback, *Rev. Sci. Instrum.*, **49**, 1206 (1978).
17. M. K. Satheeshkumar and C. P. G. Vallabhan, *Proceedings of National Conference on Instrumentation, (CS10), India*, p. 323, (1983).
18. D. P. Blai and P. H. Sydenham, *J. Phys. E.*, **8**, 627 (1975).
19. M. K. Satheeshkumar and C. P. G. Vallabhan, *J. Phys. E.*, **18**, 434 (1985).
20. W. Budde, 'Physical Detectors of Optical Radiation' (Academic Press : New York), p.94 (1983).
21. S. S. Wagal, D. R. Korhalkar and N. Y. Mehendale, *Proceedings of the Symposium on Infrared Technology and Instrumentation, (DAE), India*, p.384 (1980).
22. S. I. Yun, *J. Korean Phys. Soc.*, **15**, 144 (1982).
23. A. Rosencwaig, *Opt. Commun.*, **7**, 4, 305 (1973).
24. A. Rosencwaig and A. Gersho, *J. Appl. Phys.*, **47**, 64 (1976).
25. C. D. Hodgman, 'Handbook of Chemistry and Physics,' (Cleveland: The Chemical Rubber Publishing Co., New York) (1963).
26. R. S. Quimby and W. M. Yen, *Appl. Phys. Lett.*, **35**, 43 (1979)
27. G. Busse, K. V. Berges and D. Rogalski, *Opt. Commun.*, **28**, 341 (1979).

## CHAPTER IV

### DETERMINATION OF THERMAL DIFFUSIVITY OF METALLIC AND DIELECTRIC SAMPLES FROM PHOTO ACOUSTIC MEASUREMENTS

#### **Abstract**

*This chapter deals with the investigation of thermal parameters of copper and  $\text{CeO}_2$  thin films using PA technique. The detailed theory and experimental results are described for the measurement of thermal diffusivity of copper samples with three different backing materials. Experimental observation of thermal diffusivity of  $\text{CeO}_2$  thin film is presented using the rear surface illumination method. In the last section a detailed account of the effects of backing materials on the amplitude and phase of PA signal are described qualitatively and a complete analysis of the depth profiling studies in a multi-layered backing material is presented.*

#### 4.1 Introduction :

The PA technique offers a promising tool for measuring the thermal parameters such as thermal diffusivity, thermal conductivity and specific heat of gases, liquids and solids [1,2]. The intensity modulated electromagnetic radiation absorbed by the sample leads to an increase in the internal energy and subsequently the energy of the absorbed photon is usually released through a radiationless process that produces heat in the sample. This heat must be transferred from the sample surface to a boundary layer of the gas in the PA cell so that the resultant pressure variation acts as a piston on the bulk of the gas to produce a signal in the microphone. Both the magnitude and phase of the PA signal depend upon the amount of light absorbed, the thermal properties of the sample, gas and backing material, the modulation frequency and the cell geometry [3]. The amplitude and phase of the PA signal is directly related to the thermal diffusion process in the sample and therefore any change in the thermal parameters of the sample alters the PA signal amplitude and phase appreciably. If the sample thickness is small compared to the thermal diffusion length (thermally thin sample), then the heat generated in the sample will be transferred to the backing material depending on its thermal parameters [4].

Thus, the variation of PA amplitude and phase with chopping frequency in a thermally thin sample reveals the thermal parameters of the backing and gas medium since the chopping frequency controls the thermal diffusion process in the sample.

This chapter presents a detailed account of the experimental investigation of thermal diffusivities of copper and  $\text{CeO}_2$  thin films using PA effect. It also describes the effect of backing materials on the amplitude and phase of the PA signal which finds its application in PA depth profiling studies.

#### 4.2 Historical background :

The PA effect was mainly utilised for the absorption studies till 1970. Later in 1973 this phenomenon was effectively utilised in the measurement of thermal diffusivity of solids and liquids [5]. The Rosencwaig and Gersho theory in 1976, formulated a thermal diffusion process in the sample, gas and backing material as described in chapter II. Since the advent of R-G theory, a straight forward approach to the physical processes underlying the PA effect was established. Consequently in 1977 Adams and Kirkbright have used the PA method to obtain thermal diffusivity values for copper and glass by rear-surface illumination in which an opaque surface is illuminated and the PA signal is transferred through a thin copper or glass layer to the gas medium within a gas microphone PA system [6]. Further studies showed that they could obtain the thermal diffusivities of polymer films deposited on copper substrates and the result was in agreement with the standard values [7]. Subsequently Rosencwaig and Pines conducted experiments on rat stratum corneum and the thermal diffusivities could be accurately evaluated [8]. In 1979 Campbell et al. reported some remarkable applications of PA techniques to research in dermatology [9]. They showed that the drug diffusion, water content and thermal properties of skin at different environment could be measured and this experiment in fact proved the use of

PA technology in medicine. Later in 1981, Helander et al. refined RG theory and extended it for samples having multiple layers and using this theory he could identify the different layers which are sensitive to different colours in a photographic colour film [10]. Parpel et al, conducted depth profiling experiments using PA technique and theory could determine the thermal conductivity of Cu - Be sample [11].

Subsequently in 1982 Charpentier et al, developed new refinements to R-G theory and they could propose a more general approach to determine the thermal diffusivities of materials [12]. This method infact proved to be a prominent tool for the study of thermal parameters of samples from both PA amplitude and phase. In the theoretical model they have defined a phenomenon, called 'drum effect' which essentially is the mechanical vibration of the samples due to its periodic dilation during acoustic signal generation. Consequently in 1984 Swim and Crowley had extended this theory for thin film materials [13,14] which turned out to be an excellent method for testing the reflectivities and strain of antireflection coatings in laser optics. Yun et al. could determine the thermal diffusivities of copper and aluminium using a gas microphone PA system [15]. In 1985 Lachaine made an extensive study of the variation of PA signal phase with different sample thicknesses [16] and he could obtain the thermal parameters of Lead samples. Similarly Poulet et al. could determine the thermal diffusivity and effusivity of Hostaphan, a polymer sample with different backing materials [17]. The thermal parameters of metals and polymers in the form of thin films could be accurately obtained and this shows an excellent method to determine the thermal parameters of metals and polymer samples under varying

temperature [18, 19, 20]. Recently thermal diffusivities and thermal effusivities of teflon and polymer samples could be accurately found out by fixing the sample on to different backing materials [21].

This chapter essentially deals with the thermal diffusivity measurements of copper discs by the front surface illumination method and thermal diffusivity of  $\text{CeO}_2$  thin films by rear surface illumination method. The detailed theory and experimentation are described and a brief idea of the depth profiling studies using multiple layer thin films are presented.

#### 4.3 Front surface illumination of the sample - theory :

According to R-G theory, the expression for the complex envelope of the sinusoidal pressure variation in the PA cell is

$$\Delta P = \frac{\gamma P_0 \theta_s}{\sqrt{2} l_g a_g T_0} \quad (4.01)$$

where  $\gamma$  is the ratio of specific heats of air,  $P_0$  is the ambient pressure,  $l_g$  is the length of the air column in the PA cell,  $a_g$  the thermal diffusion coefficient of air,  $T_0$  is the ambient temperature and  $\theta_s$  is the temperature at the sample-gas interface. Since  $\theta_s$  depends on the thermal parameters of sample, air and backing material and the incident light intensity, the magnitude of  $\theta_s$  plays an important role on the generation of PA signal in the cell. Mathematically  $\theta_s$  can be expressed as,

$$\theta_s = \frac{\beta I_0}{2k_s(\beta^2 - \sigma_s^2)} \left[ \frac{(\lambda-1)(b+1)e^{\sigma_s l_s} - (\lambda+1)(b-1)e^{-\sigma_s l_s} + 2(b-1)e^{-\beta l_s}}{(g+1)(b+1)e^{\sigma_s l_s} - (g-1)(b-1)e^{-\sigma_s l_s}} \right] \quad (4.02)$$

where  $\beta$  is the optical absorption coefficient,  $I_0$  is the incident intensity of the light beam,  $k_s$  is the thermal conductivity of the sample,  $\sigma_s$  is the



complex value of the thermal diffusion coefficient of the sample,  $r = (1-i)\beta\mu_s$  where  $\mu_s$  is the thermal diffusion length of the sample which is inversely proportional to the modulation frequency,  $b = \frac{k_b\mu_b}{k_s\mu_b}$  where  $k_b$  is the thermal conductivity of the backing material,  $\mu_b$  is the thermal diffusion length in the backing material  $g = \frac{k_g\mu_g}{k_s\mu_g}$  where  $k_g$  is the thermal conductivity of air and  $\mu_g$  is the thermal diffusion length in the air column. Therefore the thermal wave reflection coefficient from the backing material is given by

$$R = \frac{1-b}{1+b} \quad (4.03)$$

where

$$b = \sqrt{\frac{k_b \rho_b c_b}{k_s \rho_s c_s}} \quad (4.04)$$

$k$ ,  $\rho$  and  $c$  are the thermal conductivity, density and specific heat of the backing material and sample respectively.

now

$$\sigma_s l_s = \frac{(1+i)l_s}{\mu_s} = (1+i)\sqrt{\pi f / \frac{\alpha_s}{l_s^2}} \quad (4.05)$$

where  $f$  is the modulation frequency of the incident light beam,  $\alpha_s$  is the thermal diffusivity of the sample and  $l_s$  is the sample thickness. Therefore  $\sigma_s l_s$  directly measures the number of thermal diffusion lengths in the sample thickness at a fixed chopping frequency.

A characteristic frequency of the sample is defined as

$$f_c = \alpha_s / l_s^2 \quad (4.06)$$

which governs the number of thermal diffusion lengths of the sample which are well confined in the sample thickness. Therefore,

$$\sigma_s l_s = (1+i)\sqrt{\pi f / f_c} \quad (4.07)$$

from the above expressions,  $\beta$  can be expressed as

$$\beta = \frac{1}{2} h \sigma_s \quad (4.08)$$

Therefore the expression for  $\Delta P$  can be rewritten as,

$$\Delta P = \frac{(1-i) \gamma P_0}{2\sqrt{2} l_g a_g k_s (\beta^2 - \sigma_s^2)} \left[ \frac{1 - \frac{(h+1)(b-1)e^{-\sigma_s l_s}}{(h-1)(b+1)} + \frac{2(b-1)e^{-\beta l_s}}{(h-1)(b+1)e^{\sigma_s l_s}}}{\frac{(g+1)(b+1)e^{\sigma_s l_s}}{(h-1)(b+1)e^{\sigma_s l_s}} - \frac{(g-1)(b-1)e^{-\sigma_s l_s}}{(h-1)(b+1)e^{\sigma_s l_s}}} \right] \quad (4.09)$$

substituting the values for  $r$ ,  $b$  and  $\sigma_s l_s$  from equations (4.03), (4.04) and (4.05) and separating out the real and imaginary parts

$$\Delta P = \frac{(1-i) \gamma P_0 \sqrt{\alpha_s}}{2 l_s T_0 \omega \sqrt{k_s \rho_s c_s}} \left[ \frac{1 + R^2 e^{-4 l_s / \mu_s} + 2 R e^{-2 l_s / \mu_s} \cos\left(\frac{2 l_s}{\mu_s}\right)}{\left[ (1 - R^2 e^{-4 l_s / \mu_s})^2 + 4 R^2 e^{-4 l_s / \mu_s} \sin^2\left(\frac{2 l_s}{\mu_s}\right) \right]^{1/2}} \right] \quad (4.10)$$

which essentially represents the pressure variation in the cell in terms of  $l_s$  and  $\mu_s$ . The corresponding expression for the phase is denoted by the imaginary part of the equation given by

$$\Delta \phi = \tan^{-1} \left[ \frac{2 R \sin\left(\frac{2 l_s}{\mu_s}\right)}{e^{2 l_s / \mu_s} - R^2 e^{-2 l_s / \mu_s}} \right] \quad (4.11)$$

For the sake of simplicity, to interpret these equations, let  $l_s / \mu_s = x$  then,

$$\Delta P = A \frac{[1 + R^2 e^{-4x} + 2 R e^{-2x} \cos(2x)]}{\left[ (1 - R^2 e^{-4x})^2 + 4 R^2 e^{-4x} \sin^2(2x) \right]^{1/2}} \quad (4.12)$$

where

$$A = \frac{\gamma P_0 T_0 l_s^2 \alpha_g^{1/2}}{l_g T_0 k_s \alpha_s^{1/2}} \quad (4.13)$$

which is a constant. Similarly the expression for phase is

$$\Delta \phi = \tan^{-1} \left[ \frac{2 R \sin(2x)}{e^{2x} - R^2 e^{-2x}} \right] \quad (4.14)$$

From the above equation it is evident that for a thermally thick sample ( $R = 0$ ), the phase is found to be zero. Therefore, in order to eliminate

any non-sample parasite phase variations, always the difference of phase  $\Delta\phi$  between the thermally thick sample and the sample whose thermal parameters are to be determined is taken into account. Similarly any variation in the thermal reflection coefficient  $R$  causes an appreciable change in the PA signal amplitude and phase. Therefore the above expressions are found to be the result of a clever modification of the R-G theory made so far [22]. It has the added advantage that this approach does not have any approximations which ensure the accurate determination of absolute values of thermal parameters of sample, backing and air medium in the PA cell.

#### 4.4 Experimental set up :

The experimental set up is shown in fig. 4.1. CW beam from an argon ion laser (Spectra Physics Model 171-17) of wavelength  $\lambda = 514.5 \text{ nm}$  is mechanically chopped using a variable frequency chopper (EG&G PARC Model 192) and is allowed to be incident normally on the copper sample kept in a nonresonant PA cell. The PA cell contains a sensitive electret microphone (Knowles BT 1753). The cell used is a cylindrical cavity (2 cm diameter, 1.75 cm height) in a solid block of aluminium with a radial microphone port as shown in fig. 4.2. The glass window and the microphone are sealed with o-rings and air at atmospheric pressure acts as the coupling gas medium. In order to mount the sample pieces rigidly, a threaded brass mount which is firmly attached in the PA cell cavity is used as shown in the inset of fig. 4.2. A plane glass disc

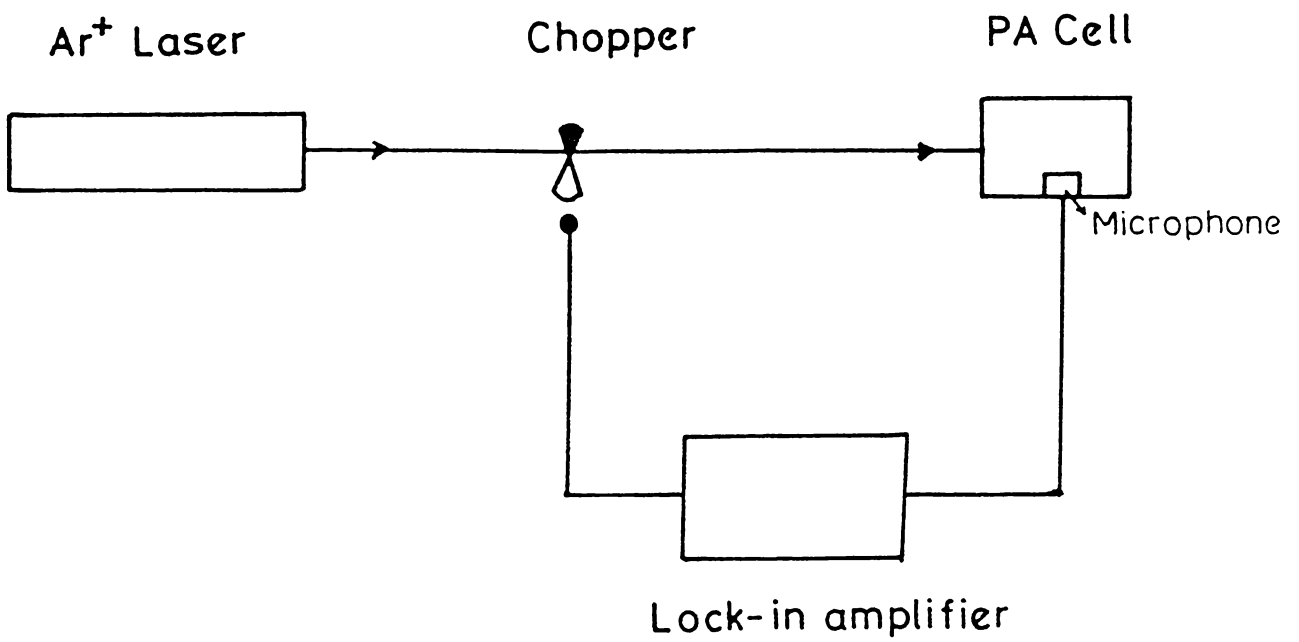


*Fig. 4.1 Experimental set up for the measurement of thermal diffusivity by using PA technique.*

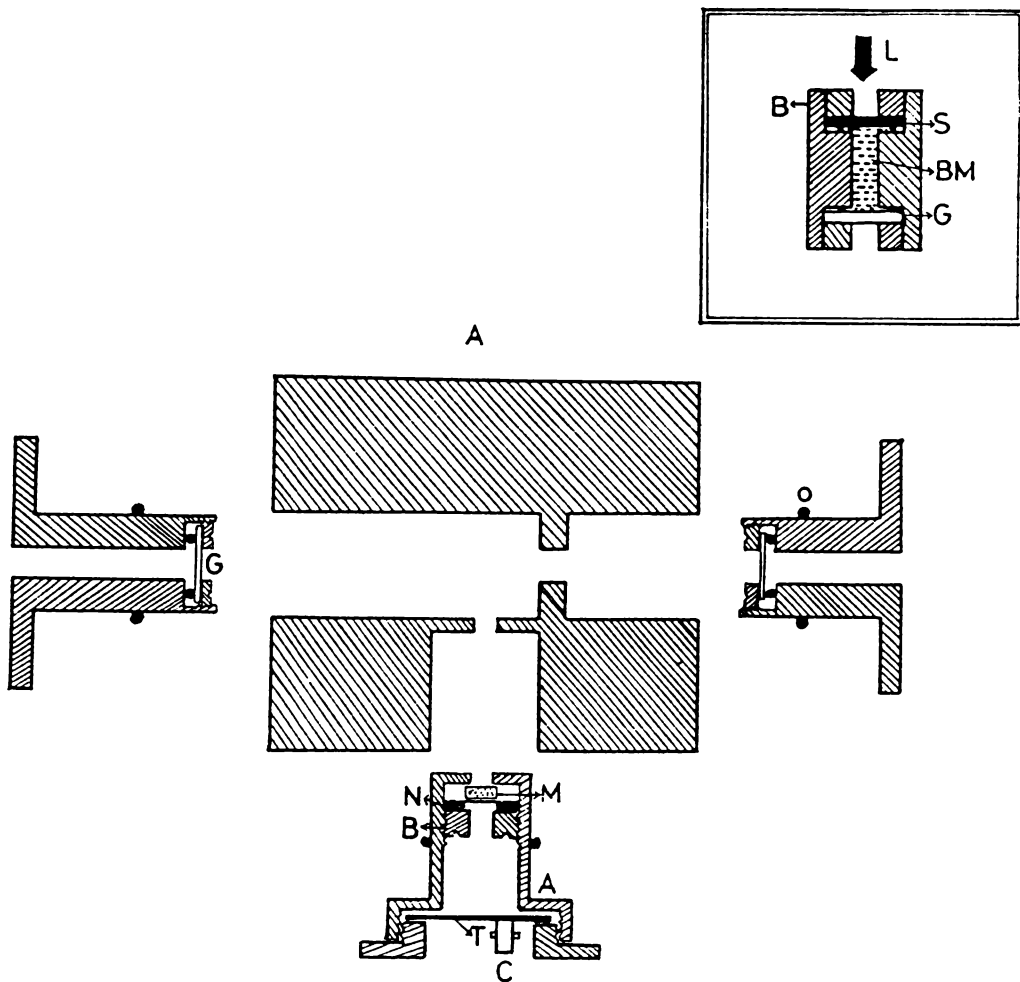
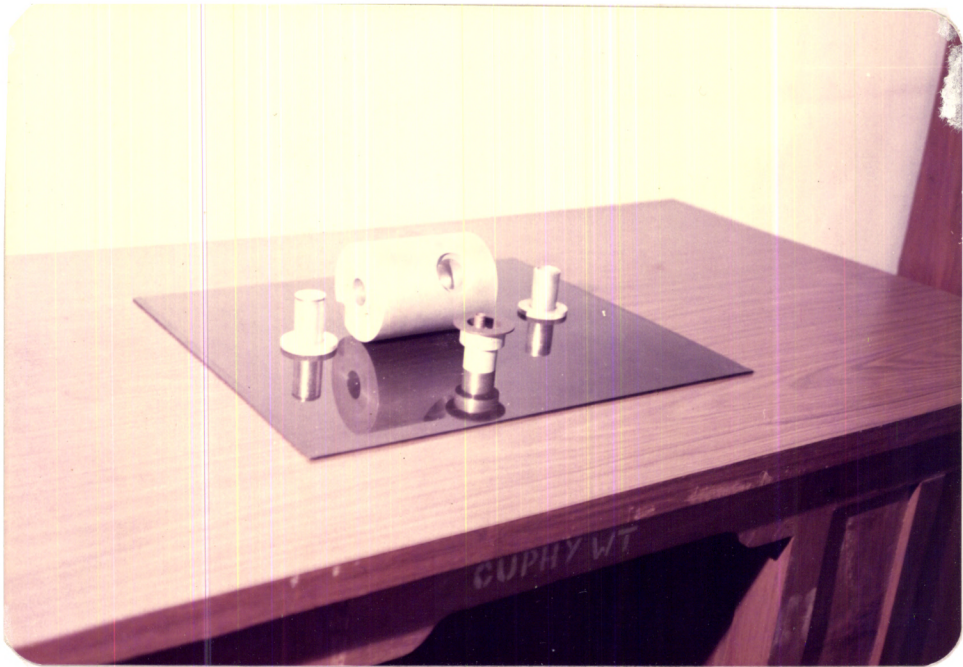


Fig. 4.2 Cross sectional view of the PA cell. Inset shows the sample holder. (A - aluminium body; B - brass housing, G - Glass window, L - laser; M - microphone; N - neoprene sheet; O - o-ring; S - sample; T - Teflon disc; C - connector and BM - backing material.)





*Photograph of the PA cell*

of transmittance 90.2 % is used as the window material for the PA cell. The microphone is rigidly fixed using o-rings and it is tightly enclosed in a cavity made in an aluminium cylinder which is inserted from the side of the PA cell so as to ensure proper coupling for the gas medium of the PA cell cavity.

The samples used in the present experimentation are copper discs the thickness of which varies from 250  $\mu\text{m}$  to 5 mm. In order to absorb the wavelength of argon ion laser, a thin layer of an organic dye is deposited on the copper discs. The copper samples are thus considered to be perfectly opaque and it provides a large optical absorption coefficient to the laser beam. Most of the heat generated by the absorption of light is transferred to this copper sample since the thermal conductivity of copper is much higher than the air medium in the PA cell. The above sample is then made to rest on different backing materials such as water, isopropyl alcohol and castor oil which prevents mechanical vibration described as the 'drum effect' of the sample due to its periodic dilation during the generation of thermal waves in the copper sample [14]. The microphone signal is processed by a lock-in amplifier (Stanford Model SR510) which simultaneously measures the amplitude and phase of the PA signal. The PA signal amplitude and phase are measured for different chopping frequencies and the values are recorded.

In order to compensate the amplitude and phase variation of the PA signal the experiment is conducted by using a copper disc of 1 cm diameter and 5 mm thickness which is the reference sample. The PA



amplitude and phase are recorded using a lock-in amplifier for different chopping frequencies. Then samples of different thicknesses are placed in the PA cell and the corresponding PA signal amplitude and phase are recorded for the same chopping frequency intervals. The advantage of this method is that the inherent phase of the PA cell geometry can be eliminated and therefore the phase difference between the reference copper sample and samples having different thicknesses directly gives the thermal parameters of the discs accurately.

#### 4.5 Results and discussion :

Fig. 4.3 shows the measured phase data for three different backing materials, viz. water, isopropyl alcohol and castor oil. The graph clearly shows the variation of phase difference  $\Delta\phi$  with the chopping frequency  $f$  for different backing materials and it is found that the variations are identical irrespective of the nature of the backing materials. As the chopping frequency increases the phase difference decreases and finally reaches zero at a frequency of 90 Hz, which is the characteristic frequency defined and  $f_c = \alpha_s / l_s^2$ . Since the thermal diffusion length in the sample is inversely proportional to the chopping frequency, at higher chopping rates the thermal diffusion length in the sample will be considerably reduced and at  $f_c$  it will be confined within the sample thickness. This behaviour can be explained from equation (4.11) and at  $f = f_c$ ,  $R = 1$  since the heat flow to the backing material is negligibly small so that the phase difference will be a minimum. Here the sample thickness is 1.1 mm and the corresponding characteristic frequency obtained from

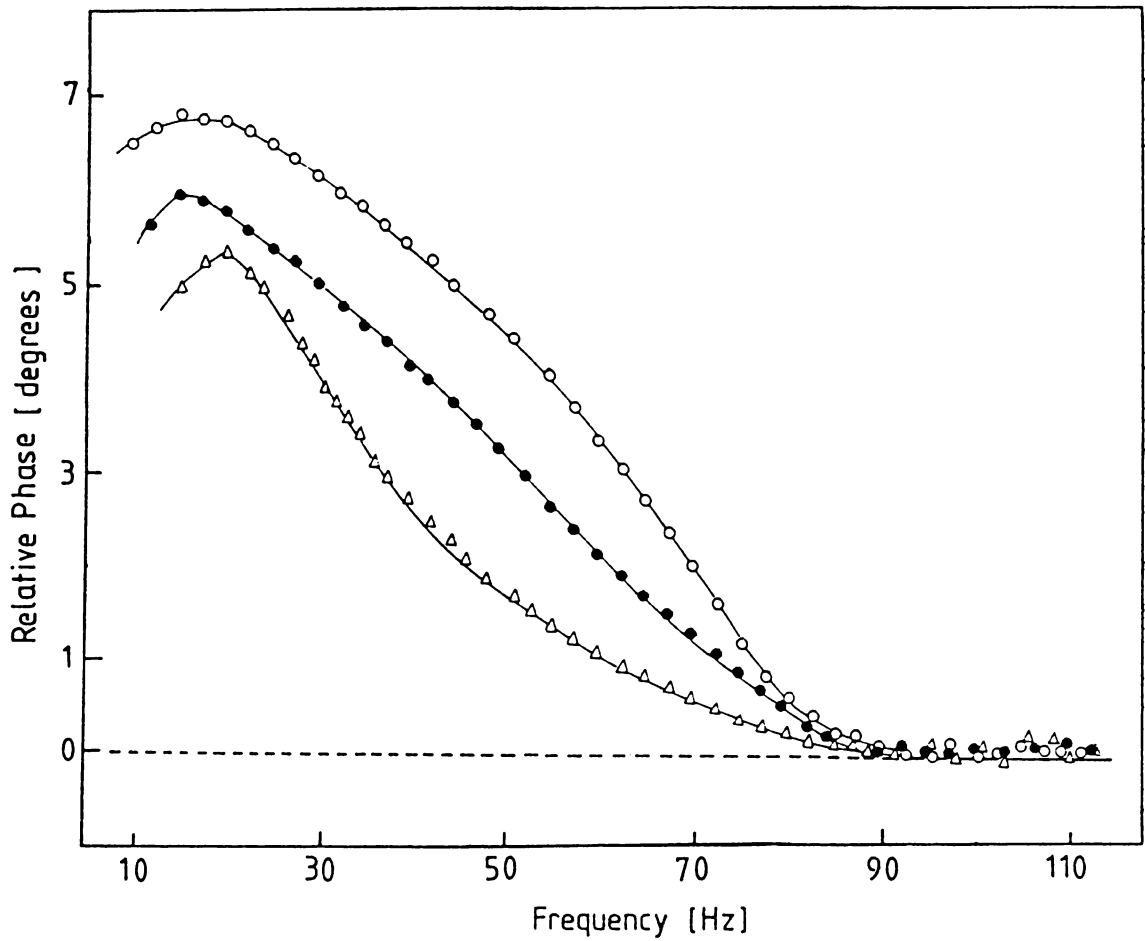


Fig. 4.3 Phase vs chopping frequency for 1.1 mm thick copper sample with different backing materials (O - castor oil; ● water and Δ - isopropyl alcohol).

the graph is approximately 90 Hz a result which is completely in agreement with the theory described in section 4.3. The values of thermal reflection coefficient  $R = 1.87 \times 10^{-3}$  and the thermal diffusivity corresponding to a characteristic frequency of 90 Hz is given by  $\alpha_s = 1.089 \text{ Cm}^2 \text{ Sec}^{-1}$ . This is in agreement with the values reported in the literature [23]. Here the observations that the phase becomes positive is due to the fact that the thermal reflection coefficient  $R$  is positive as the ratio  $b = (k_b \rho_b c_b / k_s \rho_s c_s)^{1/2}$  is always less than unity. This is so because the product  $(k \rho c)$  for copper is always larger than those for the three backing materials.

Similarly from the amplitude measurements shown in fig. 4.4 the PA signal corresponding to alcohol as the backing material is always less in magnitude and this is attributed to the difference in the magnitude of the thermal diffusivities of water and alcohol. Depending on the thermal diffusivity, more heat will be transferred to alcohol than to water and castor oil which in turn reduces the heat diffusion to the gas medium. At low chopping frequencies the slopes of the three curves in fig. 4.4 are different which directly indicate the difference in the thermal parameters of water, alcohol and castor oil. The difference in slopes clearly shows the influence of the thermal diffusivities of the backing materials since the copper sample in these cases acts as thermally thin material in the lower chopping frequency region. From the graph, it is evident that beyond the characteristic frequency  $f_c = 88 \text{ Hz}$  the curves become parallel with a slope of -1. This is readily understandable

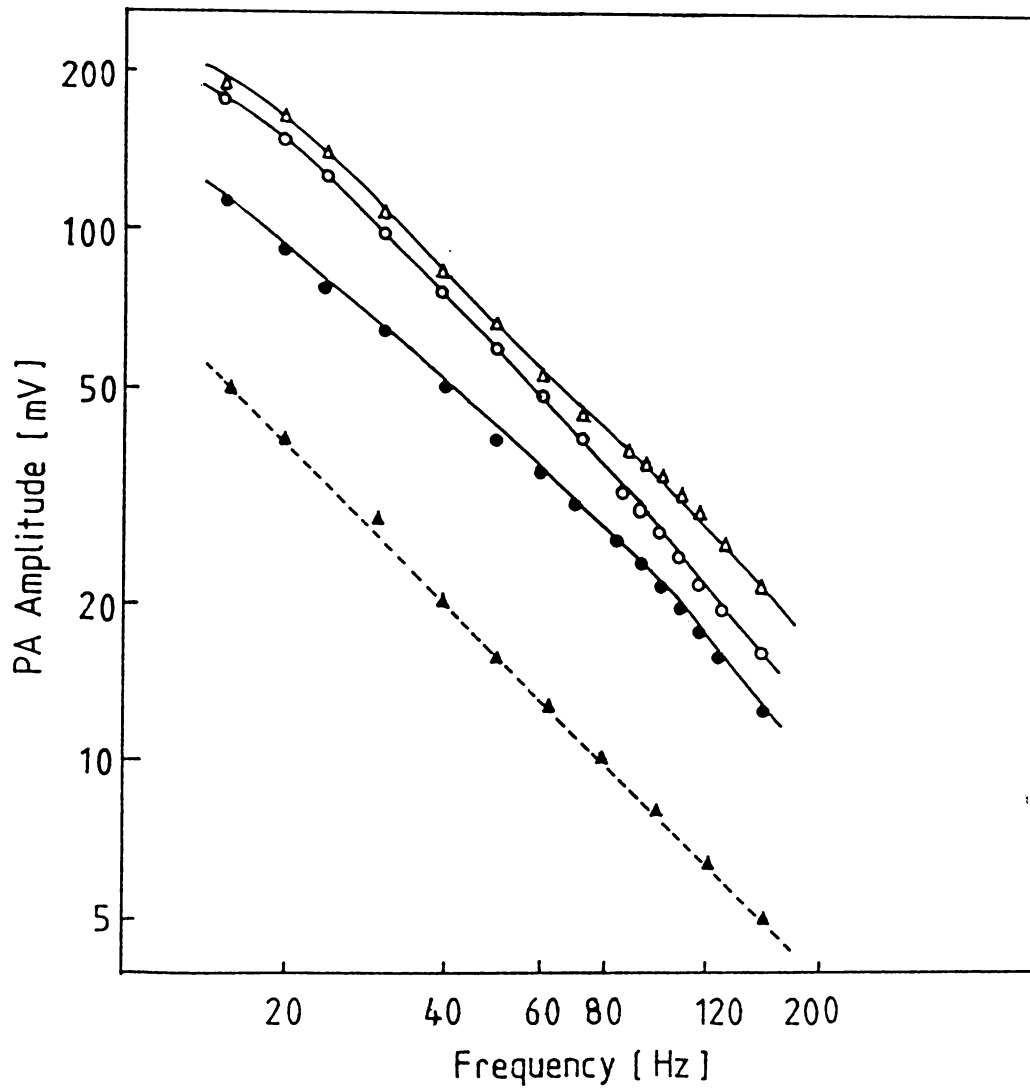


Fig. 4.4 PA amplitude vs chopping frequency for 1.1 mm thick copper sample with different backing materials ( $\Delta$  - isopropyl alcohol;  $\circ$  - water and  $\bullet$  - castor oil). Dotted line indicates the curve for a thermally thick sample.

since the sample becomes thermally thick at 88 Hz and hence the thermal wave generated in the copper disc will be confined in the sample material itself. Thus no heat will be transferred to the backing material beyond the characteristic frequency and this behaviour is evident from the slope of -1 beyond  $f_c = 88$  Hz. From the characteristic frequency obtained during PA amplitude measurements, the thermal diffusivity of copper is calculated using the relation  $\alpha_s = f_c^{-2} l_s^2$  and this value of  $\alpha_s$  is identical with the value obtained from phase measurements.

From the above experiments the results of amplitude and phase measurements are seen to be in agreement with R-G theory. The values of thermal diffusivities of copper sample of thickness 1.1 mm with different backing materials are listed in table 4.1.

Similarly the graph shown in fig. 4.5. represents the measured phase data as a function of chopping frequency for three different thicknesses of copper discs (1 mm, 1.5 mm and 2 mm) with water as the backing material. From these curves one can clearly see that an increase in the sample thickness decreases the characteristic frequency  $f_c$  and that the results are in good agreement with the RG theory described in chapter II. At low frequencies, the phases are positive, indicating a positive value for R, and decreases with chopping frequency until they reach the characteristic frequency  $f_c$ , above which they tend to zero. The figure also shows that the characteristic frequency corresponding to a sample thickness 1 mm is 110 Hz and that of 2 mm is 24 Hz.

**Table 4.1**      *Results of the amplitude and phase analysis  
for a copper sample ( $l_s = 1.1$  mm )*

<i>Backing material</i>	<i>Method</i>	$f_c$ (Hz)	$\alpha_s = f_c l_s^2$ ( $\text{cm}^2 \text{sec}^{-1}$ )
<i>Water</i>	<i>Amplitude</i>	88	1.064
	<i>phase</i>	90	1.089
<i>Isopropyl alcohol</i>	<i>Amplitude</i>	90	1.089
	<i>phase</i>	89	1.077
<i>Castor oil</i>	<i>Amplitude</i>	86	1.041
	<i>phase</i>	90	1.081

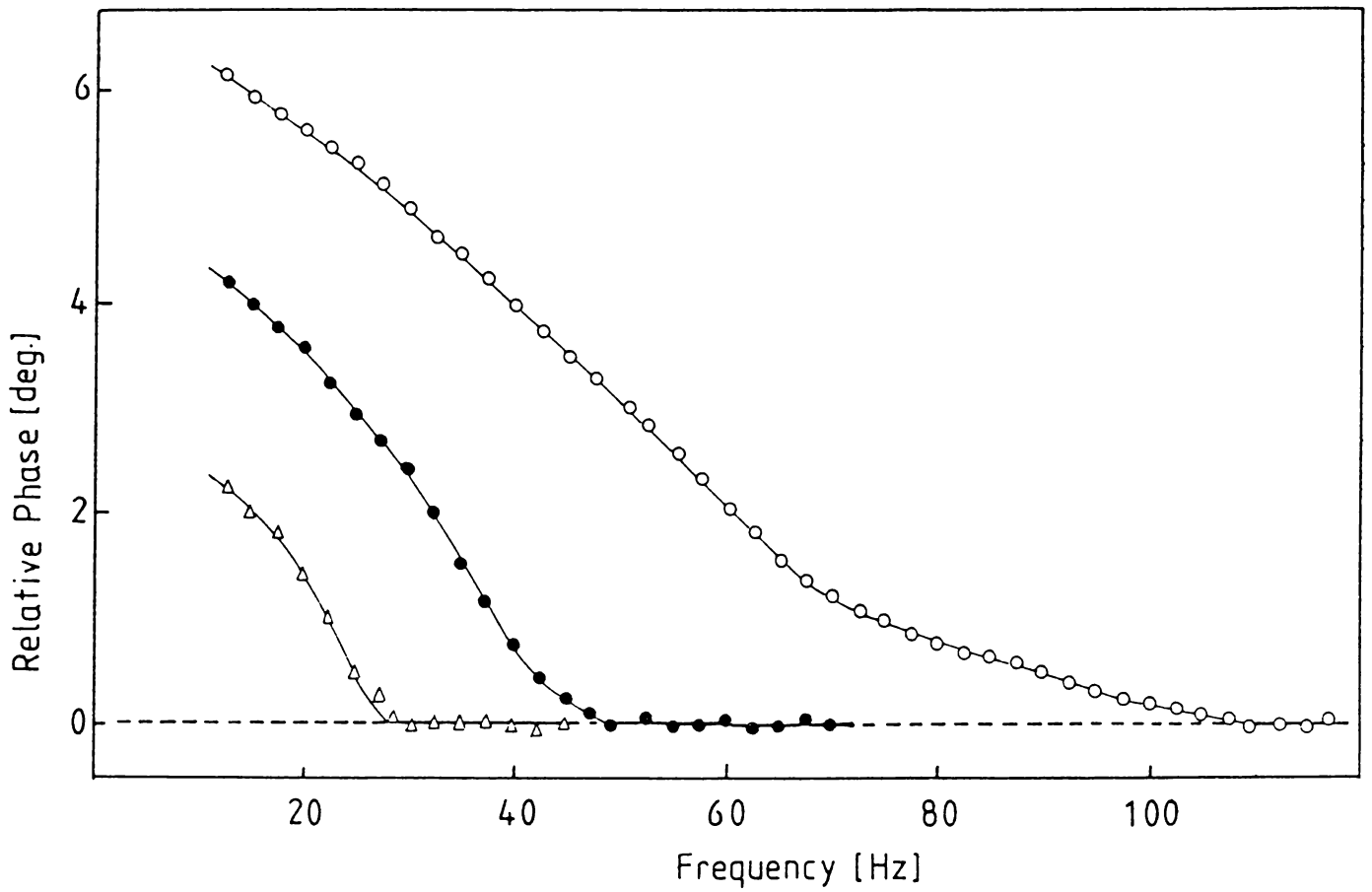


Fig. 4.5 Phase vs chopping frequency for copper samples of various thicknesses (0 - 1 mm; ● - 1.5 mm and  $\Delta$  - 2 mm)

Therefore this method is inadequate for the study of thermal parameters of thin films because the characteristic frequency will be in the MHz region as the thickness of the film is usually of the order of angstroms. Consequently in order to measure the thermal diffusivity of thin films mechanical choppers must be replaced by electro-optic or acousto-optic modulators which will provide a high frequency intensity modulation of the light beam. Thus the rear surface illumination method is usually adopted to the measurement of thermal parameters of thin films which is described in the following section.

#### **4.6 Thermal diffusivity of $\text{CeO}_2$ thin film using rear surface illumination method :**

In PA effect, the heat generated in the sample causes acoustic signal which directly measures the thermal properties of the sample. In the rear surface illumination method, the light beam is allowed to fall on the rear surface of the sample where the microphone is kept in contact with the opposite surface as shown in fig. 4.6. Here when the thermal waves generated at the surface where the light beam is incident starts propagating through the sample, it eventually generates the acoustic signal in the gas medium. Therefore the PA signal amplitude and phase directly depends on the thickness of the sample and its thermal diffusivity. Thus the knowledge of sample thickness and phase of the PA signal gives the thermal parameters of the sample. In order to find the thermal properties of thin film samples, thin films are deposited



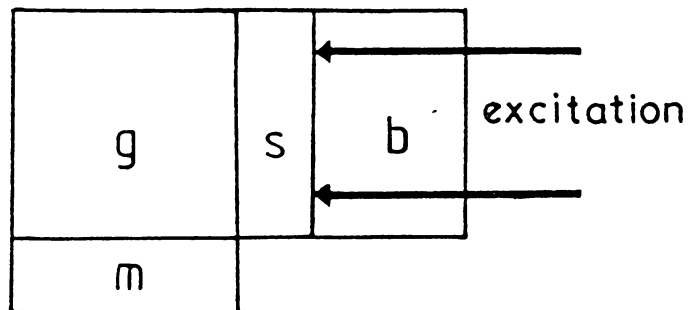


*Fig. 4.6 Schematic representation of rear surface illumination ( b - backing material S - Sample; g - coupling gas medium and m - microphone.*

on a substrate which acts as the sample material and the phase variation of the thin film samples can be found by subtracting the corresponding PA phase variation due to the substrate alone. Thus from the relative phase difference between the substrate and substrate + thin film the thermal properties of the thin film can be calculated exactly. In the present experimentation, the thermal diffusivity of  $\text{CeO}_2$  thin films deposited on copper substrate is measured by the rear surface illumination method. The detailed theory is given below.

#### 4.6.1 Theory :

Since the sample is optically opaque the intensity modulated light beam on the rear surface of the sample results the localised heat centres at the surface of the sample and as a result the thermal waves start propagating through the thickness  $l_s$  of the sample. If  $\alpha_s$  is the thermal diffusivity of the sample the thermal diffusion equation along the thickness can be expressed as

$$\frac{\partial^2 \theta_s}{\partial x^2} - \frac{1}{\alpha_s} \frac{\partial \theta_s}{\partial t} = 0 \quad (4.15)$$

where  $\theta_s$  is the temperature at the sample surface. The real part of the solution of above equation is

$$\theta_s(x,t) = \theta_0 e^{-a_s x} \cos(\omega t - ax) \quad (4.16)$$

This expression represents the temperature distribution along the thickness of the sample and it is evident that the thermal wave gets attenuated exponentially as it traverses through the sample. The term which represents

the phase of the thermal wave is  $a_s x$  where  $a_s$  is the thermal diffusion coefficient of the sample and  $x$  is the position where the temperature is found to be  $\theta_s$ . Therefore the total phase difference between the front surface and rear surface of the sample is expressed as

$$\Delta\phi = a_s l_s \quad (4.17)$$

where  $a_s$  is the thermal diffusion coefficient  $a_s = \sqrt{\omega / 2\alpha_s}$ , being the angular frequency of the intensity modulated light beam. Thus the graph between  $\sqrt{\omega}$  and  $\phi$  will be a straight line and its slope is  $(\frac{1}{2\alpha_s})^{1/2} l_s$ . From the value of  $\Delta\phi$  and  $l_s$  the value of  $\alpha_s$  can be accurately calculated. This method offers an added advantage that the knowledge of  $\alpha_s$  and  $\Delta\phi$  provides the thickness of the thin films using PA effect [24].

#### 4.6.2 Experimentation :

The experimental set up is shown in fig. 4.7. Argon ion laser beam operating at  $\lambda = 514.5$  nm at a power level of 500 mW is used as the light source. Its intensity is modulated by using a variable frequency mechanical chopper. And it is directed into the PA cell described in the previous section. CeO<sub>2</sub> thin films are deposited on identical copper discs (18 mm dia; 0.1 mm thick) using an electron beam gun. The sample is rigidly fixed in the PA cell using an o-ring seal to avoid drum effect and mechanical vibrations. The argon ion laser beam is then allowed to fall on the copper disc by means of a plane mirror held at 45° as shown in the figure effecting rear surface illumination of the sample.

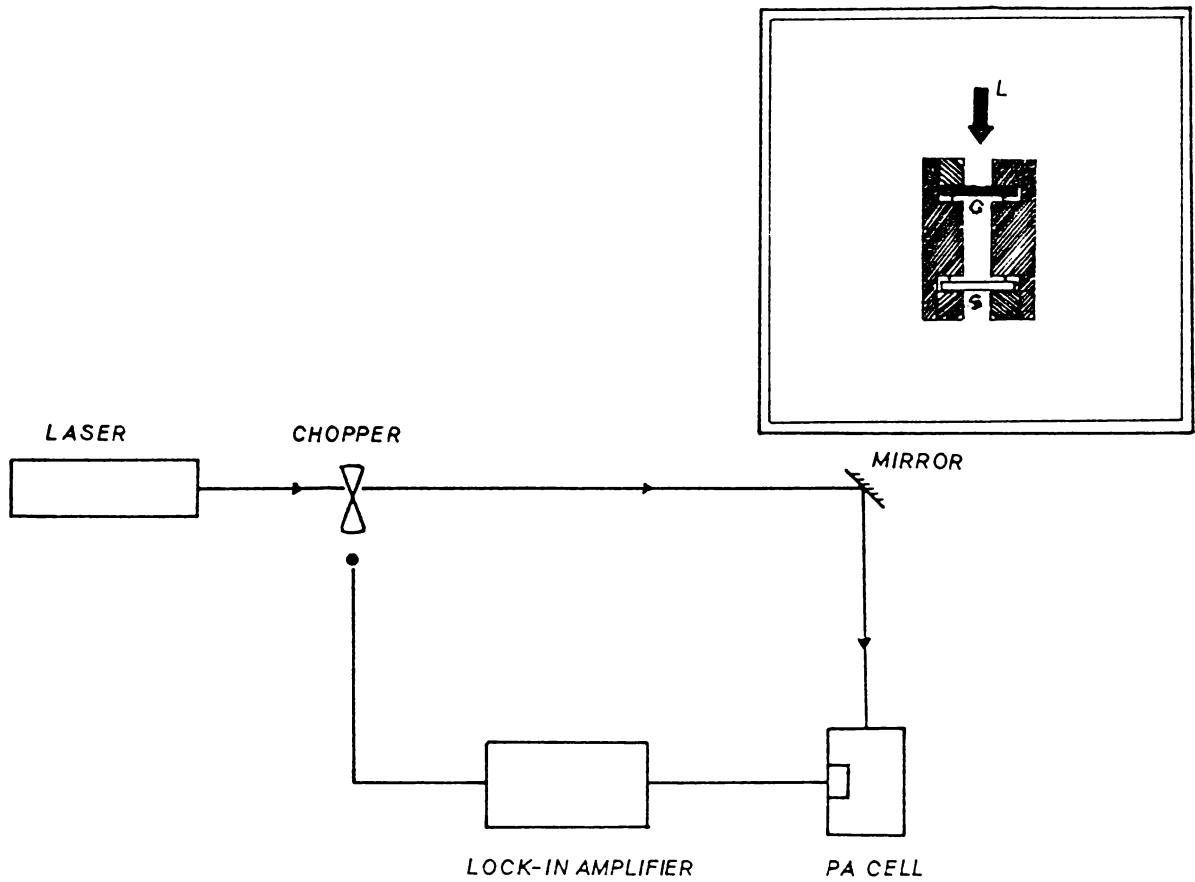


Fig. 4.7 Experimental set up for measuring the thermal diffusivity of  $\text{CeO}_2$  film. Inset shows the sample holder (  $L$  - laser beam;  $G$  - glass disc and  $S$  - Sample)

The phase difference ( $\Delta\phi$ ) occurring when copper substrate alone is used as the sample and copper + CeO<sub>2</sub> thin film is recorded against various modulation frequencies using a lock-in amplifier. The thickness of CeO<sub>2</sub> thin film is measured using optical method [25]. The time constant of the lock-in amplifier is selected as 10 msec to monitor the minute change in the variation of PA phase since the phase difference ( $\Delta\phi$ ) is found to be extremely small in the case of thin films having a few angstroms thickness.

#### 4.6.3 Results and discussion :

Fig. 4.8 shows the variation of PA phase difference between copper and copper + CeO<sub>2</sub> film with the square root of the modulation frequency at two different thicknesses of CeO<sub>2</sub> thin films (1000 Å and 2000 Å). From the straight line graph the slopes are found to be  $3.8 \times 10^{-5}$  and  $3.37 \times 10^{-5}$  for 1000 Å and 2000 Å respectively. By using the above data, thermal diffusivity of CeO<sub>2</sub> are  $0.033 \text{ cm}^2 \text{ sec}^{-1}$  and  $0.044 \text{ cm}^2 \text{ sec}^{-1}$  for 1000 Å and 2000 Å respectively. Therefore from the results it is obvious that the thermal diffusivity of CeO<sub>2</sub> films are found to increase with its thickness and approaches the thermal diffusivity of the bulk value of the material [26]. This is mainly due to the fact that as the film thickness increases there is an increase in the grain size which ultimately enhances the range of wavelength of phonons involved in the heat transfer process. This can therefore increase the thermal diffusivity of the material due to the substantial increase in the phonon distribution, in a direction perpendicular to the surface of the CeO<sub>2</sub> film [27]. As the thickness is increased further, it shows the properties of the bulk material. This method thus offers a potential tool for

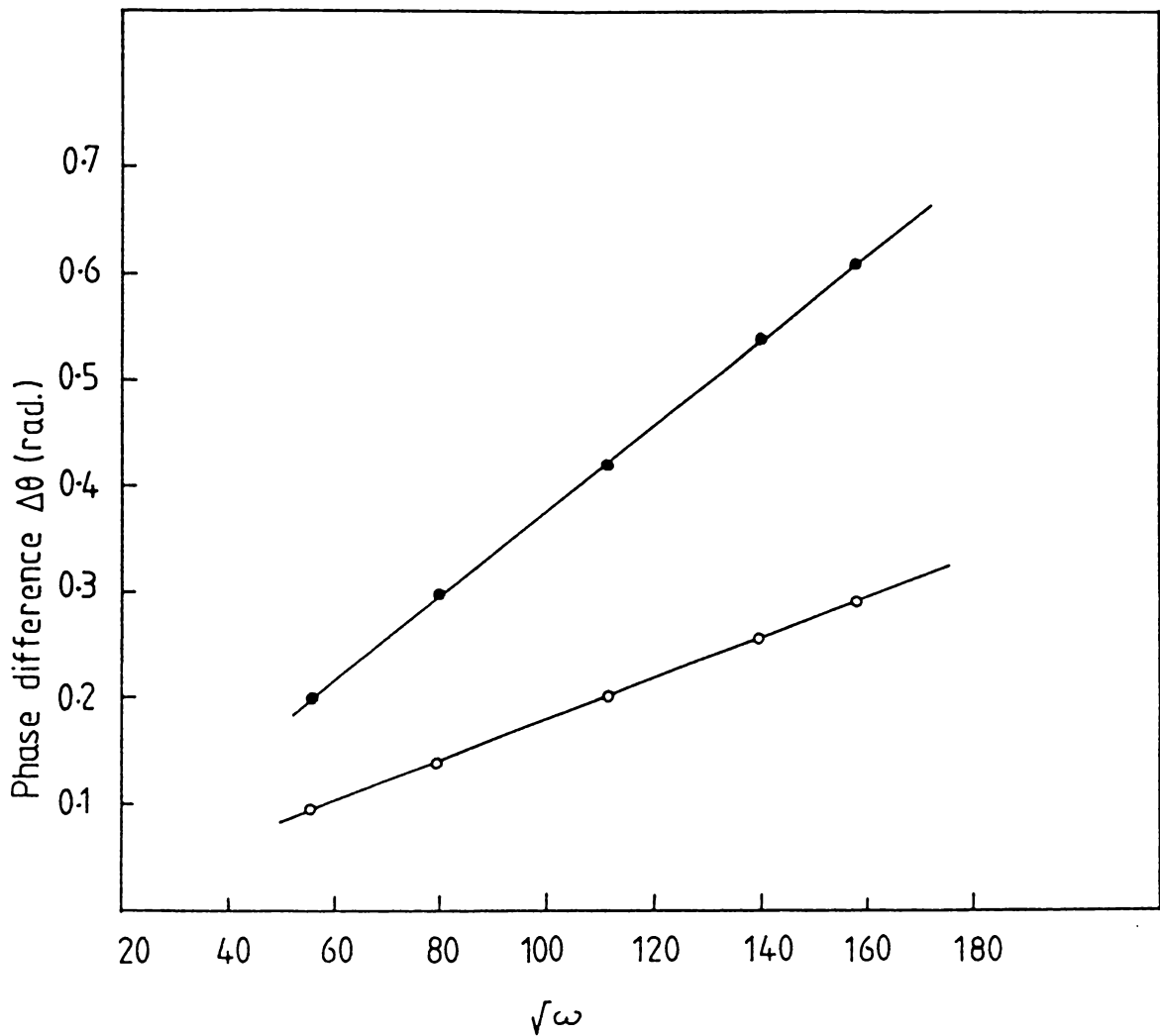


Fig. 4.8 Phase difference vs square root of the angular chopping frequency for  $\text{CeO}_2$  films having two different thicknesses (● - 2000 Å and ○ - 1000 Å)

measuring the thermal diffusivity of insulator films. The advantage of this method is that it can provide the value of the thickness of the film if the thermal diffusivity and  $\Delta\theta$  are known.

#### 4.7 Depth profiling studies using PA techniques :

The thermal waves generated by the absorption of light in the sample get transferred to the gas medium as well as to the backing material depending on the thermal diffusivity of these materials. If the sample is thermally thin then the heat waves may diffuse to the backing material and consequently the PA signal amplitude and phase directly depends on the thermal properties of the backing material. Thus if the backing material is a combination of multiple thin film layers, then the heat transfer to these materials depends on the thermal diffusivities of each thin film layer and therefore by selecting the thermal diffusion length the heat flow to each layer can be controlled precisely. This can be achieved by monitoring the PA signal with the modulation frequency and the log-log graph between them directly gives changes in slope which in turn is an indication of number of thin film layers present in the backing material [28].

In the present experimentation the effect of backing materials in the form of thin film layers on the amplitude and phase of the PA signal are studied. A brief account of the theory and the results are described in the following sections.

##### 4.7.1 Theory:

Consider a situation in which the chopped light of frequency  $f$  is incident from the right on to a sample consisting of an absorbing layer

and thin film backing materials as shown in fig. 4.9. The temperature at these layers are indicated by  $\theta_s$ ,  $\theta_b$  and  $\theta_g$  corresponding to the sample, backing and gas medium respectively. According to R-G theory the heat diffusion equation at these regions are represented by

$$\frac{\partial^2 \theta_s}{\partial x^2} - \frac{1}{\alpha_s} \frac{\partial \theta_s}{\partial t} + \frac{\beta I_0 \eta}{2k_s} e^{\beta x} (1 + e^{i\omega t}) = 0 \quad (4.18)$$

where subscript  $s$  denotes the sample,  $\alpha_s$  the thermal diffusivity of the sample,  $\beta$  the absorption coefficient,  $I_0$  is the incident intensity of the light beam,  $\eta$  is the non radiative efficiency of the sample and  $k_s$  is the thermal conductivity of the sample. The last term in the above expression represents the heat generated due to the non radiative relaxation in the sample, which gets transferred to the gas and backing material. Similarly, the thermal diffusion equation for the backing and gas medium are

$$\frac{\partial^2 \theta_b}{\partial x^2} - \frac{1}{\alpha_b} \frac{\partial \theta_b}{\partial t} = 0 \quad (4.19)$$

$$\frac{\partial^2 \theta_g}{\partial x^2} - \frac{1}{\alpha_g} \frac{\partial \theta_g}{\partial t} = 0 \quad (4.20)$$

These equations represent the heat flow through the media which essentially depend on the respective thermal diffusivities. The source term is absent here because the heat generated will be well within the sample itself. These equations are solved using appropriate boundary conditions to get the temperature at different regions and the detailed analysis of the theory is described in chapter II.



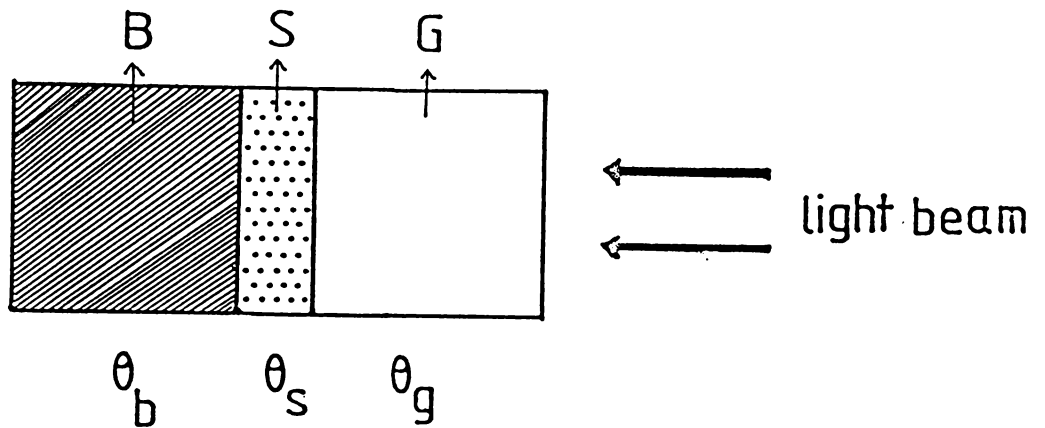


**Fig. 4.9** Schematic diagram of a PA cell.

(B - Backing material; S - Sample; G - Gas medium;

$\theta_b$  - Temperature at the backing;  $\theta_s$  - Temperature at the sample and  $\theta_g$  - Temperature at the gas.

Now, as the modulation frequency is increased, the thermal diffusion length decreases rapidly so that the probability of heat transfer to the backing materials is less and the PA signal amplitude as well as the phase varies accordingly. Thus the chopping frequency essentially controls the heat transfer to the backing material which ultimately varies the PA amplitude and phase. As the chopping frequency is increased the thermal diffusion length will be finally confined in the sample because the heat flow to the backing material is restricted completely. Therefore the variation of PA amplitude and phase with the chopping frequency directly reveals the thermal properties of the backing material which in turn can identify the multi-layered structure of the backing material. A log-log plot of the PA signal amplitude and chopping frequency is made and the different slopes of the graph is an identification of different layers present in the backing material.

#### 4.7.2 Experimentation :

The experimental set up is shown in fig. 4.10. Stable output from an argon ion laser (Spectra Physics Model 171-17) of wavelength  $\lambda = 514.5 \text{ nm}$  is modulated by using a mechanical chopper and is allowed to fall on the PA cell using a mirror held at  $45^\circ$ . The PA cell is made of solid aluminium block with a radial microphone port as described in the previous section. The glass window and the microphone are sealed with o-rings and air at atmospheric pressure acts as the coupling gas medium. The microphone signal is processed by a lock-in amplifier (EG&G PARC Model 5101) which simultaneously measures the phase and amplitude of the acoustic signal. The sample used is silver film ( $1000 \text{ \AA}$ ) coated on a thin glass slide by thermal evaporation. Another thin layer of carbon black deposited on the thin film forms the sample which is placed in the PA cell. Carbon black is deposited over the silver film because carbon possesses large optical absorption coefficient which ensures a greater amplitude for the PA signal. The studies with silver film is performed by placing the sample at the bottom end of the cell. In this configuration the distance between the window and the microphone opening is several times the thermal diffusion length of air in the frequency range used and hence the weak signal due to window absorption will be strongly damped out. Another set of measurements for the sake of comparison is taken by illuminating the carbon black of same thickness on a glass substrate which itself acts as the backing material. A log-log graph is drawn between the PA signal amplitude and chopping frequency which clearly shows different slopes corresponding to the multi-layered structure of the backing material.

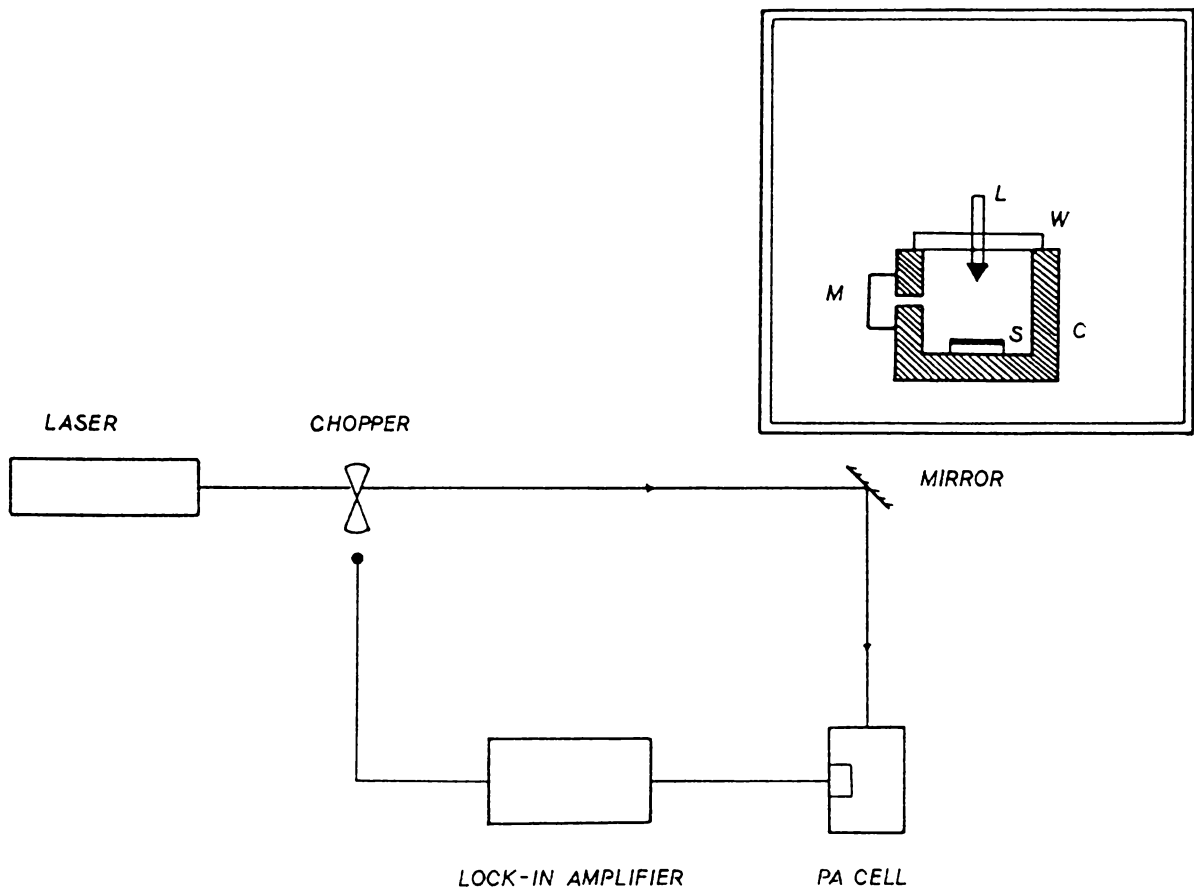


Fig. 4.10 Experimental set up. Schematic of the PA cell is shown in the inset (L - laser; W - glass window; M - microphone; C - cell cavity, and S - Sample.)

### 4.7.3 Results and discussion: :

Fig. 4.11 gives the variation of PA amplitude as a function of chopping frequency. for the two samples at an incident laser beam power level of 200 mW. The trace A shows the abrupt change in slope which occurs due the glass acting as backing material. The lower trace B gives the effect of a thin layer of silver film (1000 Å thick) sandwiched between glass and carbon black.

From the results it is evident that the change in slope of the curve of amplitude versus frequency can occur at different chopping frequencies for different backing materials [29]. Fig. 4.11 thus clearly shows that two slopes are present for glass-carbon black combination while three slopes are found to exist when glass-silver film-carbon black combination is the sample material. This indicates that backing material plays an important role on the magnitude of the PA signal at relatively low chopping frequencies. At lower chopping frequencies the thermal diffusion length in carbon black is larger than its thickness. Therefore the heat developed in carbon black will be transferred to the silver film and glass respectively. The quantity of heat transfer depends on the thermal diffusion length which in turn is inversely proportional to the chopping frequency. At higher chopping rates the amount of heat transfer to the backing material is appreciably small and the PA signal contribution arises solely from the sample surface. In the graph the region marked by  $\Delta$  in trace A gives the combined effect of glass and

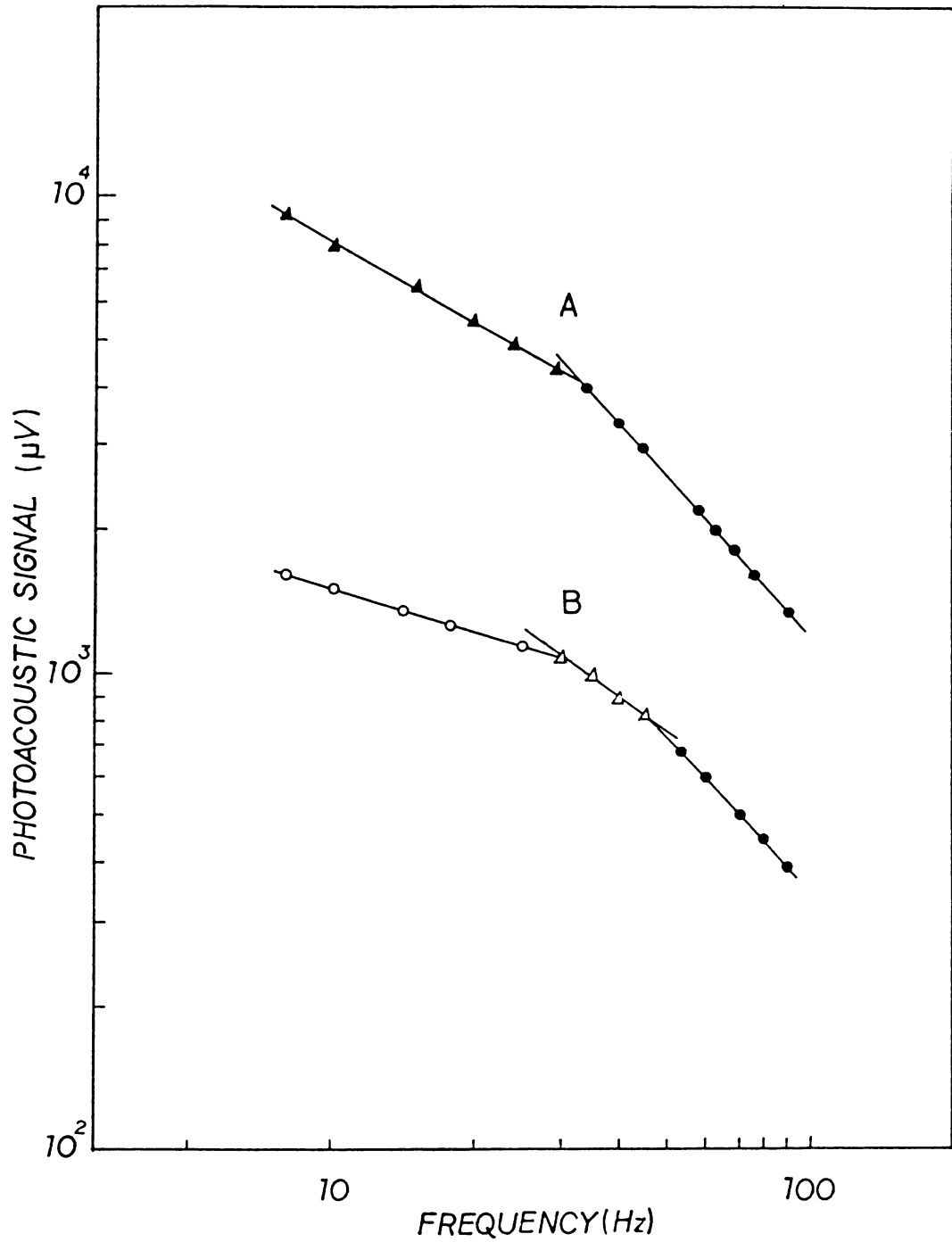


Fig. 4.11 Magnitude of the PA signal vs the chopping frequency for carbon black with two backing materials. (A - carbon black and glass; B - carbon black, silver film and glass combination)

carbon black while its lower part having a slope of -1 is the effect of carbon black only which agrees with the previous results [11]. Similarly in trace B the slope of the segment of the line marked by  $\circ$  gives the combined effect of carbon black, silver film and glass while the central portion represented by  $\Delta$  gives the total effect of silver film and carbon black and the lower region denoted by  $\bullet$  gives the effect of carbon black only. The corresponding phase difference measured by the lock-in amplifier is in agreement with the same obtained from the slopes at different regions [11] through the relation  $\Delta \phi = -\eta \pi / 2$ , where  $\eta$  is the slope of the graph. The slopes and respective phase differences are shown in Table 4.1.

This experiment infact reveals the effect of backing materials of finite extension on the amplitude and phase of the PA signal. Since this method probes the continuous heat diffusion process through the sample-backing interface, any flaw that exists in the backing material may cause an abrupt change in the heat flow which inturn induces a substantial change in amplitude and phase of the PA signal. Also if the portion represented by  $\Delta$  in the fig. 4.2, which corresponds to the slope of the silver film, can be calibrated with the frequency variation, then the thickness of the silver film can be calculated. One of the recent applications in this area is the non destructive testing and identification of light absorbing layers in the Afgachrome CT 21 colour photographic films [12].

Table 4.2                      Analysis of phase measurements

<i>Material</i>	<i>Slope</i>	<i>Phase (degrees)</i>
<i>Carbon black + silver + glass</i>	<i>-0.33</i>	<i>-30</i>
<i>Carbon black + silver</i>	<i>-0.8</i>	<i>-75</i>
<i>Carbon black + glass</i>	<i>-0.625</i>	<i>-55</i>
<i>Carbon black</i>	<i>-1</i>	<i>-90</i>



**References :**

1. A.C. Tam, Rev. Mod. Phys. 58, 2, 381 (1986).
2. C. A. Bennet Jr. and R. R. Patty, Appl. Opt., 21, 49 (1982).
3. A. Rosencwaig, Adv. Electron. Electron Phys. 46, 207 (1978).
4. A. Rosencwaig, 'Photoacoustics and Photoacoustic Spectroscopy,' (Wiley and Sons, New York) (1980).
5. Y. S. Touloukian, R. W. Powell, C.Y.Ho and M. C. Nicolasu, 'Thermal Diffusivity,' (IFI/Plenum, New York) (1973).
6. M. J. Adams and G. F. Kirkbright, Analyst, 102, 281 (1977).
7. M. J. Adams and G. F. Kirkbright, Analyst, 102, 678 (1977).
8. A. Rosencwaig and E. Pines, J. Invest. Dermatol., 69, 296 (1977a).
9. S. D. Campbell, S. S. Yee and M. A. Afromowitz, J. Bioeng, 1, 185 (1977)
10. Per Helander and Ingemar Lundstrom, J. Appl. Phys., 52, 1146 (1981).
11. J. L. Parpal, J. P. Monchalin, L. Bertrand and J. M. Gagne, J. Appl. Phys., 52, 6879 (1981).
12. P. Charpentier and F. Lepoutre and L. Bertrand, J. Appl. Phys., 53, 608 (1982).
13. R. T. Swim, Appl. Phys. Lett., 42, 955 (1983).
14. Thomas P. Crowley, Frederick R. Faxvog and David M. Rossler Appl. Phys. Lett., 36, 641 (1980)
15. K. O. Park, S.I. Yun and C.S. Sol., New Physics (Korean Physical Society) 21, 183 (1981).
16. Andre Lachine, J. Appl. Phys., 57, 5075 (1985).
17. Andre Lachine and Patrick Poulet, Appl. Phys. Lett., 45, 953 (1984).

18. D. Pessoa Jr., C. L. Cesar, N. A. Patel and H. Vargas, Digest of the 4th International Topical Meeting on Photoacoustics, Thermal and Related Sciences, Villed' Esteral (Qubec), Canada, P.W.A. 9.1 (1985).
19. R. Kordecki, B. Bein and J. Pelzl, Digest of the 4th International Topical Meeting on Photoacoustic Thermal and Related Sciences, Villed' Esteral, (Qubec), Canada, P.W.A. 3.1 (1985).
20. P. Hefferle and H. Coufal, Digest of the 4th International Topical Meeting on Photoacoustics, Thermal and Related Sciences, Villed' Esteral (Qubec), Canada, P.W.A. 2.1 (1985).
21. K. N. Madhusoodanan, Mini. R. Thomas and Jacob Philip, J. Appl. Phys. (in press).
22. Patrick Poulet, Ph.D. Thesis, L' Universities Louis Pasteur de strasbourg, (1985).
23. C. D. Hodgman, Handbook of Chemistry and Physics (Cleveland : The Chemical Rubber Publishing Co.) (1963).
24. M. J. Adams, Prog. Analyst. Atom. Spectros 5, 153 (1982).
25. R. Glang and L. V. Greor, 'Handbook of Thin Film Technology, Leon I. Maisel and Reinhard Glang (Ed.,) (McGrawhill : New York) (1970).
26. M. K. Satheeshkumar and C. P. G. Vallabhan, Proceedings of Solid state Physics Symposium (Nagpur), DAE, 28c. P.328 (1985). (1970).
27. H. L. Kwok and W. Siu, Thin Solid Films, 61, 249 (1979).
28. J. F. McClelland and R. N. Knisely, Appl. Opt., 15, 2568 (1976).
29. M. K. Satheeshkumar, K. P. Vijayakumar and C. P. G. Vallabhan, Proceedings of the Quantum Electronics Symposium, DAE, (Bombay) p. 164 (1985).

## CHAPTER V

### DESIGN AND FABRICATION OF A CURRENT STABILISED CW CO<sub>2</sub> LASER

#### ***Abstract***

*This chapter is divided into two parts in which Part A describes the historical background and theoretical aspects of CO<sub>2</sub> laser. Part B gives a detailed account of the various components of a CW CO<sub>2</sub> laser system and its working. A comprehensive description of the design and fabrication of a current stabilisation circuit for CO<sub>2</sub> laser is given in this part.*

## PART A

### 5.1 Introduction :

Since the first observation of laser action by Maiman in 1960, considerable efforts were devoted to develop new types of lasers. One of the most remarkable achievements in this regard was the discovery of a highly efficient  $\text{CO}_2$  laser working in the far infrared region by Patel in 1964 [1, 2]. In fact this discovery ushered in a new era in the field of laser applications. Subsequent work in the development in  $\text{CO}_2$  laser systems could bring out lasers having very high output power both in CW and pulsed mode operation. At present  $\text{CO}_2$  lasers are extensively being used as an industrial tool for cutting, drilling and welding purpose with great precision. They play an important role in laser fusion studies and are utilised as a pumping source for secondary lasers like Spin Flip Raman laser. Very often bloodless surgery is being successfully carried out using this laser.

A brief historical survey and the basic theoretical aspects of laser action in  $\text{CO}_2$  are given in the following sections.

Polanyi in 1961 [3] suggested the possibility of utilising rotation-vibration transitions for laser action, and it was in 1963 Legay and Barchenwitz [4] observed strong infrared emission from  $\text{CO}_2$  when it was mixed with vibrationally excited  $\text{N}_2$  and they suggested this as an indication of collisional energy transfer. Subsequently Legay and Sommaire [5] in 1964 put forward theoretical prediction for the possibility of laser action with

the rotation-vibration bands of gases excited by active  $N_2$  and mentioned specifically the  $10.6 \mu\text{m}$  transition from  $CO_2$ . At about the same time Patel [1,2] observed laser action in pure  $CO_2$  at  $10.6 \mu\text{m}$ . He used a 5 m Plasma tube and obtained a laser power of 1 mW CW output which dc excitation and 10 mW peak power with  $1 \mu\text{sec}$  pulsed excitation. Later Howe [6] investigated the effect of various molecular gases on the laser beam intensity and he could observe oscillations on R branch as well as P branch lines. Moeller and Ridgen [7] constructed a sealed tube containing  $CO_2$ - $N_2$ -He mixture in which a gain of  $10 \text{ Wm}^{-1}$  was obtained. Patel [8] modified the above system by incorporating water cooled plasma tube containing  $CO_2$ - $N_2$ -He mixture which produced over  $50 \text{ Wm}^{-1}$ . This work, in fact marked a new phase in the development of  $CO_2$  lasers. By the end of 1968 a 750 ft long CW  $CO_2$  laser was designed by Patel et al.[9] and obtained an output power of 8.8 kw.

In 1969 attempts were continued to develop high power  $CO_2$  laser systems operating in the CW mode as well as in pulsed mode. Subsequently in 1970, Beaulieu [10] could obtain laser emission from a Transversely Excited Atmospheric (TEA) laser in which the gas was flowing perpendicular to the electrical discharge. This in fact opened up the possibility of creating high densities of electronic charge using electron-beam excitation [11] or volumetric photoionization [12] independent of the discharge used to excite laser emission. By incorporating this idea microsecond pulses with energies in the kilojoule range could be obtained. Tani et al. [13] in 1972 designed a resistorless pin-curved-rod system and with an

excitation voltage upto 228 kV, he could obtain 15 MW output laser power. The advantage of this system was high pressure gases could be excited with better efficiency.

Another important achievement was the development of a gas dynamic laser which can deliver enormous amount of output power. The first laser of this type was developed by Garry [14] in which he used a mixture of 7.5% CO<sub>2</sub>, 9.13% N<sub>2</sub> and 1.2% H<sub>2</sub>O heated to a temperature of 1400 K at a pressure of 17 atmosphere before it was allowed to expand supersonically through a nozzle to create the desired population inversion.

In 1978, a combination of 8 beam CO<sub>2</sub> laser system was successfully employed for laser fusion studies [15]. This system was named HELIOS which could deliver a total output energy of 10 kJ with 0.5 nsec pulse duration.

## 5.2 Theoretical considerations for laser action :

Very often theoretical backgrounds of the nature and properties of the energy levels of the active medium of the laser are essential for a thorough understanding of the kinetic process taking place during laser emission process, its power output and efficiency. Such studies in CO<sub>2</sub> laser output has identified about 130 rotational lines in the two lasing bands [16]. Since CO<sub>2</sub> laser employs mainly a mixture of CO<sub>2</sub> and N<sub>2</sub>, the spectroscopic aspects of both gases are essential for the complete understanding of laser emission.

### 5.2.1 Vibrational energy levels of $N_2$ and $CO_2$

The ground electronic state of  $N_2$  is a  $\Sigma_g^+$  state: its first vibrational excited level lies  $2329.66 \text{ cm}^{-1}$  above the vibrationally unexcited ground state described by Lofthus in 1956 [17]; the second vibrational level lies at  $4630.83 \text{ cm}^{-1}$ . Since  $N_2$  is a homonuclear molecule, it has a zero dipole moment in the ground state. Thus the radiative rotation-vibration transitions are strictly forbidden and it implies that vibrational energy can be turned into translational energy during intermolecular collisions.

Carbon dioxide is a linear, symmetric, triatomic molecule; its rotation-vibration spectrum has been studied in detail and a fairly comprehensive description has been given by Courtoy [18] in 1957. As shown in fig. 5.1, the molecule can vibrate in three different modes. The longitudinal symmetric mode ( $\nu_1$ ) is the one in which the carbon atom remains stationary while the oxygen atoms move in opposite directions along the internuclear axis. The bending mode ( $\nu_2$ ) in which the atoms all move in a plane perpendicular to the inter-nuclear axis, the carbon atom going one way and two oxygen atoms go the other, is in fact doubly degenerate. In the longitudinal asymmetric mode ( $\nu_3$ ) the atoms all move along the inter-nuclear axis with the carbon atom moving in opposite direction to the two oxygen atoms. Usually the vibrational levels are designated by three numbers indicating the number of vibrational quanta of each mode associated with the level and represented in the order ( $\nu_1, \nu_2, \nu_3$ ). The energy levels of  $CO_2$  molecule are situated at  $2349.3 \text{ cm}^{-1}$ ,  $1388 \text{ cm}^{-1}$ ,  $1285.5 \text{ cm}^{-1}$  and  $667.3 \text{ cm}^{-1}$  above the ground

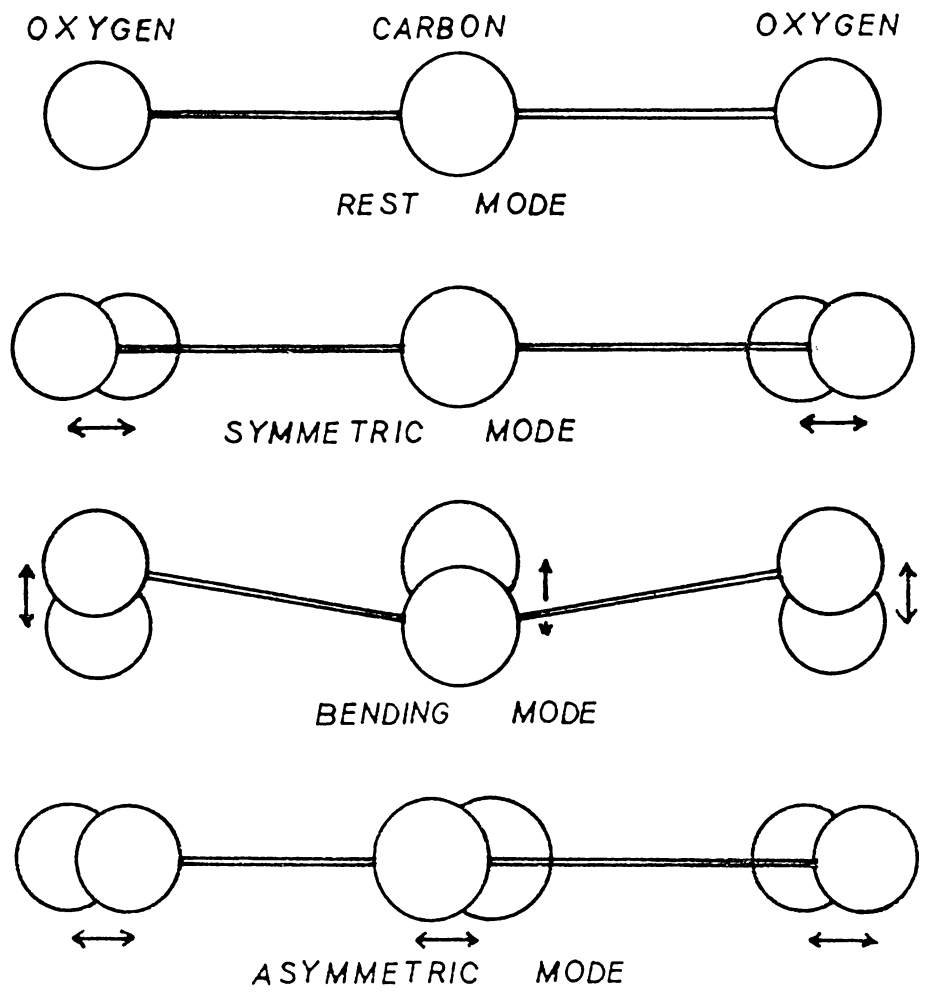


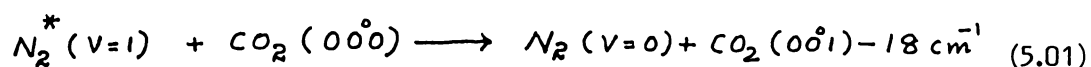
Fig. 5.1 The fundamental modes of vibration of the  $\text{CO}_2$  molecule



state as shown in fig. 5.2. These levels are represented as  $(0\overset{\circ}{0}1)$ ,  $(1\overset{\circ}{0}0)$ ,  $(0\overset{\circ}{2}0)$  and  $(0\overset{\circ}{1}0)$  respectively. The  $(0\overset{\circ}{0}1)$  level is only  $20 \text{ cm}^{-1}$  above the  $v = 1$  level of  $\text{N}_2$  and similarly the higher  $v_3$  levels are close to the corresponding higher vibrational levels of  $\text{N}_2$ .

### 5.2.2 Excitation mechanisms :

Carbon dioxide is excited primarily by two mechanisms in  $\text{CO}_2\text{-N}_2$  gas mixtures: inelastic collision with low energy electrons and the resonant energy transfer from vibrationally excited  $\text{N}_2$  molecules. Since  $\text{N}_2$  has a zero dipole moment, populations will tend to build up in excited vibrational levels of the  $\text{N}_2$  molecule when it is excited by a discharge. The first excited vibrational level of  $\text{N}_2$  ( $v = 1$ ) lies at an energy nearly coincident with the  $\text{CO}_2(0\overset{\circ}{0}1)$  level. The slight energy difference between these two levels may cause an efficient resonant energy transfer from  $\text{N}_2^*$  ( $v = 1$ ) to  $\text{CO}_2(0\overset{\circ}{0}1)$  when  $\text{N}_2$  collides with  $\text{CO}_2$ . This can be represented as



Because of the resonant nature of the above process, selective excitation of  $\text{CO}_2$  molecules to the upper laser level can be achieved quite efficiently.

Further more, the higher vibrational levels of the  $\text{N}_2$  molecule are nearly equally spaced. Hence the collisions involving  $\text{N}_2(v)$  and  $\text{CO}_2(0\overset{\circ}{0}0)$  cause an efficient vibrational energy transfer in which the excited  $\text{N}_2(v)$  loses  $v'$  quanta of vibrational energy and as a result

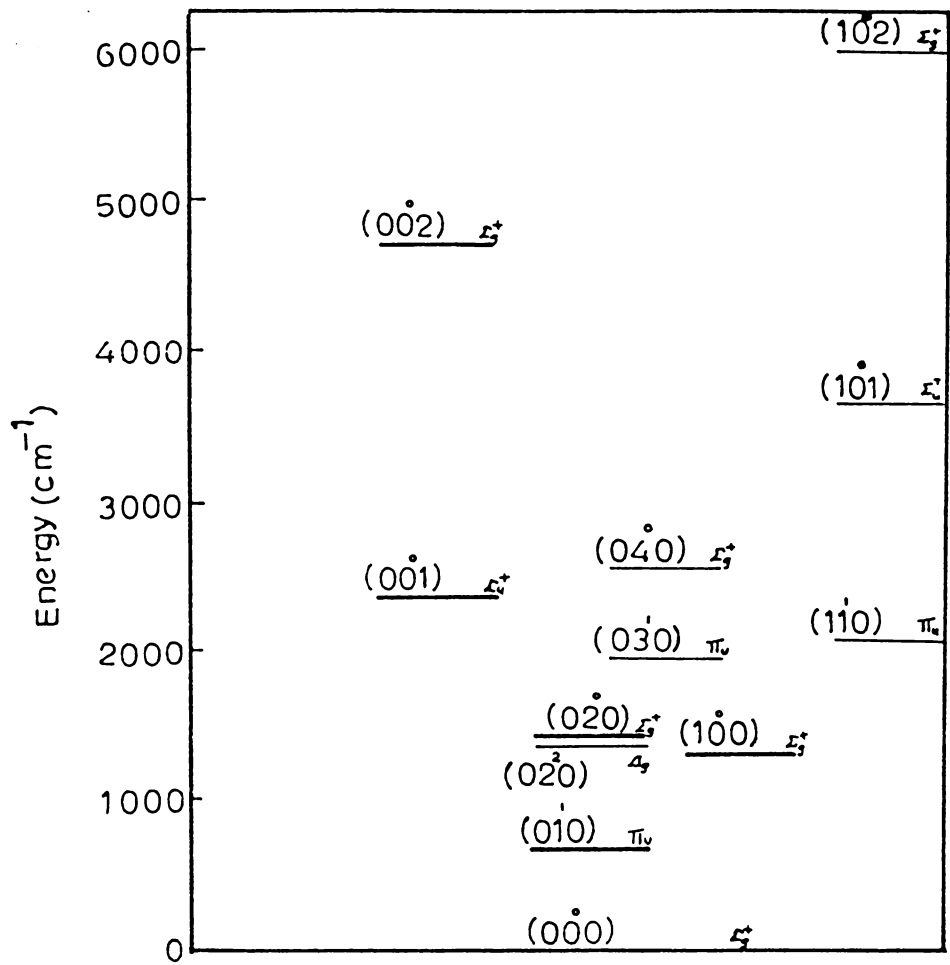
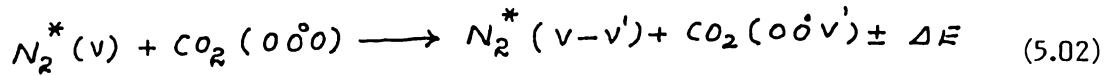
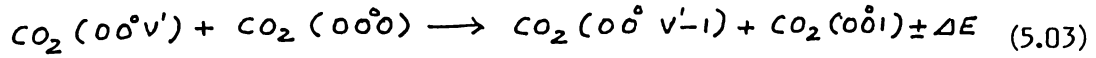


Fig. 5.2 Energy level diagram for CO<sub>2</sub> molecule

it is deexcited to the  $N_2 (v-v')$  level while the  $CO_2 (000)$  molecule gains the  $v'$  quanta of vibrational energy and it is thus selectively excited to the  $CO_2 (00v')$  level. This process can be written as

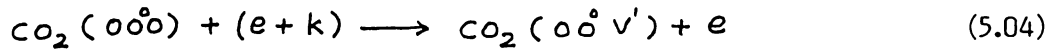


Subsequently the  $CO_2 (00v')$  molecules are converted into  $CO_2 (001)$  molecules through resonant collisions which can be represented as



Therefore by selective excitation of  $CO_2 (001)$  level, a significant increase in the efficiency and power output from a  $CO_2$ - $N_2$  laser can be achieved as compared with a laser employing pure  $CO_2$  only.

In addition to the above excitation processes, a direct electron impact can excite the  $CO_2$  molecule as



which results in exciting the  $CO_2$  molecules to the  $(00v')$  level. From this level  $CO_2 (00v')$  molecules may decay to the  $(001)$  level governed by the equation (5.03). These different excitation mechanisms have been schematically represented in fig. 5.3.

### 5.2.3 Deexcitation mechanism :

The allowed transitions from the levels involved in  $CO_2$  laser action are indicated in fig. 5.4.

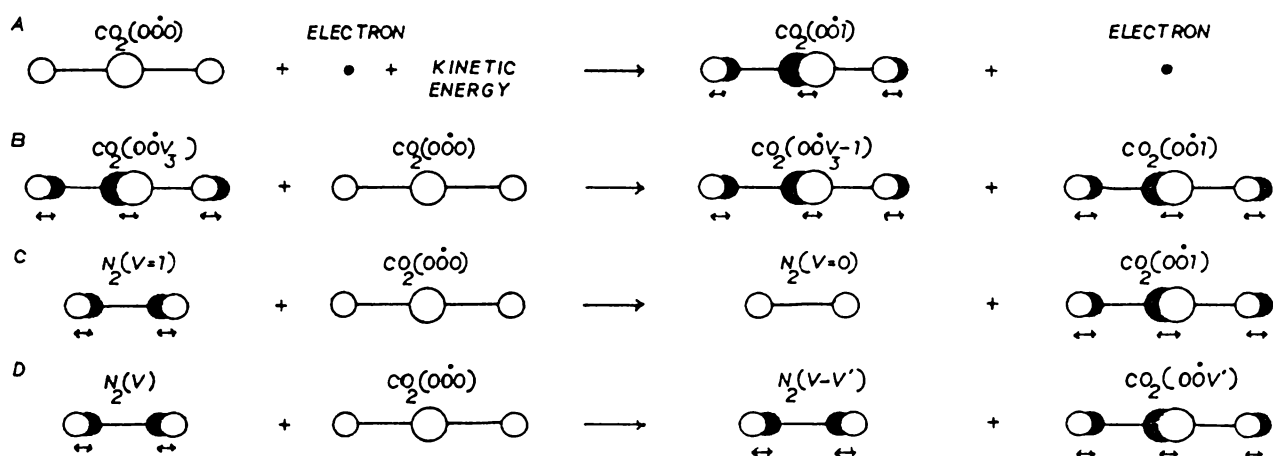


Fig. 5.3 Different excitation processes in  $\text{CO}_2 - \text{N}_2$  system

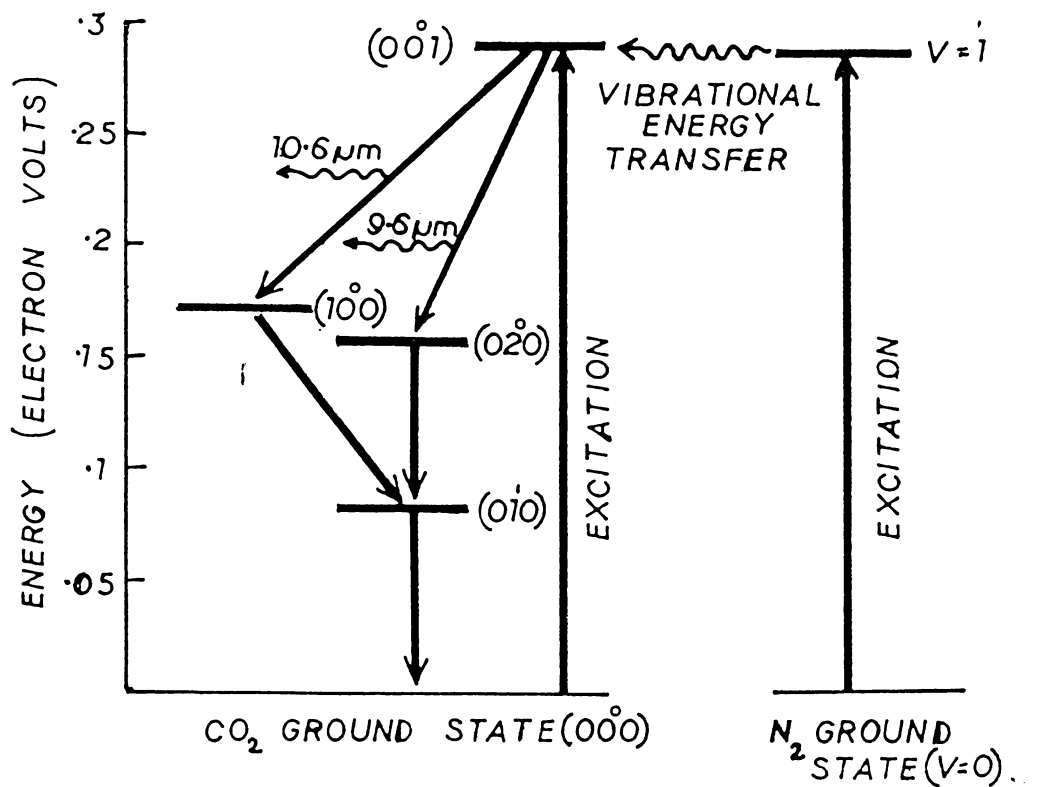
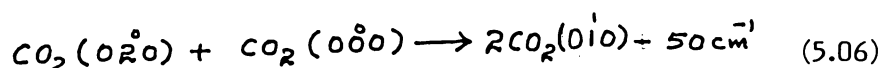
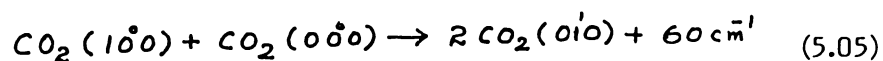


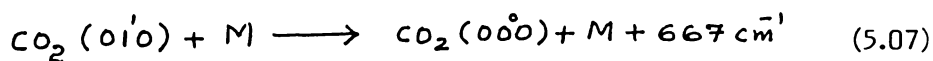
Fig. 5.4 Schematic diagram of various vibrational energy levels in CO<sub>2</sub> and N<sub>2</sub> and the laser action in CO<sub>2</sub> - N<sub>2</sub> system

Following selective excitation to the  $\text{CO}_2(00\overset{\circ}{1})$  level, the laser action occurs for the  $00\overset{\circ}{1} \rightarrow 10\overset{\circ}{0}$  transition ( $10.6 \mu\text{m}$ ) and the  $00\overset{\circ}{1} \rightarrow 02\overset{\circ}{0}$  transition ( $9.6 \mu\text{m}$ ). The lower laser levels ( $10\overset{\circ}{0}$ ) and ( $02\overset{\circ}{0}$ ) have to deexcite to the ( $01\overset{\circ}{0}$ ) level through either radiative or nonradiative decay mechanisms. The radiative decay rates are extremely low and hence the prominent route for deexcitation of  $\text{CO}_2$  molecule from the lower laser level to the  $01\overset{\circ}{0}$  state is through collisional deactivation represented as



The above processes are resonant ones and proceed at fairly rapid rate. Also the radiative life time of the ( $01\overset{\circ}{0}$ ) state is large and the collisional deexcitation assists the decay of  $\text{CO}_2$  molecule from ( $01\overset{\circ}{0}$ ) state to the ground state.

Therefore this decay can be represented as



Where  $M$  represents either a foreign gas or  $\text{CO}_2$  molecule itself. The above processes are schematically represented in fig. 5.5. Since the processes represented by eqns. (5.05) and (5.06) are resonant, presumably the process in eqn. (5.07) which determines the rate of deexcitation of  $\text{CO}_2$  molecules from lower laser levels and therefore the addition of a foreign gas considerably enhances the laser power. This in fact improves the gain and efficiency of the laser system.

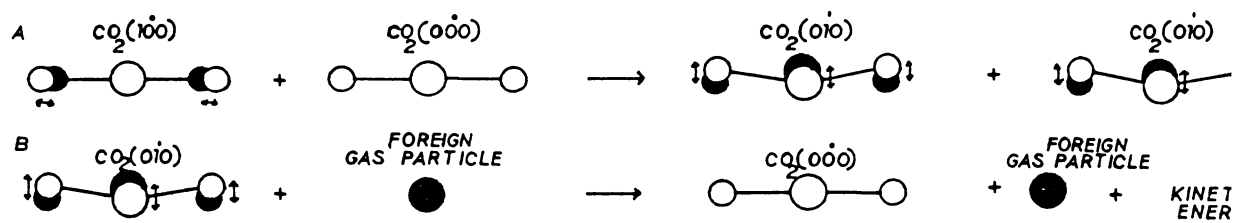
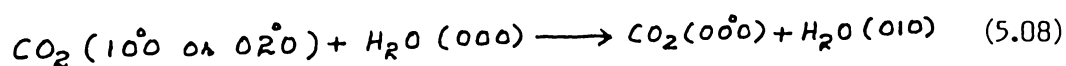


Fig. 5.5 Different deexcitation processes in  $\text{CO}_2 - \text{N}_2$  system

Therefore the addition of a foreign gas somehow changes the excitation conditions in the discharge so that it facilitates more efficient build up of population of 001 level of CO<sub>2</sub> molecules either by directly affecting the excitation mechanisms in CO<sub>2</sub> or by affecting the production rate of vibrationally excited N<sub>2</sub> molecule. Moreover the additive may

increase the power output from CO<sub>2</sub> - N<sub>2</sub> by helping to depopulate the lower laser level rapidly. The lighter gases such as Helium and Hydrogen appear to be more efficient in depopulating the (010) level [19]. It was suggested by Moeller et al. [7] that the efficiency of He is more than N<sub>2</sub> because higher powers were obtained with CO<sub>2</sub> + He mixtures than with CO<sub>2</sub> + N<sub>2</sub> mixtures. The role of He was to serve as a buffer gas reducing the number of excited molecules diffusing to the wall and becoming quenched. Latter Patel [20] suggested the role of He is to transfer energy from He\* (2<sup>3</sup>S<sub>1/2</sub>) metastable levels to the N<sub>2</sub> molecules. Besides due to its large thermal conductivity, it cools the plasma which in turn quickly depopulates the lower laser level [21]. In addition to this Helium plays an important role in maintaining the energy distribution of electrons within the discharge tube for more efficient excitation of CO<sub>2</sub> molecule.

Water vapour also enhances the laser efficiency by depopulating the lowest vibrational level of CO<sub>2</sub>. Therefore the addition of water vapour can also help to deexcite (100) level and (020) level of CO<sub>2</sub> directly to the ground level through the process.





This essentially depopulates the  $(010)$  level thereby enhancing the population inversion in the medium.

In addition to the vibration of oxygen and carbon atom with respect to one another, the  $\text{CO}_2$  molecule is free to rotate. As is well known the total energy in an electronic state of this molecule can be approximated by adding the vibrational and rotational energies. Laser transitions have been obtained from both the P-branch ( $\Delta J = -1$ ) and R-branch ( $\Delta J = +1$ ) of each band where  $J$  is the rotational quantum number. The Q-branch ( $\Delta J = 0$ ) is not allowed because these transitions occur between two  $\Sigma$  states of zero angular momentum which are forbidden by selection rules. It is pointed out that for molecular systems like  $\text{CO}_2$ , the P-branch rotational transition can be made to oscillate even when there is no substantial amount of population inversion between the two vibrational levels.

Fig. 5.6 shows the variation of population density of a number of rotational levels as a function of energy at  $400^\circ \text{K}$  rotational temperature. From this, it is evident that the spacing between the rotational levels increases as  $J$  value increases. The population density of these levels should be given by Boltzmann distribution corresponding to the rotational temperature. With stimulated emission, for a given vibrational-rotational transition one of the following two situations can occur.

- a) the vibrational level lifetime is considerably longer than the thermalization time.
- b) the vibrational lifetime becomes comparable to the thermalization time or shorter than the thermalization time.

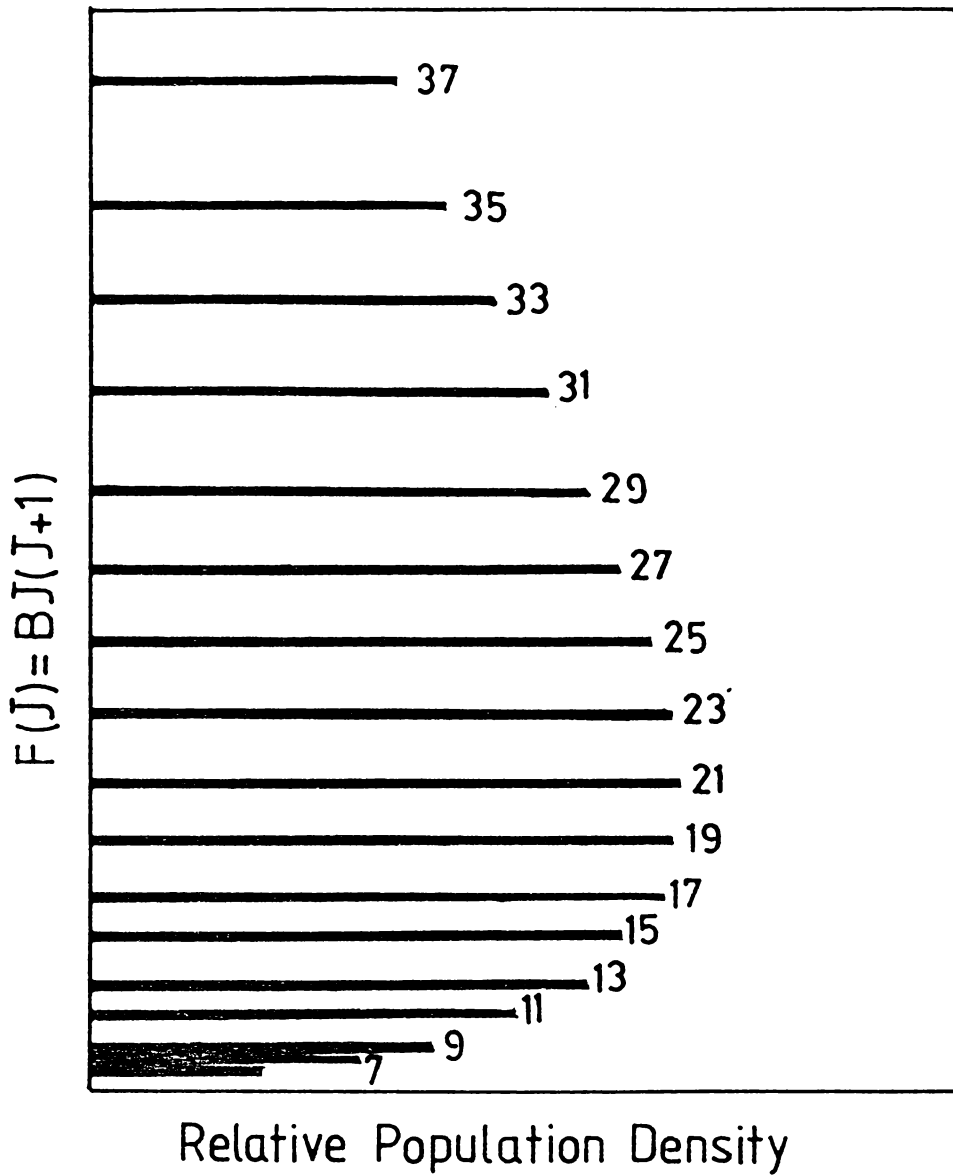


Fig. 5.6 Population density distribution among the rotational levels of 001 vibrational level of CO<sub>2</sub> molecule assuming a Boltzmann distribution at  $T = 400^\circ \text{K}$  (before laser oscillation starts).

At a rotational temperature of 400°K, the gain on the laser transition  $J = 21$  level is found to be the highest as shown in fig. 5.6. A laser transition starting from  $J = 21$  starts oscillating when the discharge is turned on. In the second case mentioned above there will not be any competition effect since the lifetime for  $J = 21$  level becomes considerably shorter than the thermalization time during the stimulated emission. Consequently the population inversion is no longer given by a Boltzmann distribution because the population density of  $J = 21$  level has been reduced to a lower value at which the optical gain on this rotational line just compensates the cavity losses as shown in fig. 5.7. Here since the gain is high for the  $(00\dot{1})$  level as a whole, no competition among other rotational transition exists.

On the other hand, if the rotational lifetime including stimulated emission is larger than the thermalization time, the population distribution is still given by Boltzmann distribution as shown in fig. 5.8. Here the optical gain on different rotational levels in the  $(00\dot{1})$  vibration level will also correspondingly reduced to a level in which gain is less than the single pass loss in the laser cavity. Therefore the laser action will take place only on the transition starting from  $J = 21$  which begins to oscillate first because the net gain on  $J = 21$  transition is the highest in the absence of stimulated emission.

Under CW operating conditions in  $\text{CO}_2$  lasers, very strong competition effects among various rotational transitions exist and in most of the high power lasers the output power is usually confined to only one or two of the rotational transitions of the  $(00\dot{1} - 1\dot{0}0)$  band at  $10.6 \mu\text{m}$ .

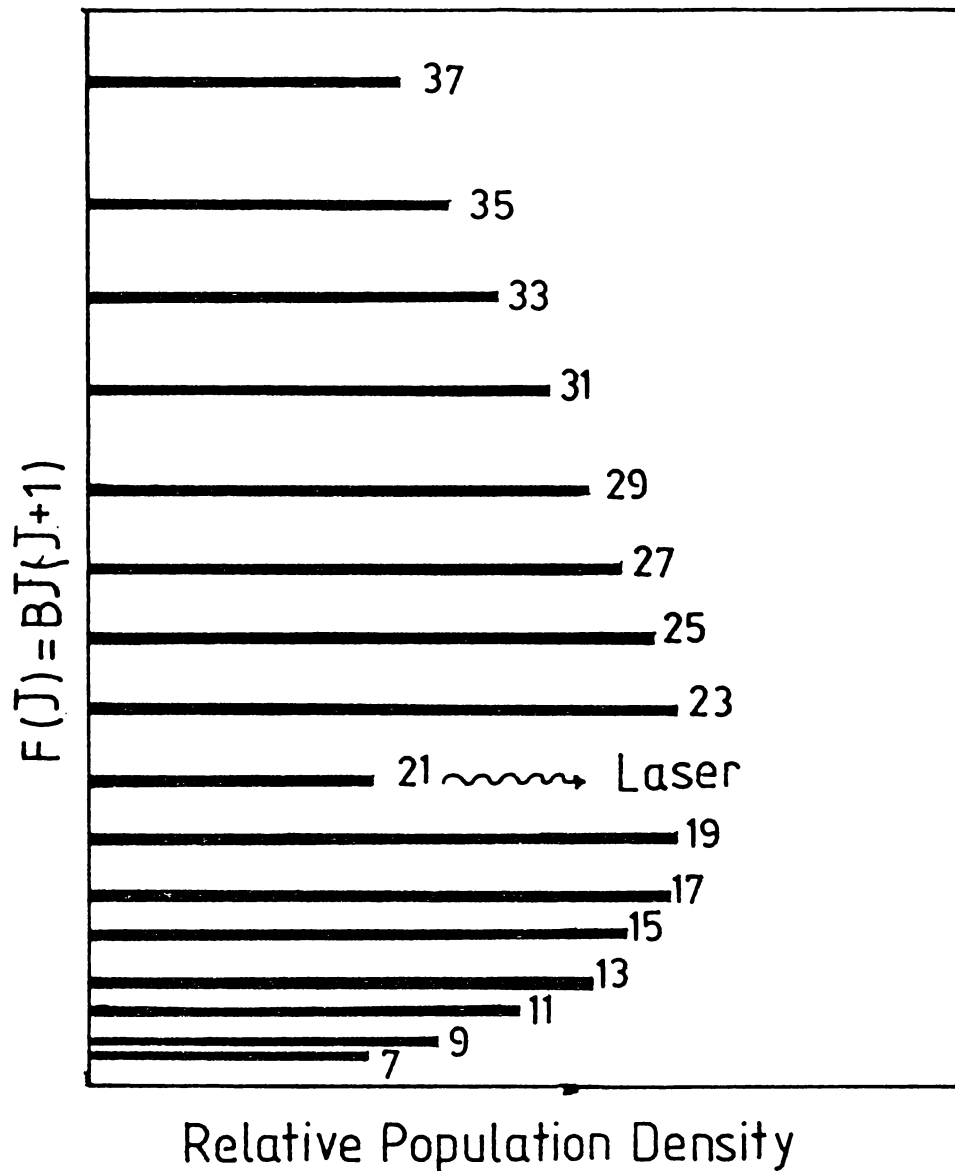


Fig. 5.7 Rotational level population density distribution of the 001 level of CO<sub>2</sub> with laser oscillation of (001 - 100) band. The transition starting from  $J = 21$  rotational level of the 001 vibrational level assuming that level life time including stimulated emission is shorter than the thermalisation time.

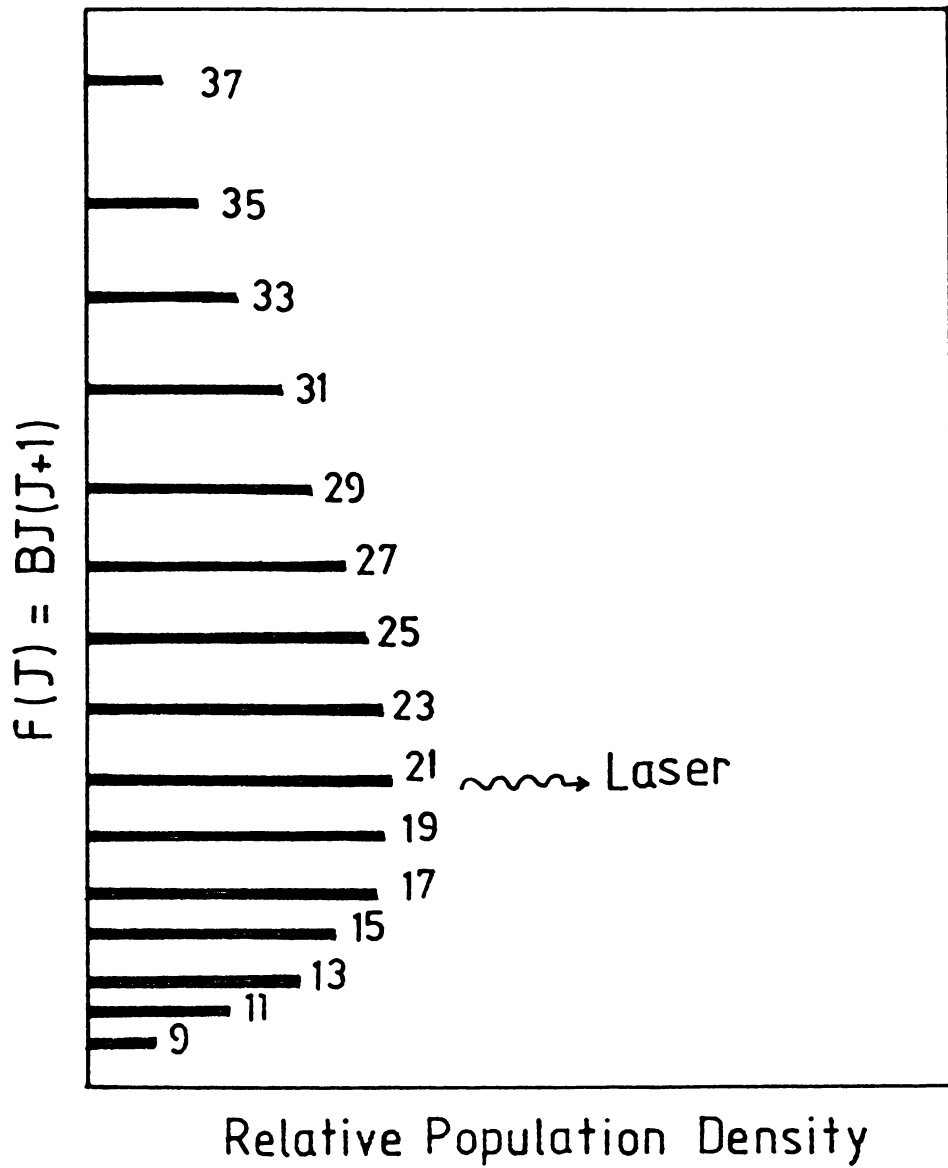


Fig. 5.8 Rotational level population density distribution of the  $00\bar{1}$  vibrational level of  $\text{CO}_2$  with laser oscillation of  $(00\bar{1} - 10\bar{0})$  band, assuming that level life time including stimulated emission is larger than the rotational thermalisation time.

Under certain conditions, some of the high power lasers oscillate on a number of P-branch transitions, at the same time various other rotational transitions do not oscillate in similar transverse modes of the cavity. Relative gain of prominent rotational lines with frequency is shown in fig. 5.9

The time development of energy densities stored in the vibrational modes of  $\text{CO}_2$  and in the vibration of  $\text{N}_2$  are given by the rate equations [22]. Let  $E_1$ ,  $E_2$ ,  $E_3$  and  $E_4$  are the energy densities ( $\text{J}/\text{cm}^3$ ) stored in the  $\text{CO}_2$   $\nu_1$ ,  $\nu_2$  and  $\nu_3$  modes and the stretching mode of  $\text{N}_2$  respectively. Temperatures  $T_1$ ,  $T_2$ ,  $T_3$  and  $T_4$  are associated with each of the molecules.

Then

$$\begin{aligned} \frac{dE_1}{dt} = & N_e(t) N_{\text{CO}_2} h\nu_1 X_1 - \left[ \frac{E_1 - E_1^e(T)}{\tau_{10}(T)} \right] - \left[ \frac{E_1 - E_1^e(T_2)}{\tau_{12}(T_2)} \right] \\ & + \left[ \frac{h\nu_1}{h\nu_3} \right] \left[ \frac{E_3 - E_3^e(T, T_1, T_2)}{\tau_3(T, T_1, T_2)} \right] + h\nu_1 \Delta N W I_{\nu} \end{aligned} \quad (5.09)$$

$$\begin{aligned} \frac{dE_2}{dt} = & N_e(t) N_{\text{CO}_2} h\nu_2 X_2 + \left[ \frac{E_1 - E_1^e(T_2)}{\tau_{12}(T_2)} \right] - \left[ \frac{E_2 - E_2^e(T)}{\tau_{20}(T)} \right] \\ & + \left[ \frac{h\nu_2}{h\nu_3} \right] \left[ \frac{E_3 - E_3^e(T, T_1, T_2)}{\tau_3(T, T_1, T_2)} \right] \end{aligned} \quad (5.10)$$

$$\begin{aligned} \frac{dE_3}{dt} = & N_e(t) N_{\text{CO}_2} h\nu_3 X_3 - \left[ \frac{E_3 - E_3^e(T, T_1, T_2)}{\tau_3(T, T_1, T_2)} \right] + \left[ \frac{E_4 - E_4^e(T_3)}{\tau_{43}(T)} \right] \\ & \text{Similarly} \quad - h\nu_3 \Delta N W I_{\nu} \end{aligned} \quad (5.11)$$

$$\frac{dE_4}{dt} = N_e(t) N_{\text{N}_2} h\nu_4 X_4 - \left[ \frac{E_4 - E_4^e(T_4)}{\tau_{43}(T)} \right] \quad (5.12)$$

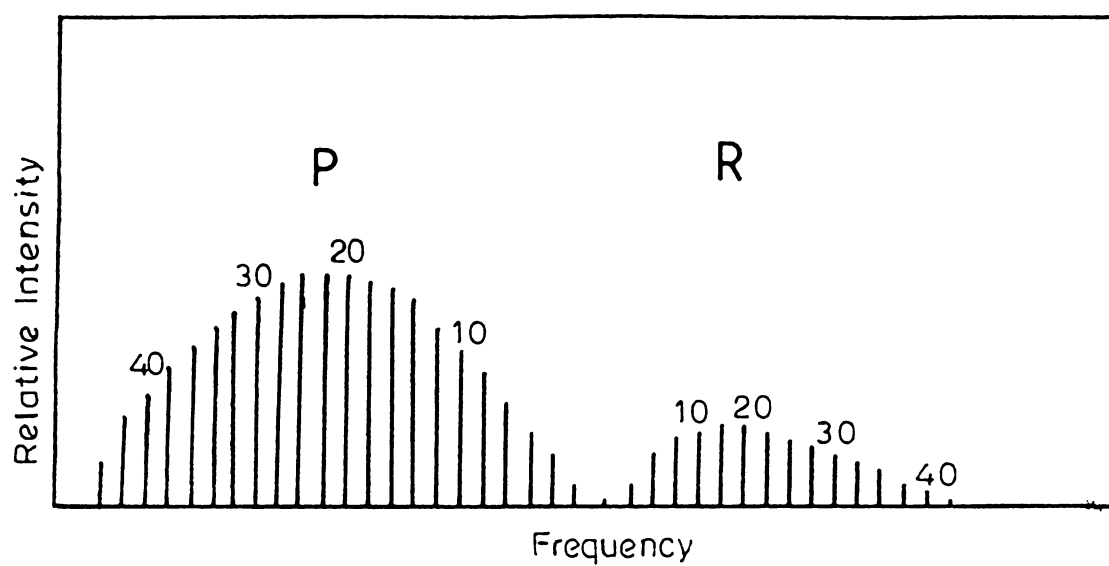


**Fig. 5.9** *Relative intensity distribution of P and R branches for the (001 - 100) band at a rotational temperature of 400 K.*

where the cavity field intensity is given by

$$\frac{dI_{\nu}}{dt} = -\left(I_{\nu}/\tau_c\right) + c h \nu_{\ell} \Delta N [W F I_{\nu} + S] \quad (5.13)$$

where

- $N_e(t)$  - density of electrons at time  $t$
- $N_{CO_2}$  - density of  $CO_2$  molecules
- $h \nu_i$  - energy of  $i^{\text{th}}$  vibrational mode
- $X_i$  - effective electron vibrational excitation rate for  $i^{\text{th}}$  mode ( $X_4 \equiv N_2$ )
- $E_i^e(\tau_i)$  - equilibrium values of  $E_i$  at temperature  $T_i$
- $\tau_{ij}$  - relaxation time associated with transfer of energy between modes  $i$  and  $j$
- $\tau_3$  - relaxation time of the antisymmetric mode
- $W$  - stimulated emission rate at the line center =  $c^2 A F / (4 \pi^2 h \nu_{\ell}^3 \Delta \nu_H)$
- $\nu_{\ell}$  - laser frequency
- $A$  - Einstein A coefficient
- $\Delta \nu_H$  - homogenous line width for laser transition
- $I_{\nu}$  - laser intensity
- $F$  - ratio of the mode volume filled with gain medium to total mode volume = (laser gain-medium length) / optical cavity length
- $\Delta N$  - population difference, =  $[N_{0,0i} P(J) - (\theta_j / \theta_{j+1}) N_{1,0o}] P(J+1)$
- $\theta_J$  -  $(2J+1)$   $J$  being rotational quantum number
- $P(J)$  -  $\left[ \frac{2hcB}{kT} \right]^J \exp(-hcBJ(J+1)/kT)$



- $B$  - rotational constant  
 $T$  - translation temperature  
 $\tau_c$  - laser cavity lifetime,  $= 2L/C \ln R$   
 $L$  - cavity length  
 $R$  - output mirror reflectivity  
 $S$  -  $ch \nu_L W$

The first term in each equation describes the pumping of the particular level by direct electron excitation. Terms with  $\tau_{10}$  are designated by the rate of vibration-translation (V-T) relaxation and those with  $\tau_{ij}^{-1}$  measure rates of vibration - vibration (v-v) exchange. The expressions with  $\tau_3^{-1}$  show the extent of (V-V) exchange involving the asymmetric stretching mode. The last terms in equation (5.09) and (5.11) depend on  $I_{\nu}$ , which is the rate of stimulated emission from upper to the lower laser levels.

The above rate equations predict the time dependence of population inversion and gain in the medium.

The first theoretical calculation concerning laser action in  $CO_2$  were to relate the gain to the population inversion. Patel [1,2] calculated the gain coefficients for the P and R branch lines and showed that for a given population inversion the P branch lines have a higher gain than the R branch lines.

The full gain expression by Patel [1] and Djeu [23] are,

$$\begin{aligned}
 \alpha_p(J) = & \frac{h}{8\pi k \nu} \sqrt{\frac{Mc^2}{2\pi k}} \frac{\lambda_{21}^3 A_{21}}{T^{3/2}} (2J-1) \left[ n_2 B_2 \exp\left\{-F_2(J-1) \frac{hc}{kT}\right\} \right. \\
 & \left. - n_1 B_1 \exp\left\{-F_1(J) \frac{hc}{kT}\right\} \right] \quad (5.14)
 \end{aligned}$$

Similarly,

$$\alpha_R(J) = \frac{h}{8\pi k} \sqrt{\frac{Mc^2}{2\pi k}} \frac{\lambda_{21}^3 A_{21}}{T^{3/2}} (2J+3) \left[ n_2 B_2 \exp\left\{-F_2(J+1) \frac{hc}{kT}\right\} - n_1 B_1 \exp\left\{-F_1(J) \frac{hc}{kT}\right\} \right] \quad (5.15)$$

Where

- h - Planck's constant
- k - Wave vector =  $2\pi/\lambda$
- C - Velocity of light
- J - Rotational quantum number
- $\lambda_{21}$  - Wavelength of the transition
- $A_{21}$  - Einstein's A coefficient
- M - Mass of CO<sub>2</sub> molecule
- T - Equilibrium gas kinetic temperature
- n - Total vibrational population
- B - Rotational constant
- F (J) - Rotational energy term.

To a good approximation the gain coefficient will be,

$$\alpha(J) = \frac{h}{8\pi k} \sqrt{\frac{Mc^2}{2\pi k}} \frac{\lambda_{21}^3 A_{21}}{T^{3/2}} (2J+1) B (n_2 - n_1) \exp\left[-B J(J+1) \frac{hc}{kT}\right] \quad (5.16)$$

where  $B = 0.37 \text{ cm}^{-1}$  and substituting the values  $\alpha \sim 3 \text{ dBm}^{-1}$ , at a rotational temperature of  $400^\circ \text{ K}$ .

## PART B

### 5.3 Design and fabrication of a CW CO<sub>2</sub> laser :

The major technological consideration in the design of a laser system is that it should have a stable optical resonator, high voltage stabilised power supply, reliable gas filling system and efficient cooling arrangement. Details of these subsystems constructed for the present studies are briefly described below :

#### 5.3.1 Optical resonator :

The optical resonator geometry plays an important role on the overall efficiency of the laser system. The present system is a longitudinally excited CW CO<sub>2</sub> laser which consists of two identical water cooled plasma tubes of length 70 cm each are arranged optically in series but electrically in parallel. The plasma tube is a commercially available glass tube of internal diameter 8 mm and wall thickness 3 mm. Since there are two plasma tubes which are electrically connected in parallel, separate anodes and cathodes must be provided in the optical cavity. The cathodes are provided at the ends of the cavity while the anodes are placed in the middle of the cavity 12 cm apart. These anodes and cathodes are tightly connected to the plasma tube using O-rings which provide vacuum sealing. Schematic diagram for the glass to metal coupling is shown in fig. 5.10. At one end of the cathode, a gold coated concave mirror (98% reflectivity) with a radius of curvature 7 m is fixed while at the other end a plane germanium window (II - VI compounds Inc., USA)

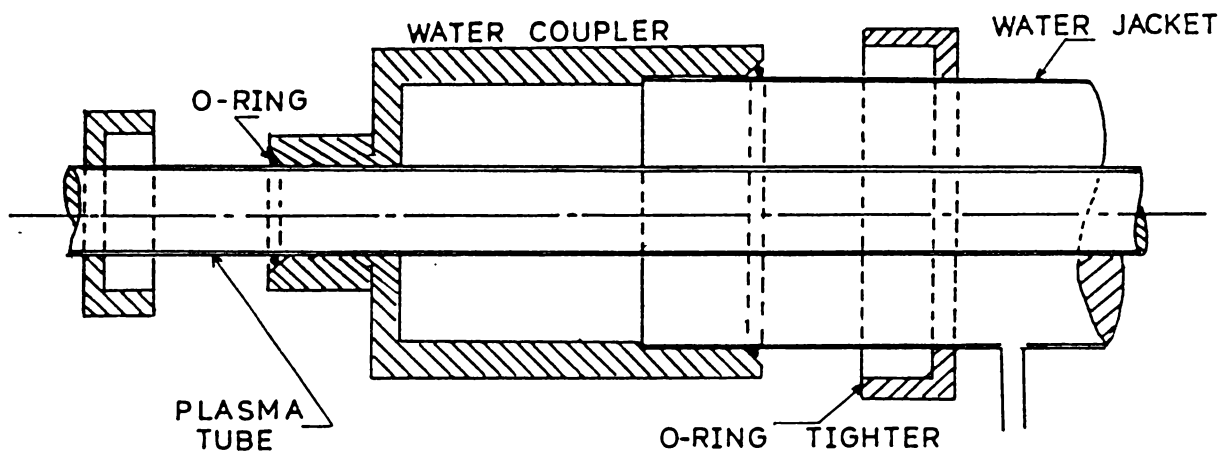


*Fig. 5.10 Schematic diagram of the o-ring coupler used at the glass-aluminium joint in the plasma tube.*

having a diameter 2 cm and thickness 3 mm is attached using neoprene o-rings. Thus the optical resonator designed for the present system is a cylindrical cavity of diameter 8 mm and length 155 cm. Since the cavity consists of a concave mirror and a flat window on the other end, only a single transverse mode will oscillate at a time and this ensures a highly stable cavity.

### 5.3.2 Electrodes :

The geometry of the electrodes play an important role and they must be highly heat dissipative, they should offer low resistance and be corrosion free against the gases. By taking into account the above requirements the electrodes are fabricated so as to suit the system in a compact way. Two identical cathode-anode pairs are made of aluminium. A schematic diagram of the cathode is given in fig. 5.11. Each cathode has an axial bore of 8 mm in which the plasma tube is fixed using o-rings. Similar arrangement has been made to fix the water cooling jacket to the cathode without any leak. Each cathode is attached to an aluminium flange of thickness 8 mm and area  $81 \text{ cm}^2$  using o-ring sealing. The gold coated mirror and germanium window mounts are separately attached on another identical aluminium flange with proper sealing. These two flanges are connected by a standard rubber bellow of length 6 cm and diameter 2.5 cm. The two ends of the bellow are rigidly mounted on the flange using aluminium rings. The bellows are provided with metal rings inside the folds to prevent them from collapsing under low pressure range. The use of these bellows

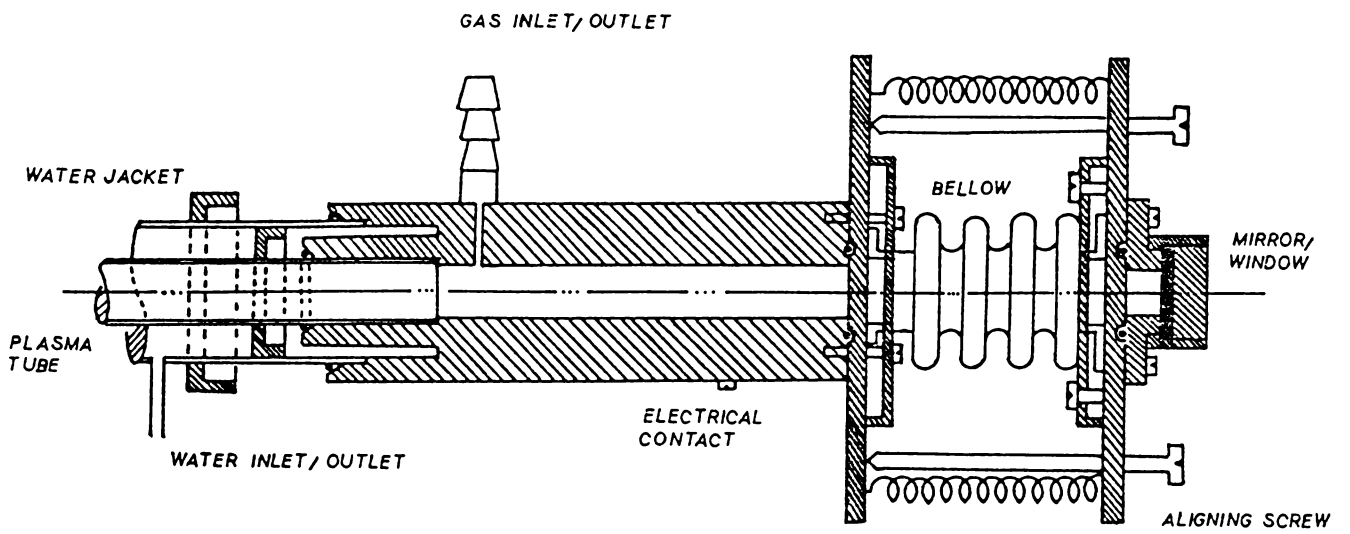


Fig. 5.11 Cross sectional view of the cathode

thus provide a convenient tilting method for the mirror or window by adjusting the aligning screws.

Since the voltage which appears at the anodes are of the order of several kilovolts, it is not practicable to cool it by water circulation. Therefore in order to provide sufficient cooling to the anodes their surface area must be increased to radiate the heat efficiently. Thus cooling fins are provided on aluminium anodes as shown in fig. 5.12 so as to provide better heat dissipation. The anode has a total length of 10 cms and axial bore of 8 mm into which the plasma tubes are inserted and kept vacuum tight with the aid of O-ring sealings. Proper high voltage leads are connected to the anodes with tags and fastners in the present design.

### 5.3.3 Gas filling system :

The gas mixture ratio is highly critical for the resonant energy transfer between  $\text{CO}_2$  molecule and  $\text{N}_2$  molecule. Therefore highly efficient and accurate methods must be selected for mixing these gases. Moreover, the rate of gas flow plays an important role on the laser power output. By incorporating these facts, a careful design of the gas filling system is adopted.

As shown in fig. 5.13, the inlets of the gas mixture are connected at the two ends of the laser cavity while the exhaust is attached to the middle of the plasma tube and this is connected to a rotary pump.

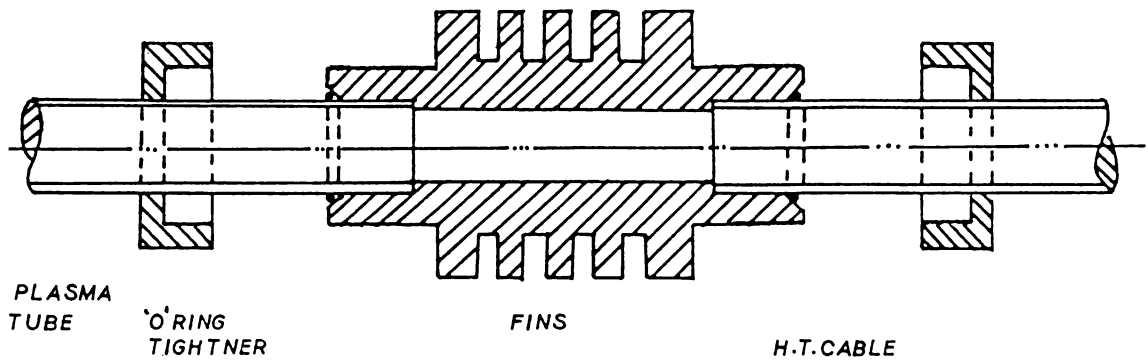


Fig. 5.12 Cross sectional view of the anode



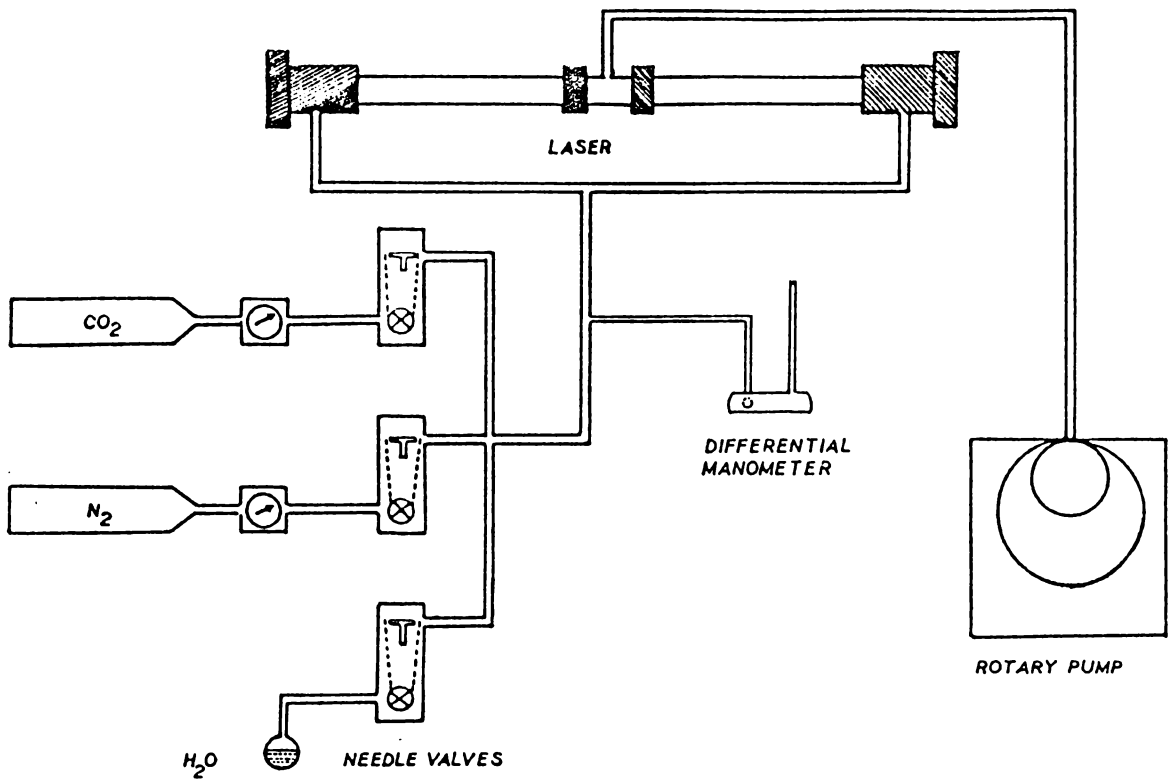


Fig. 5.13 Schematic representation of the gas filling system used in CW CO<sub>2</sub> laser

This arrangement ensures a better gas flow rate compared to a system having the inlet and outlet at the two ends of the cavity. In order to measure the partial pressures of  $\text{CO}_2$  and  $\text{N}_2$  a sensitive differential manometer is designed and fabricated. Silicon oil (sp.gr.1.08) used in the manometer provides high resolution in the measurement of partial pressures of gases. 1 cm height of the silicon oil approximately corresponds to 0.8 torr of gas pressure which ensures better sensitivity over a mercury manometer. Needle valves are used to admit different gases to the cavity with great precision. These arrangements also enable one to control the flow rate in the cavity.

#### 5.3.4 Alignment of the cavity :

In order to obtain oscillations in the laser cavity, optical feed back is necessary. To achieve this condition, it is important that axis of both the window and mirror must be aligned to be perfectly collinear and it should coincide with the axis of the plasma tube. This is usually done by fixing a He-Ne laser outside the cavity such that the laser beam from it is made to pass through the axis of the  $\text{CO}_2$  laser plasma tube. Then the gold coated concave mirror is fixed at one end of the cavity and the mirror is aligned so that the He-Ne laser beam retraces its path. Subsequently germanium window at the opposite end of the  $\text{CO}_2$  plasma tube is fixed and it is aligned to get a clear back reflected spot of the He-Ne laser on the laser itself. Thus the window and the mirror are made parallel to each other and perpendicular to the plasma tube axis.

#### 5.4 High voltage power supply :

High voltage power supply system is essential for exciting the CO<sub>2</sub> laser. It is preferable that these systems should possess simplicity and straight-forwardness in design. The conventional high voltage power supply systems do not have any stabilisation either for voltage or current. Therefore they cannot be utilised to energise a laser system from which a highly stable output is needed. Most of the sophisticated power supplies described in the literature incorporate voltage stabilisation which in fact does not ensure stable output power [23]. Since the plasma tube current of the CW CO<sub>2</sub> laser critically controls the output power, it is the current that has to be stabilised rather than the voltage to get an extremely stable output [24]. In this section the details of design and fabrication of a current stabilised high voltage power supply, with full protectional features to safeguard the plasma tube are described.

In order to excite the active medium in the laser cavity, a 20 kV, 100 mA high voltage DC power supply is fabricated. The essential features are schematically shown in fig. 5.14. High voltage upto 20 kV DC is obtained by rectifying the output voltage of a 20 kV, 100 mA oil cooled step up transformer. A bridge rectifier consists of sixty IN 4007 diodes connected in series in a single arm of the bridge to ensure the proper sharing of total voltage. Even though each diode can withstand a voltage of 1 kV, ( PIV ) sufficient number of diodes are arranged in the bridge rectifier to safeguard it against high peak inverse voltage of 40 kV. In

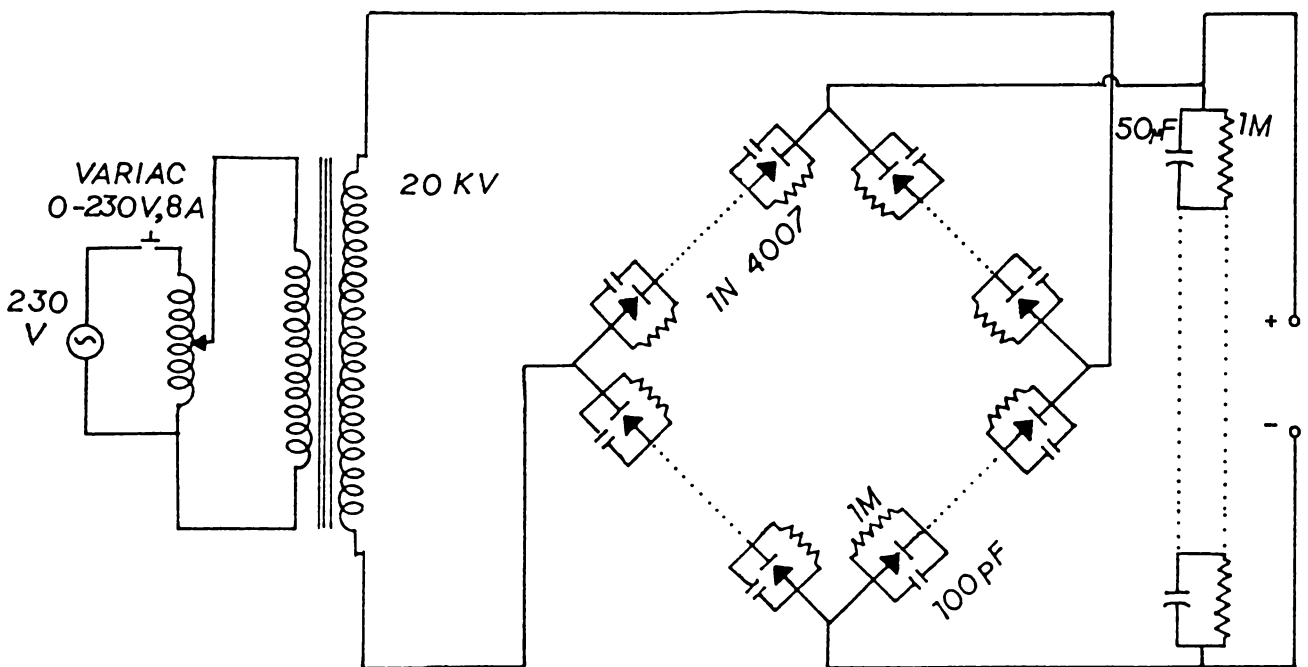


Fig. 5.14. Circuit diagram for 20 kv rectifier

order to ensure equal voltage division by these diodes a  $1\text{ M}\Omega$  resistor along with  $100\text{ pF}$  disc capacitor is arranged in parallel to each of the diodes. The rectified output from the bridge is smoothed by using a series array of 48 electrolytic capacitors ( $50\ \mu\text{F}$ ,  $500\text{ V}$ ). The diodes, resistances and capacitors are soldered and fixed on highly insulated hylem boards.

The plasma tube is divided into two sections which are electrically connected in parallel.

The advantages of this arrangement are :

- i) This reduces the striking as well as maintaining voltage for the plasma tube.
- ii) It keeps high voltages away from the optical mounts and provides a safe operation.
- iii) It offers mechanical simplicity in the design of electrode systems.

But a serious problem with such a configuration is that, because of the slight difference in the striking voltages and discharge characteristics of the plasma tubes the probability of striking a gas discharge simultaneously in the two coupled tubes is very low.

In the present system two sections of the laser tube are connected through two ballast resistors to the positive end of the high voltage power supply as shown in fig. 5.15. After switching on the power, the smoothing capacitor of the power supply reaches the maximum voltage in a few

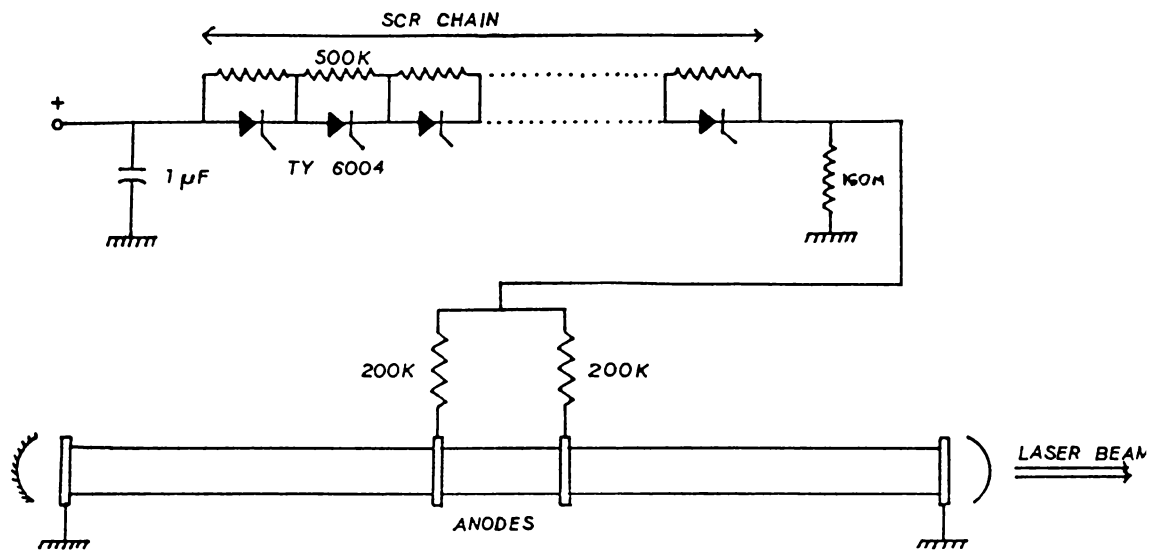


Fig. 5.15. Circuit employed for simultaneous striking of discharge in the two plasma tubes

half cycles of the mains frequency i.e., typically a few tens of milliseconds. During this slow charging the section with lower striking voltage builds up plasma discharge before the other section can strike. This in fact produces a large voltage difference between the two anodes which can result in a discharge between the two anodes. This will prevent discharge in the second section of the pair from striking.

Alternately, if the voltage applied to the two anodes is nearly a step voltage instead of a slowly rising one, simultaneous discharge can be obtained in the two sections. This voltage should be greater than that required by the tube with higher striking voltage, so that inevitably both tubes will be forced to strike simultaneously. When the discharges strike, both the anodes are maintained at nearly the same potential and there is no chance for discharge to occur in the gap between them.

The circuit used for the simultaneous striking of the discharge tube [25] is shown in fig. 51. The two sections of the plasma tube are connected to the positive terminal of the high voltage power supply through two ballast resistors each of 200 K. The circuit switches the voltage on the anodes through a series chain of eight SCRs (TY 6004) used in self breakdown mode to provide required step voltage to the anodes of the plasma tubes. In order to achieve a constant voltage division across the SCRs, appropriate resistances are ( $\sim 500$  K) connected parallel to the SCR chain. The general criteria for the selection of the SCRs are,

- a) they should have fairly low leakage current

- b) they should have low holding current so that the SCR remains in the conduction state after breakdown for the minimum desired operating current in the plasma tube
- c) they should have a large breakdown voltages so that number of SCRs can be minimised for the required step voltage.
- d) all the SCRs in the chain should have nearly equal breakdown voltages so that the parallel resistances connected to each SCR are of same value. But in most of the practical cases, the breakdown voltages are not equal therefore the shunt resistors are to be selected appropriately.

These SCRs start conducting when the voltage across them exceeds the self breakdown voltage. Therefore the step voltage available is nearly equal to the sum of the individual breakdown voltages. This breakdown in fact offers a short circuit path for the current which flows through the plasma tubes soon after it is excited. Therefore the full input voltage is applied across the tubes with a switching time of a few microseconds and this may cause the simultaneous striking of two tubes.

#### 5.4.1 Current stabilisation :

The output power of the  $\text{CO}_2$  laser is dependent on the discharge current through the plasma tube. This current, in turn, has a direct relationship on gas mixture ratio, pressure in the plasma tube, coolant temperature, line voltage and power supply ripple. The effects of above parameters on the operation of a CW  $\text{CO}_2$  laser have been extensively



studied and it is found that other conditions remaining the same, an optimum current has to be maintained for obtaining maximum output power [26]. Thus for a steady output power, a current regulated power supply is usually needed [27]. In the present design [28] a transistor network has been incorporated along with the high voltage power supply to achieve current stability. Since this circuit allows a steady desired value of current through the plasma tube to be maintained irrespective of the voltage variation across the electrodes of the cavity, high stability of output laser power is achieved. This system also incorporates a few protective features intended to safeguard the laser tube as well as the stabilisation circuit against over voltages and over currents. A novel feature of this circuit is that solid state devices have been employed for the current regulated high voltage power supply and the entire system can be fabricated at a low cost with commonly available components.

The main part of the stabilisation circuit is a string of high voltage Darlington transistor pairs (2SC 2068), the bases of which are held at successively decreasing potentials of 250 V each as shown in fig. 5. The emitters of every even numbered Darlington pair are connected respectively to the bases of high voltage power transistor (BU 536) which in turn successively reduce the voltage in equal steps in an alternate parallel chain to the Darlington pair series. The chain of high resistance (235 K each) ensure a constant voltage division for Darlington pair transistors. These Darlington pair transistors provide sufficient base current to drive the power transistors due to its enormous gain. 32 Darlington pair transistors and 16 power transistors are used in the circuit to stabilise the

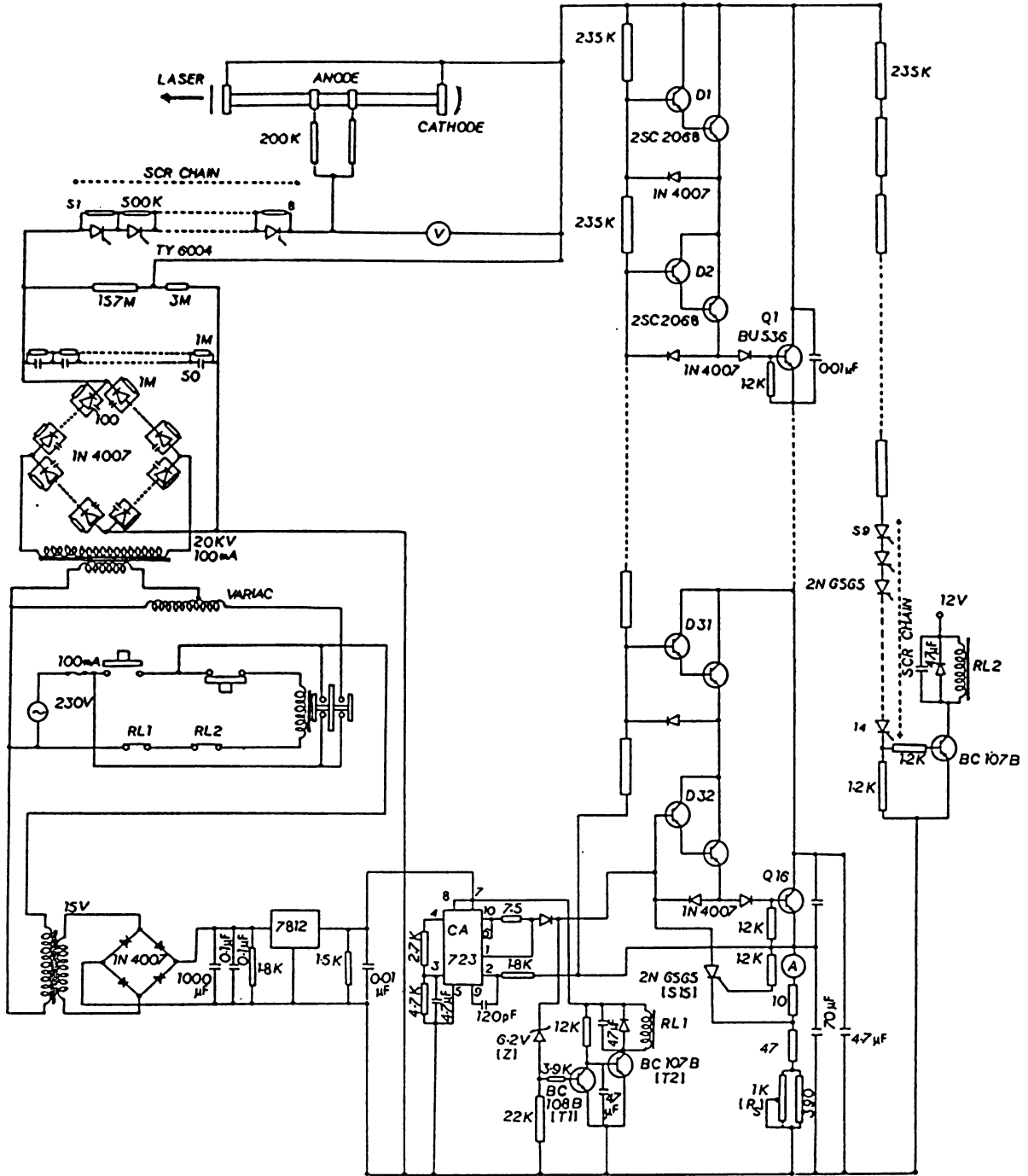


Fig. 5.16 Schematic diagram of the current regulated high voltage power supply for a dual section CW CO<sub>2</sub> laser system. (All resistances are in ohms).

current levels in the high voltage range. The diodes IN 4007 provide protection against reverse voltages which tend to damage the junctions of the transistors. Similarly the capacitor  $0.1 \mu\text{F}$  across the BU 536 prevents any surge voltages from appearing at collector-emitter side of the power transistors. The base of last Darlington pair is connected to a current regulator integrated circuit CA 723 which provides base current to drive D32. Current sensing is achieved by the 10 turn potentiometer (10 K) and the corresponding voltage is fed back to the IC through the resistor 1.8 K. The reference voltage from CA 723 is appropriately divided by the external potential divider [combination of 2.7 K and 4.7 K]. In order to provide a 12 V regulated voltage to the IC 723, a power supply is incorporated using 7812.

If the tube current exceeds 90 mA, the corresponding increase in the gate current turns on SCR 15 thereby short circuiting the base of D 32 to the emitter terminals of Q 16, driving it into a non-conducting state. As the SCR starts to conduct the voltage at the cathode of zener diode z drops to a value below its breakdown potential driving the transistor to the anode of Z to the non-conducting state and this in turn actuate the relay RLI to cut off the main supply.

Similarly, if the voltage across the series net work of the power transistors exceeds 2.7 KV, the SCR chain connected parallel to the transistors undergoes self breakdown and this in turn drive the transistor to actuate the relay RL2 connected in series with the main supply.

Since the current obtained for driving the base of D 32 is derived from the current regulator IC, the current through the transistor chain can be set to any desired value by adjusting the potentiometer  $R_s$ .

The fluctuations of plasma tube current can be calculated as follows :

The stability factor depends mainly on the gain and input resistance of D 32 and Q 16. The input impedance for a Darlington pair is  $R_i = h_{ie}(1+h_{fe})$

where  $h_{fe}$  is the current gain and  $h_{ie}$  is the input resistance of the base-emitter junction. Now if the voltage available from the output of CA 723 is  $\Delta V$ , then the base current of the D 32 will be  $I_{b_1} = V/R_i$ .

This  $I_{b_1}$  will be amplified by the total current gain of D 32. Therefore the net variation in the total current is given by  $\Delta I_c = h_{fe_1} h_{fe_2} h_{fe_3} \Delta I_{b_1}$ ,

where  $h_{fe_1}$  and  $h_{fe_2}$  are the current gain of 2SD 2068, Darlington pair while  $h_{fe_3}$  is the current gain of BU 536 power transistor.

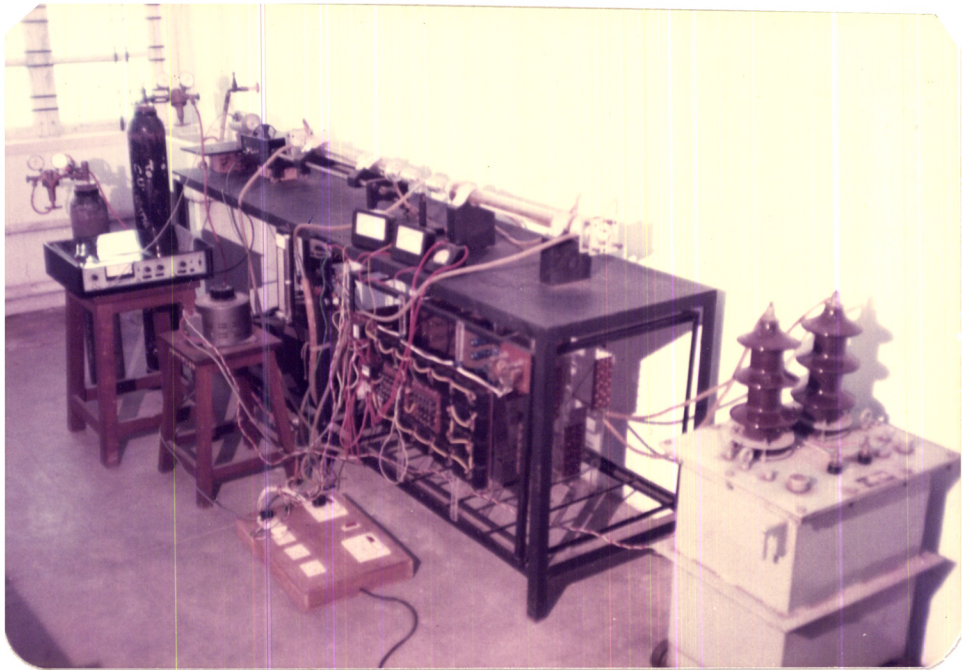
$\Delta I_{b_1}$  is the variation in the input base current which depends on the input resistance of D 32. Using the data given by the manufacturers the approximate stability of the output voltage from the IC 723 is  $7 \times 10^{-5} \text{ V/}^\circ\text{C}$  which gives a calculated plasma tube current variation

$\Delta I_c$  of  $0.14 \mu\text{A/}^\circ\text{C}$ . The tube current variation due to the thermal instability of the sensor resistance  $R_s$  is found to be  $1.5 \mu\text{A/}^\circ\text{C}$ . By incorporating the above values and the rate of variation of the laser output power with current is found to be  $0.4 \text{ mW/}\mu\text{A}$  and the fluctuation of output power of the laser beam is  $0.001\%^\circ\text{C}^{-1}$  due to the plasma current variations, change in the dimension of the optical cavity due to temperature variation, etc.

### 5.5 Operation of the laser :

To start the operation of the laser the optical cavity is aligned first as described in section 5.3.4. The rotary pump is switched on and





*Photograph of the CW CO<sub>2</sub> laser system*

the plasma tube and other flexible tubes are evacuated. Then  $\text{CO}_2$ ,  $\text{N}_2$  gases and  $\text{H}_2\text{O}$  vapour (as required) are allowed to pass through the plasma tube in a very precise manner with the aid of needle valves and manometer. Water is allowed to circulate through the outer jacket in order to cool the plasma tube walls. The power supply is switched on and the current level is set to 50 mA by adjusting the potentiometer  $R_s$ . Now the voltage to the electrodes is increased by using a variac at the input of the power supply and the discharge can be established in the two tubes simultaneously and the laser output can be sensed through the Ge window. The laser intensity can be optimised by adjusting the potentiometer which in turn vary the plasma tube current very precisely.

This laser was aligned as mentioned in section 5.3.4 and successfully made into operation. The output power was found to be 30 W which was measured by using a photoacoustic laser power meter and the details of the parametric studies are described in chapter VI.

## References :

1. C.K.N. Patel; Phys. Rev. Lett, 336A, 1187 (1964).
2. C.K.N. Patel, Phys. Rev. Lett, 12, 588 (1964).
3. J.C. Polanyi, J. Chew. Phys., 34, 347 (1961).
4. F. Legay and P. Barchenitz., C. r. Lebd. Se'anc. Acad. Sa. 256, 5305 (1963).
5. M. Legay, Sommaire, L. Henry and F. Legay., C.r. Lebd. Se'anc. Acad. Sci., 260, 3339 (1965).
6. J. A. Howe, Appl. Phys. Lett., 7, 21 (1965).
7. G. Moeller and J. D. Ridgen, Appl. Phys. Lett., 7, 274 (1965).
8. C.K.N. Patel, Appl. Phys. Lett., 7, 15 (1965).
9. C.K.N. Patel, Scientific American, 219, 2, 22 (1968).
10. A. J. Beaulieu, Appl. Phys. Lett., 16, 504 (1970).
11. C. A. Fenstermacher, M.J. Nutter, J.P. Rink and K. Boyer., Bull. Amer. Phys. Soc., 16, 42 (1971).
12. H. J. Sequin and J. Tulip., Appl. Phys. Lett., 21, 414 (1972).
13. K.O. Tan, V.Makios and R.W.Morrison, Phys. Lett., 38A, 225 (1972).
14. E.T. Gerry, IEEE Spectrum, 7, 51 (1970).
15. R.L. Carlson, P.C. James, D.E. Casperson, R.B. Gibson, R.P. Godwin, R.F. Haglund, J.A. Hanlon, E.L. Jolly and J.F. Stratton, IEEE J. Quantum Electron, QE-17,9, 1662 (1981).
16. J.D. Ridgen and G. Moeller, IEEE J. Quant. Electron., QE-2,9, 365 (1966).
17. A. Lofthus, Can. J. Phys., 34, 780 (1956).
18. C. P. Courtoy., Can. J. Phys., 35, 608 (1957).
19. C.K.N. Patel, Phys. Lett., 7, 246 (1965).



20. C.K.N. Patel, P.K. Tien and J.H. McFee, *Appl. Phys. Lett.*, **7**, 290 (1965).
21. A.J. Demaria, *Proc. IEEE*, **61**, **6**, 731 (1973).
22. W.W. Duley, *CO<sub>2</sub> lasers, Effects and Applications* (New York: Academic Press), (1976).
23. M. Djeu, Tehman Kan and G.J. Wolga, *IEEE J. Quant. Electron.* **QE-4**, 256 (1968a).
24. P.K. Cheo and H.G. Cooper, *IEEE J. Quant. Electron.*, **QE-3**, **2**, 79 (1967).
25. C.J. Walsh, *J. Phys. D*, **16**, 789 (1985).
26. B.L. Gupta, B.S. Narayan and L.M. Kukreja, *J. Phys. E: Scientific Instrum*, **13**, 1267 (1980).
27. D.C. Tyte, Carbon dioxide laser in *Advances in Quantum Electronics* ed., O.W. Goodwin (New York: Academic Press) (1970).
28. D. Courtois, C. Twietoeaux, A. Delahaigve, E. Merienne and P. Jouve., *Optics and Laser Technology*, 155 (1981).
29. M.K. Satheeshkumar, C. Raghavan and C.P.G. Vallabhan, *Int. J. Electronics*, (in press).

## CHAPTER VI

### PARAMETRIC STUDIES OF A CURRENT STABILISED CW CO<sub>2</sub> LASER

#### *Abstract*

*A detailed study of the parameters affecting the CO<sub>2</sub> laser beam intensity such as plasma tube current, gas mixture ratio and addition of water vapour using a PA laser power meter is presented in this chapter. The spectral distribution at different plasma tube currents and the divergence of the laser beam are measured. From the detailed analysis the optimum operating values of various parameters are arrived at to get a maximum power output from the CO<sub>2</sub> laser.*

## 6.1 Introduction :

A thorough knowledge of the optical as well as the electrical characteristics of the laser system is highly essential for the operation of the system with maximum efficiency and good long term stability. Very often in CO<sub>2</sub> lasers it is difficult to separate completely the influences of the various parameters that affect the working of the laser. This is primarily because many of the parameters are closely inter-related, e.g., variation in the plasma tube current will change the voltage across the plasma tube and the changes in the partial pressure of CO<sub>2</sub> - N<sub>2</sub> gas mixture causes a drastic change in the current through the plasma tube. Therefore this complex interplay of various parameters must always be taken into consideration when discussing the parametric evaluation. It is however, possible to indicate in a general way the influence of the various parameters and to give specific examples of the effect of their variation. Thus in order to carry out parametric studies of the laser, a regulated high voltage power supply for the excitation process, a highly stable resonator and an efficient gas filling system are often needed [1]. This arrangement provides the accurate measurement of the variation of laser beam intensity with one parameter while keeping the others unaltered. Consequently the precise measurement of the current, gas mixture ratio and gas pressure in the plasma tube lead to the determination of optimum operating conditions to get maximum output power. It also provides the opportunity to study the effect of additional components

like water vapour in the gas mixture on the output power of the laser. A brief account of the background regarding similar parametric studies made earlier is given in the next section.

## 6.2 Earlier work :

As mentioned earlier laser action in  $\text{CO}_2$  was first observed in pure  $\text{CO}_2$  by Patel in 1964 [2,3] and the power obtained was 1 mW with CW d.c. excitation and 10 mW peak with 1  $\mu\text{sec}$  excitation pulses. It was argued that pure  $\text{CO}_2$  will not give laser output and laser action occurs in a discharge containing  $\text{CO}_2$  because of the presence of CO formed in the discharge by the dissociation of  $\text{CO}_2$  [4]. Subsequently, Cheo showed that addition of a little CO to  $\text{CO}_2$  could enhance the laser power considerably [5]. Later Brinkschulte observed theoretically and experimentally that CO was highly needed for the laser action in pure  $\text{CO}_2$  [6]. Later Legay - Sommaire suggested the addition of  $\text{N}_2$  would enhance the laser power substantially due to the resonant energy transfer between  $\text{CO}_2$  and  $\text{N}_2$  molecules [7]. With the introduction of He gas to  $\text{CO}_2$  -  $\text{N}_2$  mixture further significant improvement in the laser power could be achieved because Helium removes the heat instantaneously from the plasma discharge [8]. Thus the effect of different concentration of these gases on the laser beam intensity was studied and it was found that a critical gas mixture ratio becomes essential for maximum efficiency and that optimum conditions vary with the geometry of the resonator cavity [9]. Variation of laser power with the addition of other vapours like water vapour and gases like argon,  $\text{SF}_6$ , Xenon etc., was extensively

studied in detail and it was concluded that the introduction of inert gases enhances the laser power substantially [10, 11, 12].

Similarly, the variation of plasma tube current with the laser power was studied in detail [13, 14, 15] and it was realised that an optimum current is always necessary for the efficient energy transfer between  $\text{CO}_2$  and  $\text{N}_2$  molecules which ensures a maximum laser beam intensity [16, 17]. Rosenberger in 1968 [18] reported a detailed account of the theoretical analysis of the variation of laser beam power with the plasma tube current. Further investigations [19, 20] revealed the fact that as the plasma tube current is increased, the laser output increases steadily to a maximum and then decreases rapidly as the current rises above the optimum. Subsequently, Tyte in 1970 showed that for a larger diameter of the plasma tube the optimum current increases significantly [15].

Alternately, studies on the temperature of plasma tube which directly affects the collisional rates in  $\text{CO}_2$  -  $\text{N}_2$  mixture revealed that the gas kinetic temperature varies radially, being maximum at tube axis [13]. Subsequently, Sviridov et al. in 1970 [21] deduced the mean gas kinetic temperature from the intensity measurements at different discharge currents. Recently, detailed numerical calculations of electron transport coefficients and vibrational excitation rates in a  $\text{CO}_2$  -  $\text{N}_2$  - He gas laser have been reported [22] and it revealed the fact that the effect of gas mixture variation on electron drift velocity is greatest in  $\text{CO}_2$  - He mixtures, but is substantially reduced when a small fraction of  $\text{N}_2$  is added [23].

Tyte in 1970 [15] reported that power output increases with the gas flow rate and this was attributed to the enhanced removal of heat from the cavity. This infact opened up the development of the convective cooled CO<sub>2</sub> lasers which gives much higher output power ( $\sim 2.7$  KW).

Similarly, Ridgen and Moeller in 1966 [24] mentioned that both the output laser power and conversion efficiency of electrical power to optical power are essentially independent of tube diameter for diameters of up to 50 mm. The gain for 10.6  $\mu\text{m}$  radiation has, however, been found to depend in a complex way on tube diameter [16] although the peak gain reduces with increasing tube diameter. Further research revealed the fact that the maximum axial gain for a CO<sub>2</sub> - N<sub>2</sub> - He mixture varies inversely with the tube diameter [25].

The external cooling of plasma tube plays an important role on the efficiency of a CW CO<sub>2</sub> laser system. Very often water cooling system has been adopted in medium power CW CO<sub>2</sub> lasers. Recently it has been reported [26] that the temperature of the water used for cooling the plasma tube must be about 10°C for maximum output power.

Extensive amount of work was carried out to identify the various laser transitions at different operating conditions [27, 28]. From the results it was found that the prominent bands are 10.6  $\mu\text{m}$  and 9.6  $\mu\text{m}$  in most of the laser geometries [29, 30]. In addition to the bands in the 9 - 11  $\mu\text{m}$  region, laser action was observed on 13 lines in the 4.3  $\mu\text{m}$  region [31, 32] and on 5 lines between 13  $\mu\text{m}$  and 17.4  $\mu\text{m}$  [33]. The line width of the CO<sub>2</sub> laser radiation so far developed is determined

mostly by mechanical, microphonic and thermal instabilities rather than the inherent molecular properties [15].

In the present chapter a detailed account of the variation of the output power of a current stabilised CW CO<sub>2</sub> laser with the plasma tube current, relative concentration of CO<sub>2</sub> and N<sub>2</sub> gas and the addition of water vapour is given. The novelty of the detection scheme is that a PA laser power meter is used to monitor the laser intensity. CO<sub>2</sub> laser power measurements using a PA cell as a laser power meter is reported here for the first time.

### **6.3 Variation of CO<sub>2</sub> laser power with the plasma tube current :**

The experimental set up for monitoring the laser beam power at 10.6  $\mu$ m region is shown in fig. 6.1. Laser beam from a current stabilised CW CO<sub>2</sub> laser is modulated by a mechanical chopper [34] and is allowed to fall normally on a PA cell containing carbon black as the sample which readily absorbs the radiation of this wavelength [35]. The details of the PA cell and its suitability to use as a sensitive laser power meter are described in chapter III. The acoustic signal is detected by a sensitive electret microphone placed in the PA cell and the PA signal is processed using a lock-in amplifier. Since the PA signal generated from carbon black has a linear dependence on the laser beam intensity, any slight variation in the laser beam power with changes in the plasma current can be precisely determined from the lock-in amplifier reading [36]. This method of detection eliminates the possibility of saturation of the detector system when one deals with higher laser beam intensities [37]. Since the CO<sub>2</sub> laser has a current stabilisation and control circuitry

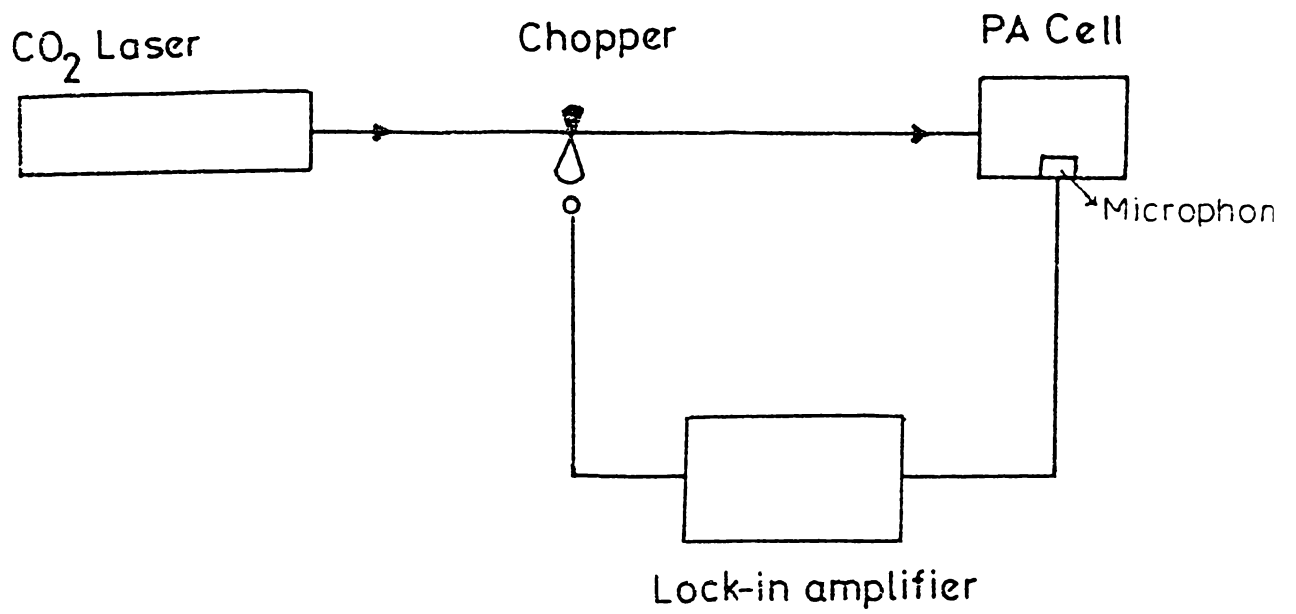


Fig. 6.1 Experimental set up for the measurement of laser beam intensity using PA technique



incorporated with its power supply, the plasma tube current can be set to any desired value irrespective of the voltage changes across the tube or the mains voltage [38]. Thus, the output power is monitored for various current levels for different combinations of gas mixture ratios.

Figures 6.2, 6.3 and 6.4 represent the variation of PA signal amplitude corresponding to different plasma tube current levels for various composition of  $\text{CO}_2$  and  $\text{N}_2$ . Here PA signal amplitude of 1 mV corresponds to a laser power of 1.07 Watts. The fig. 6.2 shows the influence of plasma tube current on the laser power for a  $\text{CO}_2$  pressure of 1.6 torr. All the curves in Fig. 6.2 show a maximum value of the output power at 24 mA and it starts decreasing with the increase in the current beyond the 24 mA except for the pressure ratio 2:3. A maximum PA amplitude of 18 mV which corresponds to a power of 20 W is obtained for a gas mixture ratio of  $\text{CO}_2 : \text{N}_2$  as 2:2. When the  $\text{N}_2$  concentration is varied the power level tends to decrease and in the case of a gas mixture ratio corresponding to  $\text{CO}_2 : \text{N}_2 = 2:3$ , two peaks are observed at different current levels of 22 mA and 26 mA respectively.

From these curves, it is seen that the gain of the  $\text{CO}_2$  laser increases sharply to its peak value at low plasma tube currents and then drops gradually with further increase in the current. This is primarily because as the current is increased above 24 mA the temperature of the gas mixture rises and consequently the centre of the gas column becomes too hot for the gain to remain optimum so that the radial gain profile in the tube dips at the centre; the larger the current, the deeper the

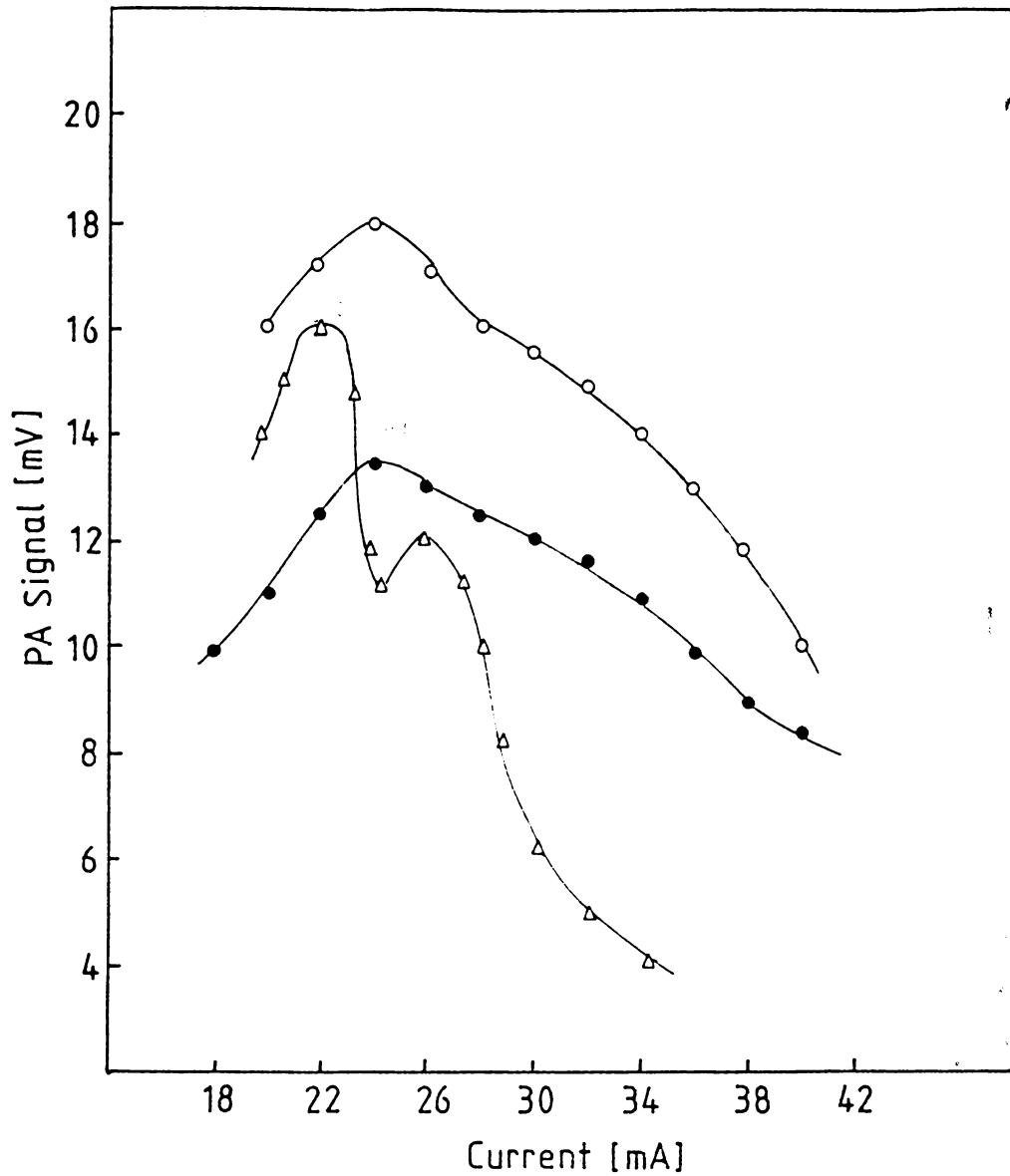
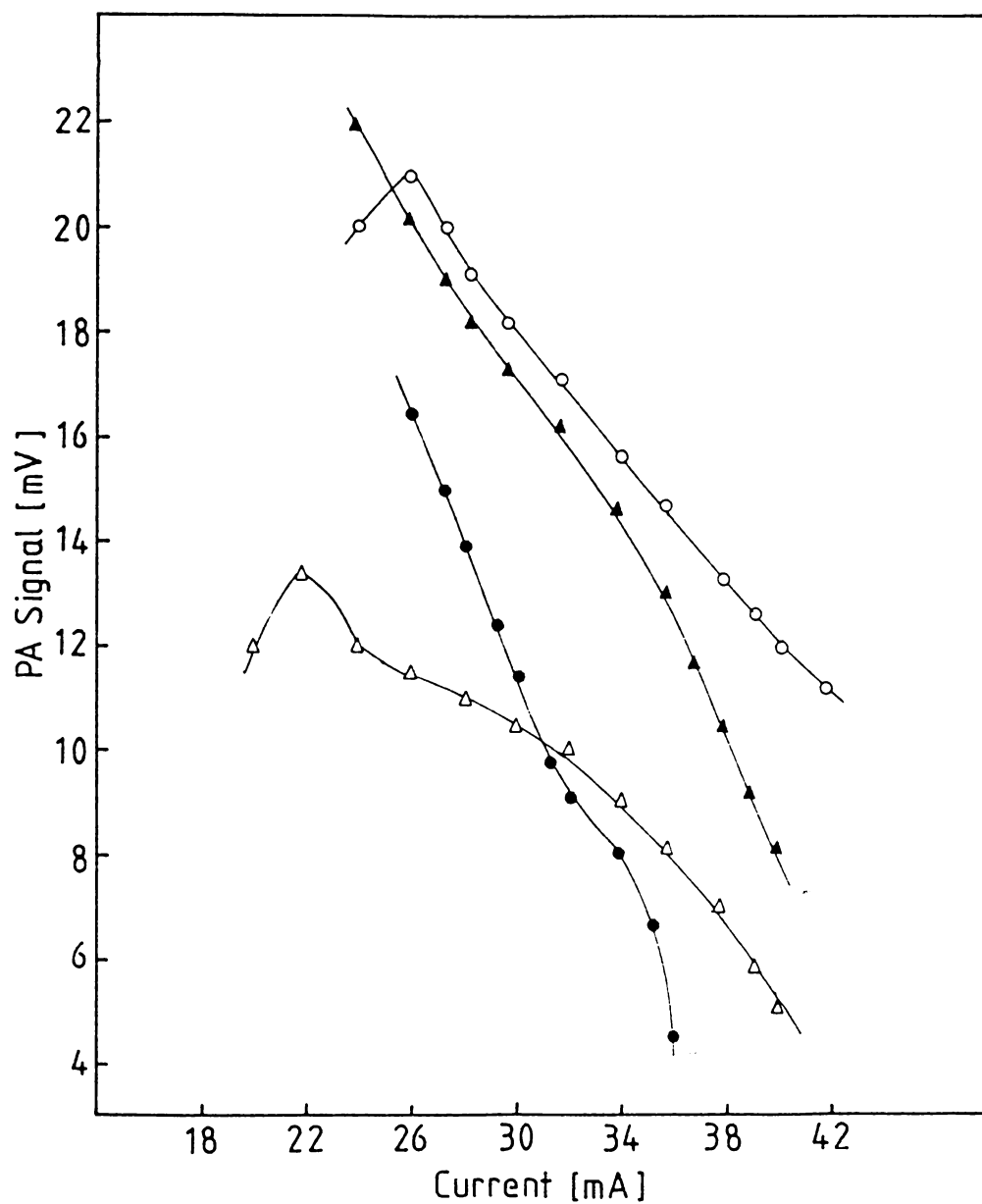


Fig. 6.2 Variation of PA signal amplitude with plasma tube current for different gas mixture ratios (●-●  $-\text{CO}_2 : \text{N}_2 = 2:1$ , ○-○  $-\text{CO}_2 : \text{N}_2 = 2:2$  and △-△  $\text{CO}_2 : \text{N}_2 = 2:3$ ) PA signal amplitude of 1 mV corresponds to a laser power of 1.07 watts.



**Fig. 6.3** Variation of PA signal amplitude with plasma tube current for different gas mixture ratios ( $\Delta$ - $\Delta$  -  $\text{CO}_2 : \text{N}_2 = 3:1$ ,  $\circ$ - $\circ$  -  $\text{CO}_2 : \text{N}_2 = 3:2$ ,  $\blacktriangle$ - $\blacktriangle$  -  $\text{CO}_2 : \text{N}_2 = 3:3$  and  $\bullet$ - $\bullet$  -  $\text{CO}_2 : \text{N}_2 = 3:4$ ). 1 mV PA signal corresponds to 1.07 watts of laser power

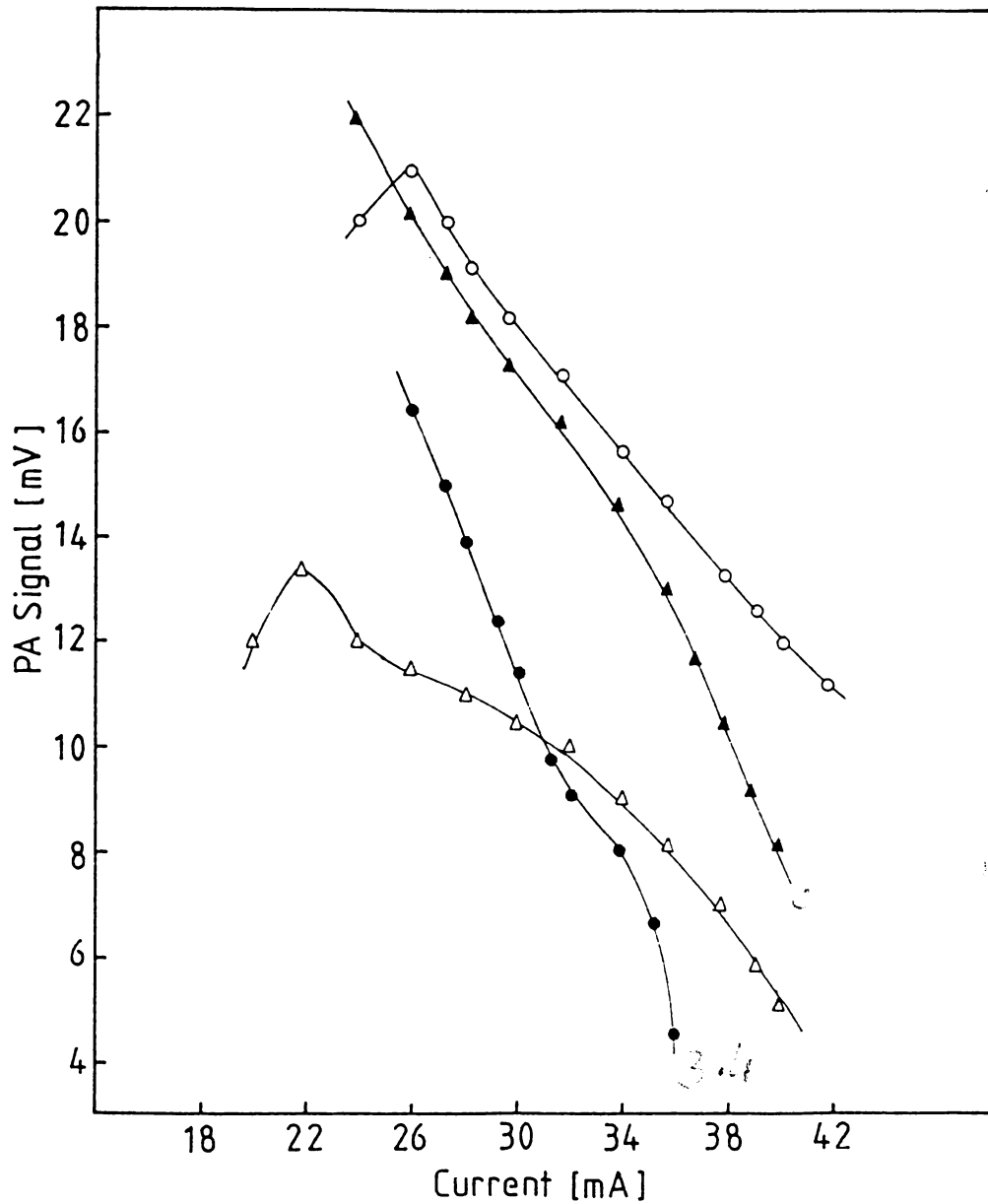


Fig. 6.3 Variation of PA signal amplitude with plasma tube current for different gas mixture ratios ( $\Delta$ - $\Delta$  -  $\text{CO}_2 : \text{N}_2 = 3:1$ ,  $\circ$ - $\circ$  -  $\text{CO}_2 : \text{N}_2 = 3:2$ ,  $\blacktriangle$ - $\blacktriangle$  -  $\text{CO}_2 : \text{N}_2 = 3:3$  and  $\bullet$ - $\bullet$  -  $\text{CO}_2 : \text{N}_2 = 3:4$ ). 1 mV PA signal corresponds to 1.07 watts of laser power

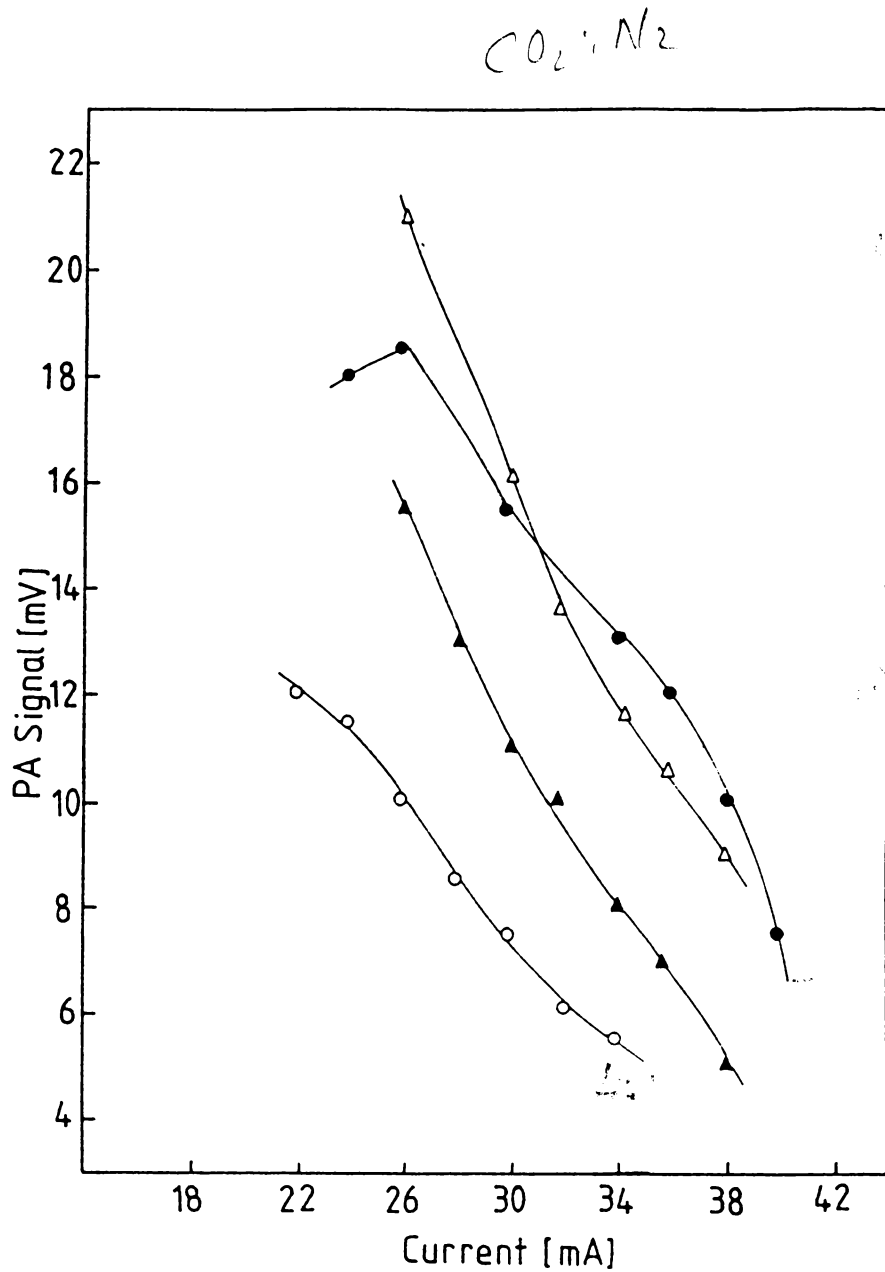
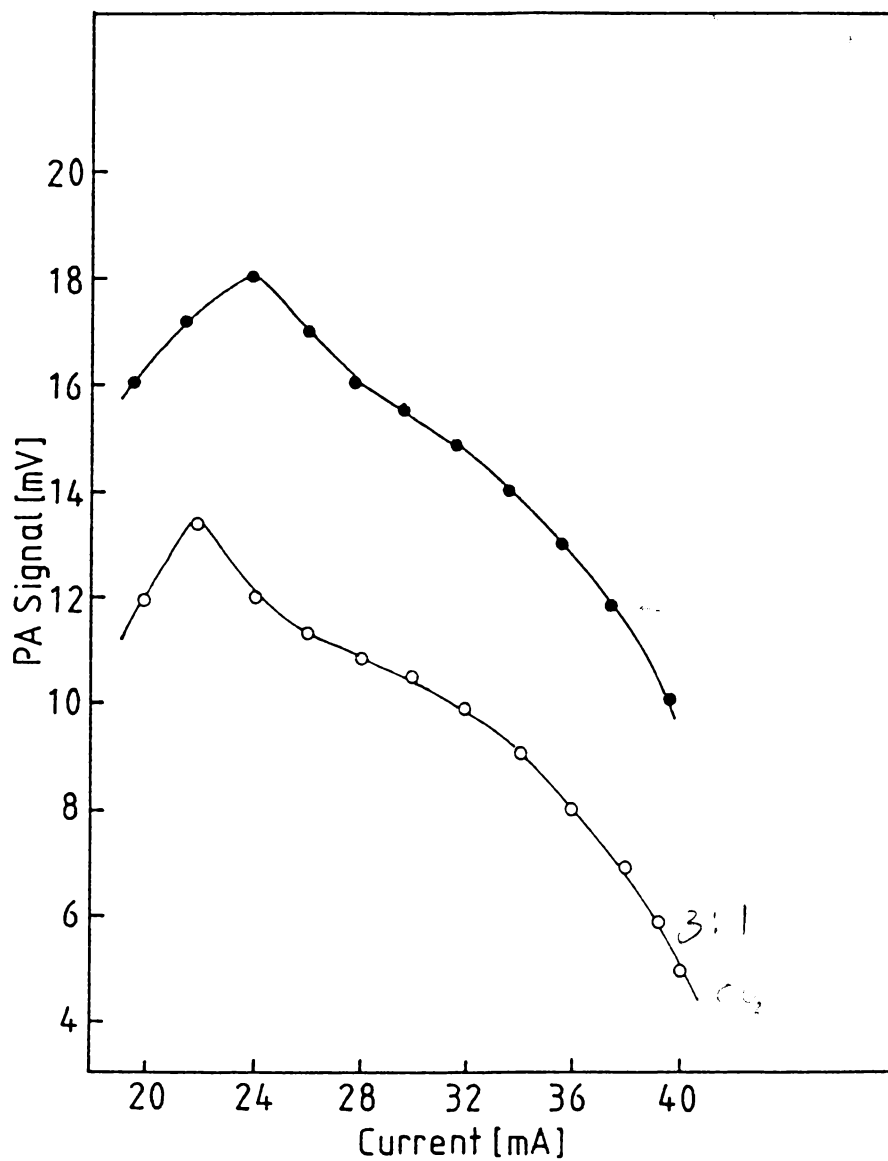


Fig. 6.4 Variation of PA signal amplitude with plasma tube current for different gas mixture ratios ( $0-0-\text{CO}_2 : \text{N}_2 = 4:1$ ,  $\bullet-\bullet-\text{CO}_2 : \text{N}_2 = 4:2$ ,  $\Delta-\Delta-\text{CO}_2 : \text{N}_2 = 4:3$  and  $\blacktriangle-\blacktriangle-\text{CO}_2 : \text{N}_2 = 4:4$ ).  $.1 \text{ mV}$  PA signal corresponds to  $1.07^2$  watts.

dip and nearer to the walls of the tube there exists maximum gain [39]. The rise in temperature may populate the (010) level of the CO<sub>2</sub> molecule by thermal excitation process which always tries to reduce the population inversion already established which in turn decreases the output power appreciably. In the case of gas mixture ratio of CO<sub>2</sub> : N<sub>2</sub> = 2:3, at lower plasma tube current levels, as shown in Fig. 6.2, excitation of the CO<sub>2</sub> molecules from the ground state (000) to the upper laser level of CO<sub>2</sub> (001) takes place by the direct collision between electrons and CO<sub>2</sub> molecules and this results in the peak obtained at a current level of 22 mA. As the current increases further, excitation of N<sub>2</sub> molecule to the first vibrational level occurs and subsequent resonant energy transfer to the CO<sub>2</sub> molecule further increases the gain which is observed as a second peak at 26 mA. The above phenomenon is apparently prominent only for a particular gas mixture ratio and at a fixed tube current [40] and this feature is reported here for the first time. This infact is an interesting special situation which can yield valuable information on excitation cross section of the CO<sub>2</sub> molecule and resonant energy transfer between CO<sub>2</sub> - N<sub>2</sub> molecules. Similarly Fig. 6.3 shows the variation of laser beam intensity with plasma tube current for various gas mixture ratios. At higher pressures of N<sub>2</sub>, a stable discharge in the plasma tube is achieved only at higher current levels which is always large compared to the optimum value. Thus at higher pressures, the optimum value of discharge current is found to be same as the minimum current required to establish a stable discharge in the plasma tube.

It is evident from these graphs that further increase in  $N_2$  concentration decreases the laser power level appreciably and this behaviour is mainly attributed to the geometry of the resonator cavity. It is also seen from the curves that an increase of 1 mA current causes a corresponding reduction of 1.6 Watts of the laser power. Since a steep slope in the operating characteristics indicate the possibility of an efficient intensity modulation of the laser beam by modulating the plasma tube current. This can be easily achieved with a current stabilised laser system in which the tube current is regulated by comparing the voltage developed across a sensor resistance in the transistor network [36] with a standard in-built reference voltage using a CA 723 integrated circuit. Therefore superposing an a.c. signal on the reference voltage may induce a corresponding variation in the plasma tube current. This variation of the current through the plasma tube can induce a corresponding change in the laser beam at  $10.6 \mu\text{m}$  region. Such an intensity modulated  $\text{CO}_2$  laser is considered to be an ideal source for optical communication.

Figures 6.5 and 6.6 represent the variations of laser power with plasma tube current at constant pressure of gas mixture in the tube. Fig. 6.5 shows the change in the PA signal amplitude at different current levels keeping total pressure of  $\text{CO}_2$  and  $N_2$  mixture at 3.2 torr. It is found that the maximum output of 19 Watts is obtained for a composition of  $\text{CO}_2$  and  $N_2$  as 2:2 at a discharge current of 24 mA. But as the gas mixture ratio is changed to 3:1 the current giving maximum power decreases as the concentration of  $\text{CO}_2$  increases. When the con-



**Fig. 6.5** Variation of PA signal amplitude with plasma tube current for different gas mixture ratios such that the total pressure in the cavity is 3.2 torr (●-● - CO<sub>2</sub> : N<sub>2</sub> = 2:2 and ○-○ - CO<sub>2</sub> : N<sub>2</sub> = 3:1). PA signal amplitude of 1 mV corresponds to a laser power of 1.07 watts.



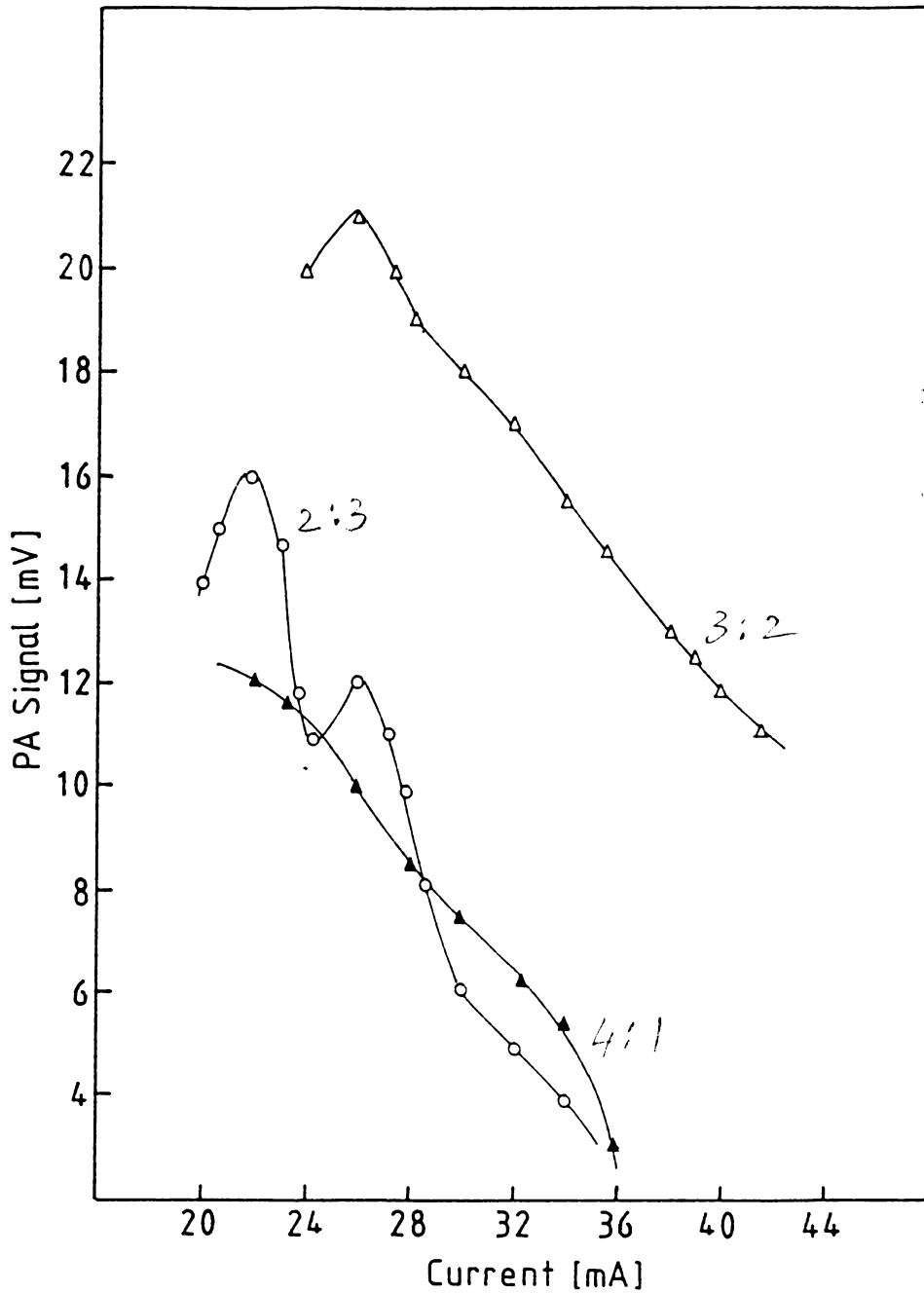
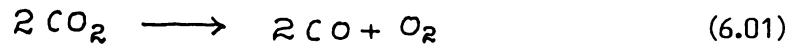


Fig. 6.6 Variation of PA signal amplitude with plasma tube current for different gas mixture ratios such that the total pressure in the cavity is 4 torr ( $\circ-\circ$  -  $\text{CO}_2 : \text{N}_2 = 2:3$ ,  $\Delta-\Delta$  -  $\text{CO}_2 : \text{N}_2 = 3:2$  and  $\blacktriangle-\blacktriangle$  -  $\text{CO}_2 : \text{N}_2 = 4:1$ ).  $1 \text{ mV} = 1.07 \text{ watts}$ .

centration of  $\text{CO}_2$  in the gas mixture increases, more and more  $\text{CO}_2$  molecules dissociate into CO according to the process,



Therefore the CO formed are excited to the upper vibrational level which matches with the  $\text{CO}_2$  ( $00\overset{\circ}{1}$ ) level. Thus efficient transfer of energy takes place from excited CO molecule to the ground state  $\text{CO}_2$  molecule, thereby  $\text{CO}_2$  molecules are raised to the upper vibration level of  $\text{CO}_2$  ( $00\overset{\circ}{1}$ ). Thus when the current is at a low value, the population inversion takes place due to the resonant energy transfer from CO molecule and also due to direct excitation of  $\text{CO}_2$  molecule by electron impact. The rate of population of the upper laser level increases upto a current of 22 mA and further increase in current reduces the population at (001) level causing a decrease in the output laser power [11]. Also when the concentration of  $\text{CO}_2$  molecules increases in the (cavity,) the probability of making collisions with the walls is considered to be larger compared to the intermolecular collision. These graphs in fact show the variation of laser power with plasma tube current for a fixed total gas pressure and hence it essentially indicates the effect of different gas mixture combinations on the laser power.

#### 6.4 Variation of output power with total pressure at fixed plasma tube current levels :

The fig. 6.7 and 6.8 represent the variation of PA signal amplitude with the total pressure at fixed current levels. These curves are obtained

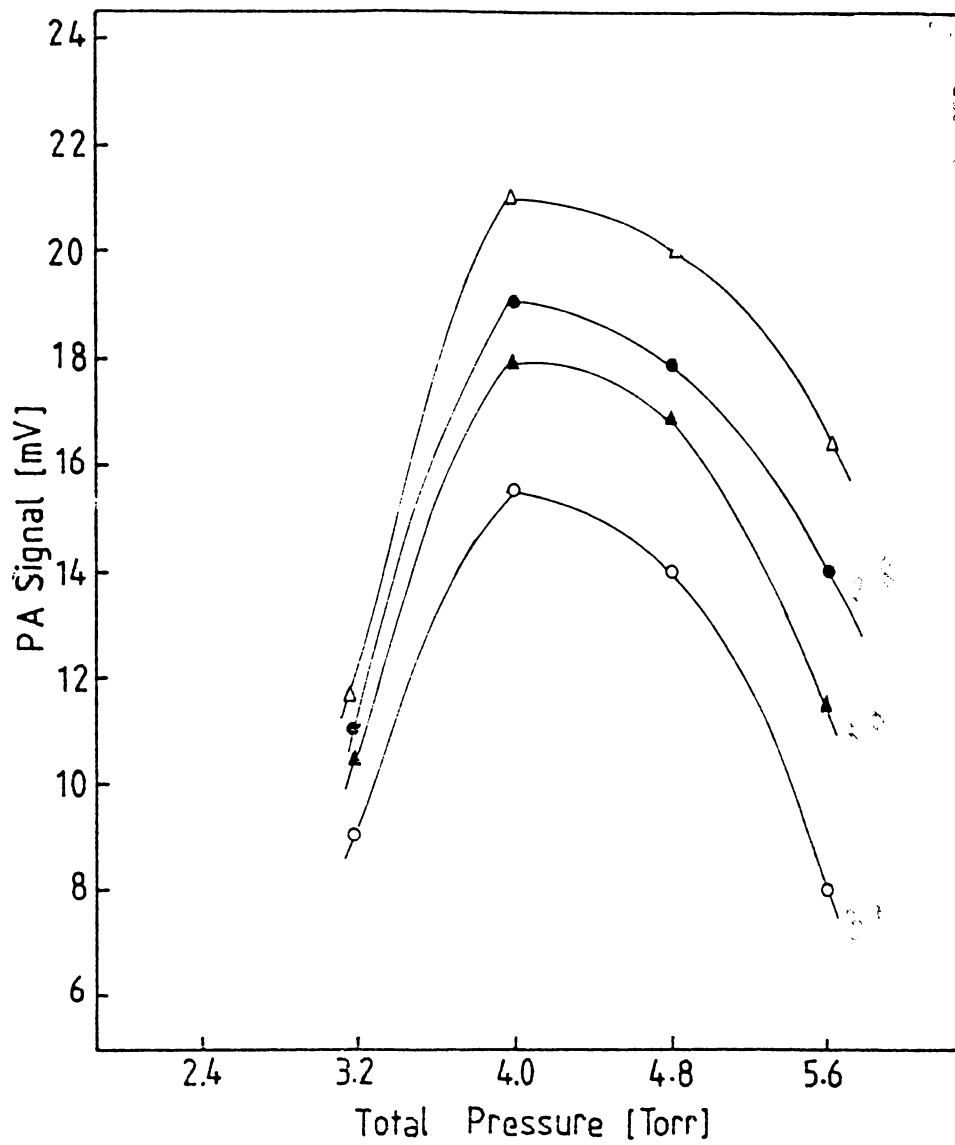


Fig. 6.7 Variation of PA signal amplitude with total pressure in the cavity for different current levels ( $\Delta$ - $\Delta$  - 26 mA,  $\bullet$ - $\bullet$  - 28 mA,  $\blacktriangle$ - $\blacktriangle$  - 30 mA and  $\circ$ - $\circ$  - 34 mA) 1 mV = 1.07 watts.

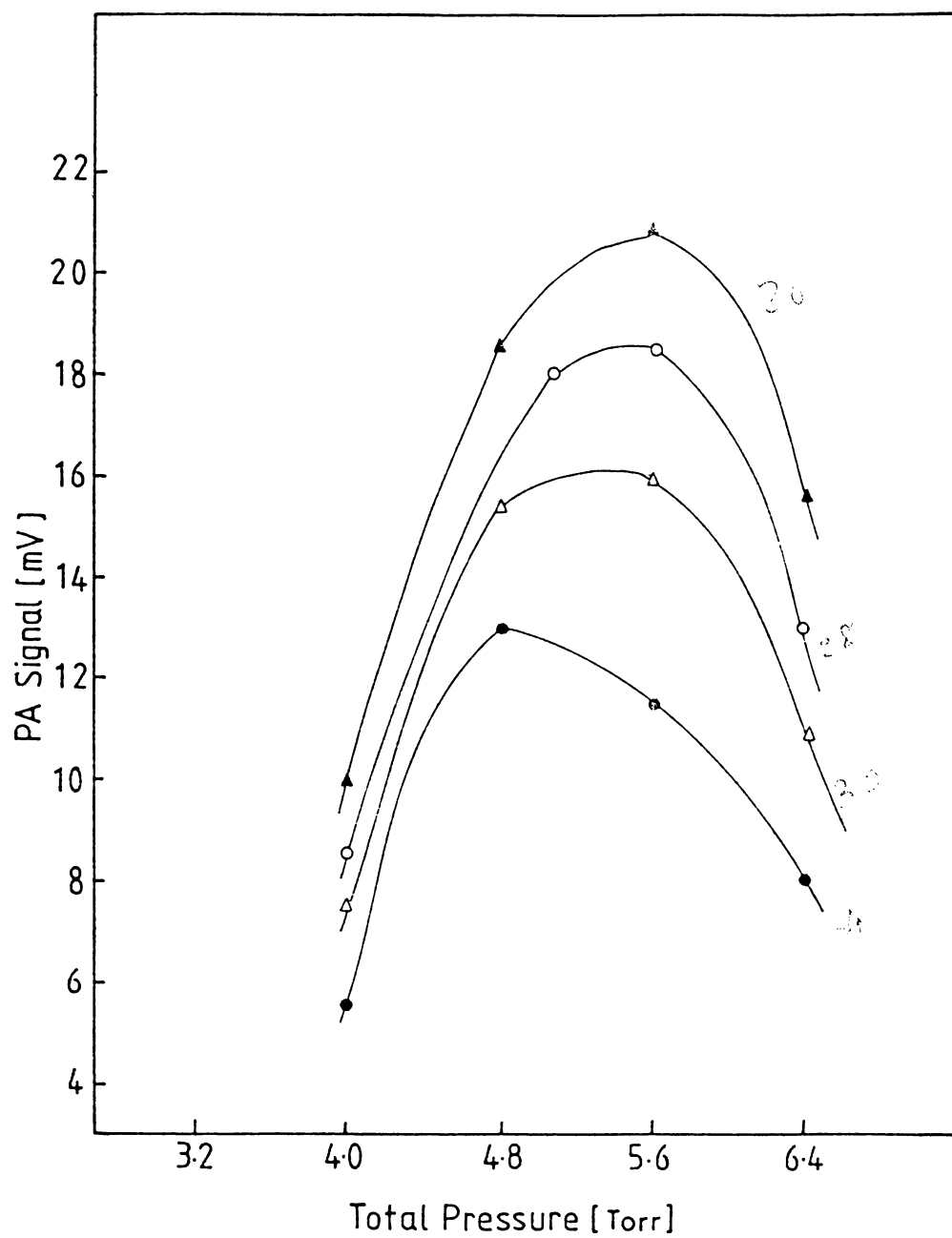


Fig. 6.8 Variation of PA signal amplitude with total pressure in the cavity for different current levels (▲-▲ - 26 mA, ○-○ - 28 mA, △-△ - 30 mA and ●-● - 34 mA). 1 mV = 1.07 watts.

by monitoring the laser power with change in total pressure in which the concentration of  $N_2$  gas varies by 0.8 torr. In fig. 6.7 the variation of output power is recorded with total pressure in the cavity when the partial pressure of  $CO_2$  is 2.4 torr. All the curves in fig. 6.7 apparently give maximum power level at a total pressure of 4 torr because at this pressure the resonant energy transfer to  $CO_2$  from  $N_2$  molecules is maximum. When the current is at 26 mA a maximum output PA signal corresponding to 22 W is obtained and beyond this limit the intensity starts decreasing. Similarly, fig. 6.7 shows the output power variation at gas mixture ratio  $CO_2 : N_2 = 4 : 1, 2, 3, 4$ . The maximum PA signal obtained is 21 mV which corresponds to an approximate power of 24 Watts at 26 mA current and at a gas composition  $CO_2 : N_2 = 3: 3$ .

Therefore from the above three figures it is found that the laser power initially increases with the total gas pressure and then decreases slowly with further increase in the pressure. It is also observed that the maximum output power obtained from the laser occurs at fairly lower current levels.

#### 6.5 Effect of the addition of water vapour on the laser beam intensity:

The variation of output power with the addition of water vapour in the  $CO_2 - N_2$  mixture is shown in the fig. 6.9. The graph corresponding to gas mixture ratios 3 : 3 and 4 : 3 and the maximum PA signal amplitude obtained are 28 mV and 21 mV respectively. From

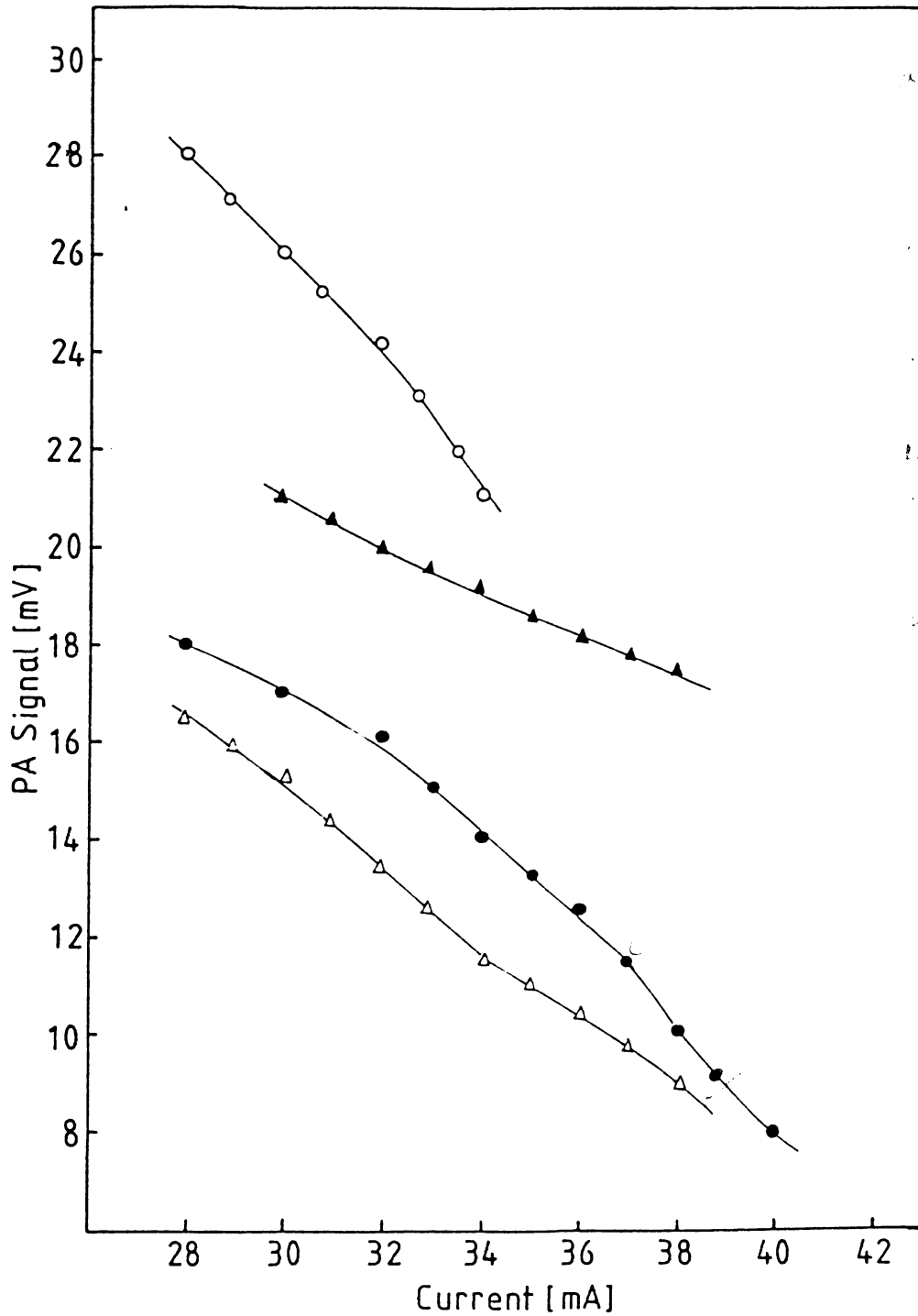
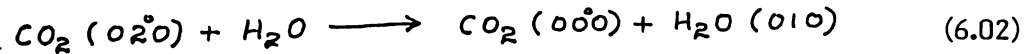


Fig. 6.9 Variation of PA signal amplitude with plasma tube current upper two curves show the enhancement of laser power due to the addition of water vapour (O-O -  $\text{CO}_2 : \text{N}_2 : \text{H}_2\text{O} = 3:3:0.3$  and ▲-▲ -  $\text{CO}_2 : \text{N}_2 : \text{H}_2\text{O} = 4:3:0.4$ ). The lower two traces represent the variation of PA signal with current for two gas mixture combinations. (●-● -  $\text{CO}_2 = \text{N}_2 = 3:3$  and Δ-Δ -  $\text{CO}_2 : \text{N}_2 = 4:3$ ) 1 mV = 1.07 watts.

the figure it is evident that the introduction of water vapour enhances the gain of the laser. When 0.3 torr of water vapour is added, there is a considerable increase in the laser power and beyond this, the laser intensity starts decreasing. Also when the amount of water vapour increases, the optimum value of the discharge current needed for the maximum power shifts to the higher current levels. Similarly, when the total pressure of the gas mixture is large, the amount of water vapour required to get maximum power is higher.

The addition of water vapour enhances the laser intensity because water vapour can help to deexcite the  $(0\overset{\circ}{2}0)$  level of  $\text{CO}_2$  directly to the ground state by the process :



and the excited water molecule then relaxes to the ground state mainly through non-radiative transitions. Therefore the addition of water vapour helps to depopulate the lower laser level which in turn improves the population inversion in the system [41]. This in fact enhances the laser power appreciably. However, there exists an optimum value for the amount of water vapour that depopulates the  $(020)$  level effectively. Below and above this value the rate of depopulation of  $(020)$  level is not large therefore the laser power decreases. Further increase of water vapour depopulate  $(1\overset{\circ}{0}0)$  and  $(0\overset{\circ}{0}1)$  levels of  $\text{CO}_2$  molecule which totally destroys the population inversion leading to a decrease of the laser beam intensity to lower values as reported previously [42].

## 6.6 Effect of plasma tube current on the spectral distribution in CO<sub>2</sub> laser emission :

There are about 160 laser lines in between 9.6  $\mu\text{m}$  and 10.6  $\mu\text{m}$  due to the various rotational level transitions [43]. A detailed study of the intensity of various lines with the plasma tube current reveals a prominence of various rotational lines in the laser emission. The experimental set up is schematically illustrated in fig. 6.10. The laser beam in the region of 10.6  $\mu\text{m}$  from a current stabilised CW CO<sub>2</sub> laser is mechanically chopped using a chopper and the beam is expanded using a gold coated concave mirror of radius of curvature 10 cm. This expanded beam is then allowed to fall on a monochromator [Oriel Model 7240] which contains a grating capable of resolving wavelengths from 8  $\mu\text{m}$  to 12  $\mu\text{m}$  with a resolution of 0.05  $\mu\text{m}$ . The expanded beam possesses a relatively small power density which safeguards the grating from any damage to its coating. Then the intensity from the monochromator is monitored by using a pyroelectric detector (Oriel Model 7090-2) and the detector output is electronically processed by using a lock-in amplifier (EG & G Model 5101). Since the monochromator has an electronic control circuit for automatic scanning of the grating angle, a recorded output can be obtained from the monochromator using a chart recorder.

Fig. 6.11 shows the spectral distribution of the output laser intensity for three different plasma tube currents at a gas mixture ratio of CO<sub>2</sub> : N<sub>2</sub> = 3 : 3. From these curves it is evident that the increase in



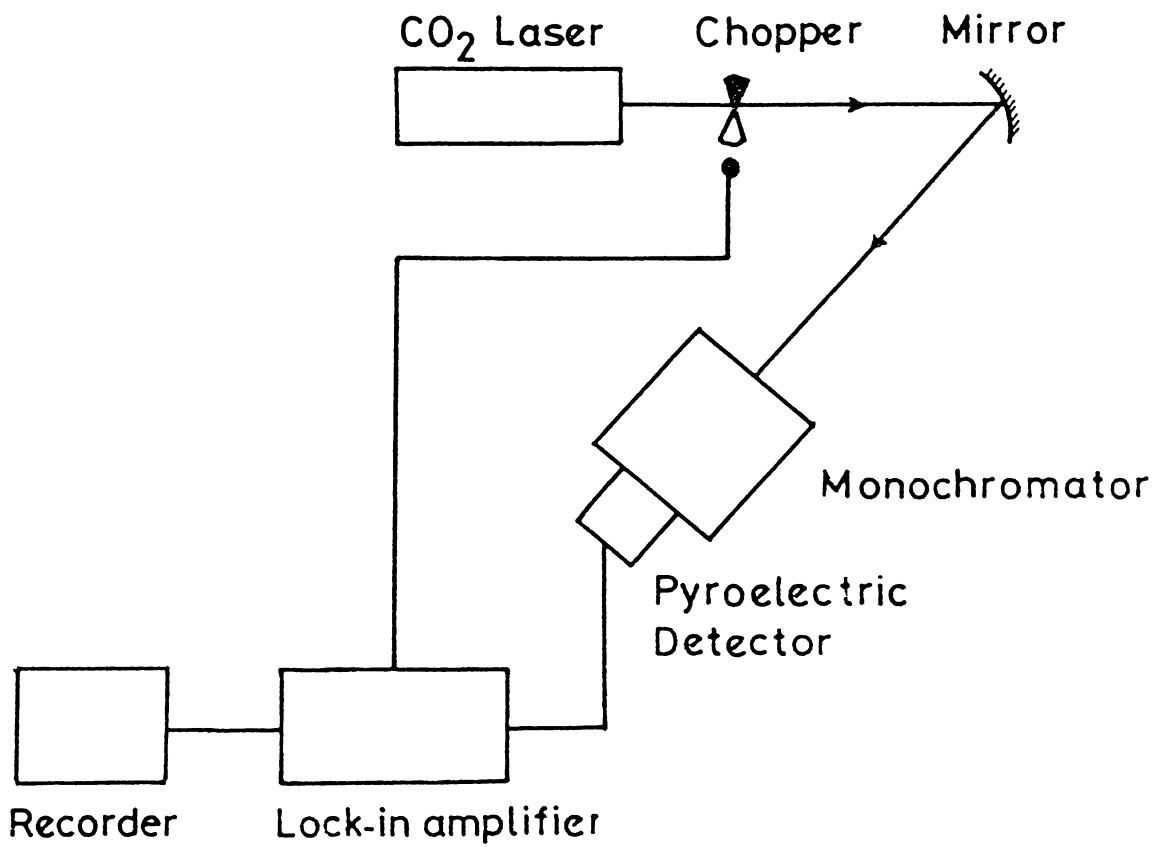


*Fig. 6.10* Experimental setup for the study of spectral distribution at different plasma tube current for an untuned CW CO<sub>2</sub> laser.

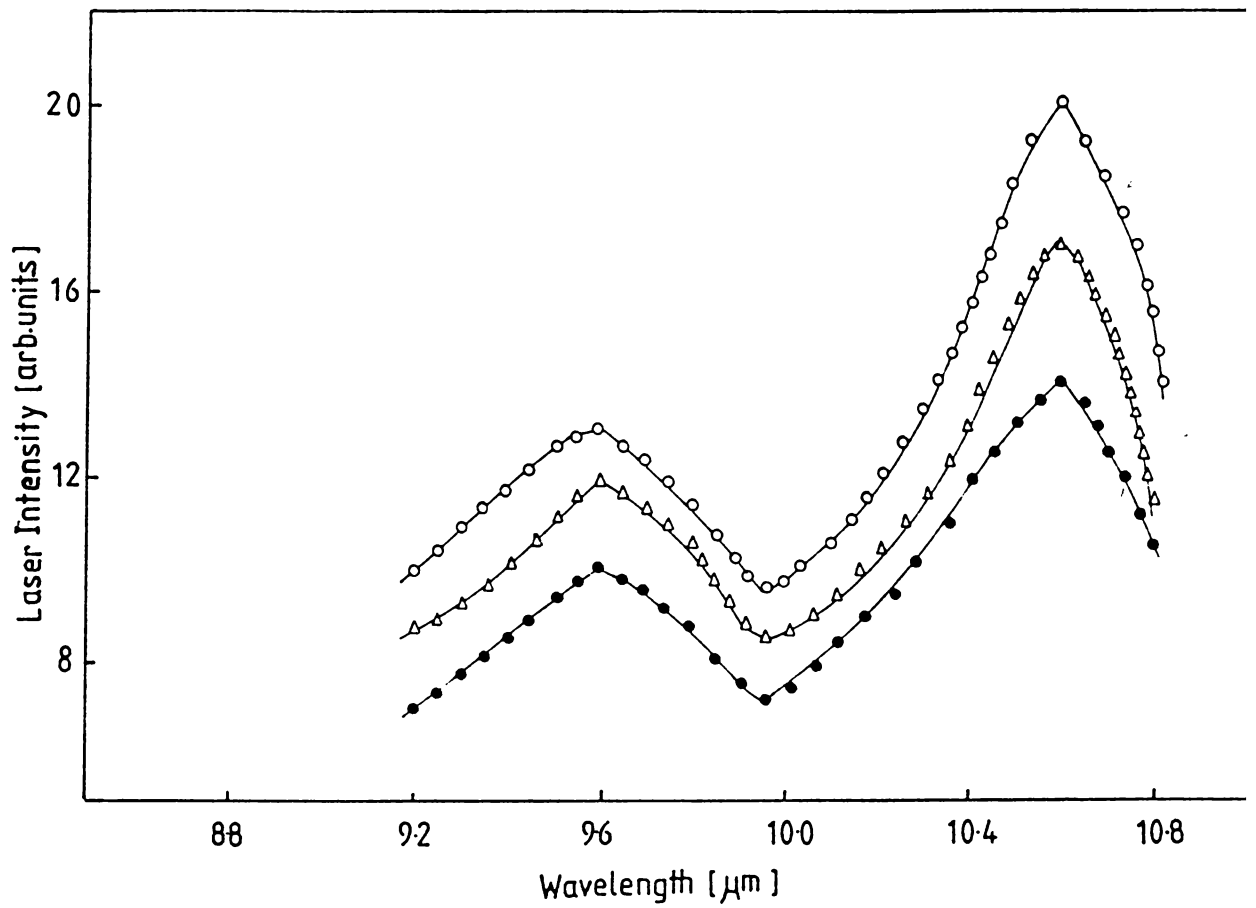


Fig. 6.11 Spectral distribution of the CW  $\text{CO}_2$  laser beam at different current levels when the gas mixture ratio of  $\text{CO}_2 : \text{N}_2 = 2:3$ . (○-○-25 mA,  $\Delta$ - $\Delta$ -30 mA and ●-●-35 mA)

tube current may reduce the intensities of various lasing lines. The intensity of 10.6  $\mu\text{m}$  radiation is always large compared to the other lasing wavelengths in a CW  $\text{CO}_2$  laser as reported earlier [44]. As a result the ratio of maximum intensities of 10.6  $\mu\text{m}$  band in  $(0\dot{0}1 \rightarrow 1\dot{0}0)$  and 9.6  $\mu\text{m}$  band in  $(0\dot{0}1 \rightarrow 0\dot{2}0)$  will indicate the change in spectral characteristics under various operating conditions [45]. This ratio is listed for different plasma tube current levels in Table 6.1.

The increase in intensity of various rotational lines at lower tube currents is mainly attributed to the fact that rise in temperature in the plasma tube tends to destroy the population inversion in the system thereby causing a reduction in the output power. Similarly in all the three curves the relative intensity of 10.6  $\mu\text{m}$  is large compared to the 9.6  $\mu\text{m}$  emission. This is primarily because the rate of deexcitation from  $\text{CO}_2(0\dot{0}1)$  to  $\text{CO}_2(1\dot{0}0)$  is fast compared to the transition between  $\text{CO}_2(0\dot{0}1)$  and  $\text{CO}_2(0\dot{2}0)$  [46] and this gives greater intensity for 10.6  $\mu\text{m}$  when compared to 9.6  $\mu\text{m}$  emission. This study indicates the spectral distribution in an untuned  $\text{CO}_2$  laser beam which reveals the relative probabilities for various rotational lines and their intensities at the various plasma tube currents.

### 6.7 Measurement of divergence of the laser beam :

Fig. 6.12 and 6.13 represent the laser beam intensity distribution in a direction perpendicular to the beam axis. The same is measured by using a pyroelectric detector firmly attached behind a pin hole on

**Table 6.1 :** *Intensities of 10.6  $\mu\text{m}$  and 9.6  $\mu\text{m}$  lines in the CW  $\text{CO}_2$  Laser at three different plasma tube currents*

<i>Plasma tube current I (mA)</i>	<i>Intensity (arb. units)</i>		<i>Ratio <math>I_{10.6}/I_{9.6}</math></i>
	<i>9.6 <math>\mu\text{m}</math></i>	<i>10.6 <math>\mu\text{m}</math></i>	
25	13.0	20.0	1.54
30	11.8	17.0	1.44
35	10.0	14.0	1.40

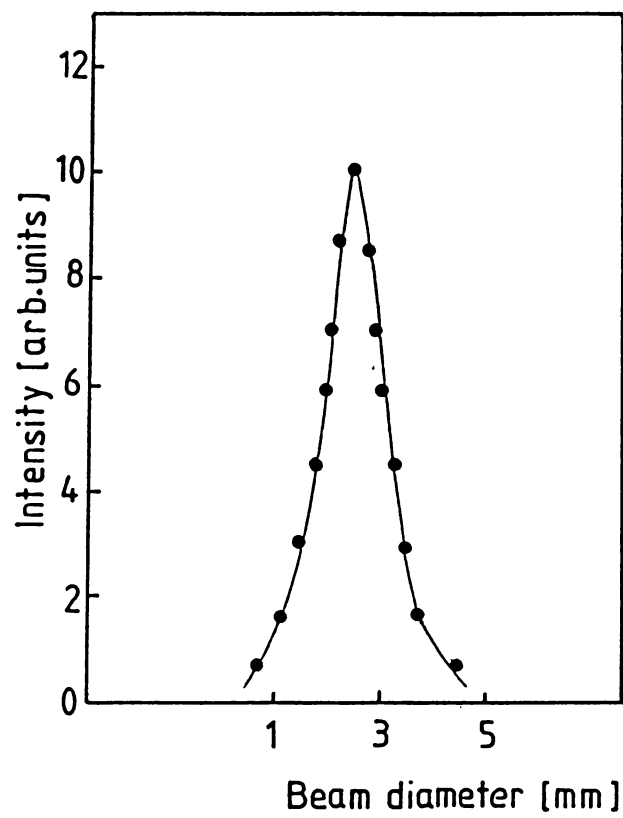


*Fig. 6.12 Laser beam profile close to the output mirror*

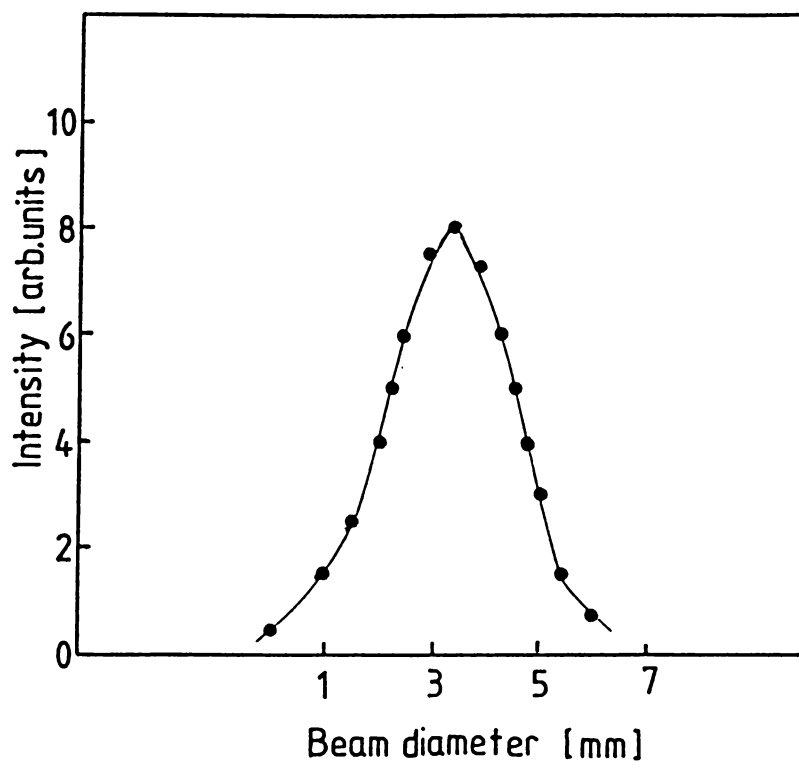


*Fig. 6.13 Laser beam profile at 60 cm away from the output mirror*

a travelling microscope. From these two figures the laser output has a gaussian profile which gives least divergence while containing maximum power in the area of the beam. Fig. 6.12 shows the beam diameter at the exist window which is found to be 3 mm while at 60 cm away from the window is 5.3 mm. Therefore these values give a divergence of 3.8 m. rad. and this is found to be comparable with the diffraction limit of 10.6  $\mu\text{m}$  radiation of above beam diameter. This is because of the 150 cm long laser cavity directs the laser beam along its axis without much divergence.

The complete parametric studies of the lab made current stabilised CW  $\text{CO}_2$  laser with indigenously available components reveal that the maximum laser power of 24 Watts can be obtained at a gas mixture ratio of  $\text{CO}_2 : \text{N}_2 = 3 : 3$  at 24 mA current. This situation could be improved by adding 0.3 torr of water vapour to the above mentioned gas mixture ratio. This optimum value of gas mixture ratio and water vapour gives a total power of 30 W at 28 mA plasma tube current. Thus the optimum condition required to get a maximum laser power is  $\text{CO}_2 : \text{N}_2 : \text{H}_2\text{O} = 3 : 3 : 0.3$  at a plasma tube current of 28 mA. The addition of Helium can further enhance the laser power. Similarly the spectral reponse confirms that the prominent wavelength which oscillates in the cavity with a maximum gain is at 10.6  $\mu\text{m}$ . It is also observed that the further increase in current from the optimum value will reduce only the intensity of various rotational transitions. The divergence of the laser beam is measured and it is found that the diver-

gence is nearly equal to the diffraction limit of  $10.6 \mu\text{m}$  radiation. The maximum attained power level of 30 Watts thus offers an efficiency of 11 % which is found to be reasonable for this system.